PHD

Catalytic Monoliths for Biodiesel Production

Asli, Umi

Award date:
2011

Awarding institution:
University of Bath

Catalytic Monoliths for Biodiesel Production

Umi Aisah Asli

A thesis is submitted for the degree of Doctor of Philosophy

University of Bath

Department of Chemical Engineering

February 2011

Abstract

Although the transesterification reaction of triglycerides with alcohols is well known and practiced on a commercial scale (using acid or alkaline catalysts), there is plenty of scope to improve this process. One approach involves the use of heterogeneous catalysts that could be retained in a fixed bed, and this would enable a continuous process to be developed. With this aim in mind, zinc proline ($Zn(C_5H_8NO_2)_2$) was used as a catalyst, which was coated onto a cordierite monolith support (62 cells/cm^2). Two different coating methods were explored, and SEM images of the surface revealed interesting crystal structures on the surface of the cordierite. Experiments were then performed in a batch reactor (120 ml) to assess the activity of the catalyst (molar ratio methanol:rapeseed oil = 12:1, T = 195ºC and P = 20 bar, 2 h duration). Although high conversions could be achieved, the catalyst was found to lose activity with time, and even the cordierite support was also found to be catalytically active. These aspects were explored further, in a continuous flow reactor, which had an i.d. = 6.2 mm, and multiple heated sections (500 mm each) into which pieces (10 mm long) of catalyst coated monoliths were inserted. Experiments were performed with packed lengths of 200 and 400 mm, and with liquid flows ranging from 0.1 to 2.9 ml min^{-1}. Although it was shown that high conversions can be achieved over extended run-times (e.g. 100 to 200 min), it was clear that the catalyst was losing its activity. Measurements also showed, that during the course of an experiment, Zn was leaching, and this clearly contributed to catalyst deactivation.

Despite the loss in activity of the zinc proline catalyst, the reaction system developed in this thesis was shown to work well, and that it could be used to evaluate the performance of catalytically coated sections of monolith. To demonstrate the use of this system, a few scoping studies were also performed using SrO as a catalyst, which was coated onto the cordierite monolith.

Acknowledgements

I would like to thank my supervisor Professor Stan Kolaczkowski for his guidance and financial support throughout my PhD. His patience, dedication and commitment were of great value to me. I would also like to thank Professor Matt Davidson and Dr Chris Chuck for their valuable advice and friendly help.

I would like to extend my gratitude to the Ministry of Education in Malaysia for the financial support of my study, and to Professor Gary Hawley for providing some financial support for the GC analysis.

I would like to express my grateful thanks to the technical staffs in the Department of Chemical Engineering; Fernando Acosta, Robert Brain, John Bishop, Richard Bull and Merv Newnes for their technical support and help with my experiments, developing a GC method and building my experimental rig. I am also particularly grateful to Alan Carver in the Department of Chemistry for his help with the Atomic Absorption Spectroscopy technique.

I would also like to thank Danniel Minett, Julia Griffen and Ben Firth, for their useful discussion during the writing up this thesis. A special thank to Kirsty Barber who helped me do the ^{1}H NMR analysis; and also to Ben Firth who helped me proof read my thesis.

I would also like to express my appreciation to the research team; Dr Serpil Awdry, Firas Al-Badran, Y.H Yap, Chris S.Ye, Chien D.L, Chen Z and all the other member for their encouragement, advice and friendship over the period I was in Bath.

Lastly, a deepest gratitude goes to my beloved family for their endless support and encouragement, especially to my Mum, husband and daughter.

To my little daughter, Sophea.

May this thesis inspire you to achieve your dream.

"If we knew what it was we were doing, it would not be called research, would it?"

Albert Einstein

TABLE OF CONTENTS

LIST OF FIGURES

LIST OF TABLES

Nomenclature

A	area, m^2
C_i	concentration of species *i* (*i*= TG, DG, MG and E), mol $litre^{-1}$
D_H	hydraulic diameter, m
$-\frac{d\,C_{TG}}{dt}$	consumption of triglyceride per unit time
F_{A0}	initial molar flow rate of reactant A, mol min^{-1}
k	rate constant, units vary
k’	reaction rate per weight of catalyst, mol min^{-1} $g_{catalyst}^{-1}$.
L	length, cm or mm
$\dot{Q}$	heat transferred to the system, W s^{-1}
Q	volumetric flowrate, ml min^{-1}
R^2	regression coefficients
S	specific surface area , m^2 m^{-3}
T	temperature, °C
T_w	wall temperature, °C
T_1	inlet temperature, °C
T_2	outlet temperature, °C
U	overall heat transfer coefficient, W m^{-2} $°C^{-1}$
V	volume of reactor, cm^3
W	weight of catalyst, g
X	fractional conversion

Greek symbols

α	order of reaction with respect to the triglyceride concentration
β	order of reaction with respect to the methanol concentration
$\in$	void fraction
μ_{mix}	dynamic viscosity of mixture, kg m^{-1} s^{-1}
υ	mean average velocity of liquid, m s^{-1}
ρ_{mix}	mass density of mixture, kg m^3

Abbreviations

DG	diglyceride
E	esters
FAME	fatty acids methyl esters
GL	glycerol
i.d	internal diameter, m
MeOH	methanol
MG	monoglyceride
o.d.	outside diameter
RTD	residence time distribution
TG	triglyceride

CHAPTER 1

INTRODUCTION

In this chapter the use of biodiesel as a fuel, and its properties, are described. In addition, a brief summary is provided of different reaction pathways by which it can be produced. Finally, the transesterification route is selected, and the outline structure of the thesis is summarised.

1.1 Background

Over the past decade, there has been a growing interest in the use of biodiesel as an alternative green fuel source. As reported by Carriquiry (2007):

> "Biodiesel has recently experienced a major surge worldwide. A rapid expansion in production capacity is being observed not only in developed countries such as Germany, Italy, France, and United States but in developing countries such as Brazil, Argentina, Indonesia and Malaysia."

As illustrated in Figure 1.1, the world biodiesel market has grown from 2.2 million tons per year in 2002, up to 32.6 million tons per year in 2008, while the production has grown from 2.2 MT per annum (in 2002) to 11.1 MT per annum (in 2008).

In many countries, there is a strong incentive to secure the supply of fuels from non-fossil fuel sources (to achieve security of fuel supply), and to use renewable energy sources (so as to reduce the carbon footprint and yield environmental benefits).

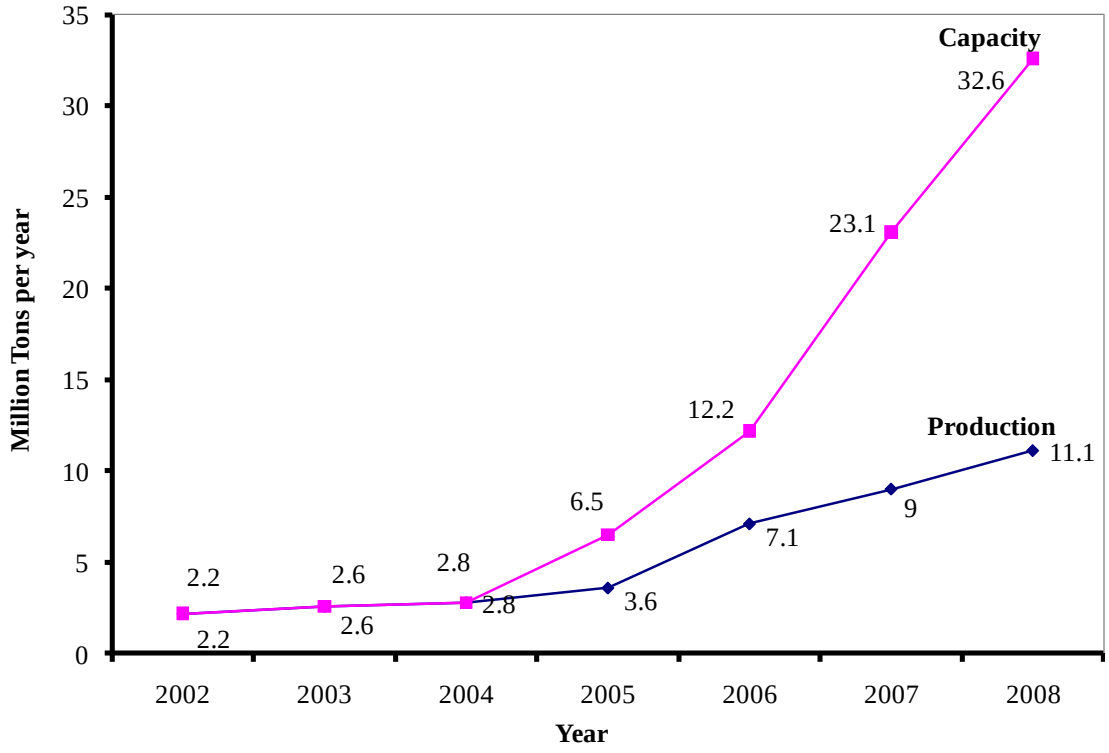

Figure 1.1: World biodiesel production and capacity (Emerging Market Online, 2008).

The use of vegetable oils to make biodiesel is a sustainable source of organic carbon, and despite concern over competition with the food supply chain, this will continue to be used in many countries as a source of fuel. Table 1.1 shows the most common oils used for the production of biodiesel.

Table 1.1: Biodiesel feedstocks for various regions of the world (adapted from Ahmad *et al.*, 2010).

Country/region	**Feedstock**
USA	Soybean
Europe/EU	Rapeseed, sunflower
Western Canada	Canola oil
Africa	Jatropha
India	Jatropha
Malaysia/Indonesia	Palm
Philipines	Coconut
China	Waste cooking oil
Spain	Linseed oil
Greece	Cottonseed

Within the European Union (EU), the demand for diesel fuel is forecast to grow by 51% from 2000 to 2030 (European Commission, 2006), and the transport sector accounts for about 32.6% of the total energy consumption (European Commission, 2010). As the transport sector is 94.5% dependent on fossil fuels, this is extremely vulnerable to disturbances in oil supply (imports into the EU) and oil prices (European Commission, 2010). Figure 1.2 shows the final energy consumption by sector in 2007.

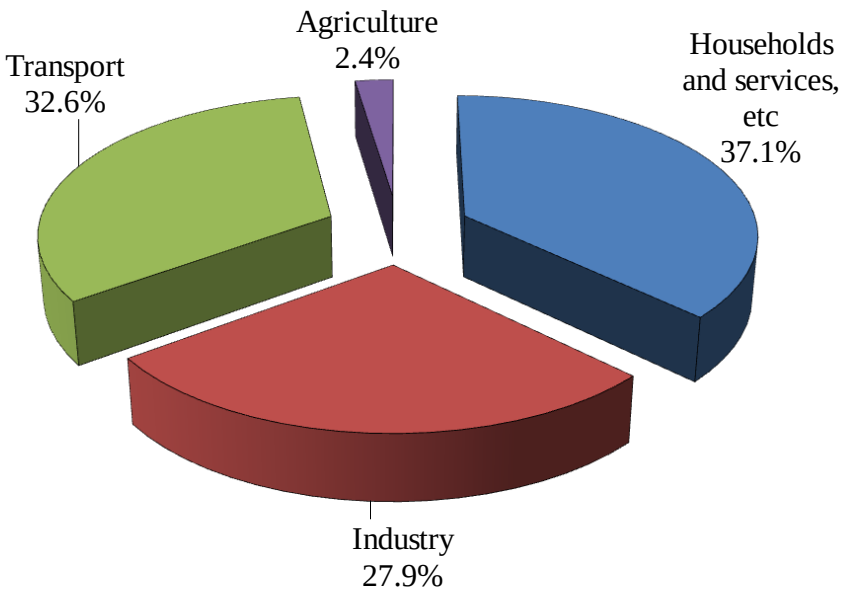

Figure 1.2: The final energy consumption by sector in 2007 (adapted from European Commission, 2010).

Alternative biofuel sources, so called second generation biodiesel feedstocks such as non-food feedstocks, have been developed to produce biodiesel to reduce the dependency on edible oil. Jatropha, mahua, jojoba oil, tobacco seed, salmon oil and seamango represent some of these energy crops. Waste cooking oils, restaurant grease and animal fats, such as beef tallow and pork lard, are also considered second generation feedstocks. Alternatively, algae oil from microalgae sources have been identified recently; which gives a high yield per unit of land (Ahmad *et al.*, 2010; Mata *et al.*, 2010). An indication of land use and oil yield for different feedstocks is given in Table 1.2.

Table 1.2: Comparison of microalgae with other biodiesel feedstocks (adapted from Mata *et al.*, 2010).

Plant source	Seed oil content (% oil by wt. in biomass)	Oil yield (litre oil/ ha/year)	Land use (m^2 year/kg biodiesel)	Biodiesel productivity (kg biodiesel /ha/year)
Corn/Maize	44	172	66	152
Hemp	33	363	31	321
Soybean	18	636	18	561
Jatropha	28	741	15	656
Camelina	42	915	12	809
Canola/rapeseed	41	974	12	862
Sunflower	40	1,070	11	946
Castor	48	1,307	9	1,156
Palm oil	36	5,366	2	4,747
Microalgae (low oil content)	30	58,700	0.2	51,927
Microalgae (medium oil content)	50	97,800	0.1	86,515
Microalgae (high oil content)	70	136,900	0.1	121,104

Note:

The value for biodiesel productivity is assumed to be estimated as follows.

Biodiesel productivity = oil yield (litre oil/ha/year) × density of oil (kg/litre) × conversion of biodiesel from raw oil

The value of oil density is varied depends on the type of oil.

The use of biodiesel complies with the agreement on the Kyoto Protocol to The United Nations Framework Convention on Climate Change (UNFCCC). As mentioned in UNFCC document (2008):

> "The major feature of the Kyoto Protocol is that it sets binding targets for 37 industrialized countries and the European community for reducing greenhouse gas (GHG) emissions .These amount to an average of five per cent against 1990 levels over the five-year period 2008 to 2012."

In Europe, renewable sources represent 7.8% of the total energy production and biodiesel accounted for 71% of the total biofuel production in 2007 (European Commission, 2010). According to European Commission (2011), European Union leaders have agreed to adopt a binding target on the use of renewable energy which is to increase the share of renewable energy to 20% in 2020. The breakdown for energy sources in Europe for 2007 is shown in Figure 1.3.

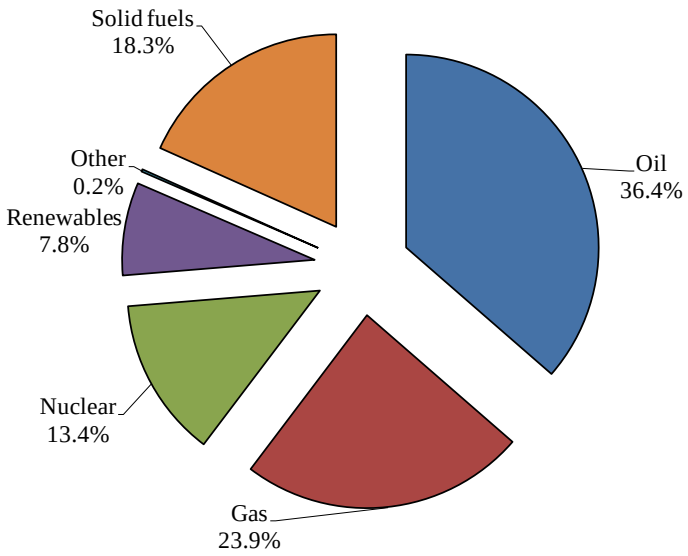

Figure 1.3: The breakdown for energy sources in Europe for 2007 (adapted from European Commission, 2010).

The development of biodiesel has its chronology. The potential of renewable fuel was first recognised by a demonstration of Rudolf Diesel's engine which ran on peanut oil in the 1900's (e.g. Knothe, 2001; Pahl, 2005). However, the direct use of vegetable oil which included blending with solvents and microemulsions, caused many problems with engine performance (Demirbas, 2003). Meanwhile, in later years, petroleum-based fuel dominated the energy sources; hence the use of vegetable oil became insignificant

(Pahl, 2005). It is believed that the global energy crisis in the 1970's was the important event that sparked the potential of biodiesel as an alternative energy source. As mentioned in Pahl (2005, p.151):

> "The oil crisis of the 1970's was a rude awakening for most Americans, dramatically underscoring the nation's dependency on imported oil. …..As the price of oil increased dramatically and long lines at gasoline stations grew even longer, people across the country began to look for alternative sources of energy."

In early biodiesel publications, the term bio-diesel has been used to describe a variety of different products. This included: neat vegetable oils, blends of conventional diesel fuel with vegetable oils, tallow and their esters, or as the alkyl esters of vegetable oils and animal fats (Maher and Bressler, 2007). Biodiesel is now formally defined as mono-alkyl esters of long chain fatty acids derived from vegetable oils or animal fats which conform to ASTM D6751 specifications for use in diesel engines (National Biodiesel Board, 2008). In Appendix A, examples of different standards are illustrated.

Biodiesel is a viable fuel in conventional diesel engines due to its significant level of similarity in terms of properties and ignition performance compared with conventional diesel (Al-Zuhair, 2007; Demirbas, 2003; Kalam and Masjuki, 2002). As claimed by Al-Zuhair (2007), biodiesel:

(a) has a relatively high flash point (150°C), which makes it less volatile and safer to transport or handle than petroleum diesel,
(b) provides lubricating properties that result from the free fatty acids present, which reduce engine wear and extend engine life, and
(c) has physical properties and an energetic content close to those of petroleum diesel (which allows it to function efficiently in conventional diesel engines without any modification).

In Table 1.3, some of the key physical and chemical properties of biodiesel fuels are described.

Table 1.3: Comparison between the physical and chemical properties of biodiesel fuels produced from various vegetable oils (adapted from Al-Zuhair, 2007); and values from Buyukkaya (2010).

Vegetable oil used	**Kinematic viscosity[a] $mm^2 s^{-1}$**	**Cetane Number[b]**	**Lower heating value[c] MJ $litre^{-1}$**	**Flash Point[d] °C**	**Density g $litre^{-1}$**
Peanut	4.9 (37.8°C)	54	33.6	176	0.883
Soybean	4.5 (37.8°C)	45	33.5	178	0.885
Soybean	4.0 (40°C)	45.7 to 56	32.7	-	0.880 (15°C)
Palm	3.6 (37.8°C)	62	33.5	164	0.880 (15°C)
Sunflower	4.3 to 4.5 (40°C)	49	33.5	183	0.860
Rapeseed	4.2 (40°C)	51 to 59.7	32.8	-	0.882 (15°C)
Used rapeseed	9.48 (30°C)	53	36.7	192	0.895
Used corn oil	6.23 (30°C)	63.9	42.3	166	0.884
Commercial diesel[e]	2.6 (40°C)	49		72	0.837

[a] relates to how fast the fuel flows.

[b] measurement of the combustion quality of diesel fuel during compression ignition.

[c] an amount of heat released by combusting a specified quantity (initially at 25°C or another reference state) and returning the temperature of the combustion products to 25°C.

[d] indicator to show how easily a chemical may burn.

[e] taken from Buyukkaya (2010).

As illustrated in Figure 1.4, the combustion of biodiesel, either pure or in mixtures with diesel, is reported to greatly reduce the emissions of carbon monoxide (CO), particulate matter (PM), total hydrocarbons (THC) and sulphur compounds. However, quite different conclusions can be formed for other substances, as an increase in NOx and SOF (soluble organic fractions) emissions has been reported (e.g. National Biodiesel Board, 2010; Pinto *et al.*, 2005).

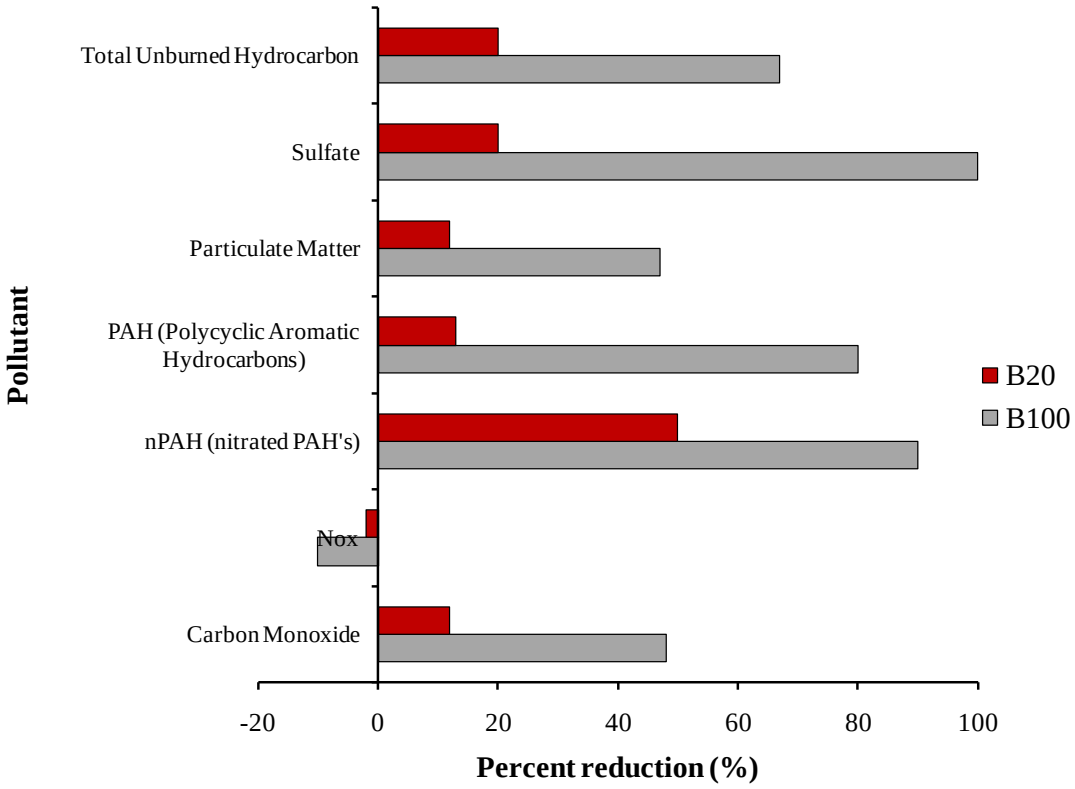

Figure 1.4: Percentage of emission reduction for B100 (100% biodiesel) and B20 (20% biodiesel blend with 80% of petroleum diesel), adapted from National Biodiesel Board (2010).

There are a number of different ways to produce biodiesel. The most common process is through the transesterification reaction. Other technologies include thermochemical processes from biomass, and these have been described in reviews by Maa and Hanna (1999), and Demirbas (2003, 2007a and 2007b). Based on a review of the literature, a summary of process routes is illustrated in Figure 1.5, and these are briefly described in the sections that follow.

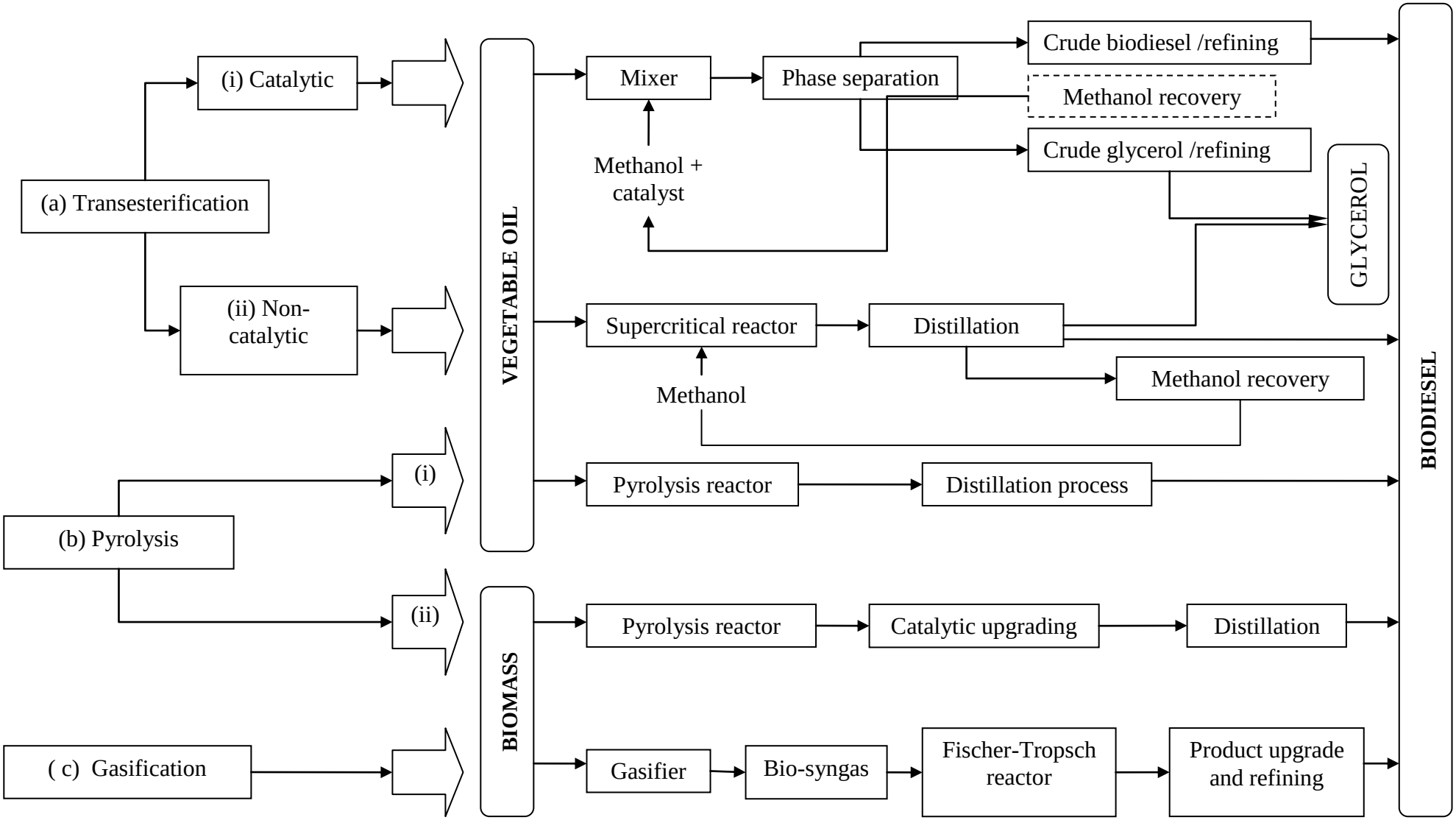

Figure 1.5: Routes to biodiesel production.

1.1.1 Transesterification

In transesterification, a triglyceride (from various natural vegetable oil or animal fats) reacts with alcohol to produce fatty acid methyl esters (biodiesel) and glycerine. The mechanism of the transesterification process is shown in Figure 1.6, where the triglyceride is converted stepwise to diglyceride, monoglyceride and finally glycerol. A mole of ester is liberated at each step. The reactions are reversible, although the equilibrium lies towards the production of fatty acid esters and glycerol. The heat of reaction for transesterification in general is small (estimated as −18.5 kJ mol^{-1} FAME at 25°C, Fjerbaek *et al.*, (2009)).

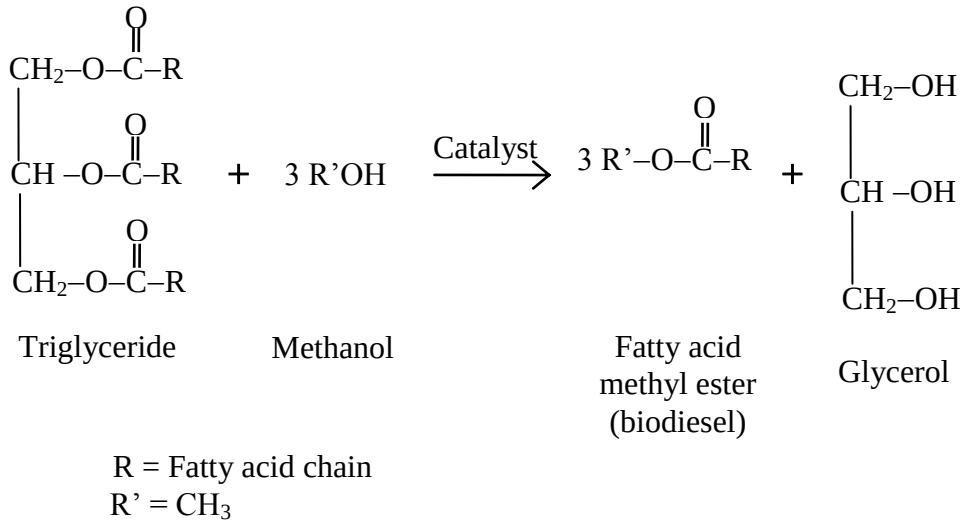

Figure 1.6: The reaction mechanism for the transesterification of triglyceride

The two main routes for the transesterification are based on:

(a) Catalytic process: Usually, in a catalytic process, a catalyst (commonly sodium hydroxide) is first dissolved in an alcohol stream; which is then mixed with the heated vegetable oils (50 to 60°C) with an alcohol in a reactor. The reaction is efficient at 60°C and ambient pressure. When the reaction is complete, the product will form two layers, biodiesel (top) and glycerol (bottom). These two layers can then be separated by means of gravity, with the glycerol settling at the bottom of the vessel. For a faster and more efficient method, a centrifuge can be used for the phase separation. The excess alcohol can then be recovered from both

raw streams (using a flash column, or a distillation column). After that, the raw biodiesel goes through a refining process, such as a neutralisation process, followed by washing and filtration processes in order to remove any residue.

(b) **Non-catalytic supercritical methanol process**: Commonly, in this process, vegetable oil and liquid methanol are charged in an autoclave vessel or reactor under supercritical conditions (e.g. 525 to 675K, and pressures of 35 to 60 MPa). At these conditions, transesterification can occur, as the oil reacts with the supercritical methanol, without the use of a catalyst. Then, the product mixture goes through a distillation process to purify both the biodiesel and the glycerol, and also to recover the excess methanol. The product is condensed before being sent into the collecting vessel.

1.1.2 Pyrolysis

In this process, large organic molecules are thermally cracked and decomposed into smaller hydrocarbon fractions (preferable diesel-like fuel or biodiesel fraction). There are two different starting materials used as a feedstock in the pyrolysis process, these are:

(a) **Pyrolysis of triglyceride** (Lima *et al.*, 2004): Here, the vegetable oil is introduced into a pyrolysis reactor and then heated at temperatures ranging from 350 to 400 °C until the oil is vaporized. Then, the vaporized product is passed through a heat exchanger (condensation process) resulting in two liquid fractions, an aqueous fraction and an organic fraction. All liquid fractions are collected and then separated by decantation, and distillation at temperatures above 200 °C.

(b) **Pyrolysis of biomass** (Chew and Bhatia, 2008): This technology is also called biomass-to-liquid (BTL) hydrocarbon. Biomass product such as crop residue and organic waste is charged into the pyrolysis reactor to produce three main products. These are (i) gas mixture (containing mainly carbon oxides, some methane and higher gaseous hydrocarbons in minor quantities) from high

temperature conditions (500 to 850°C), and (ii) carbon rich solid residue (char and coke), and (iii) liquid oil (bio-oil), from low temperature conditions (450 to 550°C). The vapour and the liquid products then undergo a catalytic upgrading process to obtain a diesel-fuel like hydrocarbon as the main product. These routes can be represented by the following equation.

$$\text{Biomass} + \text{Heat} \rightarrow H_2 + CO + CO_2 + (\text{Hydrocarbon gases}) \xrightarrow{\text{catalytic upgrading}} \text{biodiesel} \quad (1.1)$$

$$\text{Biomass} + \text{Heat} + \text{Steam} \rightarrow H_2 + CO + CO_2 + CH_4 + \text{Char} + (\text{Hydrocarbon}) \xrightarrow{\text{catalytic upgrading}} \text{biodiesel} \quad (1.2)$$

1.1.3 Gasification followed by Fischer-Tropsh Synthesis

Demirbas (2007) generalised the process into three steps; namely (i) syngas generation, (ii) syngas conversion, and (iii) hydroprocessing. Bio-mass can be converted to bio-syngas by non-catalytic, catalytic and steam gasification processes. An example of the syngas production is described in Maschio *et al.* (1994) who carried out the thermal and catalytic gasification with an operating temperature ranging from 700 to 950°C, and an initial feed of water to biomass ratio to the gasifier, ranging from 0.2 to 2.0. The chemical compositions of the bio-syngas from the biomass gasification process consists mainly of CO, H_2 and CO_2, with a small quantity (8 to 2 vol%) of methane and ethane. The bio-syngas is then fed through a gas cleaning process to remove the impurities. The remaining H_2 and CO gases are then fed into a Fischer-Tropsh reactor to produce diesel, which includes gasoline, light hydrocarbon and waxes. The typical operating temperatures and pressures for the FTS process are 475 to 625 K, and 15 to 40 bar. The long chain hydrocarbons produced are finally distilled, hydro-cracked or upgraded before being used as a liquid transportation fuel (Chew and Bhatia, 2008).

The basic FTS reactions are represented as (Demirbas, 2007):

$$nCO + 2nH_2 \rightarrow (\sim CH_2 \sim) + nH_2O \quad (1.3)$$

$$nCO + (2n+1)H_2 \rightarrow C_nH_{2n+1} + nH_2O \quad (1.4)$$

$$nCO + (n+m/2)H_2 \rightarrow C_nH_m + nH_2O \quad (1.5)$$

where n is the average length of the hydrocarbon chain and m is the number of H atoms per carbon.

$$CO + H_2 \rightarrow \sim CH_2 \sim + H_2O \qquad \Delta H = -165 \text{ kJ mol}^{-1} \quad (1.6)$$

$$2CO + H_2 \rightarrow \sim CH_2 \sim + CO_2 \qquad \Delta H = -204 \text{ kJ mol}^{-1} \quad (1.7)$$

1.1.4 Hydrodeoxygenation/ Hydrotreating Reaction

As described in Knothe (2010), biodiesel can be produced through a process called hydrodeoxygenation or hydrotreating. Hydrodeoxygenation is a process by which a feedstock that contains double bonds and oxygen moieties is converted to hydrocarbons by saturation of the double bonds and removal of oxygen (decarboxylation, decarbonylation, dehydration). Thus, the reaction requires hydrogen. Decarboxylation of unactivated carboxylic acids, although exothermic, requires high transition state energies (related with high activation energy (Ea) barrier), which is reflected in reaction conditions such as elevated temperature and pressure. An appropriate catalyst is used to reduce the activation energy (barrier), hence the energy of the transition state in the reaction profile, to release carbon dioxide from carboxylic acids. The hydrodeoxygenation of vegetable oils produces alkanes with one carbon atom less than the fatty acid chains, although the exact nature of the product mix depends on reaction conditions. Thus, a vegetable oil consisting of the typical C_{16} and C_{18} fatty acids would yield C_{15} and C_{17} alkanes (Knothe, 2010). As described in Huber and Corma (2007), most hydrodeoxygenation of bio-oils has focused on the use of sulfide Co-Mo- and Ni-Mo-based catalysts, which are used for hydrotreating industrial feedstocks. During hydrodeoxygenation, the oxygen in the bio-oil reacts with H_2 to form water and saturated C-C bonds. The straight-chain alkanes can undergo isomerization and cracking to produce fuels that are more suitable for aviation purposes. Typical reaction conditions is 250 to 450 °C at 136 atm H_2 (137.8 bar).

1.2 Selected reaction pathway for this thesis

In this thesis, rapeseed oil was selected as a vegetable oil feedstock, as this is a source of biomass that is readily available in Europe (see Table 1.1).

The transesterification reaction of glycerides with alcohols was selected for the process, as this is a relatively low energy process, is already established on an industrial scale, and this also builds on existing expertise at the University of Bath.

Although this transesterification reaction, using acid and/or alkaline catalysts is well known and practiced on a commercial scale, there is still plenty of scope to improve this semi-batch process. For example, by developing a heterogeneous catalyst that could be retained in a fixed bed, a continuous process could be developed. With this overall aim in mind, this challenge was therefore studied in more detail, and involved experimental work.

The aims of this research were:

i) to immobilize the catalyst (zinc proline) onto a monolithic support, and demonstrate applicability of the system,
ii) to develop the analytical technique on gas chromatography for monitoring the reaction,
iii) to study the viability of turning a batch reaction into a continuous process with the use of immobilised catalyst (zinc proline) on the monolith structure as a fixed bed catalyst,
iv) to design and construct the continuous flow reactor for the system,
v) to quantify the distribution of residence time under pulsatile flow conditions through Residence Time Distribution (RTD) study, and
vi) to perform reaction experiments over a wide range of conditions in the continuous flow reactor .

1.3 Structure of the thesis

In summary, the emphasis in this thesis is on the development of a reaction environment, in which the catalyst is retained in a fixed bed, and the reactor is operated in a continuous manner. This is achieved as follows.

In Chapter 2, literature on the selected transesterification reaction is studied in more detail, and zinc proline is selected as a catalyst for further work - this builds on earlier expertise with this catalyst in a powdered form in the Department of Chemistry (University of Bath). A decision is also taken to explore the viability of using a cordierite monolith support as a support structure for the zinc proline catalyst.

In Chapter 3, analytical techniques are selected, and the Gas Chromatography method for the analysis of reaction intermediates has to be developed, before the technique can be used to follow the progress of the reaction.

In Chapter 4, a novel method is developed of coating the zinc proline catalyst onto a cordierite support, and the system is tested in a batch reactor. To the author's knowledge, this is the first time this has been done and the coated system was shown to be catalytically active. This work was presented at an international conference on 3rd International Conference on Structured Catalysts and Reactors, ICOSCAR-3 (Italy, 27 to 30 September 2009) and leads to a publication in Catalysis Today (see Appendix B).

In Chapter 5, experimental apparatus is developed, which can be used to perform continuous flow experiments, where the catalyst is retained in a fixed bed. To improve the understanding of residence time in this fixed bed monolith reactor, residence time distribution studies (RTD) are performed using salt as a tracer. Then continuous flow reaction experiments are performed, using zinc proline coated monoliths, and reaction intermediates are followed. In addition, a few short feasibility experiments are performed using strontium oxide coated monoliths – this was done to assess the viability of that catalyst on a monolith and how easily it could be evaluated in the continuous flow reactor developed in this thesis.

Finally in Chapter 6, conclusions and recommendations for further work are provided. At the end of this thesis are appendices, which contain more routine calculations, listings of data, and other relevant attachments.

REFERENCES

Ahmad, A.L., Mat Y, N.H, Derek, C.J.C. and Lim, J.K., 2010. Microalgae as a sustainable energy source for biodiesel production: A review. *Renewable and Sustainable Energy Reviews*, 1, pp. 1–10.

Al-Zuhair, S., 2007. Production of biodiesel: possibilities and challenges. *Biofuels, Bioprod. Bioref.*, 1, pp. 57–66 [online]. Available from http://www3.interscience.wiley.com/cgi-bin/fulltext/ 114285965/ -PDFSTART [Accessed on 06/02/2008].

Buyukkaya, E., 2010. Effect of soybean methyl ester on diesel engine performance and emissions. *International Journal of Vehicle Design*, 54(2), pp 111-122.

Carriquiry, M., 2007. U.S. Biodiesel production: recent developments and prospects. Iowa Ag Review [online]. *Center for Agricultural and Rural Development, Iowa United States.* Available from http://www.card.iastate.edu./iowa_agreview/spring07/IAR.pdf [Accessed 8 April 2008].

Chew, T.L. and Bhatia, S., 2008. Catalytic processes towards the production of biofuels in a palm oil and oil palm biomass-based biorefinery. *Bioresource Technology*, 9, pp. 1-12.

Demirbas, A., 2003. Biodiesel fuels from vegetable oils *via* catalytic and non-catalytic supercritical alcohol transesterification and other methods: a survey. *Energy Conversion and Management*, 44. pp. 2093–2109.

Demirbas, A., 2007a. Importance of biodiesel as transportation fuel. *Energy Policy*, 35, pp. 4661–4670.

Demirbas, A., 2007b. Progress and recent trends in biofuels. *Progress in Energy and Combustion Science*, 33, pp. 1–18.

Emerging Markets Online [online]. Available from http://www.emerging-markets.com/ biodiesel /default.asp. [Assessed on 2/11/200].

European Commission, 2006. *Biofuels in the European Union : A vision for 2030 and beyond*[online]. Available from: http://ec.europa.eu/research/rtdinfo/index_en.html. [Accessed on 08/11/2008].

European Commission, 2010. *EU Energy and Transport in Figures Statistical Pocket book 2010* [online]. Available from: http://ec.europa.eu/energy/publications/statistics/doc/2010_energy_transport_figures.pdf. [Accessed on 20/01/2011].

European Commission, 2011. *Energy 2020*[online]. Available from: http://ec.europa.eu/energy/publications/doc/2011_energy2020_en.pdf. [Accessed on 21/01/2011].

Fjerbaek, L., Christensen, K. V. and Norddahl, B., 2009. A review of the current state of biodiesel production using enzymatic transesterification. *Biotechnology and Bioengineering*, 102 (5), pp. 1298–1315.

Huber, G. W. and Corma, A., 2007. Synergies between bio- and oil refineries for the production of fuels from biomass. *Angew. Chem. Int. Ed*., 46, pp. 7184 – 7201.

Kalam, M. A and Masjuki, H.H., 2002. Biodiesel from palm oil-an analysis of its properties and Potential. *Biomass and Bioenergy*, 23, pp. 471 – 479.

Knothe, G., 2001. Historical perspectives on vegetable oil-based diesel fuels . *Industrial Oils*, 12, pp. 1103–1107.

Knothe, G., 2010. Biodiesel and renewable diesel: A comparison. *Progress in Energy and Combustion Science*, 36, pp. 364–373.

Lima, D. G., Valerio, C.D., Ribeiro, E.B., Carvalho, D.A, Mundima, K.C., Rubima, J.C. and Suarez, A.Z., 2004. Diesel-like fuel obtained by pyrolysis of vegetable oils. *J. Anal. Appl. Pyrolysis*, 71, pp 987–996

Maa, F. and Hanna, M.A., 1999. Biodiesel Production: A Review. *Bioresource Technology*, 70, pp 1-15.

Maher, K.D. and Bressler, D.C., 2007. Pyrolysis of triglyceride materials for the production of renewable fuels and chemicals. *Bioresource Technology*, 98, pp. 2351–2368.

Maschio, G., Lucchesi, A. and Stoppato, G., 1994. Production of syngas from biomass. *Bioresource Technology*, 48 (2), pp. 119-126.

Mata, T.M., Martin, A. A., and Caetano, M. N., 2010. Microalgae for biodiesel production and other applications: A review. *Renewable and Sustainable Energy Reviews*, 14, pp. 217–232.

National Biodiesel Board, 2008. Fuel Fact Sheets [online]. Available from: http://www.biodiesel.org/resources/ fuelfactsheets /default.shtm [Accessed 12 January 2009].

Pahl,G., 2005. *Biodiesel : Growing a New Energy Economy* . Chelsea Green Pub. Co. United States.

Pinto, A.C., Guarieiro, L.L. N., Rezende, M. J. C., Ribeiro, N.M., Ednildo A. Torres, E.A., Lopes, W. A., de Pereira, P. A. and de Andrade, J. B., 2005. Biodiesel: an overview. *Journal of Brazilian Chemical Society*, 16 (6B), pp. 1313−1330.

UNFCC document: Kyoto Protocols [online]. Available from: http://unfccc.int/kyoto_protocol/items/2830.php. [Accessed on 24/10/ 2008]

CHAPTER 2

REVIEW OF TECHNOLOGIES FOR THE TRANSESTERIFICATION REACTION

In this chapter, the literature on the transesterification reaction is reviewed and a range of different approaches are identified. This includes processes that use acid and base catalysts. In order to gain practical experience and knowledge of these reactions, some scoping experiments are performed and described. Then, the use of heterogeneous catalyst systems is discussed, and examples are provided. The use of a monolith structure as a catalyst support is also briefly discussed, and this method is selected for the experiments in Chapter 3. Finally, methods of monitoring transesterification reaction are reviewed, including the use of H^1 NMR and gas chromatography which were used in this thesis.

2.1 An early description of the reaction

According to Demirbas (2001), transesterification reaction was conducted as early as 1853 by scientist E Duffy and J. Patrick, many years before the first diesel engine become functional.

As described in Gerpen (2005), among the early description of a transesterification reaction can be found in Bradshaw (1942), Bradshaw *et al.* (1942) and Bradshaw *et al.* (1944). Although the purpose of Bradshaw's process was to make soap (from the glycerol obtained from the transesterification process), there were a number of useful observations from the process description, such as (Gerpen, 2005):

i) Excess alcohol of more than 1.6 times the stoichiometric amount is required for complete reaction.
ii) The amount of alcohol used can be reduced by conducting the reaction in steps, where part of the alcohol and catalyst are added at the start of each step, and the glycerol is removed at the end of each step. Besides methanol, other alcohols can be used including ethanol, propanol, isopropanol, butanol, and penthanol.
iii) Water and free fatty acids inhibit the reaction. Higher alcohols are particularly sensitive to water contamination.
iv) Free fatty acids in the oils or fats can be converted to alkyl esters with an acid catalyst. This can be followed by a standard alkali-catalyzed transesterification to convert the triglycerides.
v) Acid catalysts can be used for the transesterification of oils to alkyl esters, but they are much slower than alkali catalysts.

In a later publication, Feuge and Gros (1949) reported an ethanolysis reaction of peanut oil using sodium hydroxide as a catalyst, but mainly to produce glycerol, with monoesters as byproduct. The reaction was done by mixing the solution of ethanol (15.56 g) with 0.2% (oil basis) of NaOH. Then the mixture was added to 100 g oil for 160 minutes. Both reactants were heated in a constant temperature bath (at the reaction temperature) before being mixed. They found that the optimum temperature lies close to 50°C to give a complete conversion. From the data provided, 100 g of oil reacted (with complete conversion) to produce 101.5 g of ethyl esters and 9.47 g of glycerol, with a small amount of mono- and diglyceride (3.94 and 0.8 g of respectively). They also

reported that 50% or more of the catalyst (NaOH) was destroyed in the first 15 to 20 min due to the formation of soap. They also explained that in the presence of soaps, the mono- and diglycerides decompose to yield glycerol and triglyceride.

In a study done by Hartman (1956), six different catalysts, namely:

(a) ignited potassium carbonate (or potassium oxide),
(b) sodium methoxide,
(c) sodium hydroxide,
(d) calcium oxide,
(e) barium oxide, and
(f) strontinium oxide,

were tested in an alkali-catalysed methanolysis on ox fat, coconut oil and linseed oil. In that work, all of the fat and oils were first neutralised with sodium hydroxide, then washed, and then dried in vacuum. Then, a 100 g sample of the fats was heated with 25 g of methanol and catalyst, at 60°C or (under reflux conditions). The reaction mixtures were acidified with acetic acid, and the esters were extracted with ethyl ether and thoroughly washed with water. The degree of alcoholysis was calculated from the amount of glycerol determined in the aqueous extract. Of the various catalysts employed, sodium methoxide and ignited potassium carbonate were found to set free 99 to 99.5% of total glycerol and to cause the least degree of saponification. The reaction time was 2 hours and the amount of catalyst was 0.5 wt% for sodium methoxide and 10.0 wt% of ignited potassium carbonate.

A detailed study of a transesterification process is also found in Freedman *et al.* (1984). They carried out both alkali and acid-catalysed reactions with different types of oils, at various conditions. The optimum conditions for the reaction can be summarised as follows.

i) A molar ratio of 6:1 alcohol to oil was used to achieve high conversion (93 to 98%) to esters. Ratios greater than that would not increase the yield, and they would complicate the recovery of ester and alcohol.
ii) The optimum reaction time was 1 hour for 96 to 98% ester conversion.
iii) The effective amount of catalyst used was 0.5 wt% for sodium methoxide and 1 wt% for sodium hydroxide.
iv) The content of free fatty acid in the vegetable oils should be less than 0.5 wt %.

v) The reaction temperature used was 60°C for methanol, 75°C for ethanol and 114°C for butanol.

vi) The lowest temperature used was 32°C, with 1 wt% of NaOH, for a 4 hour reaction time.

vii) For acid-catalysed reactions, a larger amount of methanol was needed, as well as a much longer reaction time. To obtain complete reaction, a 30:1 molar ratio of methanol to oil, with 1 wt% concentrated sulphuric acid, was required. A reaction temperature of 65°C was used for 69 hours.

In a transesterification reaction performed by Siler-Marinkovic and Tomasevic (1998), sunflower oil was used with sulphuric acid as a catalyst. More than 97% yield of crude esters oil was obtained in a reasonable reaction time (1 to 2 hours). The process was described as *in situ* transesterification, because of the use of pre-extracted seed oil as a feed. They found that the fuels obtained from this reaction had lower viscosities than the base-catalysed fuels. Their experimental conditions were as follows.

i) A mixture of whole sunflower oil seed with 55.5 wt% of oil and 5.5 wt % of water was used as a feedstock. The mixture was first homogenised with methanol to form a slurry.

ii) The molar ratio of methanol to oil used was 300:1 and 100 mol % of sulphuric acid was used at a reaction temperature of 64.5°C for a 60 minutes period.

iii) The lowest temperature at which a reaction was performed was 30°C, using a molar ratio of methanol to oil of 300:1, and concentrated sulphuric acid. The reaction time was 4 hours.

Interim observation:

From the literature it is evident that both conventional acid and alkaline catalysts are used. The conversion varies depending on the experimental condition (e.g. type of oil, molar ratio of alcohol: oil, temperature). An example of how process conditions vary is illustrated in Table 2.1.

Table 2.1: Example of experimental conditions for selected transesterification reactions.

Feed stock oil	Type of alcohol	Molar ratio of alcohol: oil	Type of catalyst (amount)	Temperature of reaction (°C)	Time of reaction	Conversion to FAME (%)	Reference
Sunflower oil	Methanol	6:1	NaOH (1 %w/w)	65	4 h	99.71	Vicente *et al.* (2004)
Castor oil:	Methanol	6:1	H_2SO_4 (0.5 % w/w)	60	8 h	85%	Meneghetti *et al.* (2006)
Waste frying oil	Methanol	74:1	H_2SO_4 (1.5 mol%)	80	4 h	97.4 ± 1.5	Zheng *et al.*, (2006)
Frying oil	Ethanol	12:1	KOH (1 %w/w)	78	2 h	74.2	Encinar *et al.*, (2007)
Palm kernel oil	Ethanol	3.7 : 1	KOH (1 wt %)	60	2 h	96	Alamu *et al.*, (2008)
Waste cooking oil	Methanol	9:1	NaOH (1.0 wt%)	50	90 min	89.8	Meng *et al.*, (2008)
Peanut (*A. hypogea L.*) oil	Methanol	6:1	NaOH (0.5 % w/w)	60	2 h	89	Kaya *et al.*, (2009)
Duck tallow oil	Methanol	6:1	KOH (1 wt%)	65	3 h	97	Chung *et al.*, (2009)
Soybean oil	Methanol	20:1	Trifluoroacetic acid	120	5 h	98.4	Miao *et al.*, (2009)
Rapeseed oil	Methanol	6:1	KOH (1 wt%)	65	2 h	95 to 96	Rashid and Anwar, (2009)

2.2 Preliminary experiments

In addition, in order to gain some practical experience and knowledge of these reactions, some scoping experiments were performed (labelled as Experiments P1, where the P stands for preliminary), and these are described briefly in the sections that follow.

2.2.1 Experiment P1: In this experiment, a molar ratio of 6:1, methanol: oil, with a 1 wt% of sodium hydroxide (NaOH) catalyst was used. The molar mass of oil was assumed to be 860 g mol^{-1}. A quantity of 200 ml of rapeseed oil was heated to 60°C, and 1.8 g of sodium hydroxide was mixed with 55 ml methanol (separately). Example calculations for molar ratio are shown in Appendix C. The mixture was then mixed in the reactor and stirred at 750 rpm for 1 hour. The experimental apparatus is shown in Figure 2.1. After the reaction was complete, the mixture was transferred to a measuring cylinder. Within a period of 5 to 10 minutes, a dense layer of glycerol (dark colour) was observed and this settled down to the bottom. This was then left overnight to cool and settle. Figure 2.2 shows the sample after 24 hours of settling time.

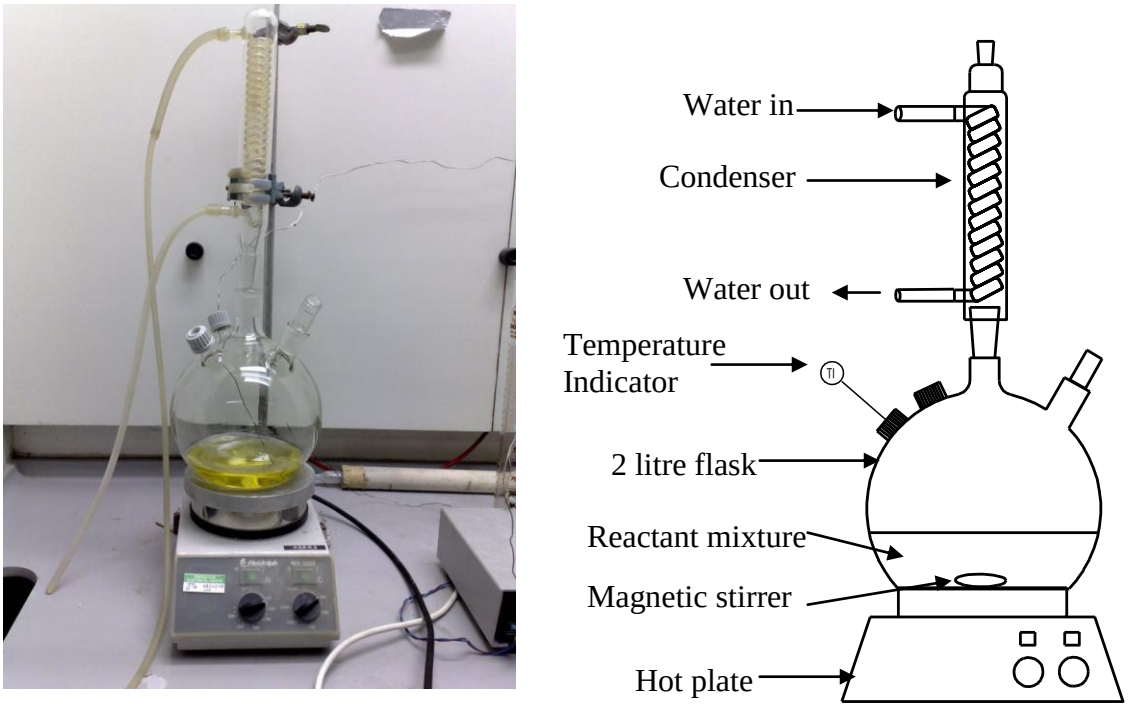

Figure 2.1: Experimental equipment for the transesterification reaction.

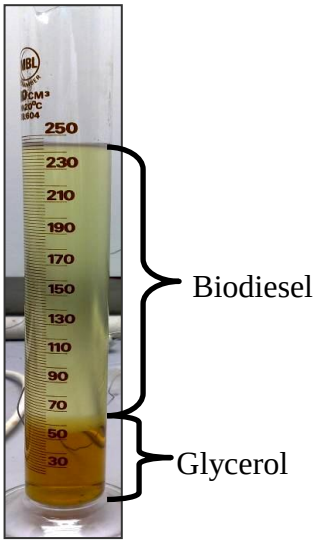

Figure 2.2: Example of the product from the transesterification process that had been allowed to settle (Experiment P1).

2.2.2 Experiment P2: In this experiment, ethanol was used as a co-reactant. The procedure was similar to Experiment P1, except that the methanol was replaced with 75 ml of ethanol. The temperature used in this experiment was 75°C (as suggested in Freedman *et al.* (1984)). After 1 hour of reaction, the mixture was poured into the cylinder for phase separation.

From this experiment, it was found that the two layers of biodiesel and glycerol were formed at a slower rate (15 to 20 minutes to settle) than in Experiment P1. This could be due to the fact that ethanol is more immiscible in glycerol that methanol.

Another observation was that the ethanol/NaOH mixing process was more difficult than methanol/NaOH. To aid the mixing process, more vigorous stirring (i.e. 1000 rpm) had to be used.

2.2.3 Experiment P3: In this experiment, sulphuric acid was used as a catalyst. A 100 ml quantity of rapeseed oil was mixed with 220 ml of methanol and 2 ml of sulphuric acid, which represented a 50:1 methanol to oil molar ratio, and an equivalent 1 wt% of oil as catalyst. The mixture was maintained at 60°C for 1 hour of reaction time. The mixture was then transferred to a cylinder and left overnight. Three different layers were formed after 24 hours of settling. The top layer was methanol, the middle layer was biodiesel, and interestingly, the colour of the bottom layer (glycerol) was clearer than the glycerol from Experiments P1 and P2.

2.3 Integration of acid-catalysed esterification and alkaline-catalysed transesterification

In a commercial process, low quality feedstock oils are usually used to minimise the cost of biodiesel. The use of these oils such as crude vegetable oils, waste frying oils and animal fats can be a problem in an alkaline transesterification process. These low cost oils contain a high amount of free fatty acid (FFA). This forms soap (through the saponification process with alkaline catalyst (Eq. 2.1)) and thus reduces the yield of esters, and complicates the separation process.

$$RCOOH + NaOH \rightleftharpoons RCOO^{-}Na^{+} + H_2O \qquad (2.1)$$

2.3.1 Ramadhas *et al.* (2005)

To overcome this problem, a 2-step esterification-transesterification process is commonly attempted. An example of this process can be found in Ramadhas *et al.* (2005). The schematic diagram of the process is shown in Figure 2.3, and they used unrefined rubber seed oils, which contained 17 wt% free fatty acid. The following is a description of this process in their study.

(a) Step 1 : Acid esterification

The first step reduces the FFA value of the crude rubber seed oil to about 2 wt%, using an acid catalyst. In this step, the oil is pre-heated, before being mixed with methanol and sulphuric acid. Heating and stirring is continued for 20 to 30 min at atmospheric pressure. The maximum conversion efficiency is achieved at a temperature of 40 to 50°C, with 0.5 wt% of sulphuric acid, and a molar ratio of methanol/oil equal to 6:1. Upon completion of the reaction, the excess alcohol with the sulphuric acid and impurities moves to the top layer which is then removed. The lower layer is separated for further processing in Step 2.

(b) Step 2 : Alkaline transesterification

In this step, NaOH is first dissolved in methanol, then mixed with preheated oil. The optimum parameters used are: molar ratio of 9:1, 0.5 wt% of NaOH, 30 min of reaction time and a temperature of 40 to 50°C. The addition of excess an amount of catalyst gave rise to the formation of an emulsion, which increased the viscosity and led to the formation of gels.

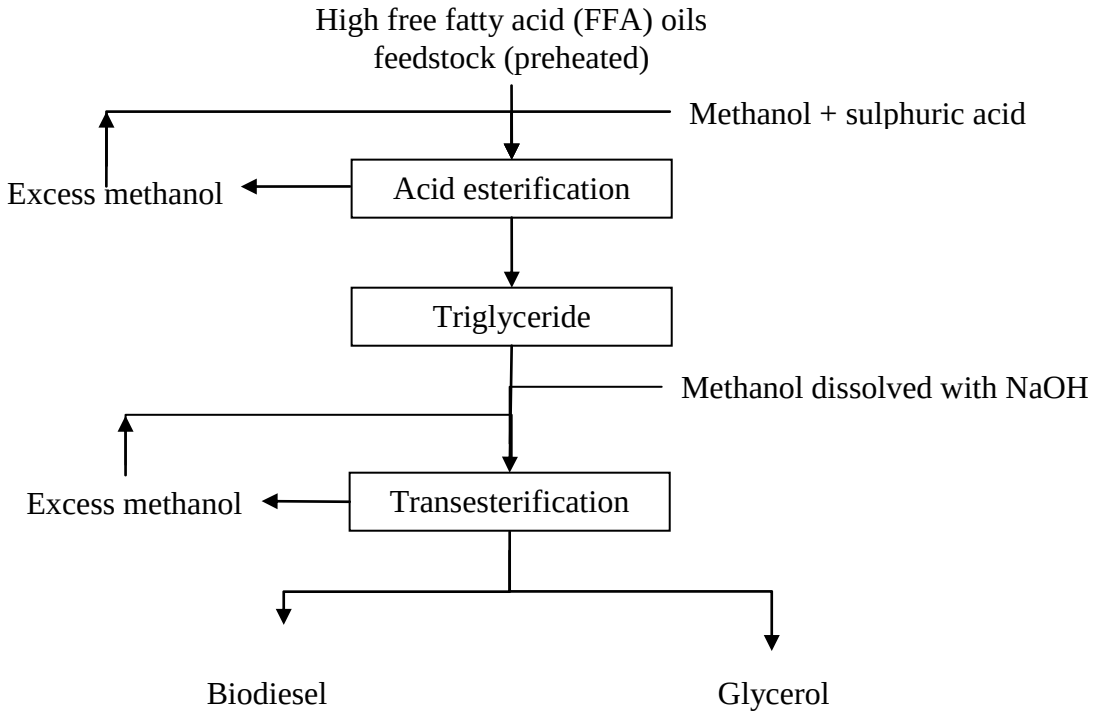

Figure 2.3: Integration of acid-catalysed and alkaline transesterification reactions.

2.3.2 Canakci and Gerpen (2003)

An extensive study to produce biodiesel from feedstocks high in free fatty acid, has been done at a pilot scale by Canakci and Gerpen (2003). Figure 2.4 shows a simplified diagram for that process. This plant typically achieves 95% yield of biodiesel. In their plant, the high FFA feedstock is first passed through the pretreatment unit before entering the main reaction unit. The acid-catalyzed pretreatment was conducted in two or more steps, with water removal taking place between the steps. As in an acid-catalysed process, the FFA reacted with alcohol and produced water. The process is briefly described as follows.

(a) Pretreatment Unit:

i) The delivered feedstock (yellow grease or brown grease) was heated at 55 to 60^{o}C and agitated with a recirculating pump in a cone-bottom storage tank.

ii) The feedstock was then transferred to a stainless steel pretreatment reaction tank. A 20 μm cellulose filter is used to remove insoluble materials.

iii) The alcohol solution with acid catalyst was prepared, and then added to the reaction tank using the air-operated pump. When the first step of the pretreatment reached steady state (after 1 hour), the reactants were transferred to a 454 litre stainless steel settling tank. This tank was used to separate the methanol-water mixture from the feedstock.

iv) After a residence time of approximately 24 hours, the solution of methanol and water rose to the top of the tank, and was removed as a single phase.

v) In a second pretreatment step, the feedstock was transferred from the first pretreatment settling tank back to the second one, and an additional mixture of methanol-acid was added. The pretreated feedstock was then transferred from the second pretreatment settling tank to the main reaction tank

(b) Transesterification (Main) Unit

i) The transesterification reaction took place in a 265 litre, stainless steel reaction tank with a 0.37 kW explosion-proof mixer, which had a fixed speed of 1750 rpm. A mixture of methanol and catalyst was added to the reaction tank. The mixture was then agitated for 8 h, and then transferred to a 492 litre cone bottom tank to separate the glycerine and to wash the ester.

ii) A Micro Motion "coriolis-type" density meter was installed at the exit of the separation tank, and this helped to identify the glycerine, water, and ester interfaces during the separation processes.

However, each single pre-treatment process required more than 25 h before biodiesel is finally produced.

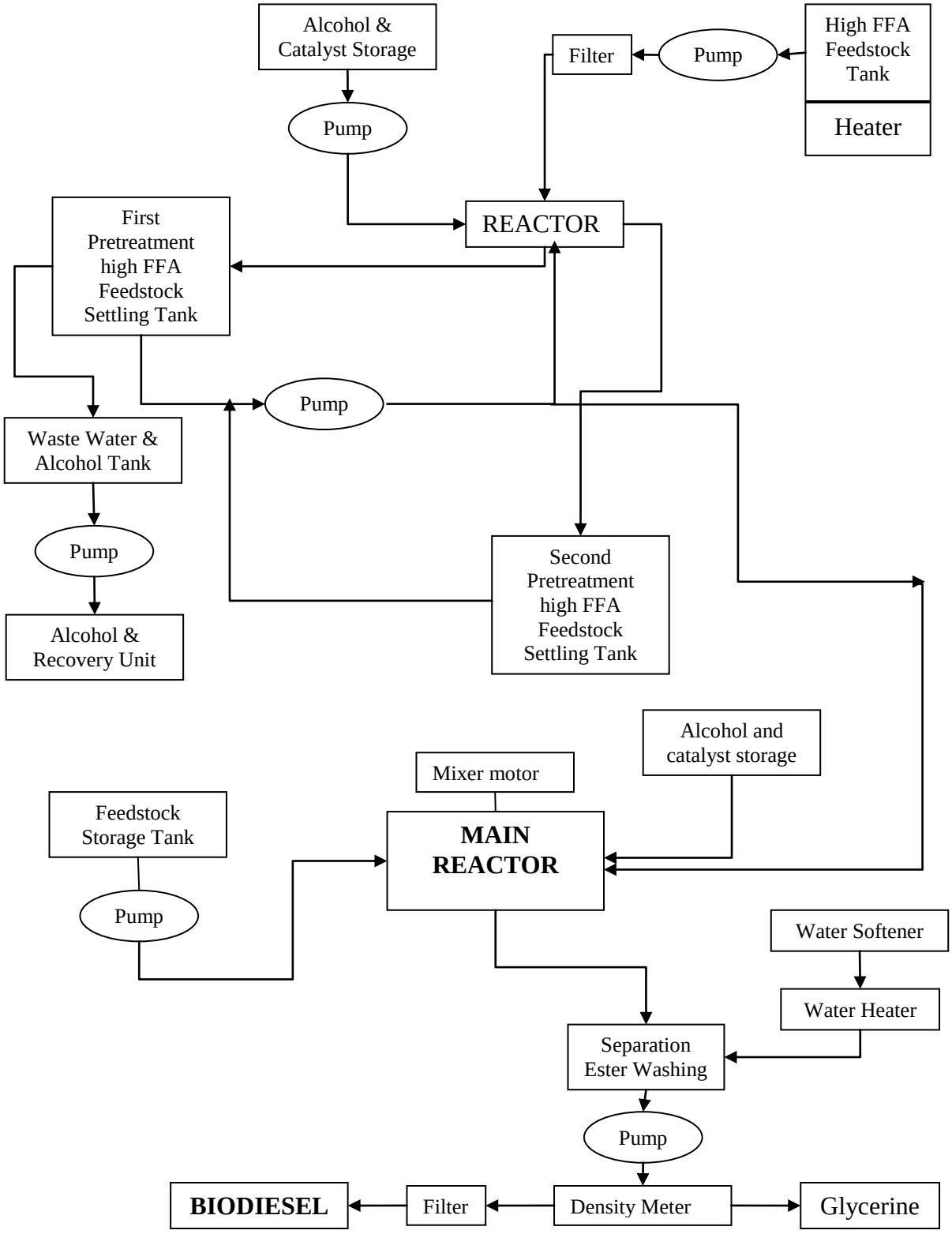

Figure 2.4: A simplified flow diagram of the process described in Canacki and Gerpen (2003).

2.4 Supercritical fluid process (Saka and Kudiana, 2001)

At supercritical conditions, the transesterification reaction can also proceed in the absence of a catalyst. This has been demonstrated by Saka and Kudiana (2001). Figure 2.5 represents a simplified diagram of the process. The reaction takes placed in a 5 ml stainless steel (Inconel-625) reactor. The pressure and temperature were monitored in real time, and were reported as 200 MPa (2 kbar) and 550°C, respectively. The molar ratio of oil to methanol was 1:42. The vessel is first charged with a given amount of rapeseed oil (2.00 g), and then liquid methanol (3.36 g) was added. The reaction vessel was then quickly immersed in a bath, and preheated to 350 or 400°C. This was then kept for a set time interval for the supercritical treatment of methanol, from 10 to 240 s. The vessel was then subsequently moved into a water bath to quench, and hence the reaction was stopped. The treated rapeseed oil was then allowed to settle for about 30 min for the three phases to be separated. The top phase consisted of methanol which was removed. The remaining phases consisted of an upper portion (consisting of biodiesel and methanol) and a lower portion (consisting of glycerol and methanol). Each portion was then evaporated at 90°C (for 20 min) to remove any remaining methanol.

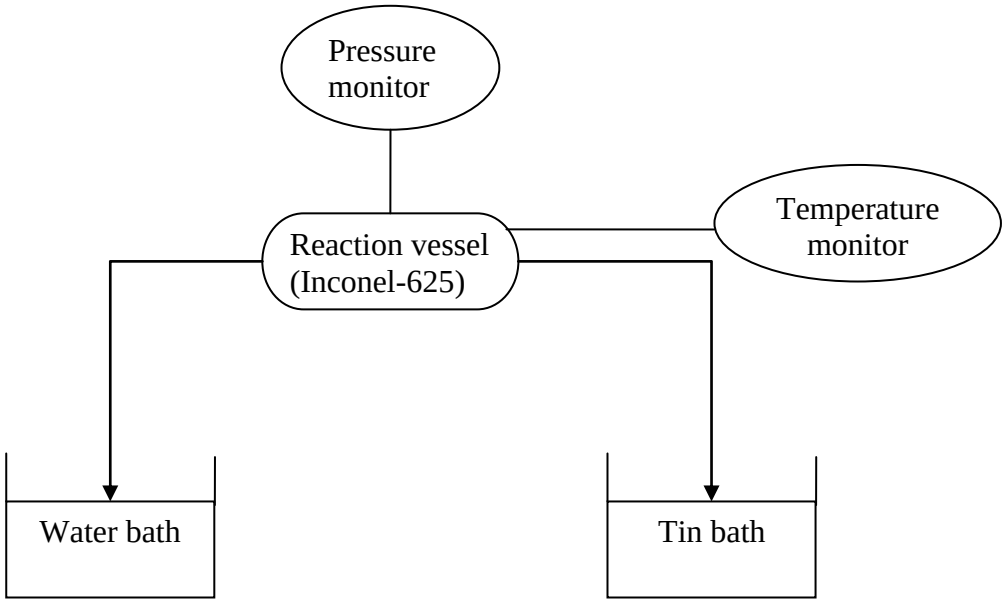

Figure 2.5: Supercritical methanol biomass system (adapted from Saka and Kusdiana, 2001).

A number of important points can be highlighted in the discussion section in Saka and Kusdiana (2001). These are:

i) The dielectric constant of liquid methanol (which tends to be decreased in the supercritical state) increases the solubility of oil in methanol to form a single phase consisting of a methanol/oil mixture.

ii) The solubility parameter of the rapeseed oil determined from a theoretical calculation was about 18 $(MPa)^{1/2}$ or 180 $(bar)^{1/2}$, while for methanol, it was 26 $(MPa)^{1/2}$ or 260 $(bar)^{1/2}$. The value for methanol decreases (to be closer to that of the rapeseed oil in supercritical state) and depends on the temperature and pressure employed.

iii) The solubility of triglycerides in methanol increased at a rate of 1 to 5% (w/w) per 10°C, as the reaction temperature was increased.

[Note: The solubility parameter is a numerical value that indicates the relative solvency behaviour of a specific solvent.]

The fact that this method required the use of a high pressure and temperature makes it unfavourable from a commercial perspective.

2.5 Enzymatic-catalysed transesterification

The use of enzyme as catalyst in biodiesel production has been reported in a number of studies (e.g. Fukuda *et al.*, 2001; Shimada, *et al*., 2002; Nie *et al*., 2006). Enzymatic production is possible using both extracellular or intracellular (whole cells) microbial lipase either as free enzyme, or immobilized onto a support to re-use the enzyme. According to Al Zuhair (2007), among the lipase type, *C. antarctica* B lipase, immobilized on acrylic resin, commercially known as Novozym 435, was by far the most commonly used enzyme for the production of biodiesel. According to the review done by Al Zuhair (2007), most of the processes using lipase are operated at a temperature of 40°C, as high temperature will denature the enzyme protein structure.

Shimada *et al.* (2002) investigated a key problem in enzymatic reaction. This consisted of the irreversible deactivation of the lipase by contact with insoluble methanol (MeOH) which results in a low degree of methanolysis in the reaction systems. Shimada *et al.* (2002) developed a stepwise methanolysis system with immobilized *Candida*

antarctica lipase, see Figure 2.6. The process involved a two-step batch methanolysis of waste oil:

(a) the first-step reaction was conducted in the presence of 1/3 molar equivalent of MeOH for the stoichiometric amount, and

(b) the second-step reaction was performed by adding 2/3 molar equivalent of MeOH.

A mixture of 28.95 g of vegetable oil, 1.05 g of MeOH (1/3 molar equivalent for the stoichiometric amount), and 4 wt.% immobilized *C. antarctica* lipase was incubated at 30°C (with shaking at 130 oscillations/min). After 10 h of reaction time, 2.10 g MeOH (2/3 molar equivalent) was added to the reaction mixture for a further 24 h. The conversion of the oil reached 33.2% at 7 h. The addition of a second 2/3 molar equivalent of MeOH at 10 h converted 96.8% of the oil to its corresponding FAMEs after 24 h (total, 34 h).

Shimada *et al.* (2002) also developed a three-step flow reaction, in case the immobilized carrier is destroyed by agitation in a reactor with an impeller. In that process, the 1^{st}-step substrates were: waste oil and 1/3 molar equivalent of MeOH. In the 2^{nd}-step, the 1^{st}-step eluate and 1/3 molar equivalent of MeOH. In the 3^{rd}-step, the 2^{nd}-step eluate and 1/3 molar equivalent of MeOH. The conversion of waste oil to biodiesel fuel reached >90% in the two reaction systems, and the lipase catalyst could be used for >100 days without any decrease in activity. The daily amount of waste oil converted to biodiesel fuel in such a two-step batch methanolysis was about 16.7 g/g lipase, while the conversion in the three-step flow reaction was 13.7 ml (11.9 g)/g lipase.

However, the main hurdle for commercialization of enzymatic transesterification process is the high cost production of lipase (Fukuda *et al*., 2001, Helwani *et al.*, 2010 and Al Zuhair, 2007).

Interim observation:

A brief summary of different approaches is presented in Table 2.2.

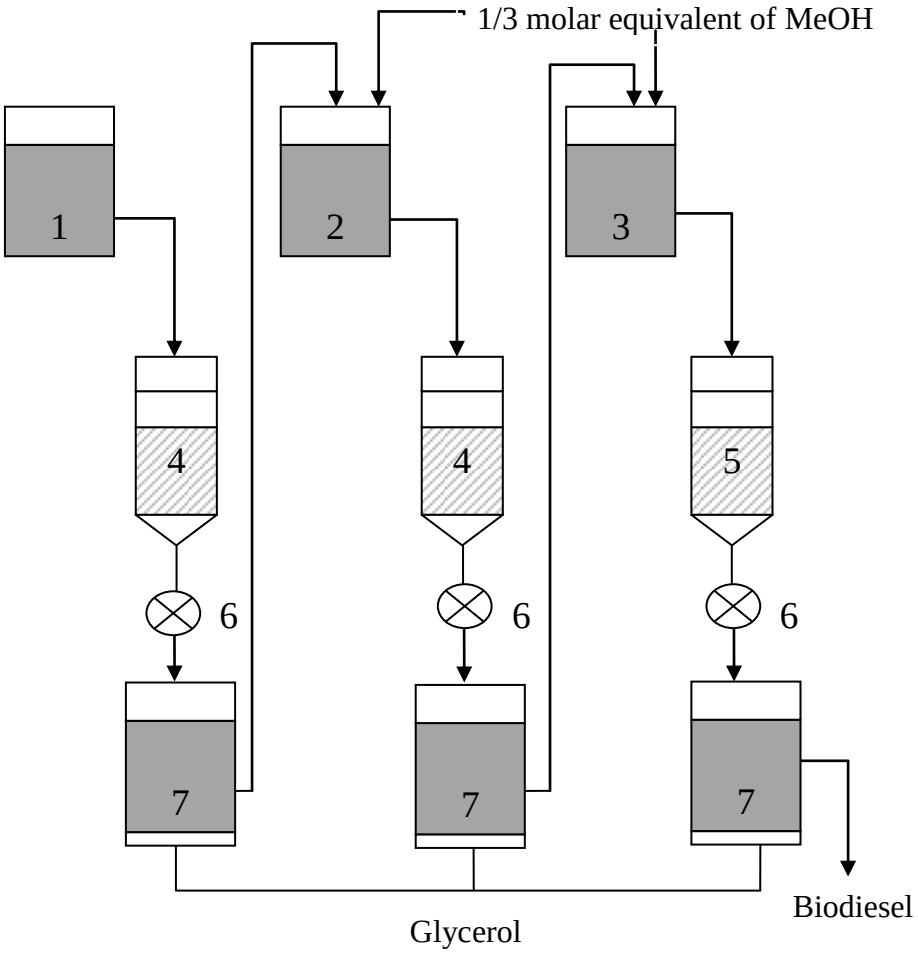

Figure 2.6: Continuous flow production of biodiesel fuel with three fixed-bed bioreactors in series (adapted from Shimada *et al.* (2002)) .

Label:

1- Storage vessel of 1st-step substrate (waste oil and 1/3 molar equivalent of MeOH).

2- Storage vessel of 2nd-step substrate (oil layer of 1st-step eluate and 1/3 molar equivalent of MeOH).

3- Storage vessel of 2nd-step substrate (oil layer of 2nd-step eluate and 1/3 molar equivalent of MeOH).

4- Fixed-bed bioreactor packed with 3 g immobilized *C. antarctica* lipase.

5- Fixed-bed bioreactor packed with 4.5 g immobilized *C. antarctica* lipase.

6- Peristaltic pump.

7- Receiver of eluted reaction mixture.

Table 2.2: Comparison of different transesterification processes.

	Alkaline-catalysed process	**Acid-catalysed process**	**Enzyme-catalysed process**	**Supercritical fluid process**
Reaction time	Fast (1 h)	Slow (4 h)	Slow (10 h)	Fast (< 5 min)
Reaction pressure	Atmospheric pressure	Atmospheric pressure	Atmospheric pressure	High (2 kbar)
Molar ratio methanol to oil	Low (6:1)	High (50:1)	Low (3:1)	High (400:1)
Tolerancy with FFA	Low (>0.5%)	High (20-30 wt%)	Low (2.5 wt %)	Not reported
Moisture tolerance	No (with absence of water)	High (no limitation)	Medium (10 wt%)	No (with absence of water)
Side reaction	Saponification with FFA	No side reaction	No side reaction	No side reaction
Commercialisation	Most preferable	Available	Less preferable due to high cost of enzyme	Less preferable due to high energy consumption

2.6 Use of heterogeneous catalyst in transesterification reaction

As already discussed, the use of conventional homogeneous catalyst such as NaOH and HCl in transesterification reaction, although effective, requires multiple stages of separation to remove the catalyst and the salt residue dissolved within the product. This is crucial in order to meet the current specification of pure biodiesel or B100 (e.g. Appendix A). In some processes, the biodiesel is washed with warm water to remove the residue, and this lead to an excessive amount of waste water. Alternatively, a dry separation technique, such as ion-exchange material can be used. This is available commercially, as was observed at the 2008 European Biofuels Expo and Conference in Nottingham (UK). However, the impression gained was that the product is high in cost and its reusability is limited. Therefore, a shift from the use of homogenous to heterogeneous catalyst is needed to lower the separation cost and to develop a more environmentally friendly process. This is also mentioned in Serio *et al.* (2007):

> "The cost of biodiesel could certainly be lowered by using a heterogeneous catalyst instead of a homogeneous one, resulting in a higher quality of esters and glycerol, which can be more easily and promptly separated."

Also, in Bournay *et al.* (2005):

> "Increasing biodiesel consumption requires optimized production processes allowing high production capacities, simplified operations, high yields, and the absence of special chemical requirements and waste streams."

Interim observation:

However, heterogeneous catalysts have limitation such as:

- They require elevated temperatures and pressures to work well.
- Those on solid support tend to show less activity than the active species in solution.
- There is the possibility of leaching which might contaminate the biodiesel.

2.6.1 Using Solid Acid/Base Catalyst

An attempt to use solid catalysts for biodiesel production has been made by several researchers, such as: Ni and Meunir (2007), Kim *et al.* (2004), Serio *et al.* (2009), Yan *et al.* (2009), and Kulkarni *et al.* (2006).

(a) Ni and Meunir (2007): They investigated the performance of solid acid catalysts:

- sulfated zirconia,
- tungstenated zirconia,
- silica-alumina, and
- resin (Nafion®) supported on SiO_2

in two different systems, and these are:

i) A batch stirred system : consisting of a three-necked 100 ml, round-bottomed flask fitted with a tap water-cooled reflux condenser. 9 ml of methanol mixed with 1 g of catalyst, was then added to 30 ml of a mixture of sunflower oil containing 10 wt.% of palmitic acid (PA). The reaction mixture was stirred at 1000 rpm to increase the dispersion of the reactants, as those were not fully miscible at the temperature used (i.e. 60 °C). The reaction was carried out at ambient pressure.

ii) A re-circulating system using a fixed bed-reactor: consisting of a stainless steel tube packed with catalyst (between two porous filters), which was connected to a peristaltic pump *via* rubber tubing. The rubber tubing was then connected to a second aperture on the 'three-neck' flask to allow recirculation of the reaction mixture in a continuous manner, see Figure 2.7. 60 ml of a mixture of sunflower oil containing 10 wt% of PA was transferred into the flask. The flask was immersed in an oil bath with a thermocouple to keep the temperature constant throughout the reaction. When the desired temperature was reached (i.e. 60 °C), 18 ml of methanol was introduced into the flask. The mixture was stirred at the desired temperature in ambient pressure and was driven by the peristaltic pump at a rate of 6.1 ml s^{-1}.

Interestingly, they found that no mass transport limitations were taking place in the re-circulation system, as;

i) the catalytic activity of the catalyst measured with the batch reactor was essentially equal to that obtained using a fixed bed-reactor in a re-circulating system,

ii) no differences in rates were observed, whether an extrudate or a powder form of the sample was used, and

iii) no differences in rates were observed when operating at various stirring speeds.

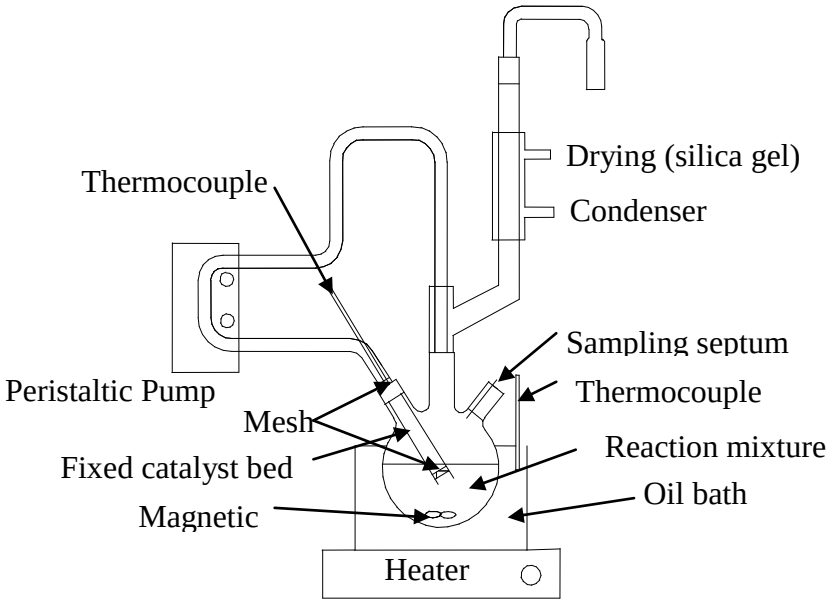

Figure 2.7: A simplified schematic layout of the reactor system used for the experiments involving the recirculation of the reaction mixture through a fixed catalytic bed (adapted from Ni and Meunir, 2007).

(b) Kim *et al.* (2004): In their paper, a conventional catalyst, sodium hydroxide, was heterogenised by impregnation onto a support surface. They developed Na/NaOH/γ-Al_2O_3 as a solid base catalyst for the transesterification reaction of soybean oil. The catalyst was prepared by impregnating γ-Al_2O_3 with sodium hydroxide and metal sodium at 320°C under nitrogen flow. From the catalyst characterisation, they concluded that; both sodium aluminate was formed (by loading NaOH on γ-Al_2O_3). They found that the higher the basic strength of the catalyst, then the higher was the yield of biodiesel. It was also mentioned that the Na/NaOH/γ-Al_2O_3 heterogeneous base catalyst showed almost the same activity under optimized reaction conditions when compared with the conventional homogeneous NaOH catalyst. For example, with a

- MeOH/oil molar ratio 6:1,
- reaction temperature 60°C,
- stirring speed 300 rpm,
- reaction time 120 min;

then the biodiesel yield with (i) NaOH catalyst: approximately 95%; and (ii) Na/NaOH/γ-Al_2O_3: approximately 75%.

They also identified a mixing problem in such a heterogeneous catalytic system. An interesting point suggested by Kim *et al.* (2004) is that:

> " In the homogenous system, the catalyst of NaOH acted as a solvent that made the reactant be miscible. When the NaOH catalyst was loaded to the reactor with methanol, small bubbles were formed and the transesterification reaction took place on the interface of the reactants. In the heterogeneous system, however, the reactants were separated in two phases by the lack of NaOH, which retarded the reaction rate."

Hence, they introduced an appropriate co-solvent (i.e. n-hexane) into the reaction to help miscibility of the methanol-oil phase. With the optimisation of other reaction conditions such as methanol and oil molar ratio, and catalyst loading, their catalyst showed almost the same activity compared to the conventional homogenous NaOH.

(c) **Zabedi *et al.* (2009)**: In their review, they identified that various solid catalysts have been investigated for biodiesel production, and this is summarised in Table 2.3.

Table 2.3: Selected activities of acid and base solid catalyst (Zabedi *et al*., 2009).

Catalyst type	**Examples**	**Catalytic behaviour**	**Operation condition**	**Conversion or yield**
Alkali earth metal oxides	Magnesium oxide	It has the weakest basic strength and solubility in methanol among group II oxides.	T = 523 °C, P = 24 MPa, t_r = 10 min	99% conversion
	Calcium oxide	It possess relatively high basic strength and low solubility in methanol and can be synthesized from cheap sources like limestone and calcium hydroxide. Leaching of active species was observed in the reaction media when the catalyst was activated at high temperature. However, the amount of leaching did not result in catalyst activity reduction and the catalyst was reusable for 8 cycles.	T = 60 °C , t_r = 100 min, alcohol/oil molar ratio = 13:1	94% conversion
Transition metal oxides	Zinc oxide	It is strong in acidity. The acidity is promoted when the surface of these metal oxides contains anions like sulfate and tungstate.	T = 300 °C, t_r = 1 h molar ratio of alcohol/oil = 6:1	86.1% methyl ester yields
	Sulphated titanium oxide	It has Bronsted acid sites formation on the catalyst surface after the introduction of sulfate anions.	T=230 °C, t_r = 8 h, alcohol/oil=12:1,	90% methyl ester yields
	Mg–Al hydrotalcite	O^{2-} anions were found to be responsible for the basicity and accordingly the activity of the catalyst. The activity of the catalyst was also correlated to porosity of the catalyst .	T=215 to 225 °C, t_r = 8 h, catalyst content = 1 wt% and ethanol/oil weight ratio of 0.45	94% biodiesel yields

2.7 Zinc-based transesterification catalysis

There are various zinc-based compounds that have been used as a catalyst in transesterification reactions such as: zinc acetate (Song *et al.*,2010), zinc hydroxide nitrate (Cordeiro *et al.*, 2010), zinc oxide (Alba-Rubio *et al.*, 2010) and zinc aluminate (Pugnet *et al.*, 2008). Currently, a zinc aluminate ($Al_2O_3/ZnAl_2O_4/ZnO$) catalyst developed by the Institute Francais du Petrole is being used in an industrial process under the commercial name Esterfip-H (Lee and Saka, 2010).

2.7.1 Song *et al.* (2010)

They investigated the use of zinc acetate for the esterification of oleic acid in a batch-type autoclave. In their work, the oleic acid conversion reached 95.0wt % (at 220°C and 6.0 MPa or 60 bar), with a molar ratio of methanol to oleic acid of 4, and 1.0 wt% zinc acetate as catalyst. Oleic acid was first added, and then the autoclave was sealed and heated to the desired temperature at a fixed heating rate. After that, methanol with dissolved zinc acetate (1.0 wt%) was pumped into the autoclave to the reaction pressure. They also provided a kinetic model for the esterification. The reaction order for this type of reaction, n, was 2.2 and the activation energy, Ea, was 32.62 kJ mol^{-1}. Since zinc acetate is homogeneous in the solution, the separation was predicted to be rather difficult.

2.7.2 Pugnet *et al.* (2010)

They studied the transesterification reaction of rapessed oil using a heterogenised $ZnAl_2O_4$ catalyst. An optimum FAME yield of ≈ 90% was obtained at 200 °C, with 4 wt% catalyst/oil and a molar ratio of MeOH:oil = 27:1. The size of catalyst powder was in the range of 315 to 125 μm. The catalyst was prepared by treating 300 g of commercial pseudo-boehmite with 175 g of water containing 5 wt% nitric acid. An amount of 95 g of commercial zinc oxide powder was then added, and the mixture was kneaded for about 45 min, and then it was extruded. The catalyst was then dried over-night at 120°C and calcined at 700°C. The transesterification reaction took place in a stainless steel batch stirred reactor. The reaction time reported was fairly long, that is 6 hours to achieve the maximum conversion.

2.7.3 Yan *et al.* (2009)

They developed heterogeneous catalysts made of zinc and lanthanum mixed oxides for biodiesel production from oil with high FFA. The catalyst was reported active in both transesterification and esterification reactions simultaneously. Lanthanum promoted zinc oxide distribution, and it also increased the surface acid and base sites. The catalyst with a 3:1 ratio of zinc to lanthanum was found to simultaneously catalyze the oil transesterification and fatty acid esterification reactions, while minimizing oil and biodiesel hydrolysis. A reaction temperature range of 170 to 220 °C was found for the biodiesel formation. A high yield (96%) of fatty acid methyl esters (FAME) was obtained within 3 h, even when using unrefined or waste oils.

2.8 Mechanism of transesterification reaction

The overall transesterification reaction may be represented by three reversible consecutive reactions. The transesterification of triglyceride (TG) with alcohol (A) (i.e. methanol) yields: fatty acids methyl esters (E), diglyceride (DG), monoglyceride (MG) and glycerol (GL) as intermediates. The reaction scheme is (e.g. Noureddini, 1999; Xu *et al*., 2005):

$$TG + CH_3OH \xleftrightarrow{k_1/k_2} DG + R_1COOCH_3 \quad (2.2)$$

$$DG + CH_3OH \xleftrightarrow{k_3/k_4} MG + R_2COOCH_3 \quad (2.3)$$

$$MG + CH_3OH \xleftrightarrow{k_5/k_6} GL + R_3COOCH_3 \quad (2.4)$$

2.8.1 Homogeneous based-acid catalysed transesterification reaction (Schuchardt *et al*., 1998)

An explanation of the mechanism of conventional base- and acid-transesterification reactions was found in Schuchardt *et al.* (1998). The mechanism of the base-catalyzed transesterification of vegetable oils is shown in Figure 2.8. The first step is the reaction of the base with the alcohol, producing an alkoxide and the protonated catalyst.

The nucleophilic attack of the alkoxide at the carbonyl group of the triglyceride generates a tetrahedral intermediate, from which the alkyl ester and the corresponding anion of the diglyceride are formed. The latter deprotonates the catalyst, thus regenerating the active species, which is now able to react with a second molecule of the alcohol, starting another catalytic cycle. Diglycerides and monoglycerides are converted by the same mechanism to a mixture of alkyl esters and glycerol.

Step 1

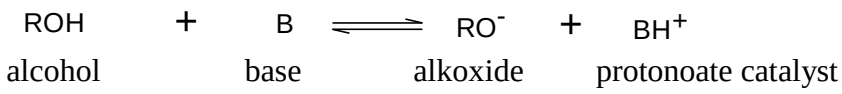

Step 2 Nucleophilic attack to the triglyceride

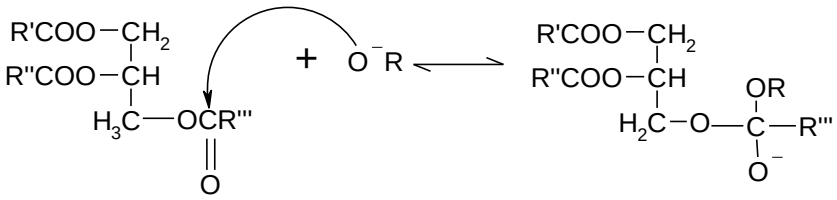

Step 3 Tetrahedral intermediate generation

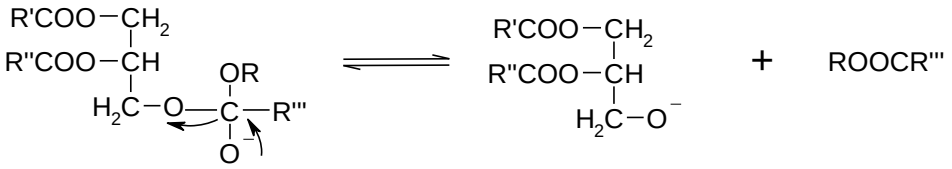

Step 4 Reaction with protonoate catalyst

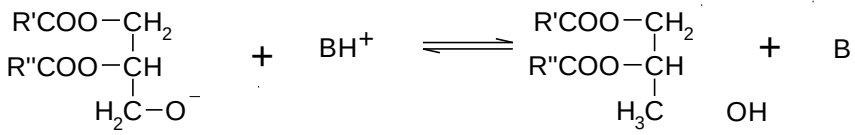

Figure 2.8: Mechanism of the base-catalyzed transesterification of vegetable oils (adapted from Schuchardt *et al*., 1998).

The mechanism of the acid-catalyzed transesterification of vegetable oils is shown in Figure 2.9, for a monoglyceride. However, it can be extended to di- and triglycerides. The protonation of the carbonyl group of the ester leads to the carbocation II which, after a nucleophilic attack of the alcohol, produces the tetrahedral intermediate III, which eliminates glycerol to form the new ester IV, and to regenerate the catalyst H^+ (Schuchardt *et al.*,1998).

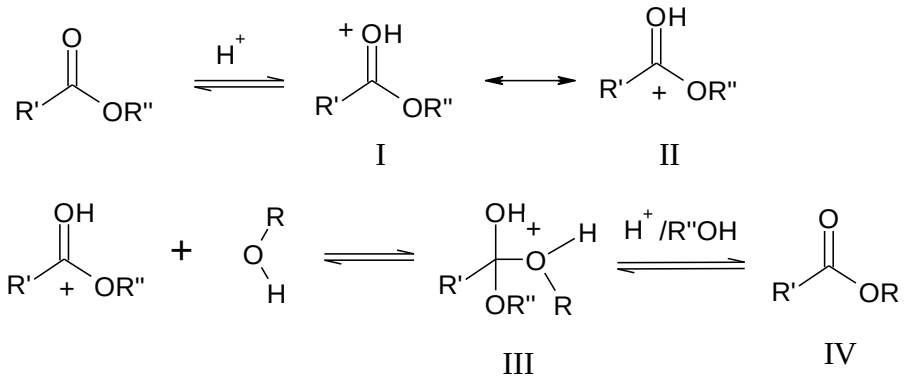

Figure 2.9: Mechanism of the acid-catalyzed transesterification of vegetable oils. (adapted from Schuchardt *et al.*, 1998).

2.8.2 Mechanism of transesterification by heterogeneous catalyst

According to Yan *et al.* (2008), the transesterification reaction by a heterogeneous catalyst with Lewis base sites, takes place between the adsorbed methanol and triglyceride (see Figure 2.10). The transesterification mechanism can be extended to di- and monoglyceride. Methanol is adsorbed on the Lewis base site (B^-) of the catalyst and forms an oxygen anion. The nucleophilic attack of the alcohol on the esters produces a tetrahedral intermediate. Then the hydroxyl group breaks and forms two kinds of esters. The use of excess methanol favours the forward reaction and thus maximizes the yield of FAME.

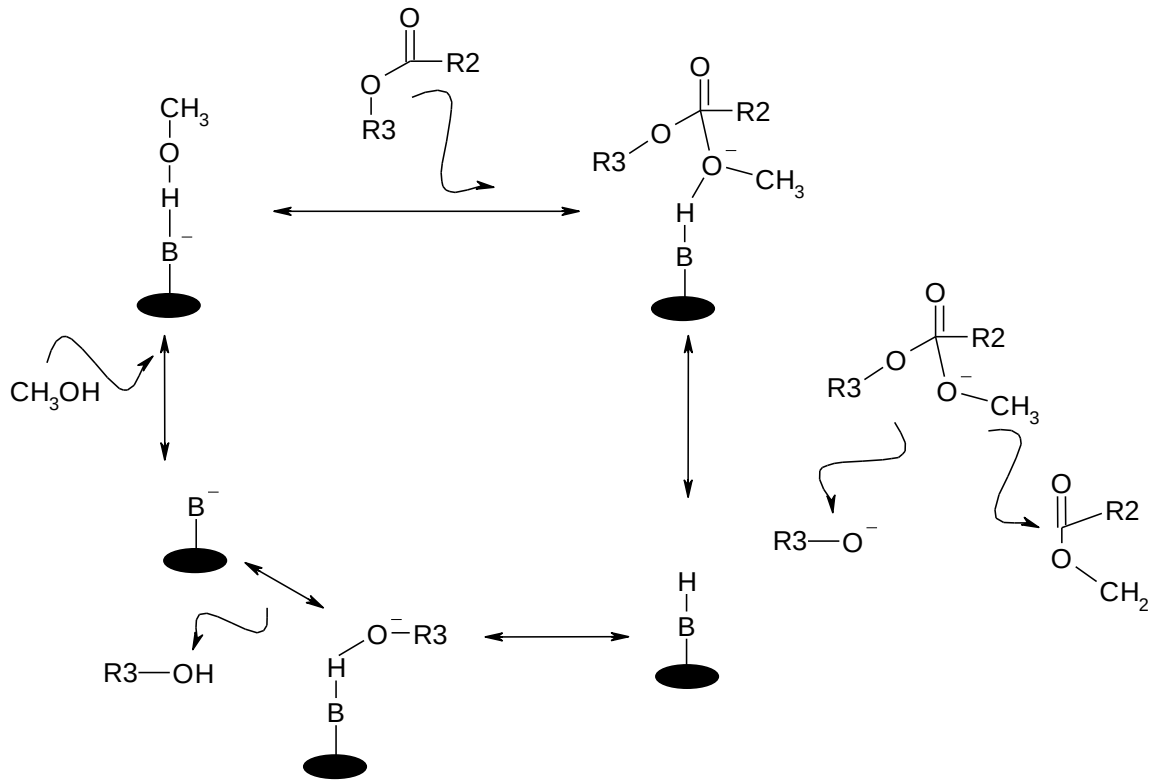

B = Lewis base site on the catalyst surface

R2 = alkyl group of fatty acid

R3 = alkyl esters of trigyceride

Figure 2.10: Schematic representation of possible mechanism for transesterification of triglyceride with methanol (adapted from Yan *et al*., 2008).

An explanation for the mechanism of transesterification with an acidic heterogenous catalyst is provided in Kulkarni *et al.* (2006). The transesterification takes place between monoglyceride ($RCOOR_9$) (taken as representative of triglycerides in this case) and methanol adsorbed on the acidic sites (L^+) on the catalyst surface. The interaction of the carbonyl oxygen of monoglyceride with the acidic site of the catalyst forms carbocation. The nucleophilic attack of alcohol on the carbocation produces a tetrahedral intermediate. The transesterification mechanism can be extended to tri- and diglyceride. It is well known that transesterification is a stepwise reaction. In the reaction sequence the triglyceride is converted stepwise to di- and monoglyceride and finally glycerol. The tetrahedral intermediate formed during the reaction eliminates di-, monoglyceride and glycerol when tri-, di- and monoglyceride come in contact with the acidic sites, respectively, to give one mole of ester ($RCOOCH_3$) in each step.

As shown in Figure 2.11, the catalyst is regenerated after the transesterification reactions. Use of excess alcohol favours forward reaction and thus maximizes the ester yield.

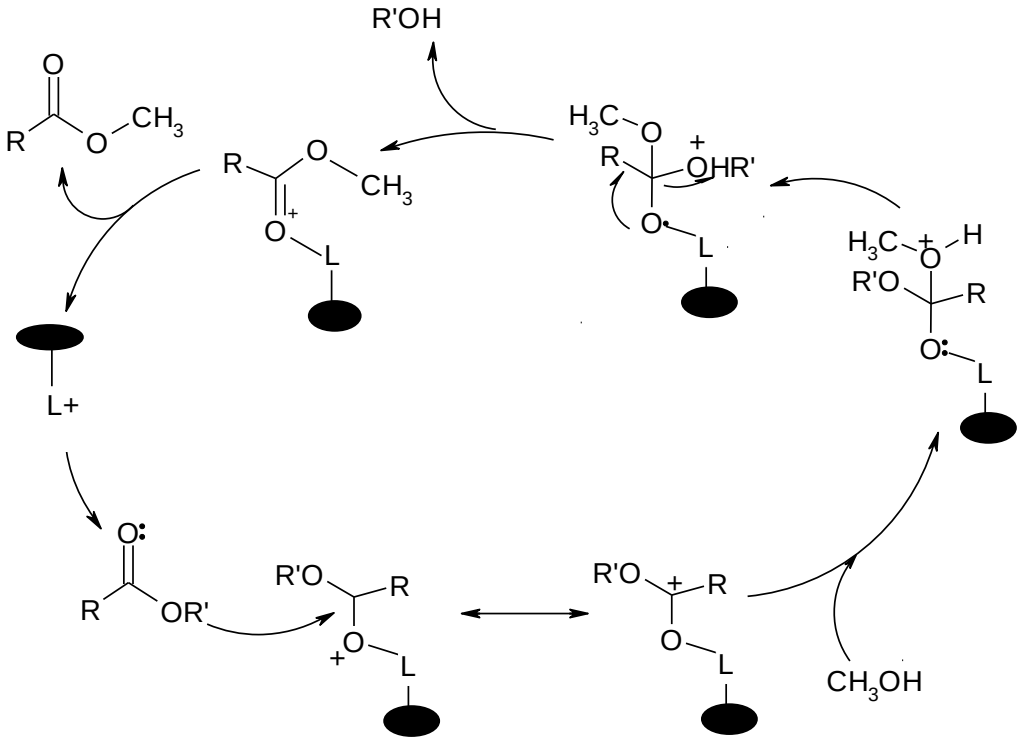

L^+ = acid site on the catalyst surface

R = alkyl group of fatty acid

R' = alkyl esters of triglyceride

Figure 2.11: Reaction scheme of transesterification reaction with Lewis acid site of solid catalyst (adapted from Kulkarni *et al*., 2006).

2.9 Batch *versus* Continuous Processing

Generally, biodiesel is produced in a batch stirred tank reactor (e.g. Behzadi and Farid, 2009; Darnoko and Cheryan, 2000; McNeff *et al.*, 2008). However, Behzadi and Farid (2009) stated that due to increase in biodiesel demand, this trend is changing and more continuous processes have been examined and used either in a laboratory, or on industrial scale. For higher volume production, a continuous process would be advantageous. There are a range of advantages quoted in the literature, for example:

As mentioned in McNeff *et al*. (2008):

> "The ideal process would involve a continuous flow reaction that does not deactivate or consume the catalyst and that further minimizes or eliminates the need for a large number of downstream separation and purification steps."

As explained by Schmidt (1997):

> "Most industrial reactors are operated in a continuous mode instead of batch because reactors produce more products with smaller equipment, require less labour and maintenance, and frequently produce better quality control. Continuous processes are more difficult to start and stop than batch reactors, but they make product without stopping to change batches and they require minimum labour."

As described by Darnoko and Cheryan (2000):

> "Batch processes suffer several disadvantages compared to continuous processes: batch processes require larger reactor volumes, thus requiring higher capital investment; they are inherently less efficient than continuous processes owing to their start-up and shutdown nature; there are batch-to-batch variations in the quality of the products; and labor costs are higher with batch processes."

In the sections that follow, examples are provided of different process routes:

2.9.1 Noureddini *et al.* (1998): Combined mixer/reactor systems

A continuous transesterification process was developed by using intensive mixing throughout the process. A flow diagram of this process is shown in Figure 2.12. In their study, two mixers/reactors, a motionless mixer and a high-shear mixer were used to obtain a better understanding of the mixing effect, by examining the performance of individual and combined mixing tools.

The description of the process provided in their paper is summarised as follows.

(i) The reactants (i.e. soybean oil, methanol and sodium hydroxide) are fed into a pump manifold, and then directed through two in-line motionless mixers.

(ii) The second motionless mixer (made from stainless steel) was inside the heater, and this also mixed the reactants and increased the heat transfer from the heater to the reactants.

(iii) A continuous high-shear mixer was used to mix the reactants further. This high-shear mixer was based on a rotor-stator design, and was considered to be excellent at converting input power into mechanical and hydrodynamic shear energy.

(iv) The residence tube (stainless tube 50.8 cm in length, 5.08 cm in diameter and 1 litre volume) was used to increase the reaction time of the transesterification process.

(v) The back-pressure regulator (BPR) was used to maintain system pressure. The regulator was rated for a maximum temperature of 220°C and a pressure of 500 psi or 34.5 bar.

(vi) After cooling in a shell and tube heat exchanger, the product was collected in a tank.

They found that: (a) both the motionless mixer and the high shear mixer were capable of providing adequate mixing for the conversion to methyl esters, (b) high conversion (>97%) was obtained when at least one mixer was in the process, and (c) the motionless mixer appeared to be more effective than the high shear mixer.

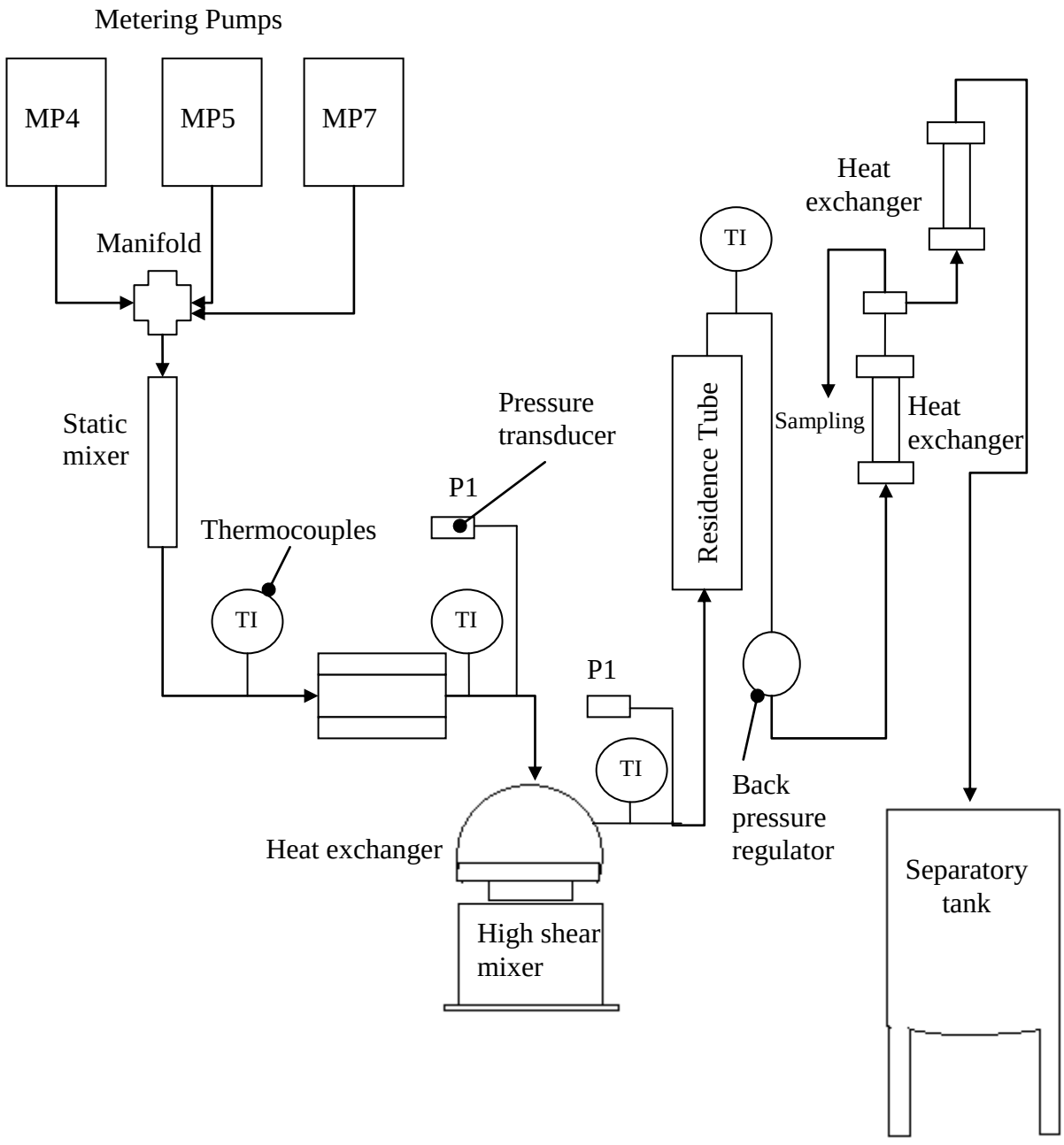

Figure 2.12: Flow diagram of the continuous transesterification process (adapted from Noureddini *et al.*, 1998).

2.9.2 Darnoko and Cheryan (2000): Continuous stirred tank reactor

Darnoko and Cheryan (2000) utilized a continuous stirred reactor system (CSTR) for the transesterification reaction of palm oil. The catalyst used was potassium hydroxide with a methanol: oil molar ratio of 6:1. In their experiment, 500 g of palm oil was heated to 60°C and stirred in 1 litre reactor. Then, the catalyst and methanol were added, and the reaction was allowed to proceed in batch mode for one residence time. The feed pumps and product pump were then simultaneously started. The two feed pumps delivered oil and catalyst to the reactor at a combined flow rate, Q, such that residence time (θ) = V/Q, where V is the volume of the reaction mixture. The product pump removed methyl esters and co-products out of the reactor. A schematic diagram for this experiment is shown in Figure 2.13.

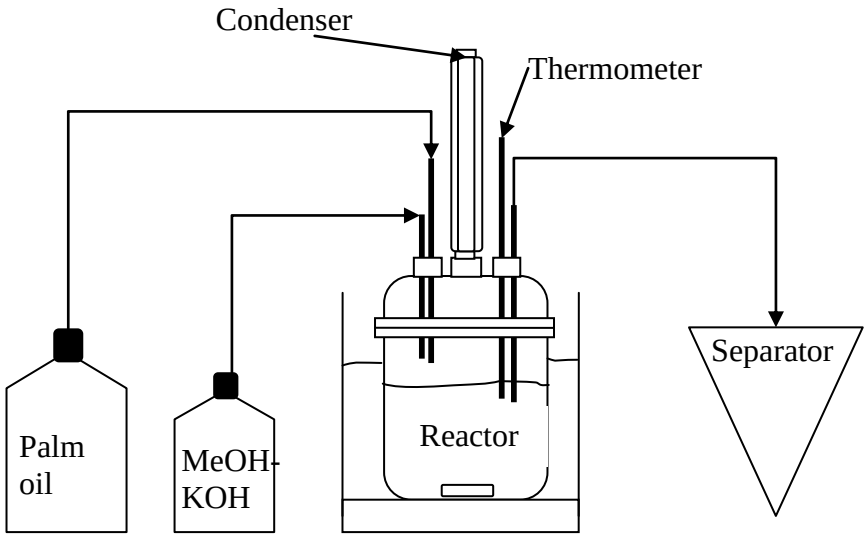

Figure 2.13: Schematic of the continuous stirred tank reactor system (adapted from Darnoko and Cheryan, 2000).

The following is a summary of important observations in their paper:

i) The yield of methyl esters decreased after start-up (i.e. from 82.7% w/w to 58.8% w/w). At the beginning (first 40 min) the reactor had been operated as a batch reactor (for one residence time period). This indicates that a residence time of 40 min is too short to complete the reaction and when operating as a CSTR, there was a dilution of the reaction products by the incoming feed. This in turn caused a build-up of intermediate products that reduced the reaction rate.

ii) Increasing the residence time to 50 min resulted in a better conversion and the average methyl esters concentration was 78.26% w/w. Further improvement was achieved with a residence time of 60 min. The average concentrations of esters and triglyceride under these conditions were 85.6 and 2.08% w/w, respectively.

iii) However, at a residence time of 70 min, a decrease in concentration of methyl esters was observed. Thus, the optimal residence time for maximal concentration of methyl esters was found to be 60 min.

iv) The lower conversion rate at the 70-min residence time could be due to a shift of the reaction equilibrium to the left at this higher residence time, e.g., free glycerol would react with methyl esters to form glycerides.

2.9.3 Zheng *et al.*, 2007: Oscillatory flow reactor

Zheng *et al.* (2007) studied the transesterification reaction in three different types of reactors:

a) Batch stirred tank reactor: this consisted of a glass vessel (42 mm i.d. and 57 mm depth) with a circulation outer jacket.

b) Batch oscillatory flow meso reactor: a vertically mounted tube (20 cm long; 5 mm i.d.), with a heating/cooling jacket.

c) Continuous oscillatory flow reactor: this consisted of a product vessel, a mixing unit, syringe pumps, feed tanks, and 8 meso tubes (with a tube length of 730 cm) with U-bends, providing a total volume of 103 ml.

They performed their experiments:

- using a refined vegetable oil (Holland UK Ltd),
- using 4.2 wt % sodium methoxide in methanol solution acting the catalyst,
- using a volume ratio of oil and alcohol solution of 4:1, corresponding to a 1:6 molar ratio, and at a temperature of 60 ºC, and atmospheric pressure.

What is particularly interesting about these oscillatory reactors, is that they achieve good mixing of the reactants. Also, by a careful choice of operating conditions, plug flow conditions can be approximated in the continuous flow reactor – avoiding any problems that may occur as a result of axial dispersion/radial velocity profiles.

From Zheng *et al.* (2007) work, the following points are relevant to this study:

(i) In the early phase of the reaction (when t < 2.5 min), there appeared to be two phases present. After t > 2.5 min, the fluid is optically homogeneous. It is therefore necessary to have an intense mixing region at the start.

(ii) The bulk of the reaction occurred in the first 10 minutes. However, in order to satisfy the EU standard for biodiesel (see Appendix A), it is necessary to continue for a further 30 min.

(iii) They showed that it is possible to directly scale the results across these three different types of reactors. For the same set of conditions, the conversion is approximately the same.

2.9.4 Tatsumi *et al* (2007) : Tubular and Fixed Bed System

Tatsumi *et al*. (2007) invented a method of producing a fatty acid ester in a continuous system in the presence of a third component. They used a third component (e.g. carbon dioxide, pentane) to make the separation of glycerine more efficient by decreasing the solubility of glycerine. A schematic of this process is shown in Figure 2.14.

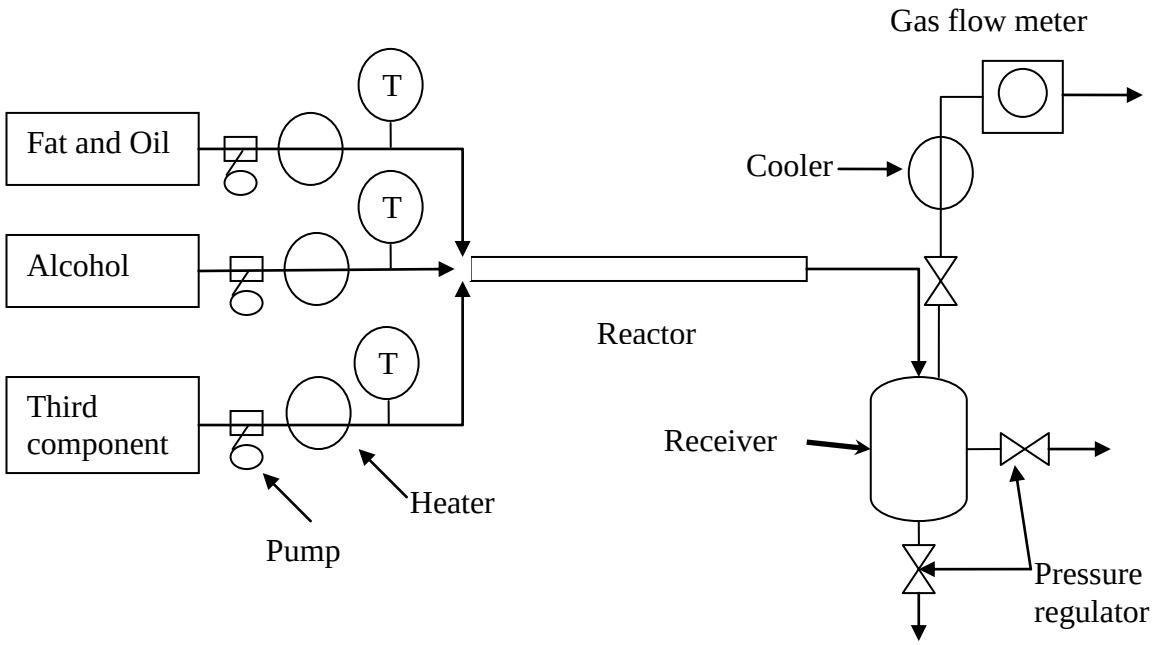

Figure 2.14: A continuous flow system adapted from Tatsumi *et al.* (2007).

In the background to Tatsumi *et al.* (2007). invention, the following important points were noted:

(i) A high purity of fatty acid esters was necessary, if they are used as a biodiesel fuel. It was pointed out that the total amount of glycerol (total amount of glycerine, monoglyceride, diglyceride and triglyceride) left in fatty acid methyl esters can affect the productivity in industrial applications. In biodiesel applications, it can cause problems with engine stains.

(ii) In the transesterification reaction step, the glycerine produced is slightly soluble in the fatty acid methyl esters. The residual amount of the monoglyceride and diglyceride (which are the reaction intermediates) can be minimised by making the fatty acid ester have an extremely low solubility. In this invention, the third component is in a subcritical or supercritical state, hence the reaction system does not form a uniform phase. Also, a third component is chosen to decrease the solubility of glycerol in oil. Therefore, it is advantageous to decrease the concentration of glycerol in the reaction. With the help of a supercritical gas in the reaction mixture, the residence time is also decreased.

A summary of reaction conditions is presented in Table 2.4, and this provides useful ideas on the design of the reactor.

Table 2.4: Summary of reaction conditions for tubular and fixed bed reactor (adapted from Tatsumi *et al.* (2007).

Type of reactor	**Tubular**	**Fixed-bed**
Dimension	i.d. = 0.004 m, L = 4.0 m, and internal volume = 50 ml	i.d. = 0.013 m, L = 0.83 m
Catalyst used	147 g phosphorus-containing metal salt powder	70 cc phosphorus-containing metal salt powder
Reaction Temperature	300°C (573 K)	200°C (473 K)
Oil feedstock	Refined palm kernel oil	Refined palm kernel oil
Reaction Pressure	13 MPa	5 MPa
Flow rate	7.5 g h^{-1} of oil 7.8 g h^{-1} of methanol 33.9 g h^{-1} of carbon dioxide	6.5 g h^{-1} of oil 5.5 g h^{-1} of methanol 15.5 g h^{-1} of pentane
Molar ratio - Methanol/ oil - Carbon dioxide/ oil	 20 71	 20 25
LHSVof oil	0.2	0.1

2.9.5 High temperature, high pressure biodiesel production system (McNeff *et al.*, 2008)

A continuous process was developed consisting of a fixed bed system using a metal oxide catalyst under high pressure (ca. 2500 psi or 172 bar) and elevated temperature (300 to 450 °C). The process was called the "Mcgyan process". It consisted of a supercritical flow of alcohol with a lipid feedstock through a tube reactor packed with sulphated metal oxide microspheres. The effluent from the reactor was further processed by adsorption onto an alumina packed-bed polisher system, called the Easy Fatty Acid Removal (EFAR) system. This removes residual unreacted free fatty acids. The excess alcohol was separated out, and then recycled back into the continuous process. A process flow diagram of the biodiesel plant using the Mcgyan process is shown in Figure 2.15.

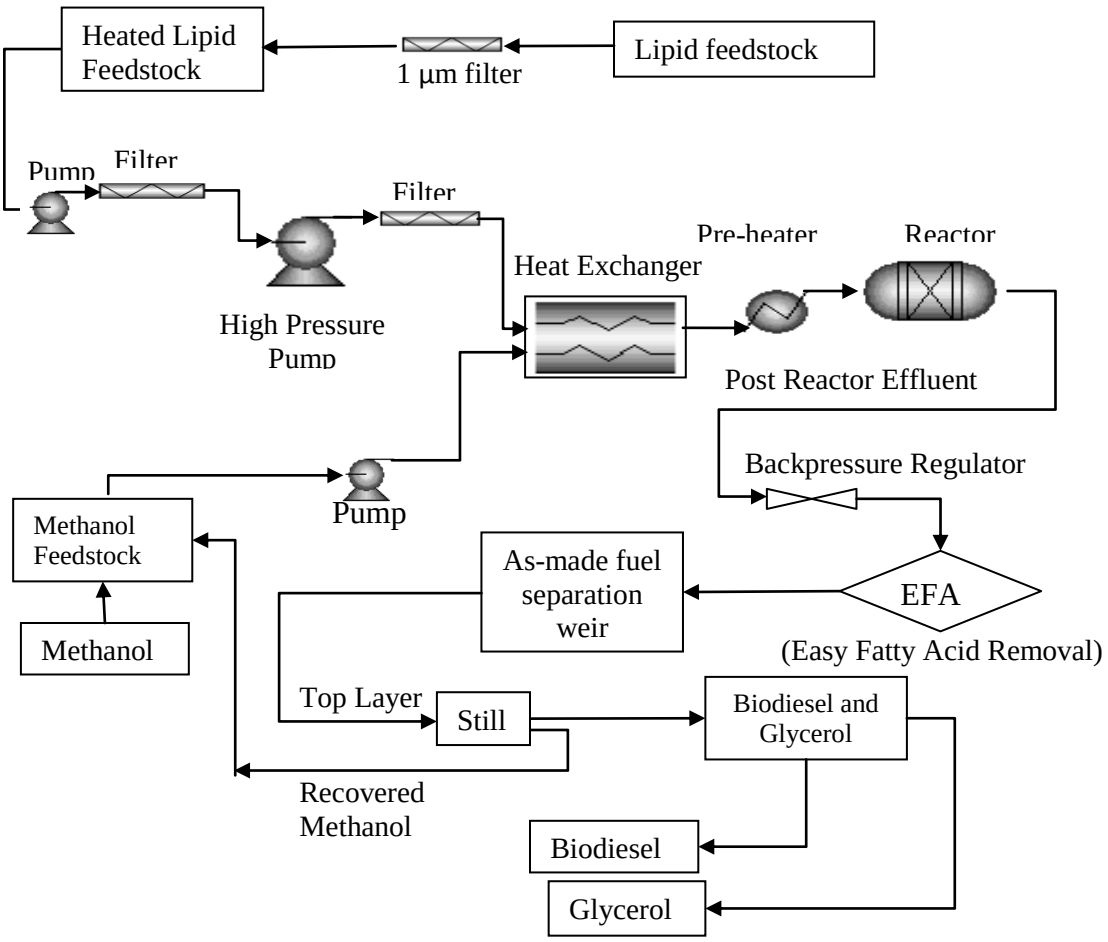

Figure 2.15: A simplified diagram for a biodiesel plant based on the Mcgyan process (adapted from McNeff *et al.*, 2008).

In the process described, the following conditions were used:

(i) Two high pressure Waters 590 HPLC pumps were used to pump the alcohol, and a heated (using a hot plate) lipid reservoir was used.

(ii) The lipid reservoir was continuously sparged with nitrogen to minimize the effect of dissolved oxygen on the system.

(iii) The reactor was a stainless steel tube (1 cm ID and 15 cm long) fitted with two 2 mm stainless steel frits.

(iv) The minimum molar ratio of alcohol:oil was 32.7 : 1.

(v) Both feedstock streams were pumped into a custom designed heat exchanger, and then sent through an electrically driven pre-heater. This pre-heater was used to bring the temperature of the flowing fluid up to the desired temperature (320 to 450°C) before it entered the reactor.

(vi) The backpressure of the system was maintained through the use of a backpressure regulator.

From their work, they found that the temperature of the reaction was a critical part of the system. The biodiesel yield increased from 15.5% to 87.3% as the temperatures increased from 322 to 434 °C. The optimum temperature range (to achieve high conversion for most of the different feedstocks tested) was between 350 and 370°C, using a residence time of about 57 s and a constant molar ratio of methanol to lipid feedstock.

2.9.6 A fixed bed reactor packed with resin as cation-exchange heterogeneous catalyst (Feng *et al.*, 2011)

Another continuous process for biodiesel production for biodiesel production was explored using a fixed packed bed reactor (with a resin type of catalyst) and waste fried oil. The resin used was a macroreticular copolymer styrene-divinyl benzene in H^+ form (purchased from commercial supplier called NKC-9). A schematic of their apparatus is shown in Figure 2.16. The reactor consisted of a water-jacket stainless steel column (i.d. of 25 mm, and height = 450 mm). The height of the catalyst bed depended on the required residence time for the experiment. The two reactants, methanol and oil, at a mass ratio of 2.8 : 1 were mixed and preheated in a feedstock tank, then were fed into the reactor using a peristaltic pump. The effluent from the reactor was then fed into an accumulation tank.

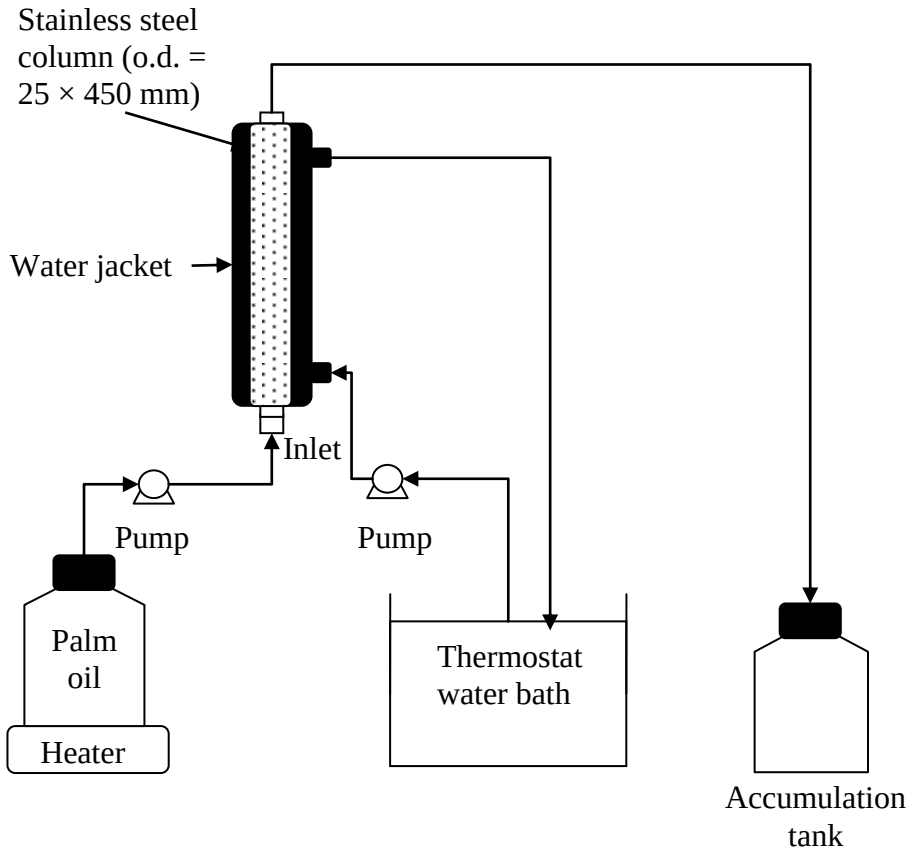

Figure 2.16: Schematic diagram of experimental apparatus used in Feng *et al.* (2011).

The important characteristics of the cation-exchange catalyst used are summarised as follows.

i) Before the experiment, the catalyst required a thorough pre-treatment step. The catalyst was first swollen in ethanol for 30 min, then dried for 24 hours at 90°C in an oven. Otherwise with about a 100% swelling ratio, the resin would plug the reactor, or create a very high pressure drop.

ii) It was necessary to remove water from the feedstock. The presence of water in the feedstock decreased the FFA conversion. The water molecule had a tendency to absorb onto the active site ($-SO_3H$) of the resin surface to form a water layer and this blocked the accessibility of the reactant to active sites.

The optimum result obtained was a 98 % FFA conversion after a 1 h reaction time at a feed flowrate of 0.62 ml min^{-1}, reaction temperature of 65°C and a mass ratio of methanol to oleic acid of 2.8 : 1. The amount of catalyst was 87.5 g packed in a 25 mm o.d. column with a height of 44 cm. The resin was reported to be stable for 500 hours of continuous running time. As mentioned in their conclusion, the resin catalyst in their system performed better than in a batch system, because the continuous packed bed reactor could : (i) avoid the breakdown of the resin particle under mechanical agitation in batch mode, and, (ii) reduce the water accumulation effect.

2.10 Monolith Reactor

To explain the monolith reactor feature, the description from Cybulski *et al.* (2006, p357) is quoted as follows:

> "A monolithic support consists of a large number of narrow parallel channels separated by thin walls. Unlike conventional packed-bed reactors, the monolith channels have a well defined geometry. The channels may have a variety of cross-sectional shapes, such as square, sinusoidal, circular, triangular, and hexagonal. The walls may contain the catalytically active material, but more frequently a washcoat consisting of a thin layer of a porous oxide is deposited onto the channel wall. Owing to its porosity it has a large surface area on which the catalytically active material is fixed. The open structure of the monolith allows high flow rates with low pressure drop."

The typical configurations of monolith reactors are shown in Figure 2.17 and a typical square cross-section channel coated with catalyst is shown in Figure 2.18.

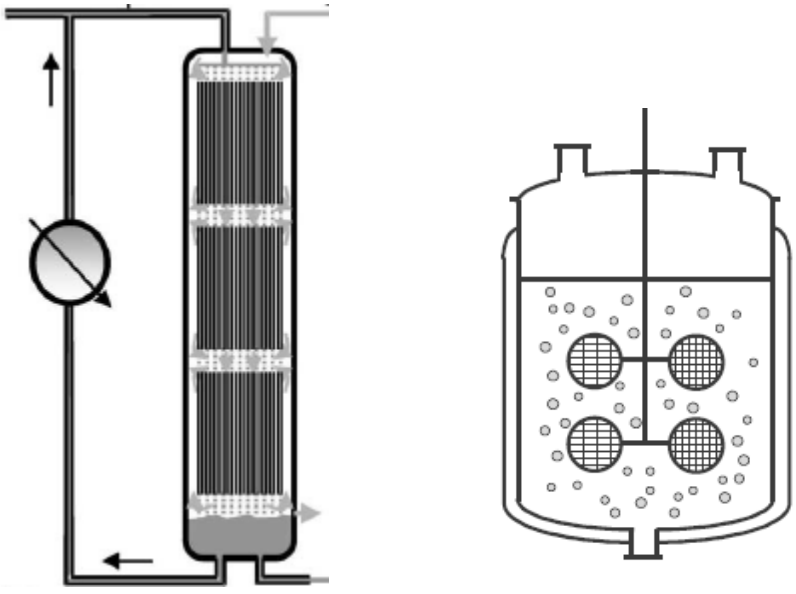

Figure 2.17: Monolith reactor in two possible configuration: (a) tubular packed reactor and (b) monolithic stirrer reactor (adapted from Nijhuis *et al.*, 2001).

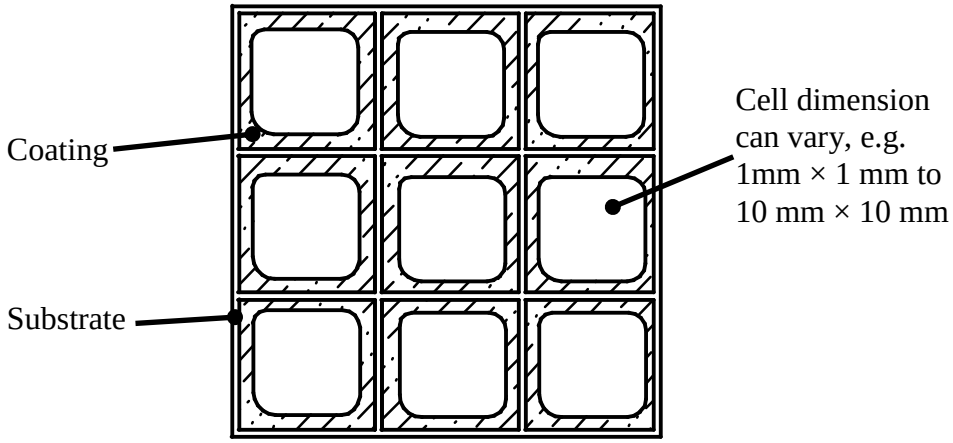

Figure 2.18: Coated monolith structure.

Monolith reactors can be operated in tubular and stirred reactor configuration. According to Smith (2005), stirred tanks become unfavourable if the reaction must take place at high pressure. Under high-pressure conditions, a small diameter cylinder requires a thinner wall than a large-diameter cylinder. Under high-pressure conditions, the use of a tubular reactor is preferred; although mixing problems with heterogeneous reaction and other factors may prevent this. Also, for a given conversion, CSTR requires a large inventory of material relative to a tubular reactor.

To the best of the author's knowledge, the use of a monolith reactor has not yet been used for the commercial production of biodiesel. The suitability of this system for the production of biodiesel is reviewed and considered in this section. Monolith reactors have been used as an alternative to conventional slurry and trickle reactors. For examples, Hoek *et al.* (2004) used a monolithic stirrer reactor for a hydrogenation process in which alkene was formed, Lathdouder *et al.* (2005) performed an enzymatic reaction by using the same type of monolithic stirrer reactor, and Addiego *et al.* (2003) utilised tubular reactor with a honeycomb monolith packing for a dehydrogenation reaction to produce styrene. General comparisons between monolith, slurry, and packed bed reactors can be found in Nijhuis *et al.* (2001) as shown in Table 2.5.

Table 2.5: Comparison between monolith and slurry and packed-bed reactors (adapted from Nijhuis *et al.*, 2001).

	Monolith reactor	**Slurry Reactor**	**Trickle-Bed reactor**
Energy Input	Low	Medium (stirring)	High (pressure drop)
Catalyst efficiency	High, thin active layer	High, small particles	Low, large particle required for pressure drop
Safety	High, self-draining reactor	Medium, easy cooling, difficult to separate catalyst from liquid	Low, difficult cooling, catalyst bed retains liquid
Catalyst separation	Easy	Costly filtering necessary	Easy
Preparation	Medium, new technology, methods have now been developed	Easy	Easy
Catalyst loading	Medium, very open structure, for washcoated systems: low	Low-medium	High, dense bed
Catalyst replacement	Difficult, shutdown required, monoliths have to be carefully stacked	Easy, continuous during operation	Medium-difficult shutdown required
Experience	Gas-phase: extensive; liquid and multiphase: very limited	Extensive	Extensive

Monolith reactors can have a number of advantages over conventional multi-phase reactors and these are discussed in Cybulski *et al.* (2006, 1999) and Boger *et al.* (2004). Among the advantages listed, the following points were relevant and applied in this thesis.

- lower pressure drop, especially under high fluid throughputs;
- higher specific external catalyst surface area for mass transfer and reactions;
- reduction of fouling and plugging, and thus extended catalyst lifetime;
- easier cleaning of particulates accumulated on the channel walls; and
- easy scale-up.

However, there are issues that must be considered, such as:

- potential low radial heat transfer rates, and, thus difficulty in temperature control for thin-wall ceramic monolith supports;
- heat transfer from the monolith to the internal reactor wall;
- potential non-uniform fluid distribution, and thus lower reactor effectiveness.

2.11 Interim conclusions

Although this transesterification reaction, using acid and/or alkaline catalysts is well known and practiced on a commercial scale, there is still plenty of scope to improve this semi-batch process. For example:

(a) By increasing the rate of the first step in the reaction (which is limited by mass transfer). The residence time for this phase could be in the region of 2.5 min (Zheng *et al.* (2007). *This could be explored further by using in-line mixers, sonic mixing, or pulsating flow techniques.* ***A static in-line mixing device will be used in this thesis.***

[Note: Italics indicate future work, when in bold the topic is considered in this thesis].

(b) By identifying a catalyst to deal with the variation in the composition of the feed (e.g. presence of fatty acids). ***This will be explored further in this thesis by studying the viability of a zinc proline catalyst system.***

(c) By decreasing the time of the separation step at the end of the reaction. ***This was a factor also considered in this thesis. By retaining the catalyst in the bed, and also using zinc proline (which was more tolerant to fatty acids), there was potential to reduce the time of the final separation step.***

(d) By turning the semi-batch reactor into a continuous process. ***This was a key consideration in this thesis, and the viability of supporting the catalyst on a monolith support will be explored.***

(e) By increasing the purity of the glycerol (which is produced as a by-product), or by converting more of the glycerol into a more useful product. *This aspect was not considered further in this thesis.*

(f) By reducing the amount of water in the reactor effluent (which then has to be separated from the products). ***This was considered, as by using a solid catalyst rather than one in a solution (e.g. acid/alkali), the amount of water would also be reduced.***

Conclusions on the reaction system:

(g) The catalyst would be supported on a monolith structure. ***Cordierite ceramic monoliths with a 1mm x 1mm cell size, are already available in the Department and these will be suitable.***

(h) The catalytic reaction with zinc proline as a catalyst requires a temperature of about 195 ^{o}C. ***The continuous flow reactor will be designed to operate at that condition, and its internal diameter will be kept relatively small (e.g. 1 cm), so as to keep the peripheral equipment relatively compact and manageable as a bench top laboratory rig. There was also a limited budget to support this project.***

(i) In a number of studies in the literature, HPLC pumps were used to pump the vegetable oil and methanol into a continuous reactor. ***HPLC pumps will also be used in this thesis.***

(j) When performing experiments at temperatures above the boiling point of the alcohol, then to maintain a liquid phase in the reactor, a back pressure valve was used. ***This will also be used in this thesis.***

(k) Heated jackets have been used around the reactor, to maintain the desired operating temperature in the reactor. ***This will also be used in this thesis, in combination with a heated oil bath.***

REFERENCES

Addiego, W.P, Campbell, S. A, Liu, W. and Odinak, M. E., 2003. Monolithic catalyst dehydrogenation reactor. *US Patent US6*,623,707 B1.

Alamu, O.J., Waheed, M.A. and Jekayinfa, S.O., 2008. Effect of ethanol–palm kernel oil ratio on alkali-catalyzed biodiesel yield. *Fuel*, 87, pp. 1529–1533.

Alba-Rubio, A.C., Santamarıa-Gonzalez, J., Merida-Robles, J.M. and Moreno-Tost, R., 2010. Heterogeneous transesterification processes by using CaO supported on zinc oxide as basic catalysts. *Catalysis Today*, 149, pp. 281–287

Al-Zuhair, S., 2007. Production of biodiesel: possibilities and challenges. Biofuels, Bioprod. Bioref., 1, pp. 57–66 [online]. Available from: http://www3.interscience.wiley.com/cgi-bin/fulltext/ 114285965/ -PDFSTART [Accessed on 06/02/2008].

Bradshaw, G.B., 1942. New soap process. *Soap,* 18, May , 23–24, 69–70.

Bradshaw, G.B., Del, W. and Meuly, W.C., 1942. Process of making pure soaps. *U.S. Patent No. 2,271*,619.

Bournay, L., Casanave, D., Delfort, B., Hillion, G.. and Chodorge, J.A., 2005. New heterogeneous process for biodiesel production: A way to improve the quality and the value of the crude glycerin produced by biodiesel plants. *Catalysis Today*, 106, pp. 190–192.

Bradshaw,G.B., Del, W. and Meuly, W.C., 1944. Preparation of detergents, *U.S. Patent No. 2*,360,844.

Canakci, M and Gerpen, J.V., 2003. A pilot plant to produce biodiesel from High Free Fatty Acid feedstock. *American Society of Agricultural Engineers*, 46, pp. 945-954 [online]. Available from: http://www3.me.iastate.edu/biodiesel/Technical%20Papers/Canakci_Paper2_ as%20revised%20after%20review.pdf [Accessed on 20/05/2008].

Chung, K.H., Kim, J and Lee, K.Y., 2009. Biodiesel production by transesterification reaction of duck tallow with methanol on alkali catalysts. *Biomass and Bioenergy*, 33, pp. 155-158.

Cordeiro, C.S., Arizaga, G.G.C., Ramos, L.P. and Wypych, F., 2008. A new zinc hydroxide nitrate heterogeneous catalyst for the esterification of free fatty acids and the transesterification of vegetable oils . *Catalysis Communications*, 9, pp. 2140–2143.

Cybulski, A., Albers, R. E., and Moulijn, J. A., 2006. Chapter 10: Monoltihic catalysts for three-phase processes. *Structured Catalysts and Reactors*. Taylor & Francis Group, LLC.

Darnoko, D and Cheryan, M, 2000. Continuous production of palm methyl esters, *Journal of American Oil Chemists Society*, 77 (12), pp. 1269-1272.

Encinar, J.M., González, J.F. and Rodríguez-Reinares, A., 2007. Ethanolysis of used frying oil. Biodiesel preparation and characterization. *Fuel Processing Technology*, 88, pp. 513–522.

Feng, Y., Zhang, A., Li, J. and He, B., 2011. A continuous process for biodiesel production in a fixed bed reactor packed with cation-ecxhange resin as heterogenous catalyst. *Bioresource Technology*, 102, pp. 3607-3609.

Feuge A.J, and *Gros* A.T., *1949.* Modification of peanut oil with ethanol. *JAOCS, 26,* pp. 97 – 102.

Freedman, B., Pryde, E.H. and Mounts, T.L., 1984. Variables affecting the yields of fatty esters from transesterified vegetables oils. *Journal of American Oil Chemists Society*, 61 (10), pp. 1638-1643.

Fukuda, H., Kondo., A. and Noda, H., 2001. Review: biodiesel fuel production by transesterification of oils. Journal of Bioscience and Bioengineering, 92 (5), pp. 405-416.

Gerpen, J.V., 2005. Biodiesel processing and production, *Fuel Processing Technology*, 86, pp 1097-1107.

Hartman, L., 1956. Methanolysis of triglycerides. *JAOCS*, 33, pp.129 - 132.

Helwani, Z., Othman, M.R., Aziz, N., Fernando, W.J.N. and Kim, J., 2009. Technologies for production of biodiesel focusing on green catalytic techniques: A review. *Fuel Processing Technology*, 90, pp. 1502–1514.

Hoek, I., Nijhuis, T.A,. Stankiewicz, A.I. and Moulijin, J.A., 2004. Performance of the monolithic stirrer reactor: applicability in multi-phases processes. *Chemical Engineering Science*, 59, pp. 4975-4981.

Kaya, C,. Hamamci, C., Baysal, A., Akba, O., Erdogan, S., and Saydut, A., 2009. Methyl ester of peanut (*Arachis Hypogea L*.) seed oil as a potential feedstock for biodiesel production. *Renewable Energy*, 34, pp.1257–1260.

Kim, H., Kang, B., Kim, M., Park, Y.M., Kim, D., Lee, J. and Lee, K., 2004. Transesterification of vegetable oil to biodiesel using heterogeneous base catalyst. *Catalysis Today*, pp. 1-6.

Knothe, G., 2010. Biodiesel and renewable diesel: A comparison. *Progress in Energy and Combustion Science*, 36, pp. 364–373.

Kulkarni, M,G., Gopinath, R., Meher, L. C. and Dalai, A.K., 2006. Solid acid catalyzed biodiesel production buy simultaneous esterification and transesterification. *The Royal Society of Chemistry : Green Chemistry*, 8, pp. 1056-1062.

Lathouder, D. K.M. , 2007. *Development of a monolithic bioreactor: design and application*. Thesis (PhD), Delft University of Technology, Netherland. [online] Available from http://repository.tudelft.nl/view/ir/uuid%3Aa214b1ce-77e5-40db-a2b1-1995e24fd73a/ [accessed on 8/11/2008].

Lee, J and Saka, S., 2010. Review : Biodiesel production by heterogeneous catalysts and supercritical technologies. *Bioresource Technology*,101,pp. 7191–7200.

McNeff, C. V., Mcneff, L. C., Yan, B., Nowlan, D. T., Rasmussen, M., Gyberg, A. E., Krohn, B. J., Fedie, R. L. & Hoye, T. R. 2008. A continuous catalytic system for biodiesel production. *Applied Catalysis A:General,* 343**,** 39-48.

Meneghetti, S.M.P., Meneghetti, M.R., Wolf, C.R., Silva, E.C., Lima, G.E.S., Silva, L. L., Serra, T. M., Cauduro, F. and Oliveira, L.G., 2006. Biodiesel from castor oil: a comparison of ethanolysis *versus* methanolysis. *Energy & Fuels*, 20, pp. 2262-2265.

Meng, X., Chena, G., and Wang, Y., 2008. Biodiesel production from waste cooking oil *via* alkali catalyst and its engine test. *Fuel Processing Technology*, 89, pp. 851-857.

Miao, X., Li, R., and Yao, H., 2009. Effective acid-catalyzed transesterification for biodiesel production. *Energy Conversion and Management*, 50, pp. 2680–2684.

Ni, J. and Meunier, F.C., 2007. Esterification of free fatty acids in sunflower oil over solid acid catalysts using batch and fixed bed-reactors. *Applied Catalysis A: General*, 333, pp. 122–130.

Nie, K., Xie, F., Wang, F.and Tan, T. 2006. Lipase catalyzed methanolysis to produce iodiesel optimization of the biodiesel production. *J. Mol. Catalysis B: Enzymatic*, 43, pp.142-147.

Nijhuis, T. A., Beers, A. E.W., Vergunst, T., Hoek, I., Kapteijn, F. and Moulijn, J.A., 2001. Preparation of monolithic catalysts. *Catalysis Review*, 43 (4), pp 345-380.

Noureddini, H., Harkey, D. and Medikonduru, V., 1998. A continuous process for the conversion of vegetable oils into methyl esters of fatty acids. *Journal of American Oil Chemists Society* ,75, pp. 1775-1783.

Pugnet, V., Maury, S., Coupard, V., Dandeu, A., Quoineaud, A., Bonneau, J and Tichit, D., 2010. Stability, activity and selectivity study of a zinc aluminate heterogeneous catalyst for the transesterification of vegetable oil in batch reactor. *Applied Catalysis A: General*, 374, pp.71–78.

Ramadhas, A.S., Jayaraj, S. and Muraleedharan, C., 2005. Biodiesel production from high FFA rubber seed oil. *Fuel*, 84, pp. 335–340.

Rashid, U. and Anwar, F., 2008. Production of biodiesel through optimized alkaline-catalyzed transesterification of rapeseed oil. *Fuel*, 87, pp 265–273.

Saka, S. and Kusdiana, D., 2001. Biodiesel fuel from rapeseed oil as prepared in supercritical methanol. *Fuel*, 80, pp. 225-231.

Schuchardt, U., Serchelia, R. and Vargas, R. M., 1998. Transesterification of vegetable oils: a review. *J. Braz. Chem. Soc.*, 9 (1) , pp199-210.

Scmidt, L.D., 1997. *The Engineering of Chemical Reactions*. Oxford University Press. United States.

Serio, M. D., Cozzolino, M., Giordano, M., Tesser, R., Patrono, P. and Santacessiaria, E., 2007. From homogeneous to heterogenuous catalysts in biodiesel production. *Ind. Eng. Chem. Res*., 46, pp. 6379-6384.

Shimada, Y., Watanabe, Y., Sugihara, A., Tominaga, Y., 2002. Enzymatic alcoholysis for biodiesel fuel production and application of the reaction to oil processing. *J. Molecul. Catal. B: Enzymatic,* 17 (3-5), pp.133-142.
Siler-Marinkovic, S. and Tomasevic, A., 1998. Transesterification of sunflower oil *in situ. Fuel* (77), No. 12, pp. 1389-1391.

Smith, R., 2005. *Chemical Process Design and Integration*. John Wiley, USA.

Song, C., Qi, Y., Deng, T., Hou, X. and Qin, Z. 2010. Kinetic model for the esterification of oleic acid catalyzed by zinc acetate in subcritical methanol. *Renewable Energy*, 35, pp. 625–628.

Tatsumi, N., Katayama, T and Tabata, O., 2007. Method of producing a fatty acid ester. *US Patent*, US 7193097, pp. 1-8.

Yan, S., Salley, S.O. and Ng, K.Y.S., 2009. Simultaneous transesterification and esterification of unrefined or waste oils over ZnO-La_2O_3 catalysts. *Applied Catalysis A: General*, 353, pp 203–212.

Vicente, G., Mercedes, M, and Jose, A., 2004. Integrated biodiesel production: a comparison of different homogeneous catalysts systems. *Bioresource Technology*, 92, pp. 297–305.

Zabedi, M., Wan Daud, W.M.A. and Aroua, M. K., 2009. Activity of solid catalysts for biodiesel production: A Review. *Fuel Processing Technology*, 90, pp 770-777.

Zheng, M., Skelton, R.L And Mackley, M. R., 2007. Biodiesel reaction screening using oscillatory flow meso reactors. *Process Safety and Environmental Protection*: *Trans IChemE*, 85 (B5), pp. 365-371.

Zheng, S., Kates, M., Dube, M. A., McLean, D. D., 2006. Acid-catalyzed production of biodiesel from waste frying oil. *Biomass Bioenenergy*, 30 (3), pp. 267-272.

CHAPTER 3

SELECTION AND DEVELOPMENT OF ANALYTICAL TECHNIQUES

In this chapter analytical techniques are discussed. The ^{1}H NMR method is tested, and the Gas Chromatography (GC) method for the analysis of intermediates is developed. This is done by making use of available information in the literature, and applying it to the GC that was available in the Department of Chemical Engineering. This required a enormous amount of 'trial and error', but in the end the technique worked very well.

3.1 Introduction

Analytical methods used to monitor transesterification reactions include techniques such as: thin layer chromatography (TLC), gas chromatography (GC), high performance liquid chromatography (HPLC), gel permeation chromatography (GPC), size exclusion chromatography (SEC), ^{1}H Nuclear Magnetic Resonance (^{1}H NMR) and near-infrared spectroscopy (NIR) (Arzamendi *et al.*, 2006 and Meher *et al*., 2006).

In Chapter 4 in this thesis, the ^{1}H NMR method was used to determine the conversion to FAME and then later, in Chapter 5, the conversion and concentration of the intermediate components was determined using GC. The ^{1}H-NMR equipment was based in the Department of Chemistry (see Figure 3.1), and the GC used was in the Department of Chemical Engineering (see Figure 3.2).

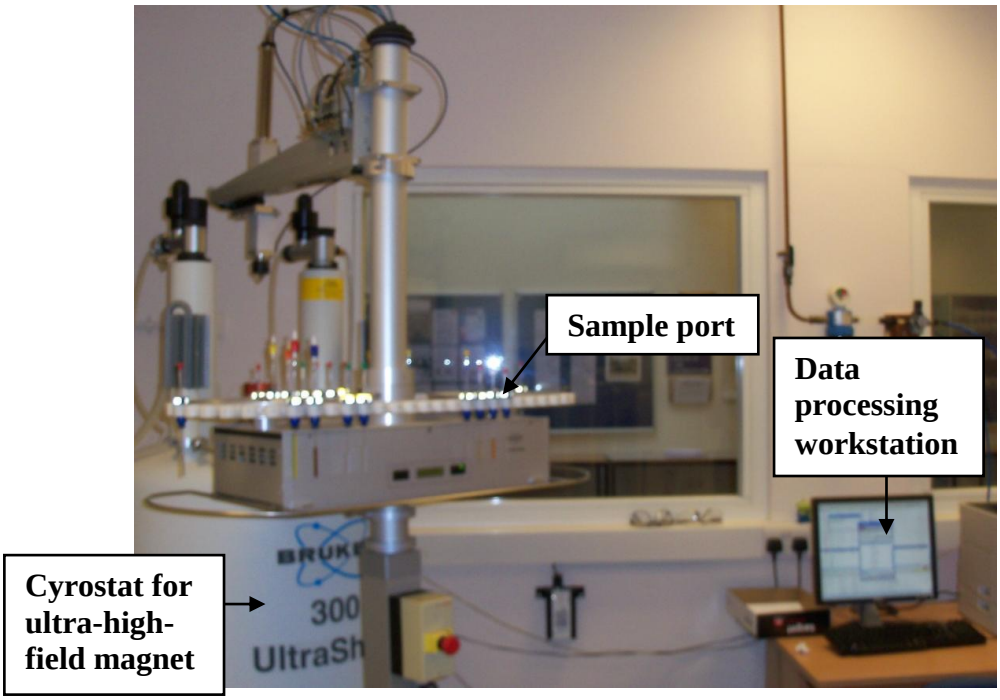

Figure 3.1: Photograph of ^{1}H NMR in the Department of Chemistry.

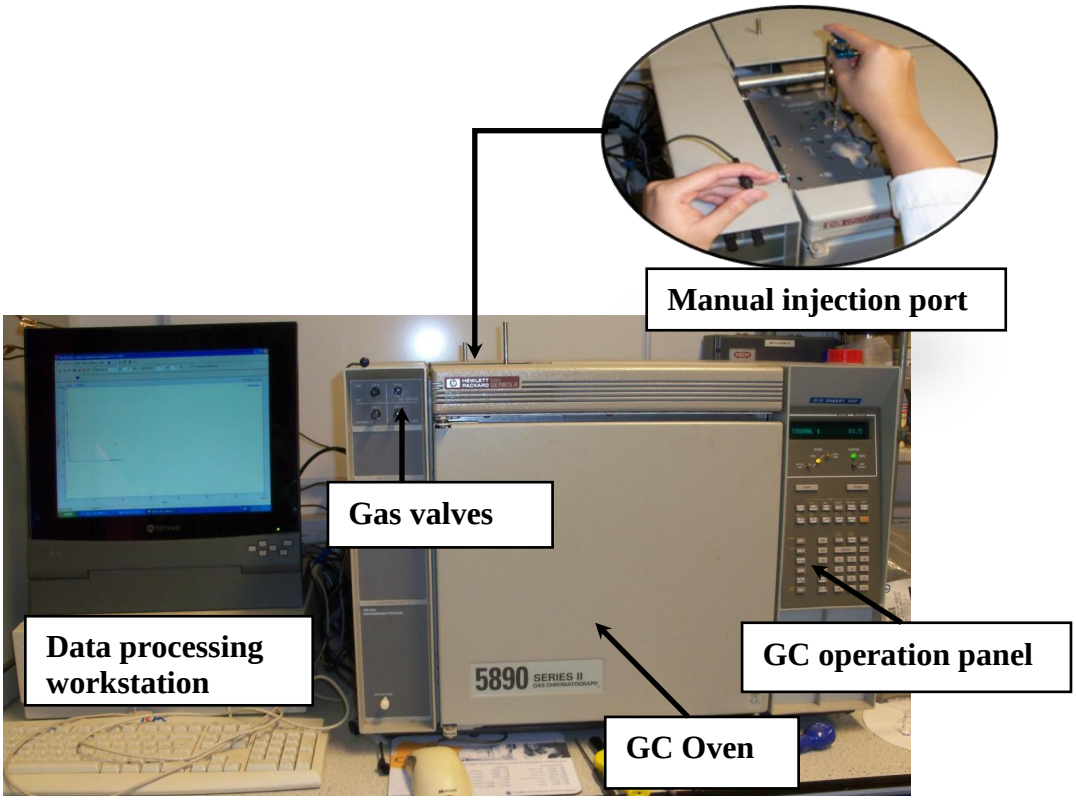

Figure 3.2: Photograph of GC in the Department of Chemical Engineering.

3.2 ^{1}H NMR method

According to Knothe (2000), there are two ^{1}H NMR approaches, one being the use of methyl esters protons and the protons on the carbons next to the glyceryl moiety (a-CH_2). The second approach in the use of methyl ester protons and the protons of the glyceryl moiety in the triglycerides.

In this work, the second approach was used, where FAME yield is calculated by taking the integral value of the methoxy group of the FAME against the remaining proton signals adjacent to the glycerol backbone of the triglyceride Chuck (2007). Chuck (2007) compared the value from this method using HPLC and found small error (i.e. standard deviation of 3%).

The conversion to FAME (in %) can be calculated from:

$$\text{Conversion to FAME}(\%) = 100 \times \frac{5 \times I_{ME}}{5 \times I_{ME} + 9 \times I_{TG}} \qquad (3.1)$$

where I_{ME} is the integration value of the methyl ester protons and I_{TG} is the integration value of the glyceridic protons in ^{1}H NMR.

According to Knothe (2000), the factors 5 and 9 in Eq. 3.1 result from the fact that the glyceryl moiety of a triglyceride has five protons and the three methyl ester moieties resulting from one triglyceride molecule have nine protons. This is shown in Figure 3.5. The mono- and diacylglycerides, which are formed as intermediates in the transesterification reaction, exhibit signals of their glyceridic protons in the same regions as glyceridic protons of the triacylglycerides in the feedstock .

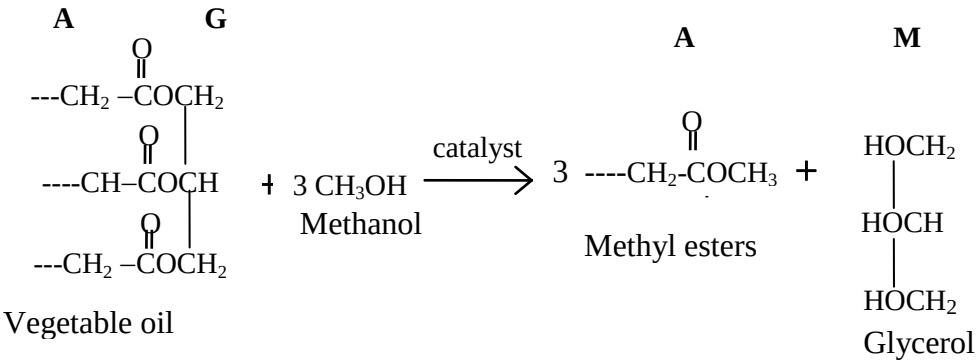

A = a-CH_2 protons, G = glyceridic protons and M = methyl esters protons

Figure 3.3: Reaction scheme of transesterification (adapted from Knothe, 2001).

A standard ^{1}H NMR spectrum of a blend of pure FAME and vegetable oil is illustrated in Figure 3.3. Every peak represents a chemical structure as shown in the legend. Figure 3.4 shows the difference in molecular structure between the triglyceride and FAME.

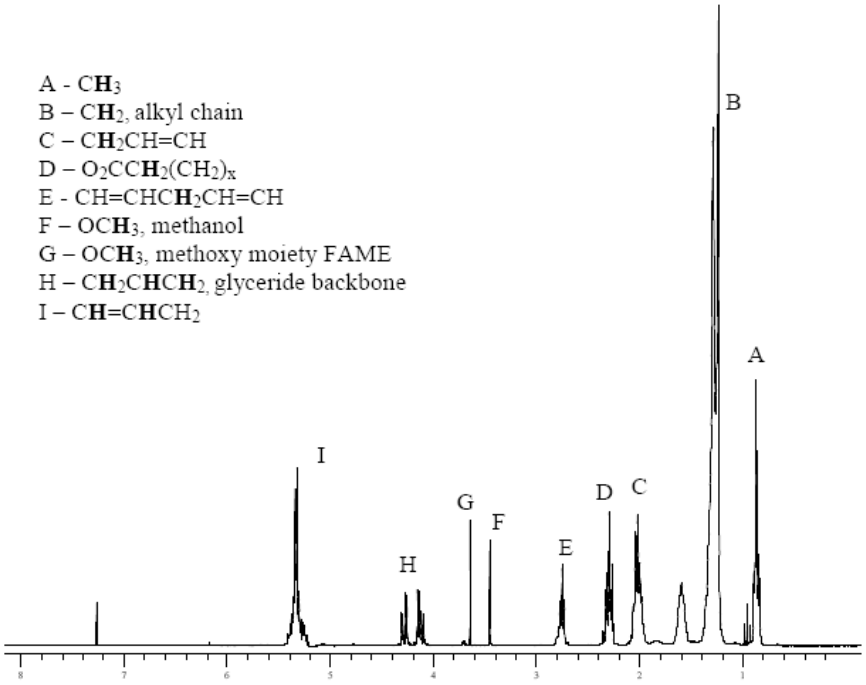

Figure 3.4: ^{1}H NMR spectrum of a blend of FAME and soybean oil (adapted from Chuck, 2007, p.49).

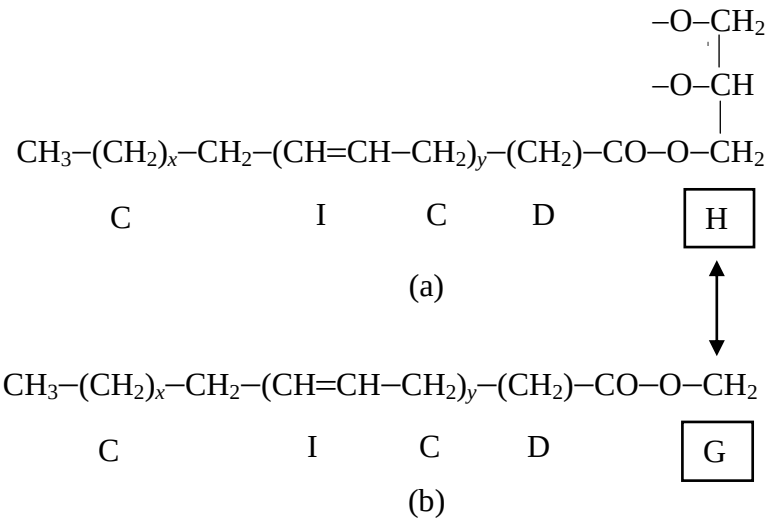

Figure 3.5: Molecular structure of (a) triglyceride and (b) fatty acid methyl ester.

<u>Example calculation No 1</u>: Determining the conversion of FAME from ^{1}H NMR spectrum.

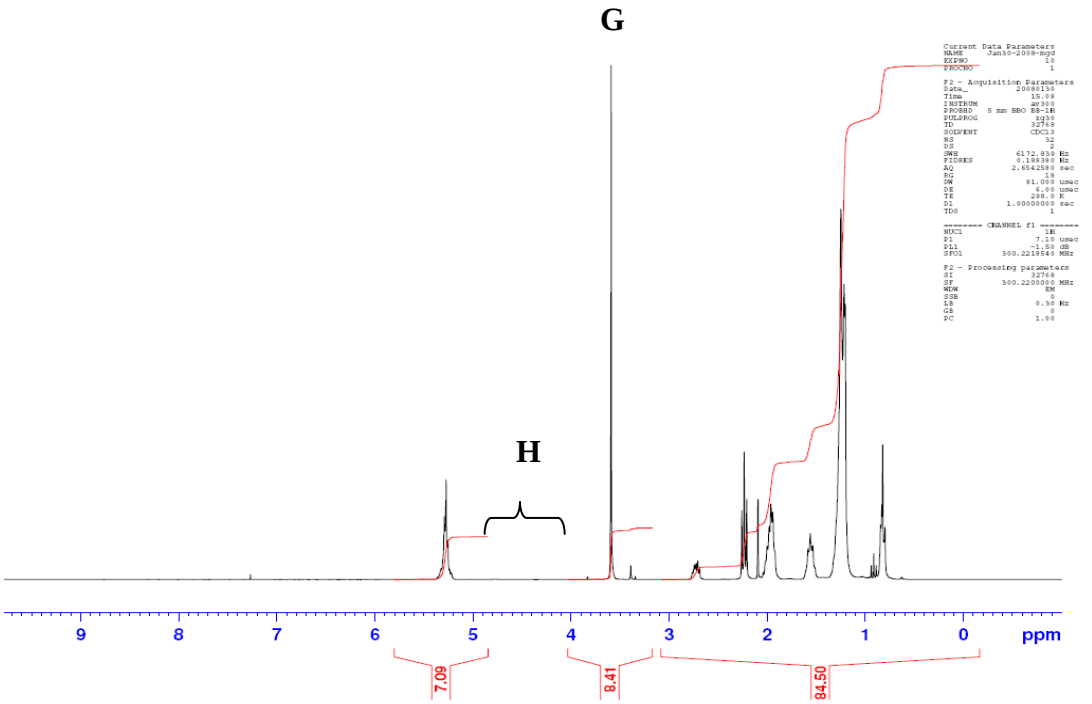

Figure 3.6: ^{1}H NMR spectrum of 100% FAME.

First in Figure 3.6, the peak G at 3.6-3.7 ppm was identified as the biodiesel peak, and then the peak H at 4.0-4.2 ppm was identified as the triglyceride peak. For 100% conversion, there was no peak at the H region. For information, all the preliminary experiments, P1, P2 and P3, achieved almost 100% conversion of oil to FAME. Therfore, for 100% conversion, it is not necessary to make use of Eq. 3.1.

End of example**.**

Example calculation No 2:

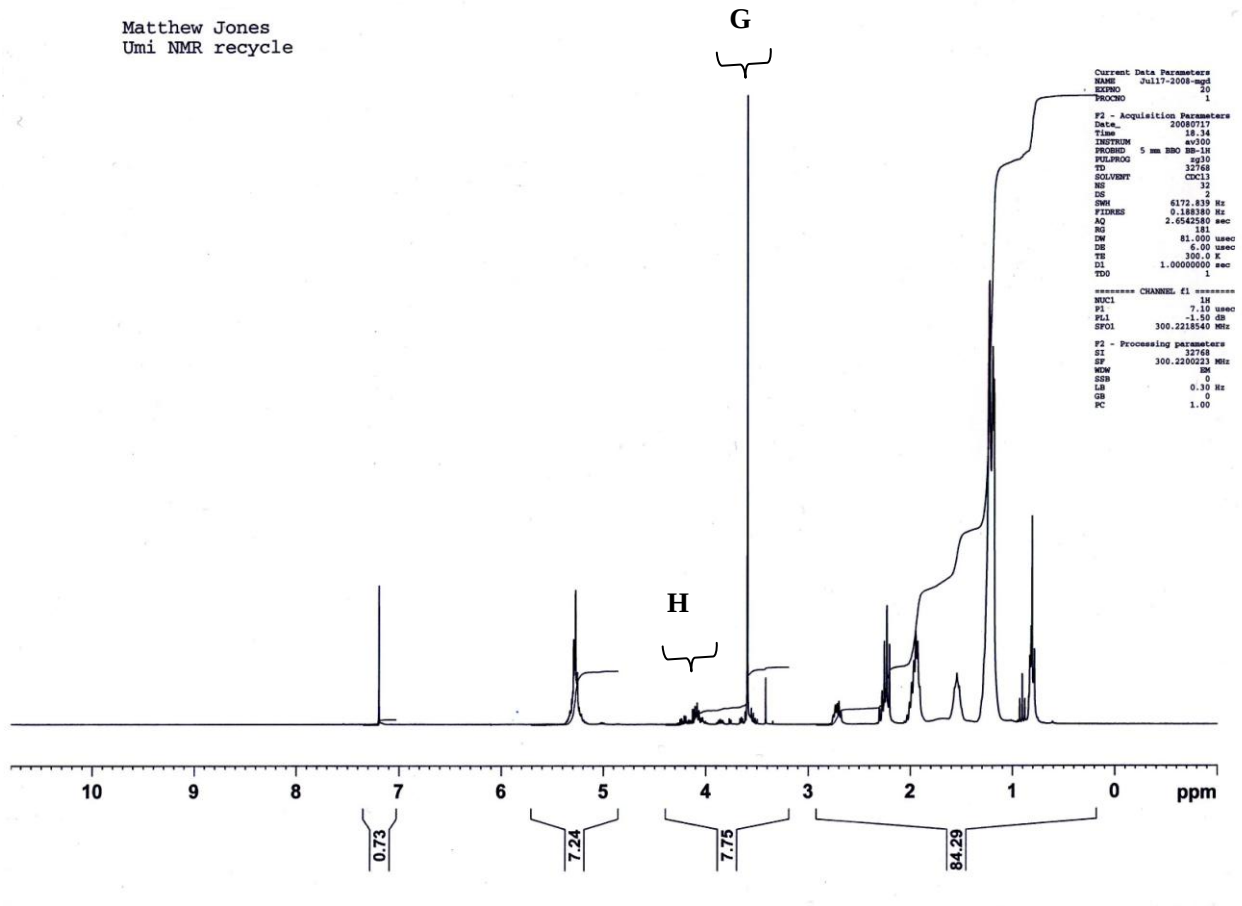

Figure 3.7: ^{1}H NMR spectrum of 57% FAME.

From the spectrum in Figure 3.7, there is a peak in the H region. The biodiesel peak, G is compared with peak H, by doing the integration in the software provided within the machine. The results were:

I_{ME} (is the integration values of the methyl ester) = 2.3687

I_{TG} glyceridic = 1

Using Eq. 3.1, then

$$\text{Conversion to FAME}(\%) = 100 \times \frac{5 \times I_{ME}}{5 \times I_{ME} + 9 \times I_{TG}}$$

$$= 100 \times \frac{5 \times 2.3687}{(5 \times 2.3687) + 9} = 57\%$$

End of example.

3.3 Gas Chromatography method

Gas chromatography (GC) analysis has been developed to determine the component mixtures containing fatty acid esters, glycerol, mono-, di-, and tri-glycerides derivatives from transesterification reaction of vegetable oil (e.g. Plank and Lorbeer,1995; Ruppel and Huybright, 2008).

The following important points are highlighted from Plank and Lorbeer (1995):

(i) In principle, glycerol, mono-, di- and triglycerides can be analyzed on highly inert columns coated with a polar stationary phase without derivatization. The inertness of the column, required to obtain good peak shapes and satisfactory recoveries, cannot be easily maintained in routine analysis.

(ii) Trimethylsilylation of the free hydroxyl groups of glycerol, mono- and diglycerides, ensures excellent peak shapes, good recoveries and low detection limits. [Trimethylsilylation is the addition of trimethylsilyl groups (consists of three methyl groups bonded to a silicon atom) to a molecule].

(iii) For complete silylation of glycerol and partial glycerides, the conditions of the derivatization reaction have to be controlled carefully. This can be achieved by employing silylating agents such as MSTFA or BSTFA. The use of an internal standard, 1,2,4-butanetriol, serves as a very sensitive indicator of incomplete derivatization.

(iv) Peak identification was achieved by analysis of samples spiked with a reference substances, or by comparison with reference chromatograms.

According to McCurry and Wang (2008), it was recommended that a retention gap be used between the GC inlet and the column. The retention gap (see Figure 3.8) would improve peak shape and sample vaporization, as well as maintain column efficiency. This recommendation was adapted in this thesis.

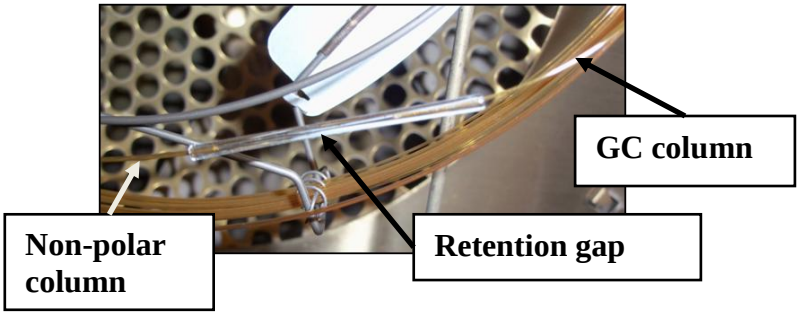

Figure 3.8: Retention gap in GC column.

A number of GC methods that have been used for the determination of biodiesel and its components has been compared in order to develop a new suitable method for this thesis. These are summarised in Table 3.1.

It is important to emphasize, that this method had not been used previously either in the Department of Chemistry by Chuck (2007), or in the Department of Chemical Engineering. Therefore, the method had to be developed for the available GC (see Figure) in the department.

3.3.1 Instrumentation

For this work, GC analysis was performed using a Hewlett Packard 5890 Series II Gas Chromatograph (UK/US) equipped with a Flame Ionisation Detector (FID) and an on-column injector. The type of column used was a 5 % phenyl fused silica capillary column (10 m × 0.32 mm ID × 0.1 μm), supplied by: Thermo Scientific, UK. A number of trials were done to establish the method by referring to earlier works (in Table 3.1). The selected temperature programme and GC conditions for this thesis are shown in Table 3.2.

Table 3.1: Selected GC operating conditions for simultaneous determination of methyl esters, glycerol, mono-, di- and triglycerides.

Instrument	Column	Detector	Oven temperature	Carrier gas	Injector	Reference
Fisons Instruments GC 8000	Pre-column: uncoated deactivated fused-silica (2 m × 0.53 m ID) connected in series with fused-silica capillary column (10 m × 0.32 mm ID × 0.1 μm film)	Flame Ionization Detector (FID) at 370°C	Initial at 50°C for 1 min Rate 1: 15°C min^{-1} to 180°C Rate 2: 7°C min^{-1} to 230°C ballistically to 370°C, then hold for 10 min	H_2 at 3 ml min^{-1} N_2 as make-up gas at inlet pressure of 0.5 bar	On-column injector at oven temperature program	Plank and Lorbeer (1995)
Agilent 7890A GC	Agilent DB-5ht (15 m × 0.32 mm ID × 0.1 μm film) with 2 m × 0.53 mm ID retention gap	Flame Ionization Detector (FID) at 380°C	Initial at 50°C for 1 min Rate 1: 15°C min^{-1} to 180°C Rate 2: 7°C min^{-1} to 230°C Rate 3: 30°C min^{-1} to 380°C hold for 10 min	Helium at 3 ml min^{-1}	On-column injector at oven temperature program	McCurry (2009)
PerkinElmer Clarus GC	Elite-5HT (15 m 15 m × 0.32 mm ID × 0.1 μm film) with a guard column of (254 mm × 0.53 mm ID)	Flame Ionization Detector (FID) at 380°C	Initial at 50°C for 1 min Rate 1: 15°C min^{-1} to 180°C Rate 2: 7°C min^{-1} to 230°C Rate 3: 30°C min^{-1} to 380°C hold for 10 min	Helium at 3 ml min^{-1} Air at 450 ml min^{-1} H_2 at 45 ml min^{-1} as make-up gas	On-column injector at oven temperature program	Ruppel and Hall (2007)

Table 3.2: GC condition for biodiesel and its derivatives.

Oven Program Initial Temperature: Hold Time 1: Ramp 1: Oven Program Temperature 2: Hold Time 2: Ramp 2: Oven Program Temperature 3: Hold Time 3: Ramp 3: Oven Program Final Temperature Hold time	60°C 1 min 15°C min^{-1} 180°C 0 min 7°C min^{-1} 230°C 0 min 30°C min^{-1} 330°C 10 min
Carrier Gas:	Helium (30 ml min^{-1})
FID Temperature Hydrogen Flow: Air Flow:	300°C 33 ml min^{-1} 400 ml min^{-1}
Injector Temperature: Injection volume:	oven temperature track mode 1 μl

In Figure 3.9, the temperature ramp set for the components is illustrated. The chromatogram of all the components produced by this GC is shown in Figure 3.10.

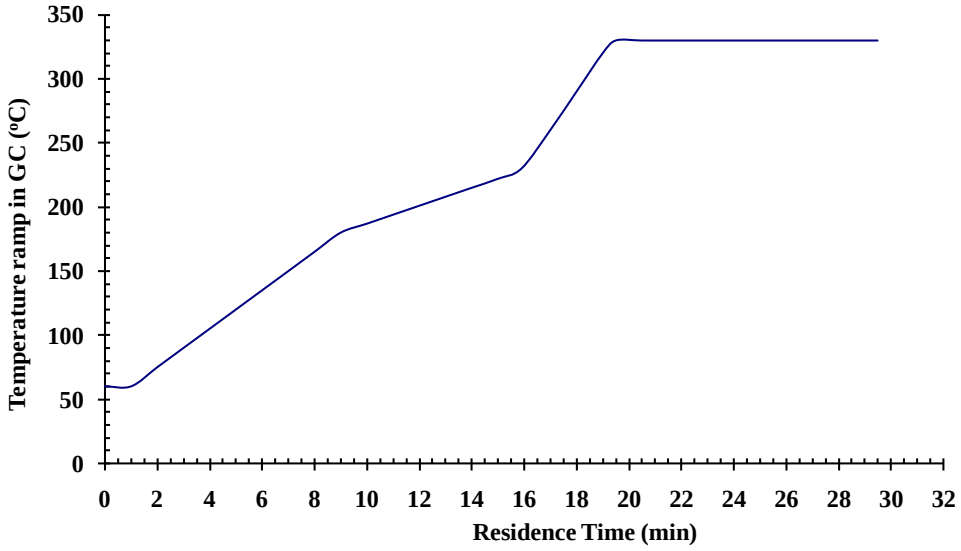

Figure 3.9: Temperature ramp for GC.

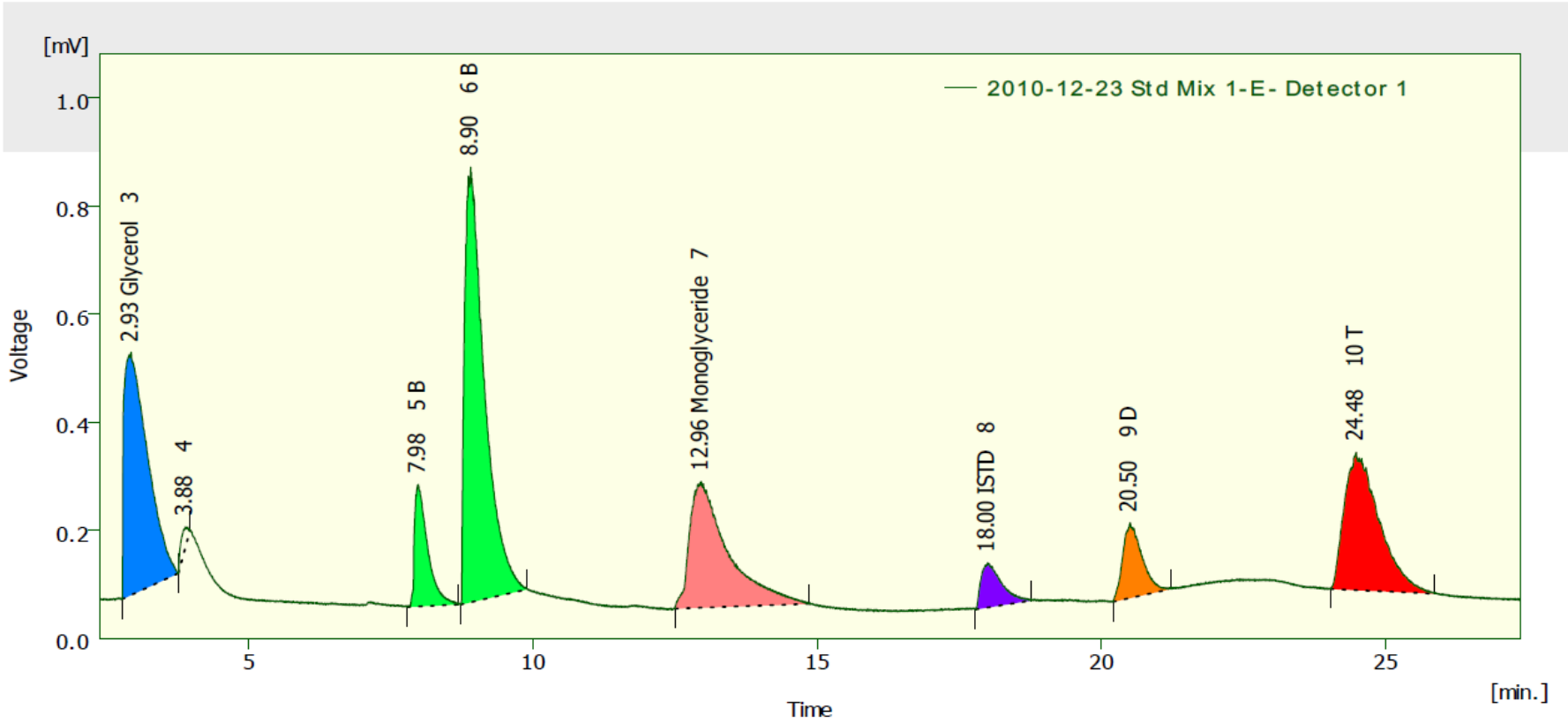

Figure 3.10: Chromatogram of biodiesel product and its intermediates (Abbreviation used in the GC programme: B = Fatty acid methyl esters or biodiesel, D = Diglycerides, T = Triglyceride and ISTD = Internal standard (tricaprin)).

3.3.2 Data Acquisition

The signal from the GC was processed by using ClarityLite Software in combination with a WindowsXP compatible personal computer. The Clarity Lite chromatography station was purchased separately from DataApex to acquire and evaluate data from the chromatographs (with standard analog output using an A/D (Analog-to-digital) converter). The chromatogram from each analysis was linked to a calibration file in the software, giving the calibrated result for every analysis. The amount of each standard (methyl esters, tri-, di- and monoglyceride, methyl ester and glycerol) was first calibrated by obtaining a linear calibration at different known concentrations. The calibrations for all of the standard components are included in Appendix D.

To represent tri-, di- and monoglyceride, reference standards of Triolein, Diolein, Monoolein were used respectively. For the methyl ester compound, a commercial biodiesel (B100) from rapeseed oil (BroadLand Fuel Brand) was used. The known 100% biodiesel made in the lab (using base catalyst) was also used, and demonstrated the same result.

3.3.3 Preparation of samples and standard solutions

The method to prepare the solution of samples and standards was taken from Plank and Lorbeer (1995) with some modification. Standard stock solutions in pyridine were used:

- Glycerol (Sigma-Aldrich, ≥ 99%) 5 mg ml^{-1}
- Monoolein (Sigma-Aldrich, ≥ 99%) 4.0 mg ml^{-1}
- Diolein (Sigma-Aldrich, ≥ 99%) 4.0 mg ml^{-1}
- Triolein (Sigma-Aldrich, ≥ 99%) 5.0 mg ml^{-1}
- Rapeseed methyl ester (B100, Broadland Fuels, UK) 3.0 mg ml^{-1}.

These were used to prepare standard solution mixtures at 5 different concentration levels. The silylating agent used was MTSFA (trimethylsilyl trifloruoroacetamide). The internal standards used were 8.0 mg ml^{-1} of 1,2,4-butanetriol and 8.0 mg ml^{-1} of Tricaprin.

The preparation of standard solution mixtures was as follows:

i) An appropriate amount (varied from 20 to 380 μl) of the standard solution was transferred and mixed in a screw cap vial. [Note that the total amount must be 380 μl].
ii) Then 60 μl MSTFA (N-methyl-N-trimethylsilyl-trifluoroacetamide) was added to the mixture and left at room temperature for at least 30 minutes.
iii) After that, 30 μl butanetriol and 30 μl of tricaprin was added to the solution.
iv) Then, 1.0 ml of n-heptane was added.

The samples were prepared as follows:

i) Preparation of sample solution in pyridine :
   - The sample from the experiment was shaken prior to sample solution preparation.
   - An amount of 20 to 30 μl of the sample was drawn using a 1 ml syringe. Then, the sample was filtered using syringe filter (Millex hydrophobic, PTFE membrane, non sterile and 0.2 μm pore size) while transferring the sample to a vial.
   - The filtered sample was then diluted to 1 ml with pyridine.
ii) Silylation process: 380 μl of sample solution in pyridine was taken and diluted with 60 μl of MSTFA (N-methyl-N-trimethylsilyl-trifluoroacetamide) and left at room temperature for at least 30 minutes.
iii) Then the internal standards, 30 μl butanetriol and 30 μl of tricaprin were added to the solution.
iv) Finally, the mixed solution was diluted with n-heptane to achieve a total volume of 1.5 ml.

Note:

MSTFA solution was only used in sample preparation (for silylation reaction).

Calibration using these standards are included in Appendix E.

3.3.4 Calculation and expression of results

The mass content of component i, in the sample, as a wt (%) can be calculated from the formula

$$\left(\text{wt\% of component } i\right)=\frac{\left(\text{Mass concentration of component } i\right)}{\sum_{i=1}^{i=5}\left(\text{Mass concentration of component } i\right)}\times 100 \tag{3.2}$$

where i = 1 to 5 representing the five components.

The overall conversion of triglyceride (TG) can be expressed as:

$$X=\frac{\mathrm{Wt_{TG,0}}-\mathrm{Wt_{TG}}}{\mathrm{Wt_{TG,0}}} \tag{3.3}$$

where $\mathrm{Wt_{TG,0}}$ is the amount of TG at t = 0, and $\mathrm{Wt_{TG}}$ is an amount of TG at t = t, the unit of Wt is wt %.

To check the accuracy of this method, three different standard mixtures (containing known concentrations of all key components) were injected into the GC. The results obtained were expressed as wt % according to Eq. 3.2. The error was calculated from:

$$\text{Error (\%)} = \frac{\text{Actual value-value obtained}}{\text{Actual value}}\times 100 \tag{3.4}$$

The maximum error values are shown in Table 3.3.

Table 3.3: Maximum error for GC method.

Component	Maximum error (%)
Triglyceride	0.10
Diglyceride	0.40
Monoglyceride	1.00
Glycerol	0.20
Biodiesel	0.2

3.4 Conclusions

(a) The ^{1}H NMR method is suitable to calculate the conversion to FAME. This was tested and will be used in Chapter 4.

(b) The GC method was developed and tested. This will be used in Chapter 5 to determine the composition of individual species.

(c) The comparison for both methods as follows.

	^{1}H NMR	**GC**
Determination of intermediates compounds	Not possible.	Possible.
Sample preparation	Simple	Difficult
Analysis time	Short (less than 5 minutes per sample)	Long (35 to 45 mins per sample)
Reproducibility and accuracy	Good. Std Dev = 3% (Error was calculated by comparing the result analysis with HPLC method).	Good. (Error = see Table 3.3) Accuracy of GC analyses can be influenced by factors such as baseline drift, overlapping signals, etc (Knothe, 2000).

REFERENCES

Arzamendi, G., Arguinarena, E, Campo, I and Gandia, L.M., 2006. Monitoring of biodiesel production: Simultaneous analysis of the tranesterification products using size-exclusion chromatography. *Chemical Engineering Journal*, 122, pp 31-40.

Chuck, C.M., 2007. *Lewis Acid Catalyst Design for the Transesterification of Lower Quality Feedstock for Biodiesel Production*. Thesis (PhD). Department of Chemistry, University of Bath.

Knothe, G., 2000. Monitoring a processing transesterification reaction by fiber-optic near infrared spectroscopy with correlation to ^{1}H Nuclear Magnetic Resonance spectroscopy. *Journal of American Oils Chemists Society*, 77 (5), pp. 489-493.

McCurry, J. D. and Wang, C. X., 2007. Analysis of Glycerin and Glycerides in Biodiesel (B100) Using ASTM D6584 and EN14105. *Application Note. Agilent Technologies, Inc. 2007* [online]. Available from: http://www.chem.agilent.com/Library/applications/5989-7269EN.pdf [accessed on 6/4/2009].

Meher, L.C., Vidya Sagar, D. and Naik, S.N., 2006. Technical aspects of biodiesel production by transesterification—a review. *Renewable and Sustainable Energy Reviews*, 10, pp 248–268.

Plank, C. and Lorbeer, E., 1995. Simultaneous determination of glycerol, and mono-, di and triglycerides in vegetable oil methyl esters by capillary gas chromatography. *Journal of Chromatography A*, 697, pp. 461-468.

Ruppel, T. and Huybrighs, T., 2008. Fatty Acid Methyl Esters in b100 biodiesel by gas chromatography (Modified EN 14103). *Application Note, Gas Chromatography. Perkin Elmer Inc*. [online] available from http://las.perkinelmer.com/Content/ApplicationNotes/APP_FAMEbyGCinB100Biodiesel.pdf. [Accessed on 7/3/2008].

CHAPTER 4

USE OF ZINC PROLINE AS A CATALYST ON A MONOLITH SUPPORT

In earlier work in the Department of Chemistry (University of Bath), Chuck (2007) identified that zinc proline in powder form was a suitable catalyst for the transesterification reaction. So, in this chapter this aspect is considered in more detail, and a method is developed of immobilizing the catalyst onto a cordierite monolith. The performance of the coated monolith in a batch reactor is then studied.

Part of the work done in this chapter was presented at an international conference on 3rd International Conference on Structured Catalysts and Reactors, ICOSCAR-3 (Italy, 27 to 30 September 2009) and leads to a publication in Catalysis Today (see Appendix B).

4.1 Introduction

4.1.1 Zinc proline catalyst

Among many others, catalysts based on amino acid complexes were studied by Chuck (2007), zinc proline was identified as the most highly active catalyst in a situation where the quality of the oil feedstock was low. It is reported that 93 to 96% conversion of FAME was obtained for vegetable oil feedstock, with a 0.56% FFA and 2 wt% of water. The reaction conditions used for this catalyst were 180°C at a pressure of 20 bar. The details of the conditions and results of the experiments are shown in Table 4.1.

Table 4.1: Experimental conditions and results for catalytic activity of zinc proline (based on data in Chuck, 2007).

Experiment	**(i)**	**(ii)**
Feedstock oil	Soybean oil	Rapeseed oil
Stearic acid content	0 to 30 wt %	0.56 %
Water content	0 to 5 wt %	0 wt %
Molar ratio of oil to methanol	1 : 12	1 : 6
Amount of oil	36.8 ml	330 g
Amount of methanol	19.5 ml	72 g
Catalyst amount	0.9 wt % of oil	0.9 wt % of oil
Mass of zinc proline	0.3 g	3 g
Temperature	195 °C	200 °C
Speed of rotation	1500 rpm	1500 rpm
Operating pressure	20 bar	20 bar
Conversion of oil into FAME	69 % with 0 % FFA and 0 % water 96% with 0% of FFA and 0.5% water 93% with 2% of FFA and 0 % water	83.3%

The discussion found in Chuck (2007) includes, the following set of important remarks about the zinc proline catalyst:

(a) Zinc proline is presumably catalysing the esterification of the stearic acid, producing FAME and water. There is not a high enough FFA content to explain the large rise in activity and so it is likely that the water is increasing the activity of the zinc proline catalyst. This trend is also observed on the addition of water alone to the reaction. If all the stearic acid (2 wt%) was esterified it would produce 2.5 mmol of water.

(b) Water has a large effect on the activity of the zinc proline catalyst. Counter intuitively, an increase in water increases the activity of the catalyst. Just a 0.25 wt% (~5 mmol) amount of water increases the activity of the zinc proline catalyst. This reactivity is slightly diminished on addition of larger volumes but is still far greater than in the absence of water.

The structure of zinc proline is shown in Figure 4.1, and Table 4.2 contains data on the properties of zinc proline. Zinc proline is probably tetrahedral - though its crystal structure has water bound into the complex, so it is more than four co-ordinate in the structure (Chuck, 2011).

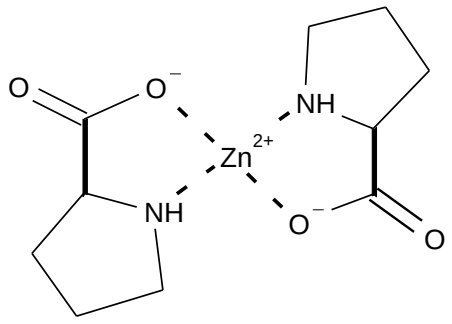

Figure 4.1: Molecular structure of zinc proline (adapted from Chuck 2007).

Table 4.2: Physical properties of zinc proline catalyst.

General formula	$Zn(C_5H_8NO_2)_2$
Solubility	Soluble in water Insoluble in methanol, vegetable oil or biodiesel
pH in solution	Neutral (i.e. pH 7) in a water solution
Melting point	250+° C
Stability	Very stable in light or air
Toxicology	Harmless

It is important to emphasize, that in Chuck (2007), experiments were performed in a batch reactor, and the zinc proline was used as a very fine powdered catalyst (16 to 144 µm in size), that was then discharged with the product. There was no attempt made to immobilise the catalyst and retain it in the reactor.

4.1.2 Monolithic Catalysts

Monolithic catalyst supports offer an interesting alternative for conventional catalysts in randomly packed beds or slurry reactors (Nijhuis *et al*., 2001 and Hoek *et al*., 2004). The following are the significant advantages of monoliths over other types of structured packing found in Nijhuis *et al*. (2001):

i) The most common material for monolithic structures is cordierite. This is a ceramic material consisting of magnesia, silica, and alumina in the ratio of 2:5:2, which has high mechanical strength, can stand high temperatures and temperature shocks, and has a low thermal expansion coefficient.

ii) The porous ceramic material is easier to use as a catalyst support than the metal of the conventional structured packing (easier to bond the catalyst to the support). When coating metal supports with a catalyst or catalyst support material, an intermediate layer of a ceramic is often used for a better binding.

iii) The cost of monolithic supports is relatively low, mainly due to the large-scale production for the automotive industry and relatively simple production method (i.e. *via* an extrusion process).

Due to these benefits (i to iii), it was decided to use the cordierite monolith as a support for the zinc proline catalyst. As mentioned in Nijhuis *et al.* (2001), ready-made catalysts or other catalysts that do not need a specific support material, such as zeolites, can be coated or synthesized directly on a monolith body. Different techniques for coating a layer of material on a monolith support e.g. colloidal coating, sol–gel coating, slurry coating, and polymer coating have been discussed in Nijhuis *et al.* (2001). The same procedures can be utilized for the deposition of the active phase on a monolith support with some adaptations. Because zinc proline is dissolved into water, it is possible to make a slurry or colloidal solution which later can be coated onto the cordierite monolith surface.

Principally, there are two possible methods to anchor the catalyst layer onto the monolith surface (see Figure 4.2): (i) pore filling coating - the macroporous catalysts (partly) are filled with the high surface-area material, or (ii) slurry coating - the catalysts are deposited as a layer in the pores on the monolith surface (Nijhuis *et al.*, 2001).

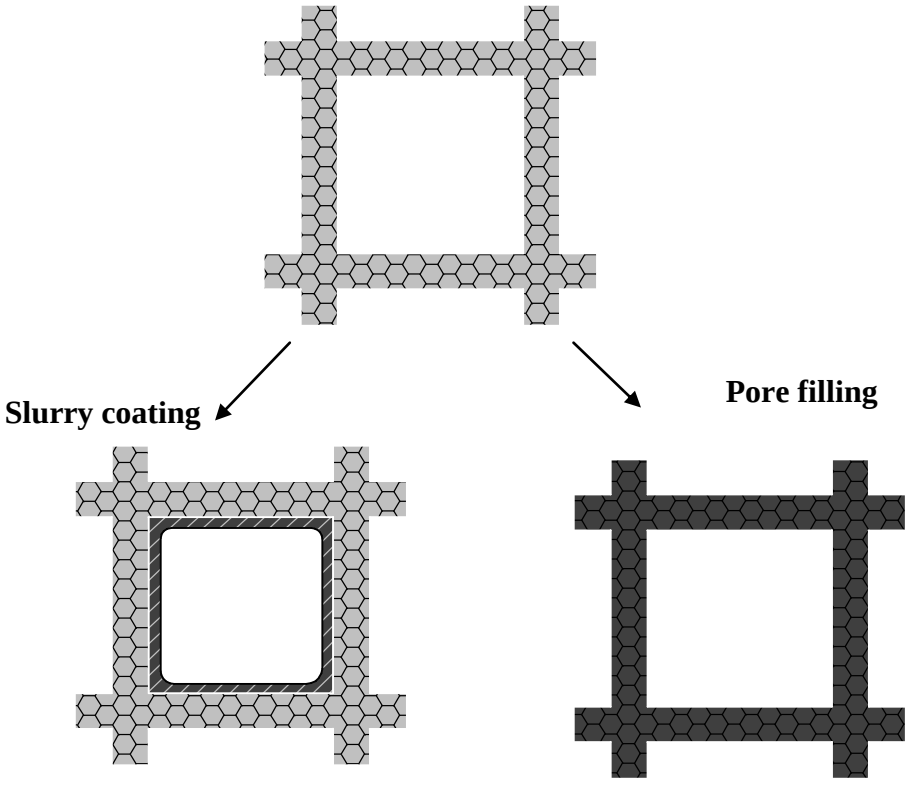

Figure 4.2: Schematic representation of the difference between slurry-coating and pore-filling-coating methods (adapted from Nijhuis *et al.*, 2001).

The following are important guidelines presented in Nijhuis *et al*. (2001):

i) **Coating using colloidal solutions for pore-filling method**: A typical procedure for coating a monolith in this manner is to dry the monolith (a few hours at 383 K) and then to submerge it in the colloidal coating solution for a few seconds after cooling the monolith. The excess liquid is shaken out, and the liquid still remaining in the channels is gently blown out using pressurized air. The monoliths are dried horizontally at room temperature while continuously being rotated around their axes. Finally, the monoliths are calcined in air (for alumina or silica typically at 723 K).

ii) **Coating using slurry solution for slurry coating**: The basic principle of slurry-coating procedures is demonstrated in Figure 4.3. Because the coating is carried out using relatively large particles, the contact surface between these particles and the support is small. Therefore, a binding agent should be added to increase the contact surface. All components of the coating slurry should be well mixed using a high-shear mixer until the slurry is homogeneous. A dried monolith should be dipped into this slurry for a short period. Very short (a few seconds) dipping times result in a slightly higher loading (5 to 10% relative increase) than longer dipping times (a few minutes), because a dry monolith will rapidly absorb liquid and draw extra particles against the wall (slip-casting). A longer period of dipping will reduce this amount. After dipping, excess liquid is shaken out of the monolith and the channels are cleared using pressurized air. The monolith is dried horizontally while continuously being rotated around its axis. Finally, the monolith is calcined in air, typically at 673 to 1173 K depending on the catalyst coated. The minimum calcination temperature of 673 K is used to obtain a good physical interaction among catalyst, binder, and support. However, the applicability of this method is limited to catalysts that are thermostable up to that temperature.

Based on these guidelines, the process in Figure 4.3 was developed to coat monolith with the zinc proline catalyst.

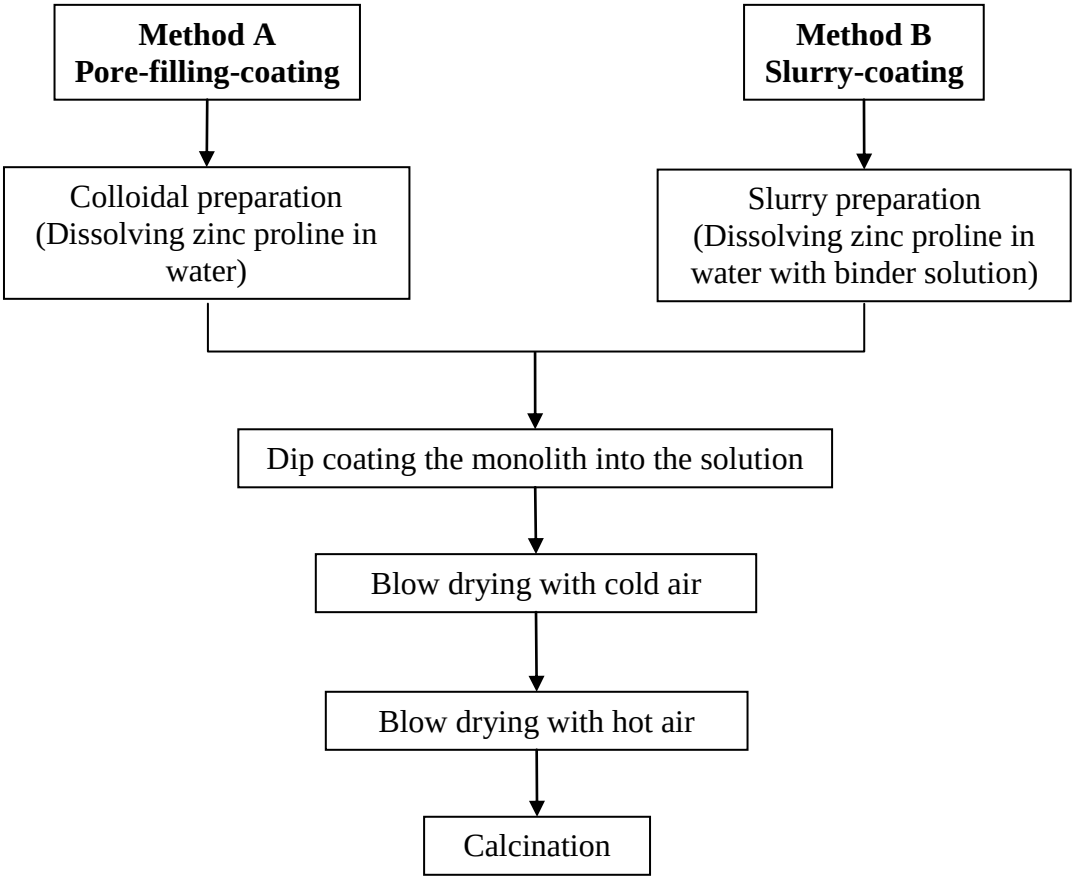

Figure 4.3: Summary illustrating the two methods used to coat the cordierite monolith with zinc proline catalyst.

The drying steps in the slurry-coating process are illustrated in Figure 4.4.

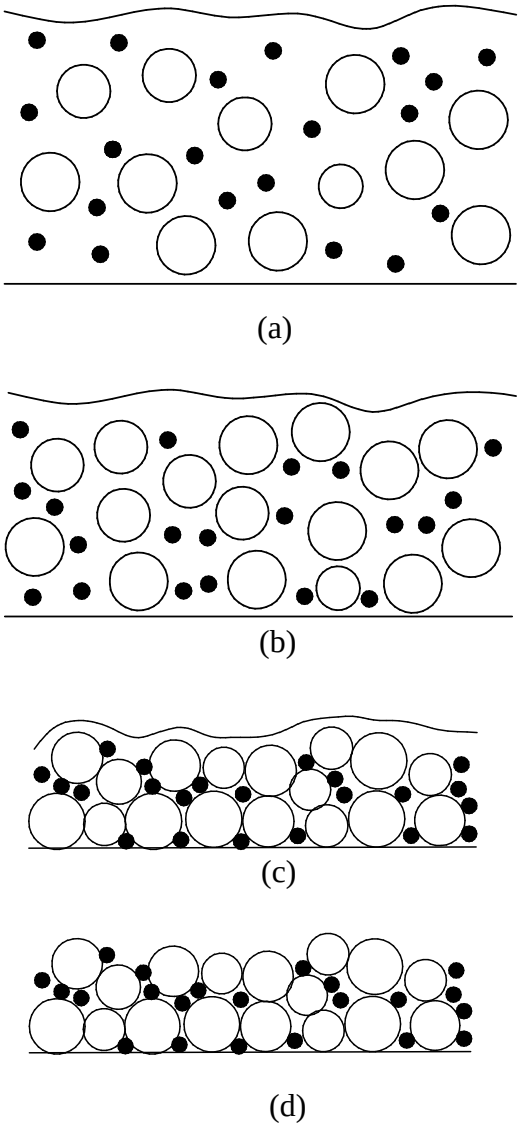

Figure 4.4: Schematic representation of the drying steps in the slurry-coating process:

(a) wet slurry on surface [large white circles: material to be coated (catalyst support or catalyst, typically 5 μm); black dots: binder (typically 20 to 50 nm)];

(b) first stages of drying, particles still suspended in liquid;

(c) large support/catalyst particles touch each other, binder still free-floating;

(d) binder deposited at interfaces between particles by capillary forces during final stages in drying.

In developing the coating procedure, a number of issues relating to the use of zinc proline were taken into consideration:

i) According to Kofoed *et al.* (2006), the addition of acid or base into zinc proline will denature the zinc proline structure. The change of zinc proline structure with pH is shown in Figure 4.5.

ii) Zinc proline tends to start to oxidise at a temperature above 150°C, and this was discovered in preliminary experimental trials.

iii) Zinc proline has a limited solubility in water. Although zinc proline is considered water-soluble, it was observed that a prepared solution of zinc proline in water was not homogeneous (i.e. the zinc proline in water solution separated into two layers).

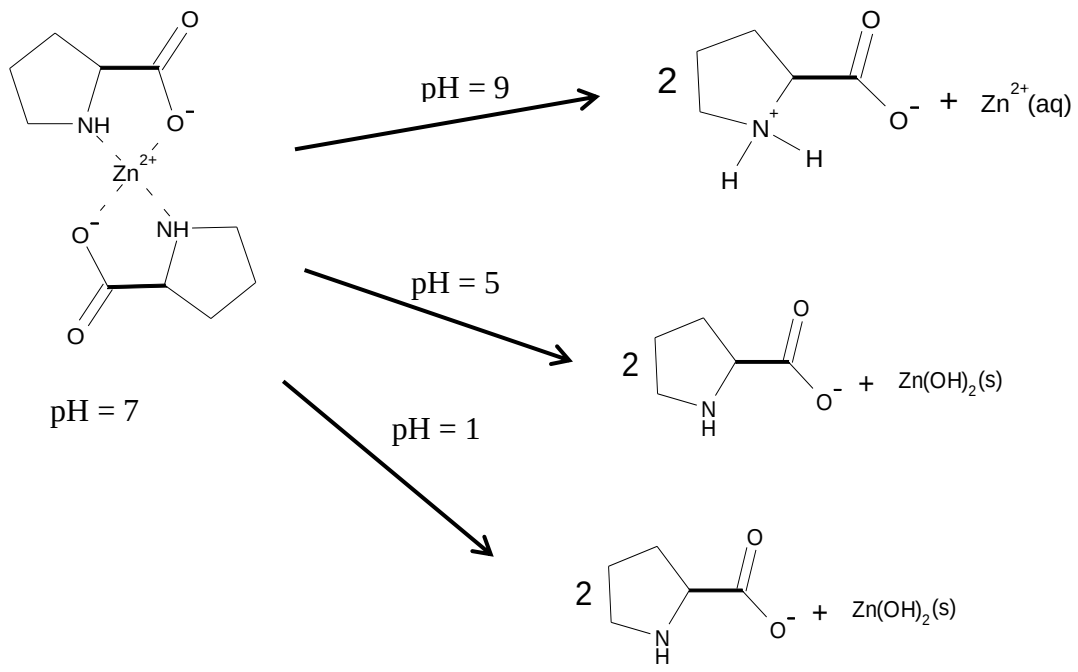

Figure 4.5: Zinc proline compound decomposed with pH (adapted from Kofoed *et al.* (2006)).

4.2 Experimental

4.2.1 Catalyst preparation

These were prepared as powders, and also in the form of coated monoliths.

4.2.1.1 Zinc proline powder

The catalyst was prepared (Chuck, 2007) by mixing:

- proline (or 2-carboxypyrrolidine) (Sigma-Aldrich) 36.81 wt %,
- triethylamine (Sigma-Aldrich) 28.16 wt%,
- zinc acetate (Sigma-Aldrich) 35.03 wt%,

for one hour. Triethylamine in this reaction was acted as a catalyst for zinc proline formation. Immediately after mixing, a white aqueous solution was formed (see Figure 4.6 (a)). After one hour, the solution was filtered and washed with 200 ml of methanol. The filtered colloid was then dried by leaving it for two or three days to obtain a powdered form of zinc proline. Figure 4.6 (b) shows the sample of zinc proline powder after being dried and crushed.

(a) (b)

Figure 4.6: Zinc proline catalyst preparation (a) colloidal solution after mixing process and (b) after drying process.

4.2.1.2 Supporting the catalyst on a monolith structure

A coating procedure was developed to immobilize the zinc proline on a cordierite monolith support (supplied by Johnson Matthey, UK) (see Table 4.3), such that the catalyst still remained active for the transesterification reaction studied. Two methods were developed in this work called Method A and B.

Table 4.3: Properties of monolith.

Material	Cordierite ($2MgO\ 2Al_2O_3\ 5SiO_2$)
Square channel	1.1 mm × 1.1 mm
Cell density	62 cells/cm^2
Thickness of monolith wall	0.2 mm

a) Method A: Pore-filling coating

First, the zinc proline powder (0.5 g) was dissolved in 50 ml of water. The solution was then mixed and heated at 100°C for 20 to 30 minutes, until the solution became homogeneous as shown in Figure 4.7. After that, monolith pieces (10 mm × 10 mm × 10 mm) were dipped into the solution 2 to 3 times, for one second each time. Excess liquid was then blown out using a jet of air to remove any excess solution. Then, the coated monoliths were dried using a hot blower at a temperature of approximately 100 °C. The coating process was repeated three times in order to increase the amount of catalyst. Finally, the coated monoliths were heated at 200°C in the presence of nitrogen. The apparatus for this process is shown in Figure 4.8. The final weight of the coated monolith was recorded.

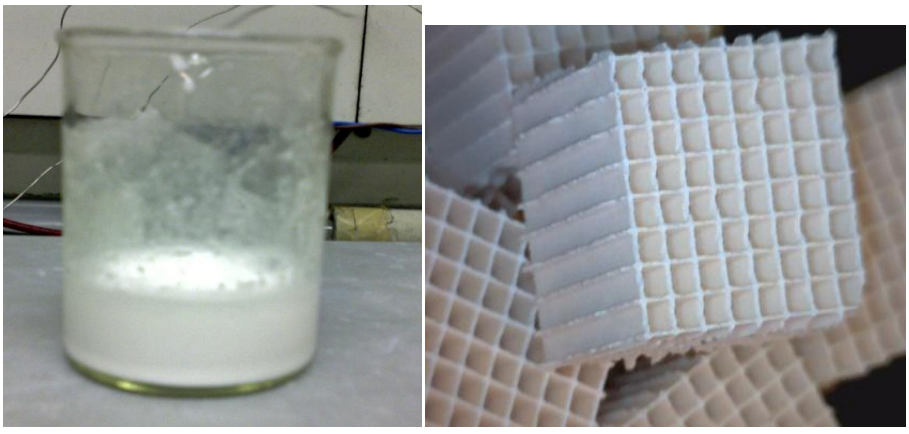

(i) (ii)

Figure 4.7: (i) Zinc proline solution, and (ii) Bare cordierite monolith.

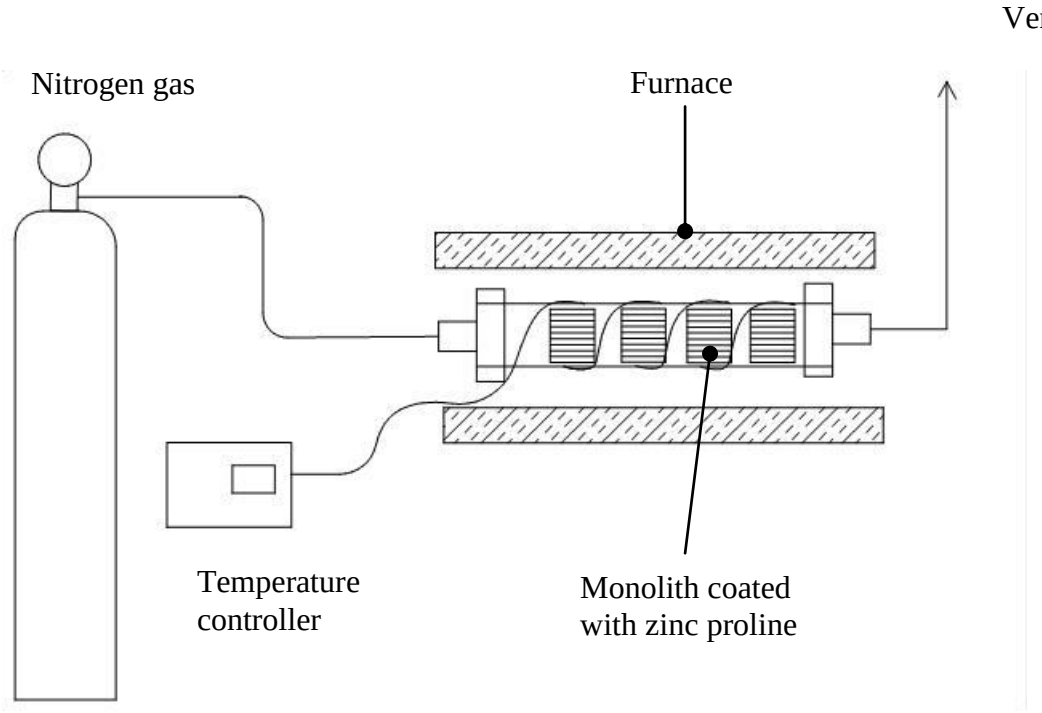

Figure 4.8: A schematic diagram of apparatus used to 'heat treat' the coated monolith.

b) Method B: Slurry coating

In the slurry method, the commercial colloidal silica, Ludox AS30 (Sigma-Aldrich), was used as received. In this method, a zinc proline slurry was prepared by dissolving the zinc proline powder (1.2 g) in 60 ml of water and mixed with 1.0 ml of Ludox AS30 (Aldrich) colloidal silica solution (which is 30 wt% SiO_2 in H_2O). The dipping, coating and calcination processes were the same as in the colloidal coating method.

4.2.2 Catalyst loading

The catalyst loading on the monolith was determined by measuring the mass before and after the preparation steps, using the following formula:

$$\text{Loading} = \frac{W_{coated} - W_0}{W_0} \times 100\% \qquad (4.1)$$

where

W_{coated} is the mass of the coated monolith,

W_0 is the mass of the monolith before dip-coating.

After preparing a number of batches of coated monolith, it was discovered that it was not easy to maintain the same catalyst loading. Although the consistency of each step was maintained as precisely as possible, such as concentration of solution and dipping time, the catalyst loading at the end varied. The comparison of the catalyst loading of zinc proline onto monoliths prepared by the two methods, Method A (colloidal coating) and B (slurry coating) was done by comparing the maximum amount of zinc proline loaded, see Table 4.4. In each method 10 monoliths were used (each piece was 10 mm × 10 mm × 10 mm).

Table 4.4: Maximum zinc proline loading onto 10 pieces of monolith.

Coating Method	**Mass of zinc proline in coated layer on 10 pieces**	**Catalyst Loading**
Method A : Colloidal	0.297 g	4.8 wt%
Method B : Slurry	0.458 g	7.5 wt%

The surface characteristics of: the zinc proline catalyst powder (Figure 4.9), the blank monolith (Figure 4.10), and the zinc proline deposit on the monolith (Figure 4.11 and 4.12) were observed by a Scanning Electron Microscope (SEM). Also, comparing the surface morphology in the SEM in Figures 4.9 and 4.11, similar forms of the rod-like zinc proline structures (≈ 1μm in diameter and 1 to 10 μm long) appear in the magnified pictures of the surface of the particle and on the coated monolith support. The SEM images in Figure 4.12 (a) and (b) show the top view of the cordierite surface covered with zinc proline catalyst with a silica binder. The morphology of the surface is totally different, as the previous rod-like structures now appear attached in petal-like layers. Most of the pores have been covered, as the number of visible pores seems less than in Figure 4.11 (a).

To confirm that zinc proline is being coated onto the monolith, X-ray microanalysis was performed to detect the presence of chemical elements. Figure 4.13 (a) shows the x-ray profile for the cordierite monolith structure. It can be seen that Mg, Al, O and Si peaks appear in both Figures 4.13 (a) and (b), which correspond to the cordierite composition (i.e. $2MgO\ 2Al_2O_3\ 5SiO_2$), while in Figure 4.13 (b), the presence of Zn is detected. This shows that the Zn from the zinc proline catalyst is anchored on the monolith surface.

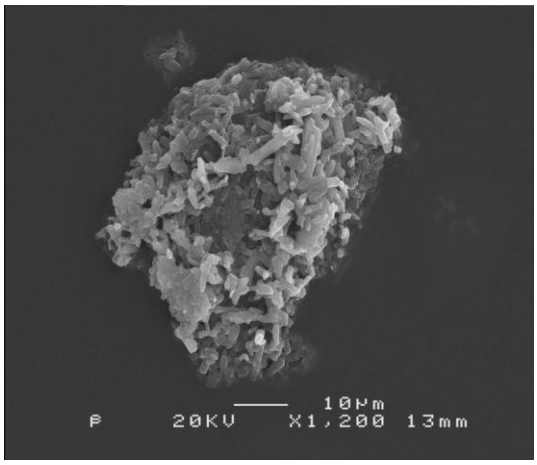

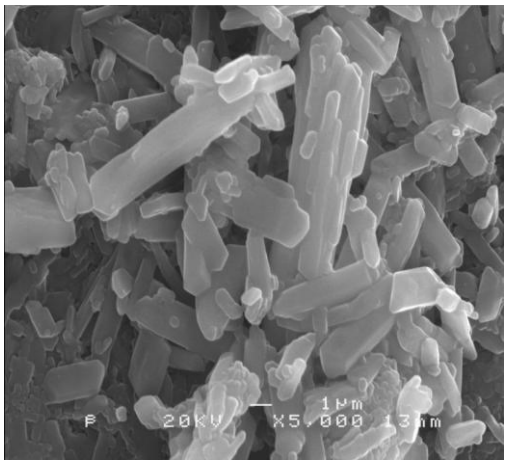

10 μm

1 μm

(a) **(b)**

Figure 4.9: Example SEM of the powdered zinc proline catalyst: (a) example of a particle, (b) magnified view of surface.

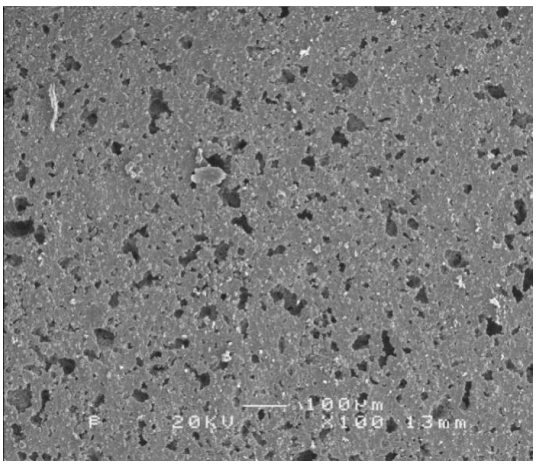

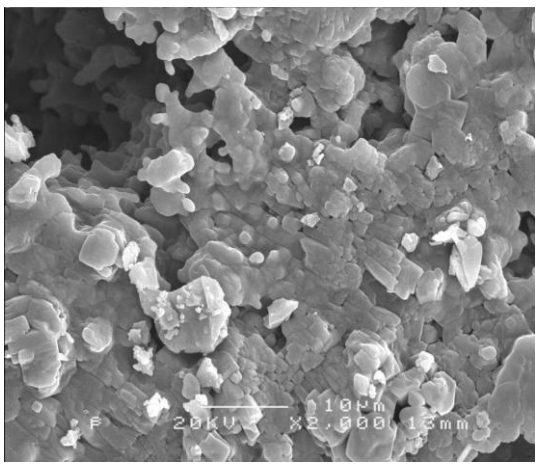

100 μm

10 μm

(a) **(b)**

Figure 4.10: Example SEM of the cordierite monolith: (a) view of surface, (b) magnified view of surface.

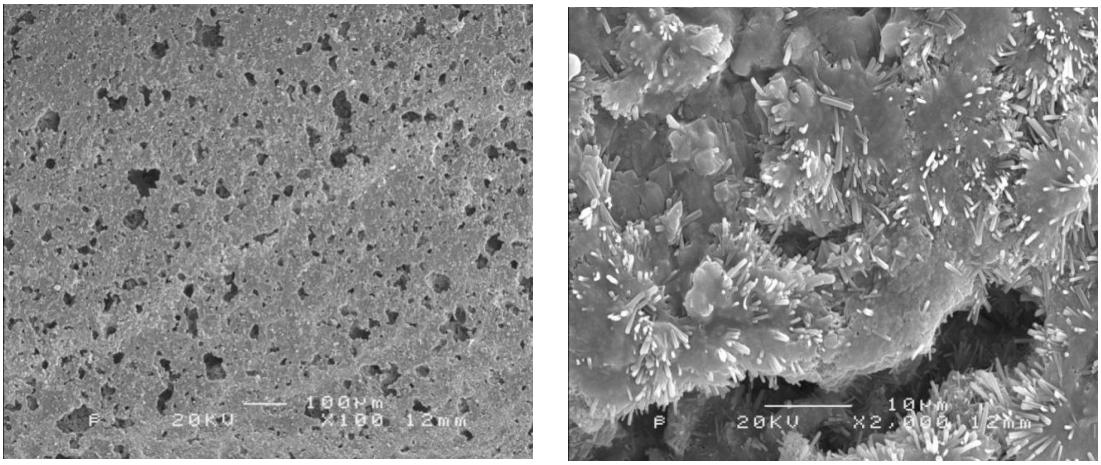

100 μm 10 μm

(a) **(b)**

Figure 4.11: Example SEM of the zinc proline coated cordierite monolith using pore-filling/colloidal Method A: (a) view of surface, b) magnified view of surface with zinc proline rod-like structures.

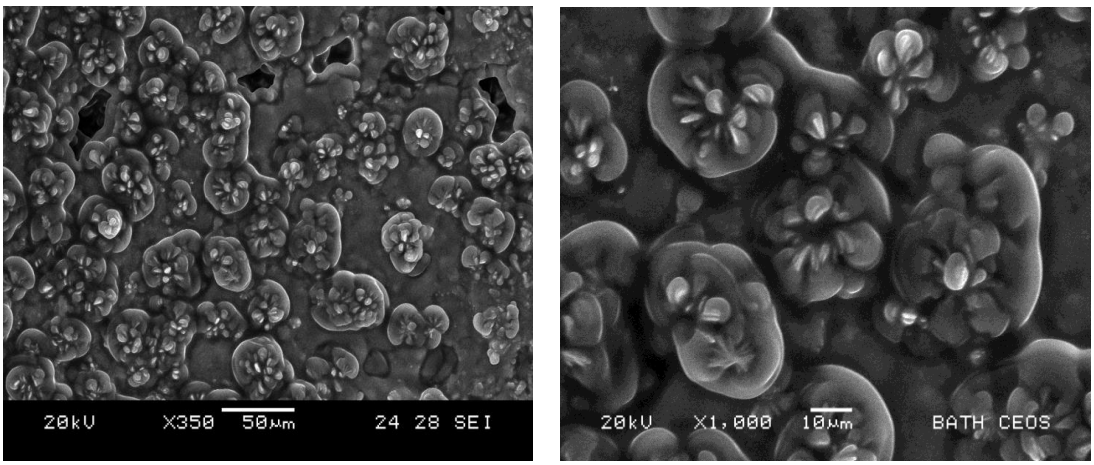

(a) **(b)**

Figure 4.12: Example SEM of the zinc proline coated cordierite monolith using slurry Method B: (a) view of surface, (b) magnified view of surface with zinc proline petal-like structures.

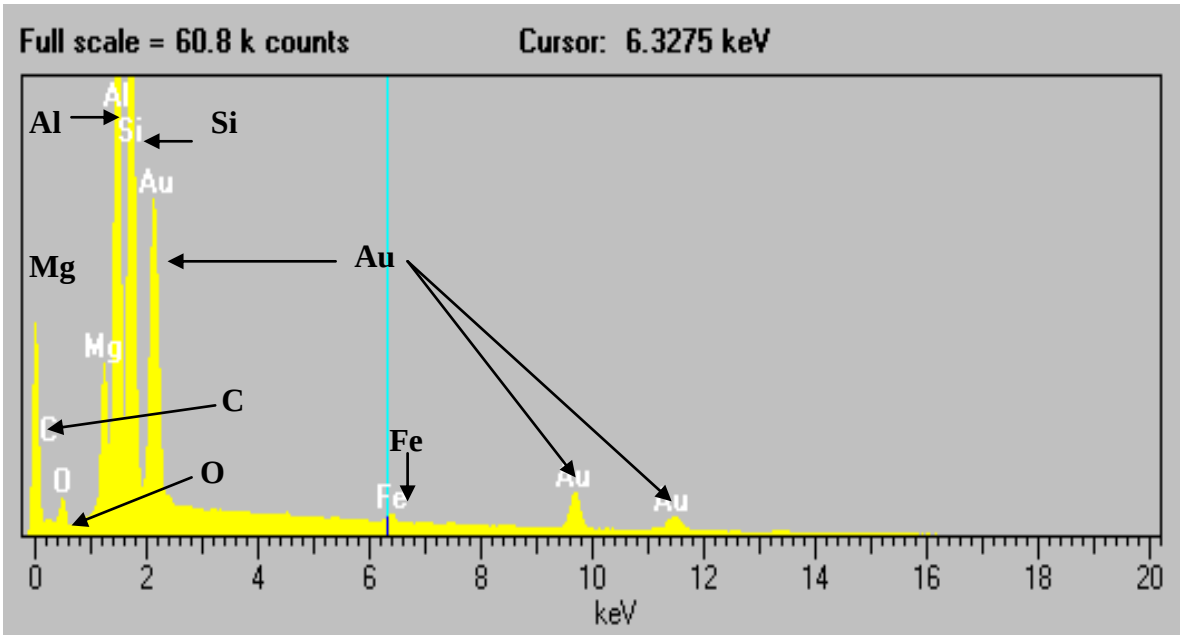

(a)

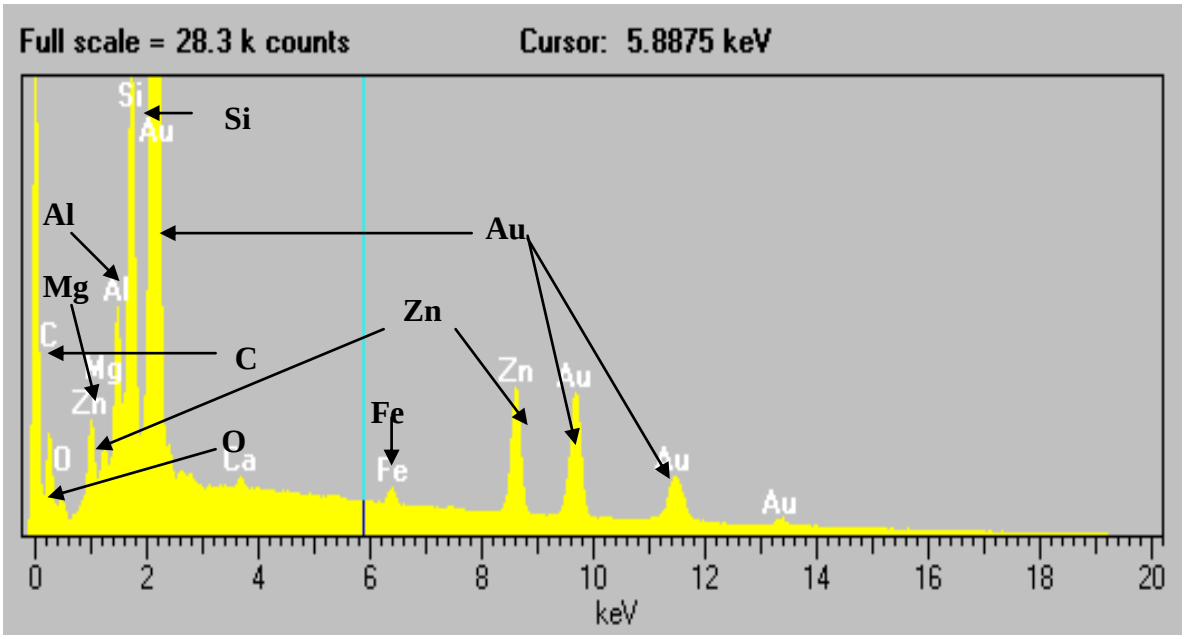

(b)

Figure 4.13: X-ray analysis profile for a) cordierite monolith and b) monolith coated with zinc proline using coating Method A.

4.2.3 Experimental condition for the batch reaction

A 37 ml quantity of rapeseed oil and 20 ml of methanol, which represents a 12:1 MeOH:oil molar ratio, was placed in a 120 ml autoclave with magnetic stirrer set at 1500 rpm. Then, 0.29 g of zinc proline (2.5 mol %) was added, the autoclave sealed and then it was placed in a graphite bath. For the process using the monoliths coated with zinc proline, the prepared monoliths were inserted in the autoclave. The mixture was then heated to a temperature of 195ºC. The time of reaction started from the point at which a temperature of 195°C was reached. After two hours of reaction time, the autoclave was quickly cooled in a stream of water. The product mixture was then poured into a conical flask filled with water. The biodiesel layer remained on the top, while the glycerol, excess methanol and catalyst were dissolved in an aqueous layer on the bottom. Figure 4.14 shows the experimental rig used for the reaction, and Figure 4.15 the products at the end of the reaction.

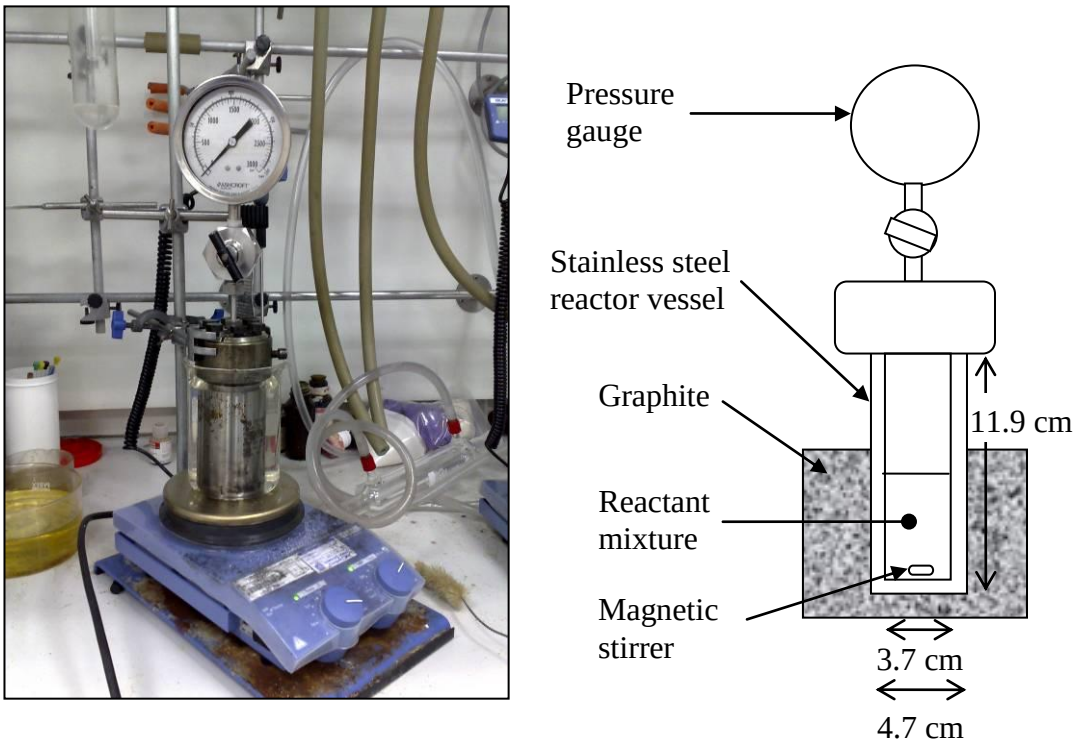

Figure 4.14: Experimental rig for the transesterification reaction using zinc proline.

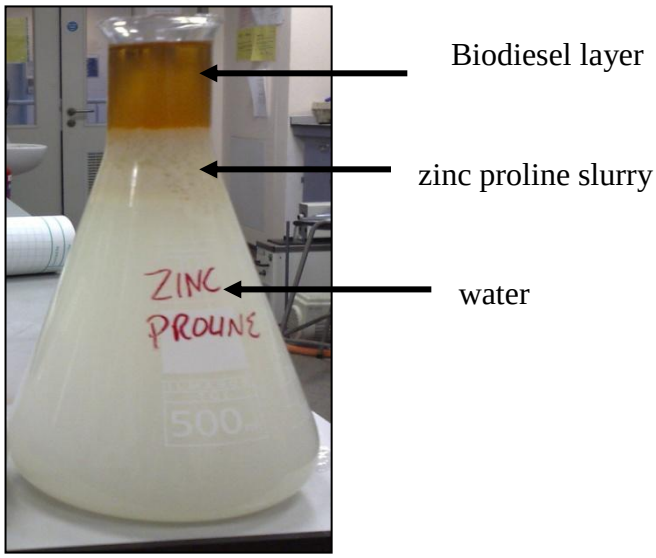

Figure 4.15: Products at the end of the transesterification reaction using zinc proline.

4.3 Result and Discussion

4.3.1 Batch reaction with zinc proline powder

The experiment was repeated for reaction time intervals of: 10, 20, 30, 40, 60, 80 and 120 minutes. Because liquid samples could not be taken during the reaction, the experiments were done with different batches. Figure 4.15 shows the product after the reaction was quenched with water. The zinc proline catalyst agglomerates in the water solution, leaving the biodiesel and unconverted oil in the top layer. The results from this experiment are shown in Figure 4.16. The final conversion to FAME after 2 hours was 69%.

In Figure 4.16, it can be seen that the graph shows a sigmoidal pattern (S-shape), which consists of a slow rate at the beginning followed by a sudden surge and finally a slow rate again. The S shape is typical in transesterification reactions (e.g. Freedman *et al.* (1984), Noureddini and Zhu (2003) and Darnoko and Cheryan (2000)). In general, a reaction mechanism for the transesterification of vegetable oils consists of an initial mass transfer-controlled region followed by a kinetically controlled region. The lag time

at the initial stage occurs because of poor diffusion between alcohol and oil (Noureddini and Zhu, 2003). The beginning of a kinetically controlled region can be observed at around 60 minutes. One possible explanation is found in Dasari *et al.* (2003):

> "the fact that for <20% conversions in transesterification reactions the methanol was predominantly in liquid phase separate from the oil phase. After approximately 20% conversion, the methyl esters, MG, and DG acted as cosolvent, enhancing the solubility of methanol in the oil phase and forming a homogeneous solution".

Comment:

It is worth mentioning that the result in Figure 4.16 was the best data obtained with the equipment limitation. The equipment was not equipped with sampling port and temperature indicator. The accuracy of the result might be slightly affected by following possible source of errors.

i) The time for the autoclave to reach 195°C was approximately 20 minutes. Also, the sampling was done after the autoclave was quenched and cooled. The reaction was assumed stopped immediately during the process, however, the cooling process time was taken at least 5 minutes. The reaction might have taken place during the heating and cooling period. However, this was not measured in this work.

ii) The batch reaction was repeated 7 times continuously. There was a possibility that the autoclave was contaminated with the spent catalyst before the next batch was taken place.

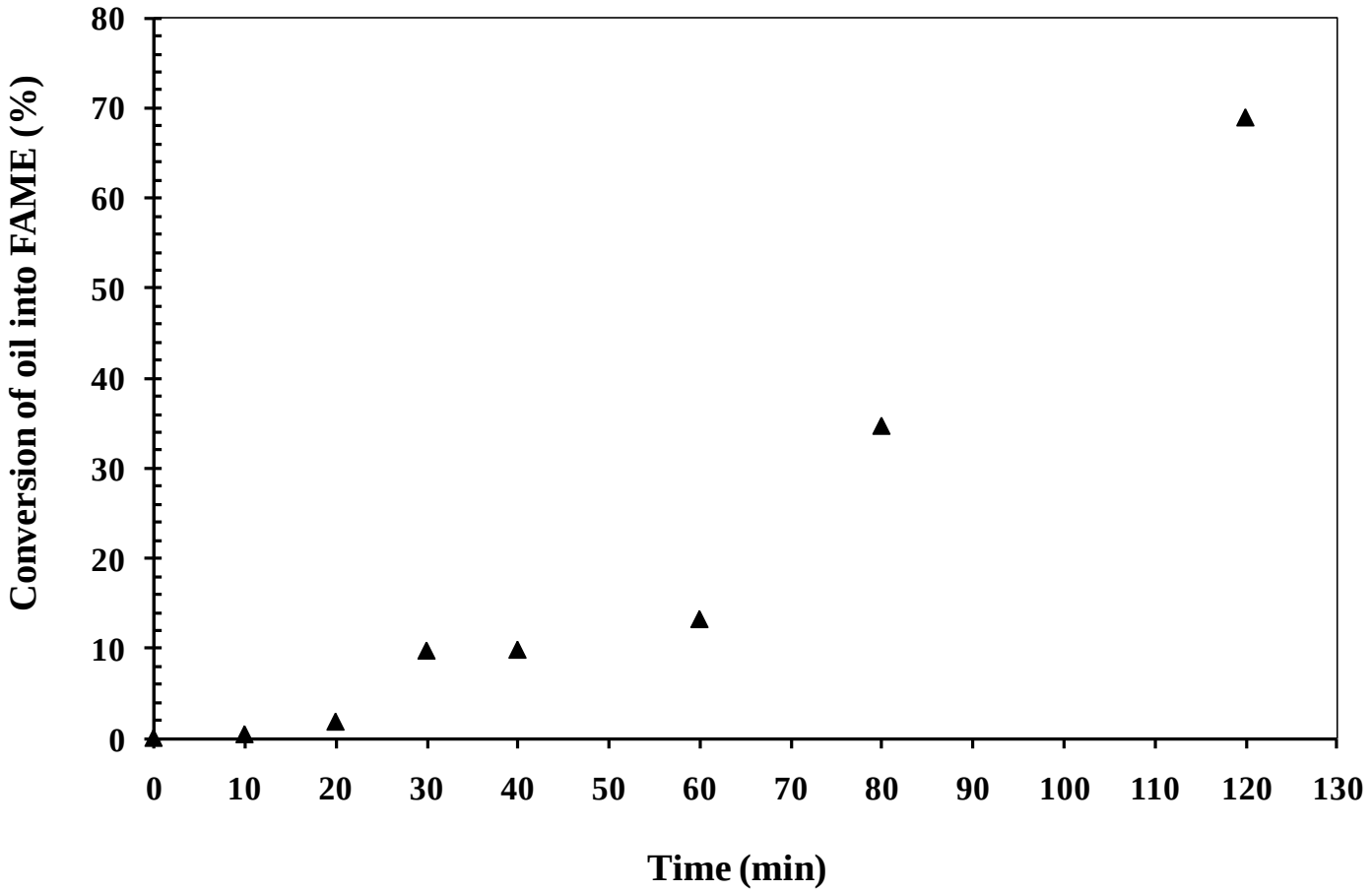

Figure 4.16: Batch experiments using zinc proline in powder form (T = 195°C, P = 20 bar, molar ratio MeOH : oil = 12:1, initial concentration of oil, $C_{TG,0}$ = 0.7 mol litre^{-1} and initial concentration of MeOH, $C_{MeOH,0}$ = 8.5 mol litre^{-1} and mass of zinc proline = 0.3 g).

Batch reaction with coated monolith

Batch reaction experiments were performed using the monolith coated with zinc proline prepared according to the procedure described in Section 4.2.3. Because the zinc proline catalyst was trapped in the monolith pieces, it was possible to withdraw a small amount (e.g. 0.5 ml) of liquid (without removing the catalyst). After allowing the mixture to cool down for approximately 10 to 15 minutes, 0.5 ml of sample was removed with a pipette from the mixture. Then, the reactor was assembled, and the reaction was allowed to continue after the temperature reached 195°C. This was done for a total reaction time of: 10, 20, 30, 40, 60, 80 and 120 minutes. After 2 hours of total reaction time, the monolith was removed from the mixture, and the mixture was then poured into a flask filled with water to quench the reaction, see Figure 4.17. All the samples were analysed using ^{1}H NMR. The sampling routine in this method was not ideal and could affected the accuracy of the result. The time for the autoclave to reach 195°C was approximately 20 minutes of the heating and 5 minutes of cooling each time of sampling process. The reaction might have taken place during that time. Due to the limitation of the autoclave available, this approach was the best achievable in this thesis (see the comment on Section 4.7.1).

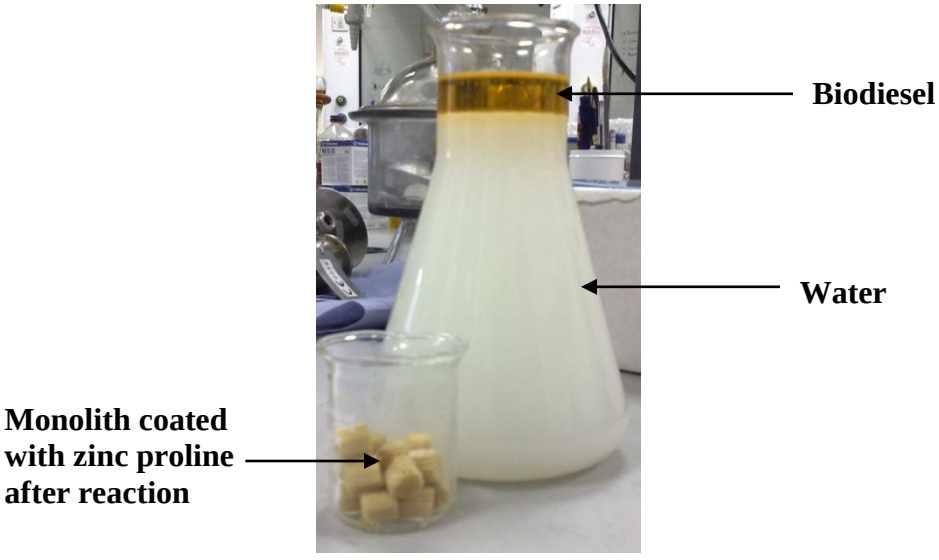

Figure 4.17: Products of the reaction quenched in water, using zinc proline coated monoliths. The zinc proline slurry was not seen in the waste water, indicating that the zinc proline remained on the monolith surface.

Method A (pore-filling/colloidal):

In this experiment, the conversion to FAME after 2 hours was approximately 53.7 %. The result is relatively good, especially as the stirring in the reactor was not very effective, (as the movement of the magnetic stirrer was restricted because of the sections of monolith). This compares very favourable with the earlier batch experiments with the zinc proline catalyst where a conversion of 69 % was achieved. The result is encouraging, especially as it is estimated that the geometric external surface area of the monolith was about 30 times lower than the powdered catalyst.

Method B (slurry coating):

The same experiment was repeated using monolith pieces impregnated with zinc proline and binder solution using a slurry-coating-method, called Method B. The plot of the experimental results from these two sets of experiments is shown in Figure 4.18. Both coated monoliths gave a similar conversion during the reaction time even though the catalyst loading is higher in the monolith with the binding agent (coating with Method B).

As can be seen from Figure 4.18, a slow initial reaction region was observed for both reactions (coating Methods A and B). A slight increase in FAME conversion was observed in the first 30 minutes, compared with the zinc proline powder (see Figure 4.16). It may even be that the method of coating the monolith had actually increased the activity of the catalyst, or the cordierite itself exhibited catalytic activity.

Looking more closely at the SEM pictures of the monolith surface, the zinc proline deposition is illustrated in Figure 4.19. The coated monolith surface obtained from the colloidal coating method shows that the zinc proline structure is deposited in such a manner that the external surface area is increased. In the SEM image of the cordierite surface obtained from the slurry-coating-method (see Figure 4.20 (a)), it can be seen that there are petal-like layers with zinc proline rod structures on top of them. It seems that the petal layers consist of the binder (used in Method B), to which the zinc proline crystals have bound. Although the binder increased the catalyst loading (see Table 4.4), it does not appear to have increased the rate of reaction, see Figure 4.18.

At similar conditions, further experiments were then performed with uncoated monolith, to see if the cordierite exhibited any form of catalytic activity. From these it was found that 27% conversion was achieved (*versus* 54%). This would suggest that the cordierite is catalytically active, and further evidence may be obtained from the literature. For example, in Kouza *et al.* (2006) the use of a number of alkaline-earth metal oxides (MgO, CaO, SrO) as catalysts for the transesterification reaction (edible soybean oil with methanol) were studied. They found that both SrO and CaO were very active catalytically, whereas the MgO had a low level of activity. As the structure of cordierite corresponds to $2MgO{\cdot}2Al_2O_3{\cdot}5SiO_2$ (Alexender and Umera,1995), then the MgO could have exhibited some activity in these experiments (especially as temperatures were a lot higher than in Kouza *et al.* (2008)). Also, in work by Li and Rudolf (2008), the catalytic activity of MgO functionalized mesoporous materials for the transesterification of blended vegetable oil with ethanol was studied. These experiments were also performed at higher temperatures (220 ºC), and silica loaded with MgO was found to be the most effective of all of the catalysts tested in that paper. So this provides further evidence that the MgO in the cordierite could show catalytic activity especially at elevated temperatures.

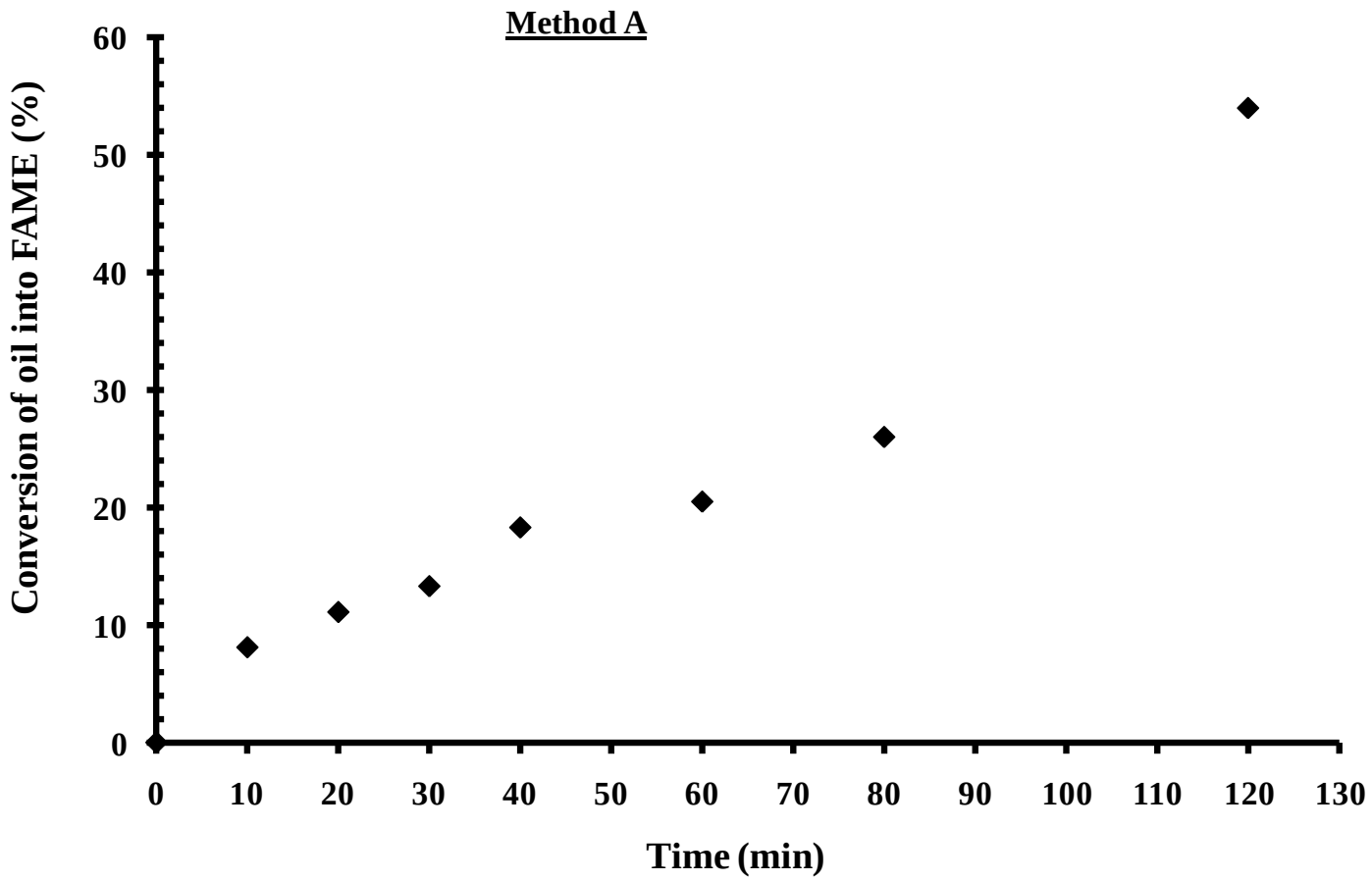

Figure 4.18: Batch experiment using monolith coated zinc proline using Method A, (T = 195°C, P = 20 bar, molar ratio MeOH : oil = 12: 1, initial concentration of oil, $C_{TG,0}$ =0.7 mol litre^{-1} and initial concentration of MEOH, $C_{A,0}$ = 8.5 mol litre^{-1} and mass of zinc proline 0.3 g, coated onto monolith pieces).

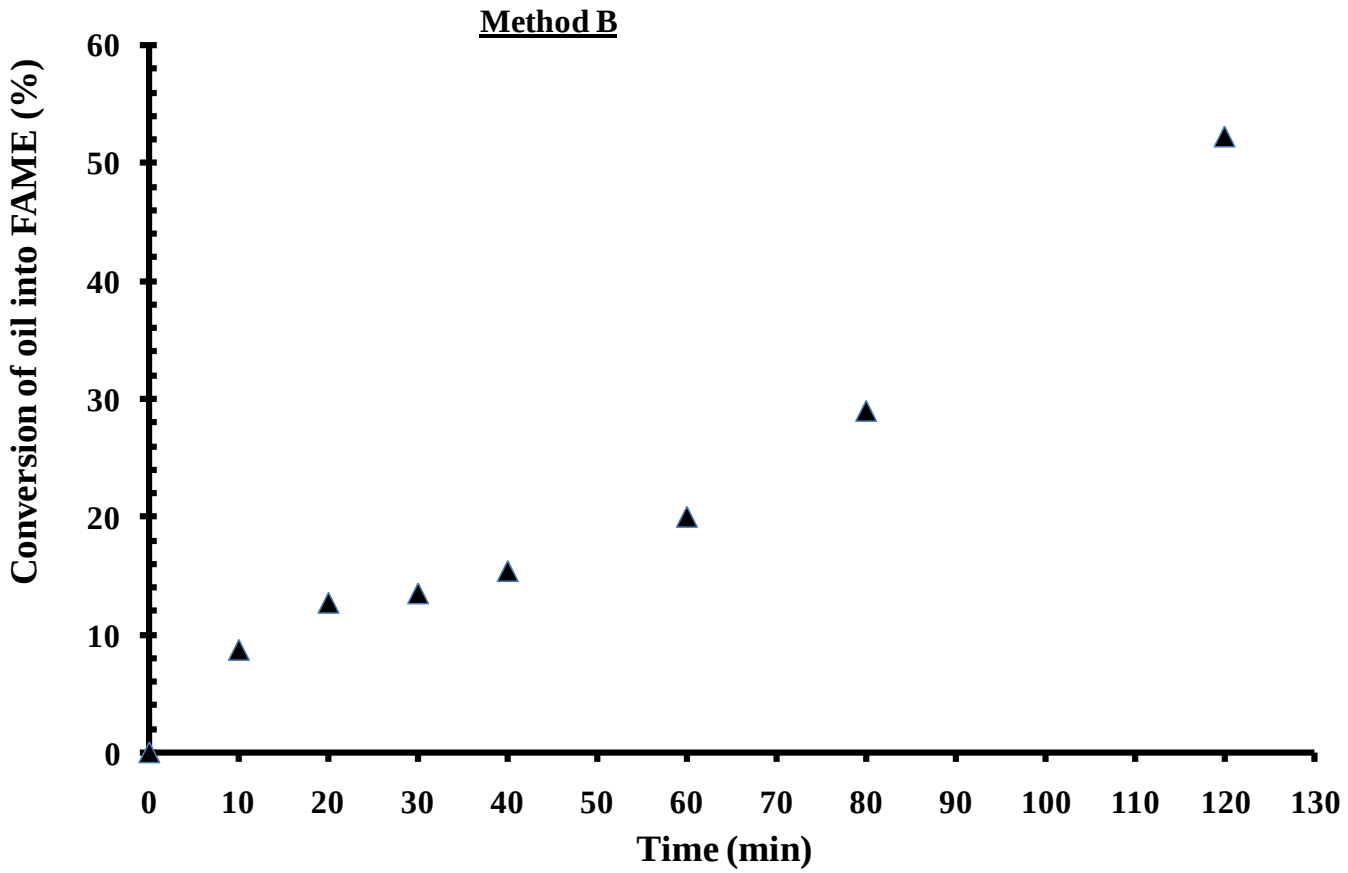

Figure 4.19: Batch experiment using monolith coated zinc proline using Method B, (T = 195°C, P = 20 bar, molar ratio MeOH : oil = 12: 1, initial concentration of oil, $C_{TG,0}$ = 0.7 mol litre^{-1} and initial concentration of MEOH, $C_{A,0}$ = 8.5 mol litre^{-1} and mass of zinc proline = 0.46 g coated onto monolith pieces).

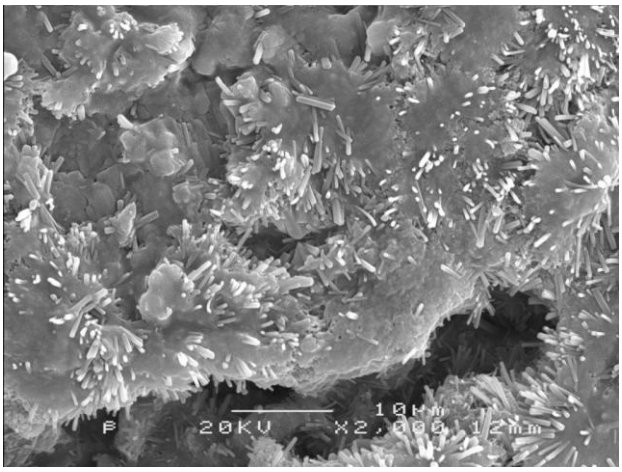

(a)

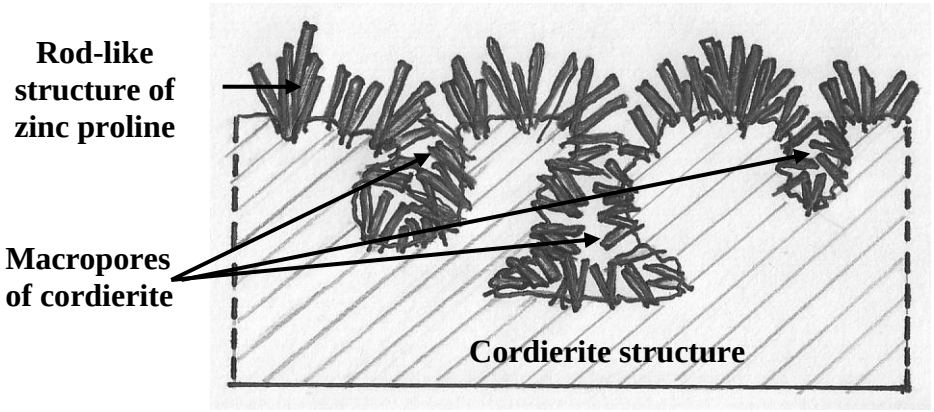

(b)

Figure 4.20: Colloidal coating Method A showing zinc proline on the surface: (a) SEM image, (b) visual representation of the structure.

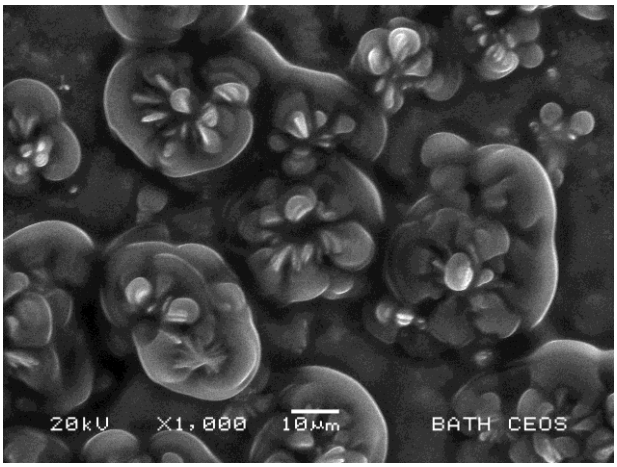

(a)

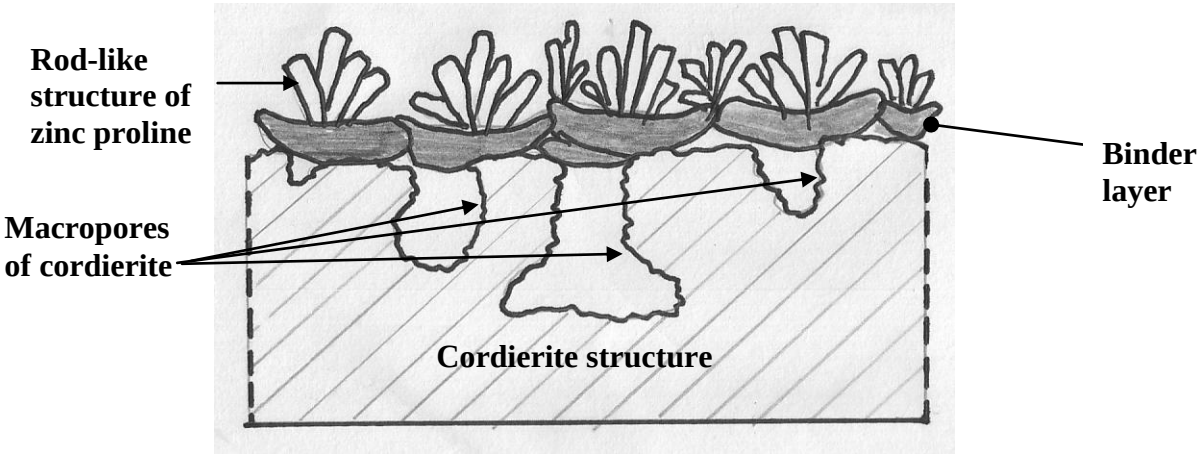

(b)

Figure 4.21: Slurry coating Method B showing zinc proline on the surface (a) SEM image, (b) visual representation of the structure on the surface showing the binding layer.

4.3.3 Analysis of rate data

The data was obtained to determine the overall initial rate constant for the reaction. This aspect had not been studied by Chuck (2007), but is important in order to estimate the length of a continuous flow reactor (if the catalyst is fixed in the bed).

The overall rate of reaction may be represented by the simplified expression:

$$TG + 3CH_3OH \xrightarrow{k} GL + 3RCOOCH_3 \quad (4.2)$$

The reaction rate constant is derived from the general rate equation :

$$r_{TG} = \frac{d\,C_{TG}}{dt} = -k\,C_{TG}{}^{\alpha}\,C_{MeOH}{}^{\beta} \quad (4.3)$$

where $-\frac{d\,C_{TG}}{dt}$ is the consumption of triglyceride (mol l^{-1} min^{-1}),

k is the rate constant (units vary),

α is the order with respect to the triglyceride concentration,

β is the order with respect to the methanol concentration.

In order to obtain the reaction order and rate constant, the procedure described in Singh and Fernando (2007) was followed.

The concentration of triglyceride, C_{TG} may be expressed in terms of the fractional conversion, X:

$$C_{TG} = C_{TG,0}(1 - X) \quad (4.4)$$

where $C_{TG,0}$, represents the initial concentration when t = 0.

The methanol concentration, C_{MeOH} may be expressed in terms of conversion, as:

$$C_{MeOH} = C_{TG,0}(\theta_A - X) \quad (4.5)$$

where

$$\theta_A = C_{MEOH,0} / C_{TG,0} \quad (4.6)$$

where C_{MeOH} is the initial methanol concentration at t = 0.

Therefore, Eq. 4.3 can be written as:

$$\frac{dX}{dt} = kC_{TG,0}^{(\alpha+\beta-1)}(1-X)^{\alpha}(\theta_A - 3X)^{\beta} \tag{4.7}$$

Different values of reaction order for β and α were tested. This is similar to the technique used by Cheng (2009). Eq. 4.7 was integrated using the following values of α and β:

Case 1 : (α = 0,β = 0), then:

$$C_{TG,0}\ X = k\ t \tag{4.8}$$

Case 2 : (α = 1,β = 0), then:

$$\ln\left(\frac{1}{1-X}\right) = k\ t \tag{4.9}$$

Case 3 : (α = 0,β = 1), then:

$$-\frac{1}{3}\left[\ln\frac{(\theta_A - 3X)}{\theta_A}\right] = k\ t \tag{4.10}$$

Case 4 : (α = 1,β = 1), then:

$$\frac{1}{(\theta_A - 3)}\ln\left[\frac{\theta_A - 3X}{(1-X)\theta_A}\right] = k\ C_{TG,0}\ t \tag{4.11}$$

Case 5 : (α=2,β=0), then:

$$\frac{X}{(1-X)} = k\ C_{TG,0}t \tag{4.12}$$

Each of these equations can be presented in the form of $y = m\,x$, where the slope (m) is the reaction rate constant.

Using the data over 120 minutes of the reaction (see Figures 4.16 and 4.18), the experimental data was plotted in this form. The regression coefficients, R^2 from the plots for each case were then compared. Table 4.5 shows the value of R^2 for the five cases tested. Based on the highest value of R^2, Case 1 was selected for all three of the zinc proline reaction systems. The reaction was determined to be zero order with respect to TG concentration, and also zero order with respect to MeOH concentration. Because MeOH is in excess, then a value of $\beta = 0$ is to be expected. In a paper by Singh and Fernando (2007), $\alpha = 0$ and $\beta = 1$, but the catalysts were different (i.e. PbO, MgO and CaO).

Table 4.5: The value of regression coefficient, R^2 for Cases 1 to 5.

Zinc proline catalyst	**Powder form 0.29 g catalyst**	**Method A (colloidal) 0.29 g catalyst**	**Method B (slurry) 0.458 g catalyst**
Values of α and β	**Regression coefficient, R^2**		
Case 1: ($\alpha = 0$, $\beta = 0$)	0.8562	0.9378	0.9495
Case 2: ($\alpha = 1$, $\beta = 0$)	0.7596	0.8894	0.9151
Case 3: ($\alpha = 0$, $\beta = 1$)	0.8406	0.9326	0.9470
Case 4: ($\alpha = 1$, $\beta = 1$)	0.7414	0.8755	0.9036
Case 5: ($\alpha = 2$, $\beta = 0$)	0.6569	0.8076	0.8445

The initial rate constant was then determined, using the initial values of experimental data from t = 0 to t = 40 min. Then, the rate constant was expressed in terms of the geometric surface area of catalyst, k_s. In this calculation, it is assumed that the whole surface area of the monolith is covered with catalyst, thus the surface area of the monolith is used in this estimation. To calculate k_s, the following was used:

$$k_s = \frac{k}{\text{surface area of catalyst}, A} \qquad \left(\frac{mol\ litre^{-1} \min^{-1}}{m^2} \right) \qquad (4.13)$$

The overall and the initial rate constants are shown in Table 4.6. The overall rate of reaction (over t = 0 to 120 min) based on the volume of the reactor is similar, however, when calculated on the basis of geometric surface area, then the rate for the monolith is significantly higher by a factor 30. Initial rates of reaction for the monolith are also higher than the powder form. Also, from the result, the coated monolith using Method B did not result in an increase in the rate of reaction. Example calculations are included in Appendix F.

Table 4.6: Values of rate constants.

Zinc proline catalyst	**Powder form 0.3 g catalyst**	**Method A (colloidal) 0.3 g catalyst**	**Method B (slurry) 0.458 g catalyst**
Overall reaction rate (mol l^{-1} min^{-1})	0.4588	0.4096	0.4072
Overall reaction rate (mol l^{-1} min^{-1} m_{cat}^{-2})	0.425	12.33	12.2578
Overall reaction rate (mol min^{-1} g_{cat}^{-1})	1.582	1.412	0.889
Initial rate constant (mol l^{-1} min^{-1})	0.0016	0.0033	0.0031
Initial rate constant (mol l^{-1} min^{-1} m_{cat}^{-2})	0.001	0.100	0.094
Initial rate constant (mol min^{-1} g_{cat}^{-1})	0.0055	0.0114	0.0068

4.3.4 Re-usability of monolith coated with zinc proline

To investigate the re-usability of a coated monolith, the procedure described in Section 4.3.2 was repeated. In this experiment, all of the monoliths were placed in a wire-mesh cage inside the reactor in order to make it easier to remove the monolith after one reaction. After one reaction in the batch reactor, the wire-mesh cage was removed, and then re-used for the next batch reaction. This was repeated for 9 cycles of the reaction. The conversion for every cycle was determined by ^{1}H NMR analysis, and the results are shown in Figure 4.21. From this it is clear that the activity of the catalyst has reduced by 30% after 8 cycles (total reaction time = 16 h), and then further 53% after the 9th cycle (total reaction time = 18 h).

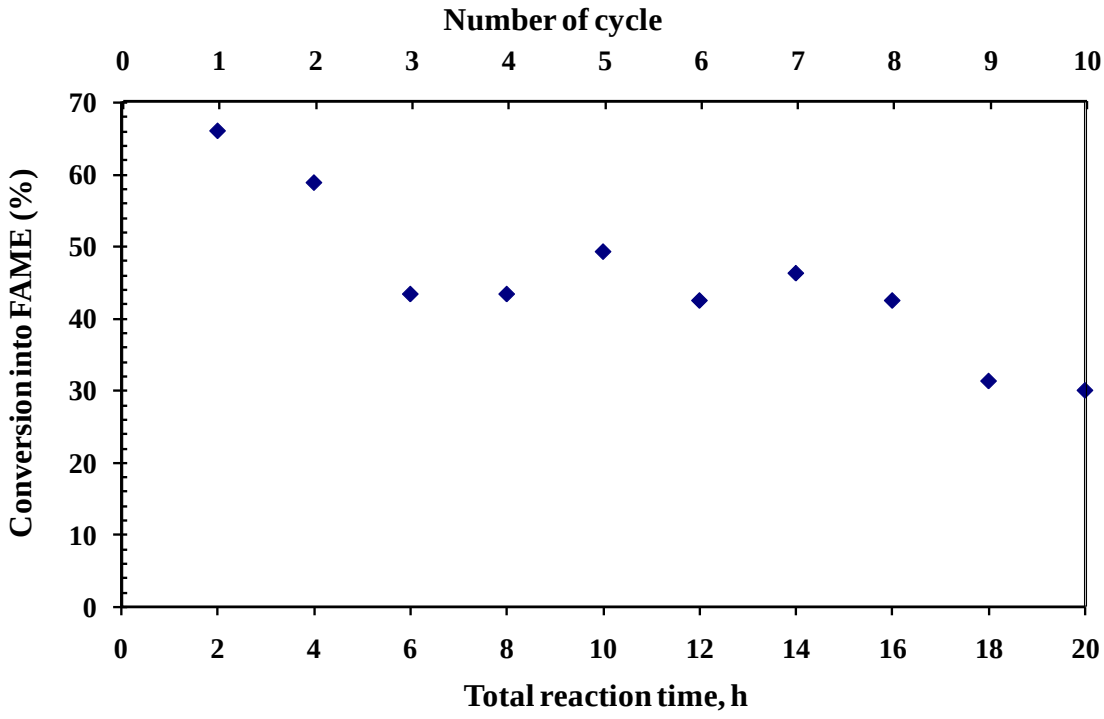

Figure 4.22: Reusability of zinc proline coated monolith (Note: the reaction time per cycle was 2 h).

4.3.5 Identification of zinc proline as heterogeneous catalyst

One of the important questions in this work was whether the zinc proline acts as an homogeneous or a heterogeneous catalyst. In Chuck (2007), this was not considered in any detail. Actually, it is difficult to determine. When the zinc proline was in powder form, this was very dispersed in the reaction mixture, and hence difficult to recover (after the reaction) in order to be examined. In Chuck (2007), the zinc proline was washed out of the product with water. When zinc proline was coated onto the monolith, it became easier to explore this aspect.

An experiment to explore the heterogeneity of zinc proline was done by one researcher in the group (Minnet, 2010) in a supporting and collaborative short project. In the initial test to determine whether zinc proline dissolved into the reaction medium and was the cause of activity, some impregnated monolith in a wire-mesh cage was placed into 20 ml methanol, heated to 200 °C for 2 hours, and then cooled. The monolith was subsequently removed, and 37 ml of oil was added to the methanol, and a standard batch reaction was performed. In these tests, the reaction in which the coated monolith was removed gave no yield, whilst the reaction with a zinc proline coated monolith gave a yield of 42%.

These results suggest that the zinc proline behaves more as a heterogeneous catalyst, rather than a homogeneous one. However, this clearly requires more exploration, and it would be interesting to see what happens to the catalyst when it used in a continuous flow reactor.

4.4 Conclusions on batch experiments

i) It was shown that it is possible to coat a cordierite monolith support with the zinc proline catalyst, and the catalyst was shown to be active.

ii) Two methods of catalyst coating were explored, one based on a colloidal solution (Method A), and the other made use of a slurry solution (Method B). The surface of the catalyst made by Method A exhibited clear rod-like structures, which also penetrated the macropores on the surface. These rod-like structures resembled the structure of the powder form of the catalyst. The surface of the catalyst made by Method B, consisted of the binder which had bonded with the cordierite support in blob form (blocked some of the macropores) to which the zinc proline rod-like crystal structures attached themselves creating petal-like shapes on the surface.

iii) Using the slurry Method B, it was easier to achieve a higher loading of catalyst, although the level of catalytic activity (based on fluid volume, and also geometric surface area) remained similar to Method A.

iv) The coated monoliths exhibited a similar level of activity (based on the volume of the fluid) as the powdered form. However, when comparisons were made based on geometric surface area (assuming a flat smooth surface), then the monolith form exhibited a higher level of activity than the powdered form (by a factor of 30). When based on mass of catalyst, then the colloidal form (Method A), showed a slightly higher level of activity than Method B. ***It was decided to try monoliths prepared using Methods A and B in the continuous flow reactor in Chapter 5.***

v) When the reaction rate was matched to a rate expression, then the best fit was found with a rate expression that was zero order with respect to TG and MeOH ($\alpha = 0$ and $\beta = 0$). This suggests that the reaction was independent of the concentration of either TG or MeOH.

vi) Repeat experiments in which the re-usability of the coated monolith was tested, demonstrated a gradual loss in activity (30% after the 8^{th} repeat cycle (total

reaction time of 16 h), and 53% after the 9th repeat cycle (total reaction time of 18 h)). This was a little surprising, as in earlier preliminary trials, such a loss in activity had not been observed. ***Catalyst loss/deactivation will be explored further in the continuous flow reactor in Chapter 5.***

vii) Preliminary tests (by a student working on a short collaborative project) to establish if the catalyst was active as a homogeneous dissolved catalyst, or as a heterogeneous catalyst, suggest that it does not dissolve in methanol in a catalytically active form. *However, further work is necessary, and a special experiment will need to be devised – this was not done in this thesis.*

viii) Reaction experiments with an uncoated monolith showed that the cordierite monolith on its own exhibited significant catalytic activity. This was an interesting finding, and evidence was found in the literature that the presence of MgO (present in cordierite) could have been responsible. ***It was decided to try uncoated monoliths in the continuous flow reactor in Chapter 5.***

REFERENCES

Alexander, J.T. and Umehara, K., 1995. Ceramic honeycomb for air pollution control. NGK Insulator Ltd., Nagoya, Japan, *Reference JH-952128*, July 1995.

Cheng, Y., 2009. *Lower Emissions from A Biodiesel and Microemulsion Fuelled Diesel Engine*. Thesis (PhD). Faculty of Health and Medical Sciences, Chemical Science Division. University of Surrey.

Chuck, C.M., 2007. *Lewis Acid Catalyst Design for the Transesterification of Lower Quality Feedstock for Biodiesel Production*. Thesis (PhD). Department of Chemistry, University of Bath.

Chuck, C.M., 2010. Chuck, C.M. (cc245@bath.ac.uk). 10 March 2010. *Re: Zinc proline*. Email to Asli,U.A. (U.A.Asli@bath.ac.uk).

Darnoko, D. and Cheryan, M., 2000. Continuous production of palm methyl esters *Journal of American Oil Chemists' Society*, 77 (12), pp. 1269–1272.

Dasari, M. A., Goff, M. J. and Suppes, G. J., 2003. Noncatalytic alcoholysis kinetics of soybean oil. *Journal of American Oil Chemists' Society*, 80 (2), pp. 1-4.

Freedman, B., Pryde, E.H. and Mounts, T.L., 1984. Variables affecting the yields of fatty esters from transesterified vegetables oils. *Journal of American Oil Chemists' Society*, 61 (10), pp. 1638-1643.

Hoek, I., Nijhuis, T.A,. Stankiewicz, A.I. and Moulijin, J.A., 2004. Performance of the monolithic stirrer reactor: applicability in multi-phases processes. *Chemical Engineering Science*, 59, pp. 4975-4981.

Kofoed, J., Darbre, T. and Reymond, J., 2006. Dual mechanism of zinc-proline catalyzed aldol reactions in water. *Chemical Communication*., pp. 1482–1484.

Kouza, M., Kasuno, T., Tajika, M., Sugimoto, Y. S. and Hidaka, J., 2008. Calcium oxide as a solid base catalysts for the transesterification of soybean oil and its application to biodiesel production. *Fuel*, 87, pp. 2798-2806.

Li, E. and Rudolph, V., 2008. Transesterification of vegetable oil to biodiesel over MgO functionalized Mesoporous Catalysts, *Energy Fuels*, 22 (1), pp. 145–149.

Minnet, D. 2010. *Kinetic Study Of A Zinc Proline Catalyst System For Biodiesel Production*. DTC Project II Report. Department of Chemistry, University of Bath.

Nijhuis, T. A., Beers, A. E.W., Vergunst, T., Hoek, I., Kapteijn, F. and Moulijn, J.A., 2001. Preparation of monolithic catalysts. *Catalysis Review*, 43 (4), pp 345-380.

Noureddini, H. and Zhu, D., 1997. Kinetics of transesterification of soybean oil. *Journal of American Oil Chemists' Society*, 74, pp. 1457–1463.

Singh, A.K. and Fernando, S.D. , 2007. Reaction kinetics of soybean oil transesterification using heterogeneous metal oxide catalysts. *Chemical Engineering Technology*, 30 (12), pp. 1716–1720.

Stamenkovic, O.S., Todorovic, Z. B., Lazic, M. L., Veljkovic, V.B. and Skala, D.U., 2008. Kinetics of sunflower oil methanolysis at low temperatures. *Bioresource Technology*, 99, pp. 1131–1140.

CHAPTER 5

CONTINUOUS FLOW REACTOR

In this chapter, experimental apparatus is developed, which can be used to perform continuous flow experiments, where the catalyst is retained in a fixed bed. To improve the understanding of residence time in this fixed bed monolith reactor, residence time distribution studies (RTD) are performed using salt as a tracer. Then continuous flow reaction experiments are performed, using zinc proline coated monoliths, and reaction intermediates are followed. In addition, a few short feasibility experiments are performed using strontium oxide coated monoliths – this was done to assess the viability of that catalyst on a monolith and how easily it could be evaluated in the continuous flow reactor developed in this thesis.

5.1 Introduction

As a reminder, at the end of Chapter 2, the following decisions were taken when the interim conclusions were formed:

- An in-line mixing device would be used.
- Experiments would be performed using cordierite ceramic monolith as a catalyst support.
- The internal diameter of the flow reactor would be kept relatively small (e.g. 1 cm), so as to keep the peripheral equipment relatively compact and manageable.
- HPLC pumps would be used to pump the vegetable oil and methanol.
- A back pressure valve would be used to maintain a liquid phase in the reactor.
- A heated jacket would be used to maintain the desired temperature.

These are now considered and implemented.

In designing an experimental reactor for biodiesel production, it is necessary to estimate the size of the reactor, and this is done in the following section.

5.1.1 Estimating the size of the experimental reactor

In this section, use is made of a number of short-cut design techniques, in order to estimate the size of the experimental reactor, that has to be designed for the experiments in this chapter.

Making use of a design equation for a packed bed reactor as presented in Fogler (2006, p.60), then:

$$W = F_{A,0} \int_0^X \frac{dX}{-r_A'} \tag{5.1}$$

where:

W is the weight of catalyst (g),

F_{A0} is the entering molar flow of reactant A (mol min^{-1}),

X is the fractional conversion of reactant A, and

$-r_A'$ is rate of reaction of reactant A per unit mass of catalyst (mol min^{-1} $g_{catalyst}^{-1}$).

Let the initial molar flow of triglyceride (TG) be:

$$F_{TG0} = \upsilon_0 C_{TG,0} \tag{5.2}$$

where:

υ_0 is the inlet volumetric flow of the stream TG (litre min^{-1}), and

$C_{TG,0}$ is the concentration of TG (mol $litre^{-1}$).

Assuming that the rate of reaction is of the following form:

$$-r_{TG}^{'} = k' \ C_{TG}^{m} \tag{5.3}$$

In Chapter 4, in the Section 4.3.3, it was established that the reaction order m = 0, therefore $-r_A = k'$, and the unit of k' is mol min^{-1} $g_{catalyst}^{-1}$.

Substituting into Eq. (5.1) and integrating, then the weight of catalyst , W, to achieve a fractional conversion X, is given by:

$$W = \left(\upsilon_0 \times C_{TG,0}\right) \frac{X}{k'} \tag{5.4}$$

Using Eq. 5.4, a plot of conversion as a function of zinc proline catalyst loading at different entering flows, ν_0, is shown in Figure 5.1. A sample calculation is also presented in Appendix G (G1).

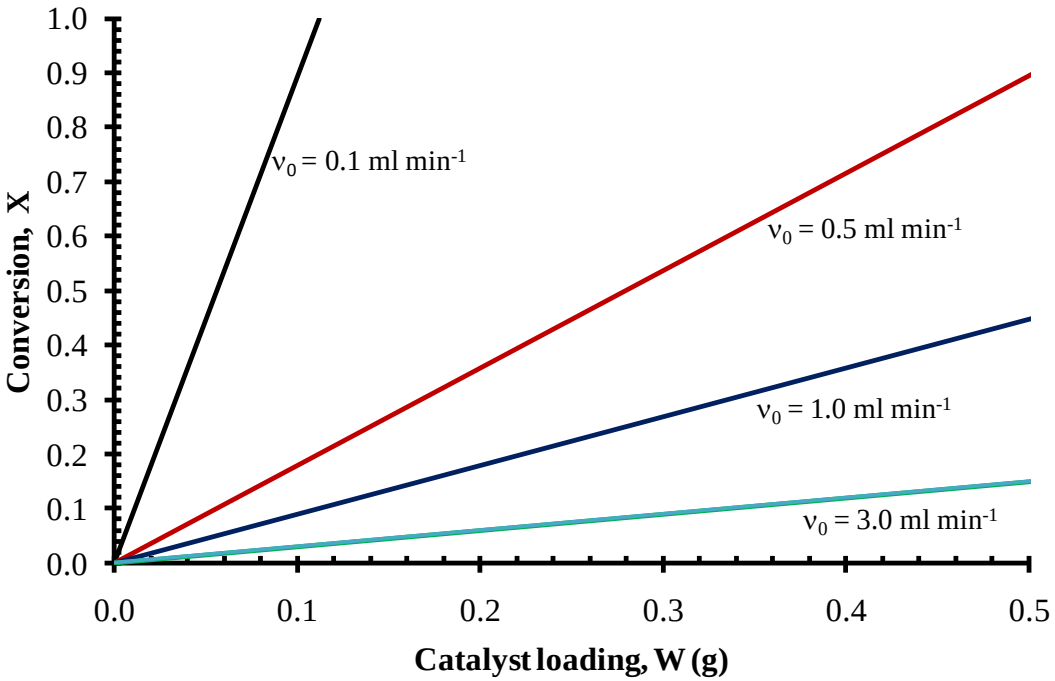

Figure 5.1: Estimating the amount of catalyst required in an experimental continuous flow monolith reactor.

By assuming the catalyst loading per unit volume of monolith remains the same, the size of the reactor can be estimated. This was obtained from a number of coating experiments. The average weight of zinc proline catalyst that was deposited on a 10 mm × 10 mm ×10 mm monolith piece was 0.03 g. Thus the average zinc proline loading per unit volume of monolith is 0.03 g cm^{-3}.

The required volume of monolith in the reactor, may then be estimated from:

$$V = \frac{W\ V_1}{W_1} \qquad (5.5)$$

where

V is volume of monolith in the reactor, cm^3.

W_1 is the average weight of catalyst on one piece of monolith, g,

V_1 is the volume of one piece of monolith, cm^3.

An example calculation is presented in Appendix G (G2). The data in Figure 5.1, may then be presented in the form of monolith volume as illustrated in Figure 5.2.

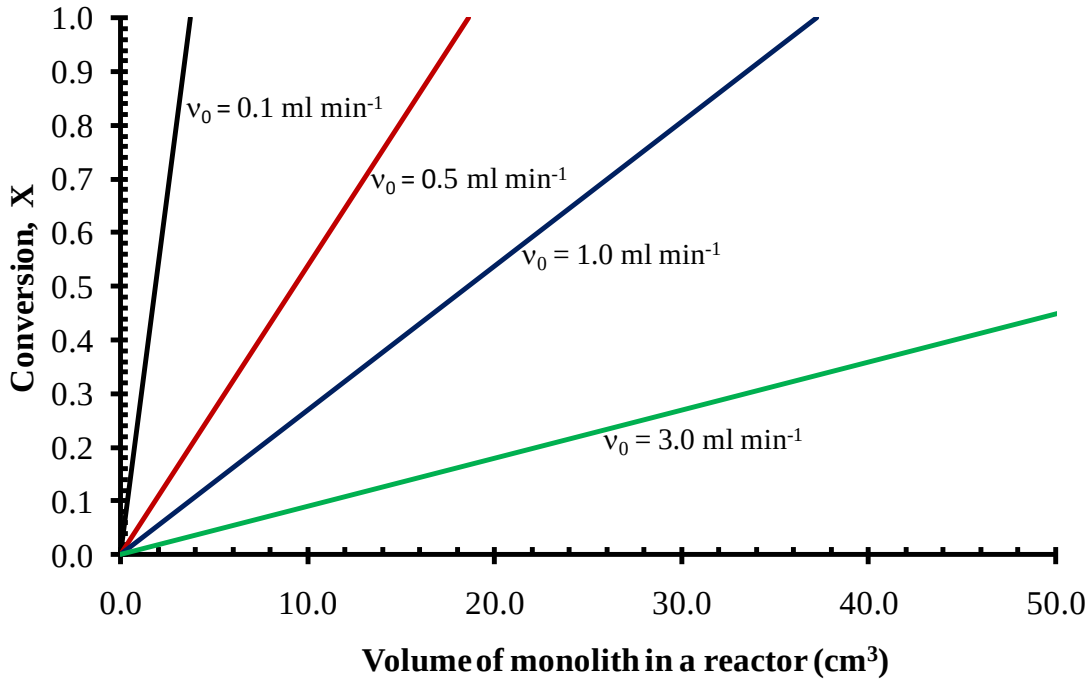

Figure 5.2: Estimating the volume of monolith required in an experimental continuous flow monolith reactor.

Other useful parameters may also be estimated, such as:

(a) The weight of catalyst per unit surface area:

$$W_S = \frac{W_1}{S_1} \tag{5.6}$$

where S_1, is the geometric external area of one piece monolith.

(b) The geometric external surface area of monolith in the reactor:

$$S = \frac{S_1}{V_1} \times V \tag{5.7}$$

Further useful relationship such as space time, τ and space velocity (SV) can be calculated. Space time, τ is the time necessary to process one reactor volume of fluid, given a particular set entrance conditions (Fogler, 2006). This is given by:

(c) Space Time (min), $\tau = \frac{V}{Q}$, (5.8)

where

Q is the volumetric flowrate, ml min^{-1}; and

V is the volume of void in the reactor, ml.

and space velocity (SV) indicates how many reactor volumes of feed can be treated in a unit time. In fogler (2006), SV regarded as the reciprocal of the space time.

(d) SV (min^{-1}) = $\frac{1}{\tau}$ (5.9)

The space velocity commonly used is LHSV, which is defined as

(e) LHSV = Liquid hourly space velocity, h^{-1}

After considering a number of options, it was decided to use a 3/8" stainless steel tube (o.d. = 9.5 mm, wall thickness = 1.7 mm and i.d. = 6.2 mm) that would be packed with monolith pieces that were 5 (± 0.5) in diameter and 10 mm long (see Figure 5.3). The overall length of monolith in the reactor could be varied from 20 cm to 40 cm, providing a range of possible conversions.

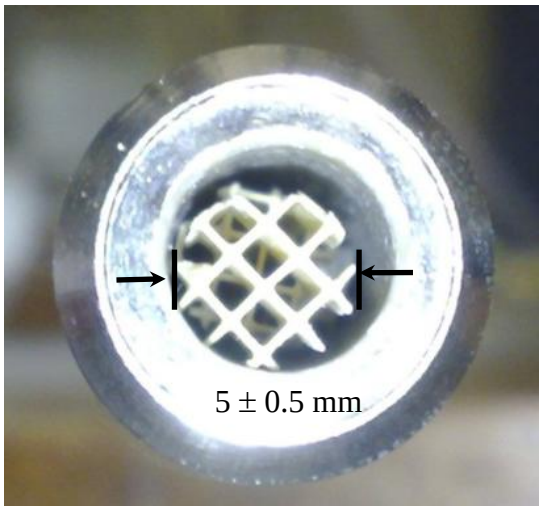

Figure 5.3: Front view of a monolith piece in the experimental reactor.

For example, if $\nu_0 = 1.0$ ml min^{-1} is chosen, the comparison of all the useful values is shown in Table 5.1.

Table 5.1: Estimation of parameters for reactor design.

Number of monolith pieces	**20**	**40**
V, cm^3	4 ± 0.8	8 ± 1.5
W, mg	≈ 100	≈ 270
X (from Figure 5.2)	≈ 0.1	≈ 0.3
τ, min	≈ 3	≈ 6
SV, min^{-1}	≈ 0.4	≈ 0.2
LHSV	≈ 20	≈ 10

5.1.2 Configuration of a continuous flow reactor packed with monolith for biodiesel production

The design of the experimental apparatus is illustrated in Figure 5.4. This consists of:

- Two HPLC pumps (supplied by SSI Lab Alliance).
- One reactor with a heated oil jacket (manufactured in the workshop, University of Bath).
- One back pressure regulator valve (supplied by Tescom, Germany)
- Cooling coil (L= 1.5 m and o.d. = 6 mm).
- Hot oil circulating bath (Grant GP200), with oil flow = 17 litre min^{-1}.

The temperature of the reactor was regulated by circulating a heat transfer fluid (Julabo Thermal HC20S) through a heated outer tube. The i.d. of the reactor was 6.22 mm (o.d. = 9.53 mm), and the i.d. of the outer heated oil tube was 22.25 mm (o.d. = 31.8 mm). The liquid feed inlet and the heat transfer fluid inlet were both at the base of the reactor and flowed in a co-current direction. The overall length of a heated section was 500 mm, and it was possible to clamp extra sections as illustrated in Figure 5.4. The reactor tube was filled with short lengths of monolith coated with zinc proline (prepared using the methods described earlier in Chapter 4). A 10 mm slice of monolith was first cut from a cordirite monolith block, and then a core cutter (6 mm o.d.) was used. Each piece was:

$$\text{o.d.} = 5 \text{ mm} \pm 0.5 \text{ mm}$$

$$L = 10 \text{ mm} \pm 0.5 \text{ mm}$$

A cooling coil was connected to the reactor outlet. At the base of the reactor, space was provided to enable a pulsating device to be installed in the future (not done in this thesis).

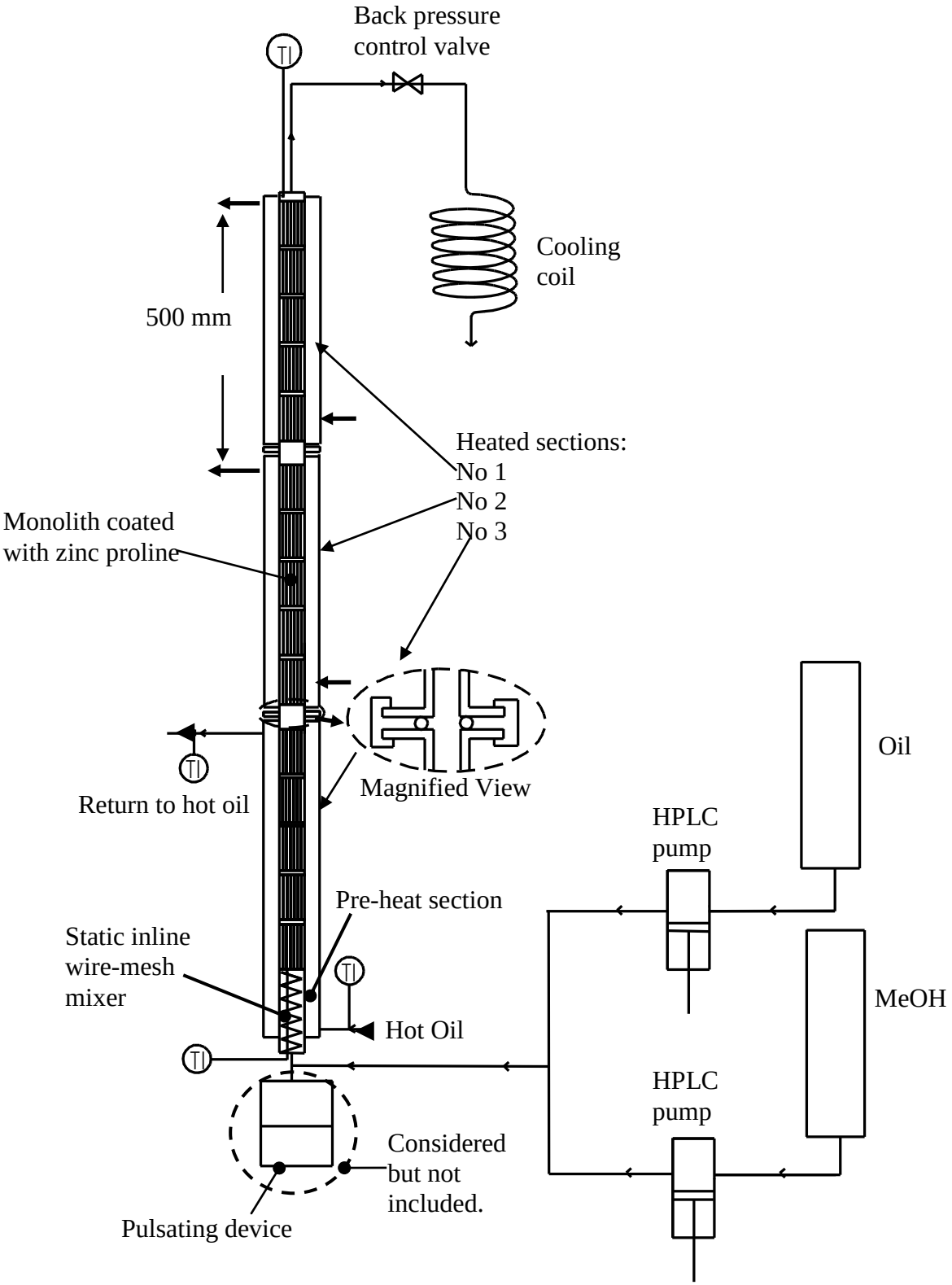

Figure 5.4: Schematic diagram of the experimental rig for the continuous monolith reactor system.

In order to improve the mixing between the two reactants, the first part of the reactor was filled with wire mesh to act as an in-line static mixer (length = 100 mm). Although it was initially planned to use a pulsating devise to aid mixing, this was not explored in this thesis. The mixing section also acted as a pre-heating section. The length of this wire mesh section was considered adequate to raise the temperature from 20°C to a reaction temperature of about 195°C. This was checked by performing a simple heat transfer calculation using (e.g. Geankoplis, 2003) :

$$\dot{Q} = \frac{U\ A\ (T_2 - T_1)}{\ln[(T_w - T_2)/(T_W - T_1)]} \tag{5.8}$$

where

$\dot{Q}$ is the heat transferred to the system (W s^{-1})

U is the overall heat transfer coefficient (W m^{-2} K^{-1})

A is the area of heat exchange (m^{-2})

T_w is the wall temperature

T_1, T_2 are the outlet and inlet oil temperatures respectively.

These calculations were supported by a simple experiment in which the fluid flowed through a coil immersed in a hot water bath, and the temperature was measured for a known liquid flow. Useful thermal properties of the fluids are presented in Appendix H.

5.2 Residence time distribution (RTD)

In order to explore the nature of flow inside the experimental reactor, some RTD studies were performed.

5.2.1 Theoretical background

The measurement and analysis of residence time has become a tool in continuous flow reactor systems to analyse and characterise the flow non-idealities and mixing that occurs in a chemical reactor. The RTD is determined experimentally by injecting an inert tracer into the reactor, at some time t = 0 and then measuring the tracer concentration, C, in the effluent stream as a function of time (Fogler, 2006).

As described in Fogler (1999):

> "In an ideal plug-flow reactor, all the atoms of material leaving the reactor have been inside it for exactly the same amount of time. Similarly, in an ideal batch reactor, all the atoms of materials within the reactor have been inside it for an identical length of time. The time the atoms have spent in the reactor is called the *residence time* of the atoms in the reactor."

In a tubular reactor, plug flow, or an approach to plug flow conditions is often considered desirable.

In order to understand the concept of plug flow, the velocity profile for plug flow is often compared with that obtained in laminar or tubulent flow (Ni, 1999). The three profiles are shown in Figure 5.5, and are described in Ni (1999):

(i) In laminar flow, the velocity at the centre of the tube (along the dotted line) is equal to that of the incoming flow, u, while the velocity at the wall equals to zero (due to viscosity), giving the well-known parabolic velocity profile. Hence, there is a velocity gradient along the radial direction. As a consequence, the fluid element at the centre would come out of the tube first and that at the wall would come out last – that is, the fluid elements would have different residence times in the tube.

(ii) In turbulent flow, the laminar parabolic velocity front is significantly flattened; however, there is still a laminar sublayer remaining in the velocity profile. For a given fluid (ρ and μ) and tube diameter (d), the main criterion that separates laminar from turbulent flow is the fluid velocity – generally the net flow Reynolds number, Re_n.

(iii) In plug flow, all the velocity components in the tube equal that of the incoming flow, u; hence there is no velocity gradient in the radial direction, indicating complete mixing across the tube. Also, because of the velocity profile, all fluid elements travelling through the vessel will have an equal residence time.

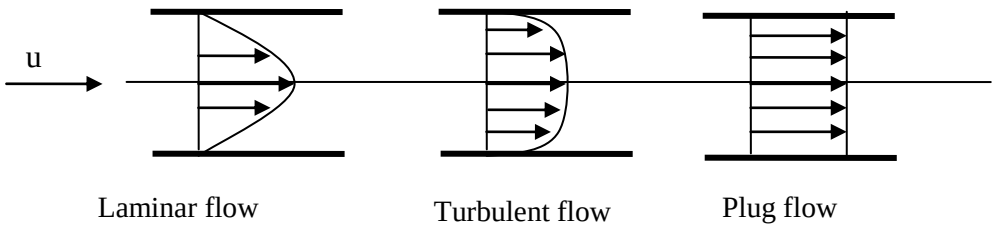

Figure 5.5: Velocity profiles for laminar, turbulent and plug flows (adapted from Ni, 1999).

One of the methods used to study RTD is to use a pulse input. In a pulse input, an amount of tracer is suddenly injected in one shot into the feed stream entering the reactor in a short interval of time. The outlet concentration is then measured as a function of time. The effluent concentration-time curve is referred to as the C curve in the RTD analysis.

5.2.2 Experimental set-up

The set-up for the experiment is shown in Figure 5.6. An HPLC pump was used to feed deionised water from a water reservoir to the reactor (a stainless steel tube with i.d. 6.2 mm, L = 700 mm). A 'cross-fitting' with one injection port was used to connect the feed stream to the reactor. The experiment was started by flowing the deionised water until the water filled the conductivity meter. The water flow was assumed to be representative of oil and MeOH mixture. The difference of estimated superficial velocity for the water and oil/MeOH mixture is considered small (*e.g* at flowrate of 1.0 ml min^{-1}, υ_0, without monolith packed is 0.55 mm s^{-1} for water, and 0.96 mm s^{-1} for oil/MeOH mixture). Then, 2 ml of tracer was injected into the deionised water flow, and the salt concentration at the reactor outlet was measured (using a conductivity meter). In this experiment, potassium chloride solution (0.025 M) was used as a tracer and the response was monitored. The conductivity probe was first calibrated with a known concentration of salt solution. The calibration plot is shown in Appendix I (I1).

Using this technique, experiments were performed:

(a) With no monolith in the tube (L = 700 mm),

(b) With 20 pieces of monolith (200 mm) inside the 700 mm tube, and

(c) With 40 pieces of monolith (400 mm) inside the 700 mm tube.

The monolith pieces had to be pre-treated with a commercial sealant to seal the monolith pores to prevent the salt from being adsorbed into the pores of the monolith. surface. It is worth mentioning that a PVA type of sealant was found to be unsuitable for this application. This pre-treatment procedure was developed after preliminary trials with untreated monoliths showed no conductivity response (*i.e.* no salt solution tracer at the reactor outlet). To seal the pores, the monolith pieces were soaked in a solvent-based sealant solution (Thompson's Water Seal brand) overnight, and then dried with a cold air blower to remove the excess solution. In order to make sure the monoliths were fully dried, they were left in the fume cupboard for 3 to 4 hours.

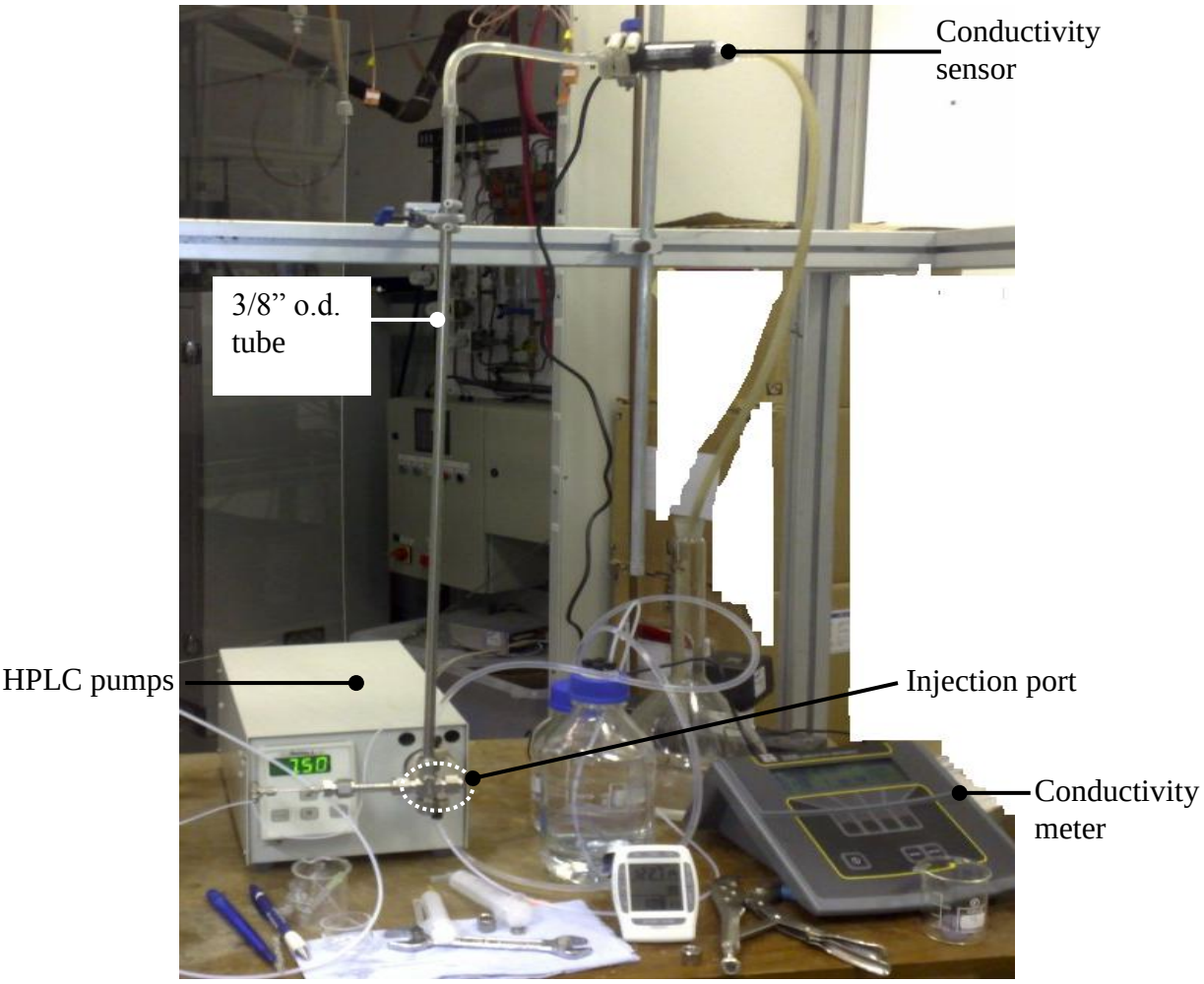

Figure 5.6: Experimental set-up for the RTD experiment.

5.2.3 Measurement of response curve

Experiments were performed at three different flowrates:

(a) low flowrate = 0.1 ml min^{-1},

(b) medium flowrate = 1.0 ml min^{-1}, and

(c) high flowrate = 2.9 ml min^{-1}.

The results are presented as C curves in Figures 5.7 to 5.10.

From this set of experiments, there are a number of interesting observations:

(a) At the high liquid flow, the mean residence is less than at the lower flows, and as expected the shape of the C curve is sharper and closer to plug flow.

(b) The use of monoliths increase the sharpness of the peak in the curves and approach to plug flow conditions.

(c) At both medium and low flows, the RTD remains very broad.

(d) At the very low flow (see Figure 5.9), the mean residence time is very long (i.e. 300 to 400 min), and experiments were not performed on the 40 pieces monolith reactor.

(e) The area under the C curve needs to be checked to ensure that total mass of tracer in = mass of tracer out.

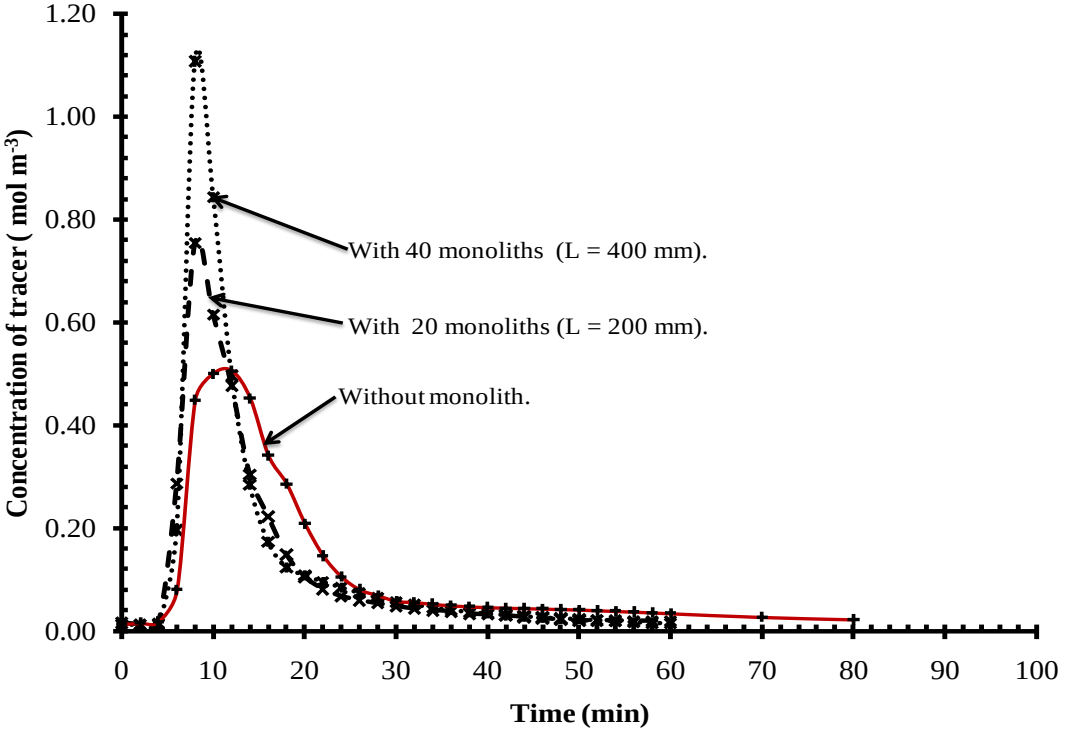

Figure 5.7: Comparison of C curves with and without monoliths at a flow of 2.9 ml min^{-1}.

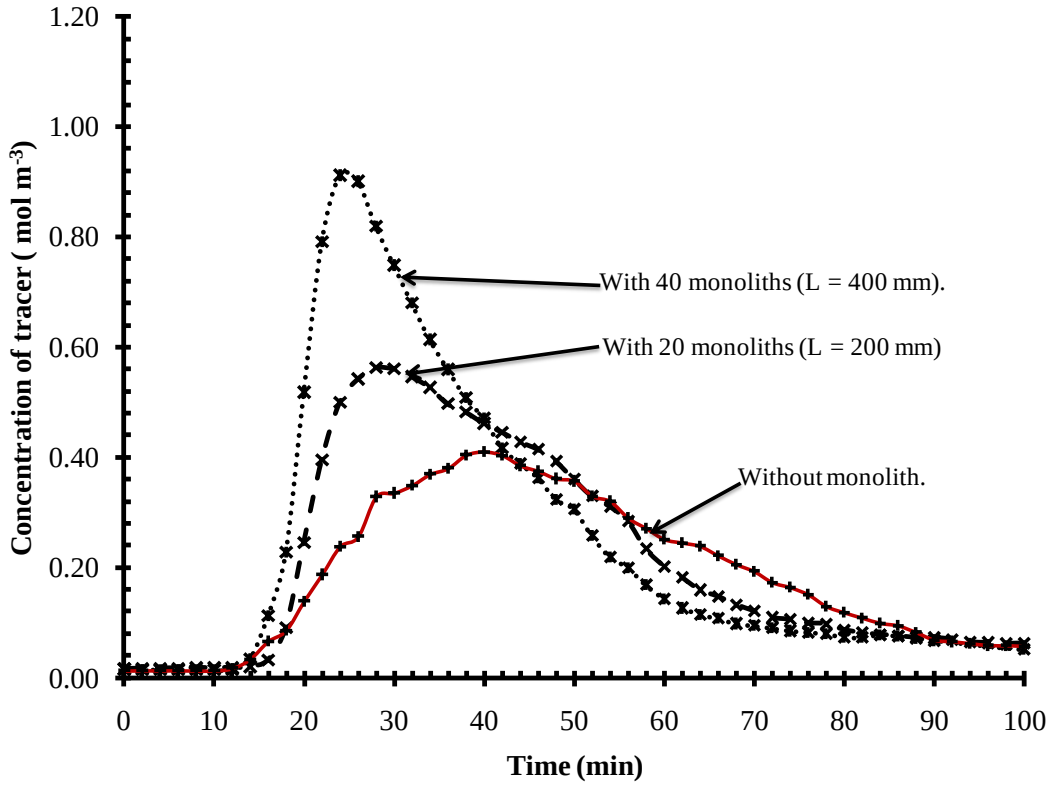

Figure 5.8: Comparison of C curves with and without monoliths at a flow of 1.0 ml min^{-1}.

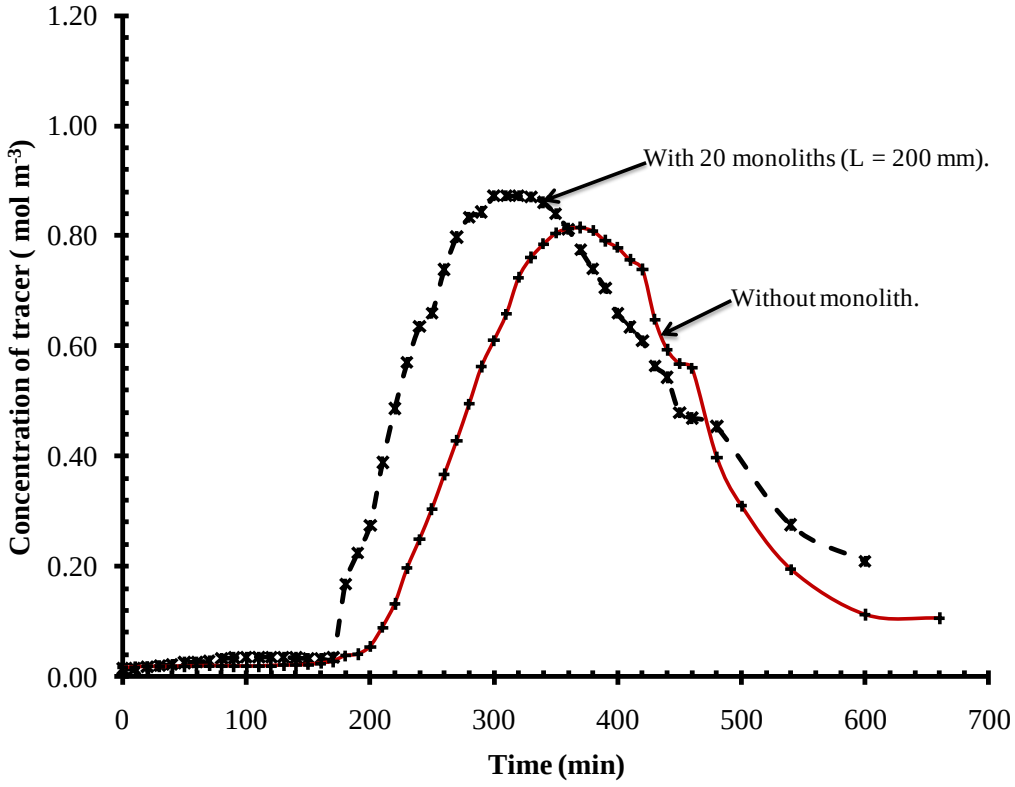

Figure 5.9: Comparison of C curves with and without monolith at a flow of 0.1 ml min^{-1}.

In theory, the total area under C curve should match the amount of tracer injected into the system. The total amount of material injected into the reactor was calculated using the following equation (Fogler, 2006):

$$M_{tracer} = \int_0^\infty \nu\, C(t)dt \qquad (5.9)$$

From this type of calculation, the % tracer injected that was detected in the outlet stream is shown in Table 5.2.

Table 5.2: The % of tracer detected in the outlet stream.

Inlet Flowrate	**2.9 ml min^{-1}**	**1.0 ml min^{-1}**	**0.1 ml min^{-1}**
Without monolith.	95 %	~40 %	~14 %
With monoliths	21 to 47 %	36 to 50%	~25%

From the results in Table 5.2, it is clear that in many of these experiments, a significant amount of tracer is unaccounted for. Only in the high flow (2.9 ml min^{-1}) experiment without monolith was 95% of the tracer present in the outlet stream. Although it was known that superficial velocities were low in this experiment (see Table 5.3), it was only after performing this experiment that the difficulty of this experimental technique at such flows was appreciated. This problem is also mentioned in Reis *et al.* (2010): "A major issue with this technique is the effect of the tracer density (solution of NaCl or KNO_3) which affects the sensitivity of the determination." This most probably relates to possible density differences between the injected tracer and the feed fluid.

Table 5.3: Superficial liquid velocity value for each flowrate.

Flowrate (ml min^{-1})	2.90	1.00	0.10
Superficial water velocity, μ (mm s^{-1})	1.60	0.55	0.06

To explore possible causes a repeatability experiment was performed, which is described in the following section.

5.2.4 Repeatability study

(a) Very high flow (10 ml min^{-1}):

To test the accuracy and sensitivity of the conductivity meter, a tracer was injected into a higher flow (10 ml min^{-1}) three times consequently after each cycle of response. The results are shown in Figure 5.10, showing that the technique is repeatable.

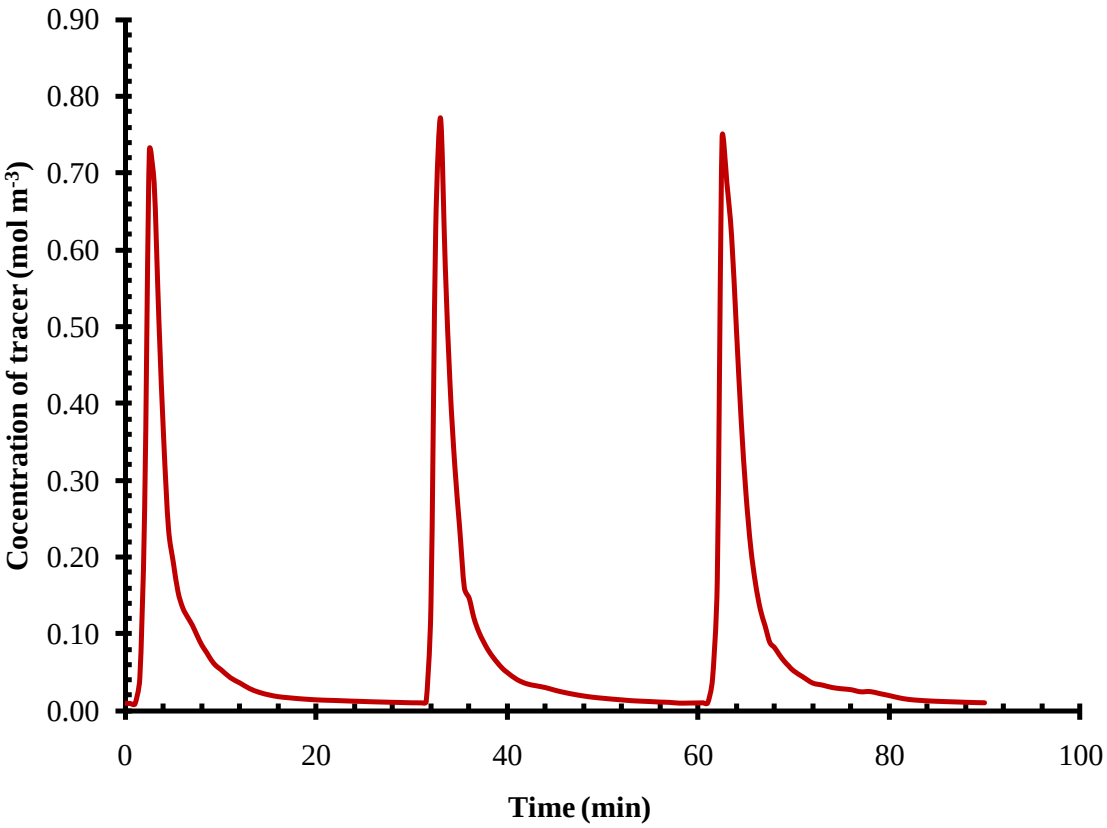

Figure 5.10: Concentration curve for three impulses of tracer injection in continuous RTD experiment at a flow of 10 ml min^{-1}.

(b) Low flow (0.1 ml min^{-1})

To check the accuracy of the conductivity measurement at the lowest flowrate (i.e 0.1 ml min^{-1}), it was decided that it was necessary to find a method that could record the result over a lengthy time period. A new way to record the reading was developed with help from colleagues. For this purpose, the conductivity meter was connected to a computer and the result was recorded using LabView software. After the injection of tracer, the experiment was left running continuously for 2 days. The response measurement was recorded and is reported in units µS cm^{-1}. Figure 5.11 shows the response curve after the injection of two pulses of tracer:

(i) The 1st pulse was inject at t = 0.

(ii) The 2nd pulse was injected at t = 22 h.

In the first day, between 10 to 15 hours, there was a technical problem with the software, and the recording of conductivity stopped temporarily. Since the aim was to check the consistency of measurement, a general observation can still obtained. The result showed that at that flowrate, it took almost 4 hours before the tracer was detected and then it took another 10 h before the signal from the tracer decayed. This technique is not suitable at very low flowrates (e.g. 0.1 ml min^{-1}). To explore this problem further, it was decided to perform experiments in a glass tube, and to use a dye.

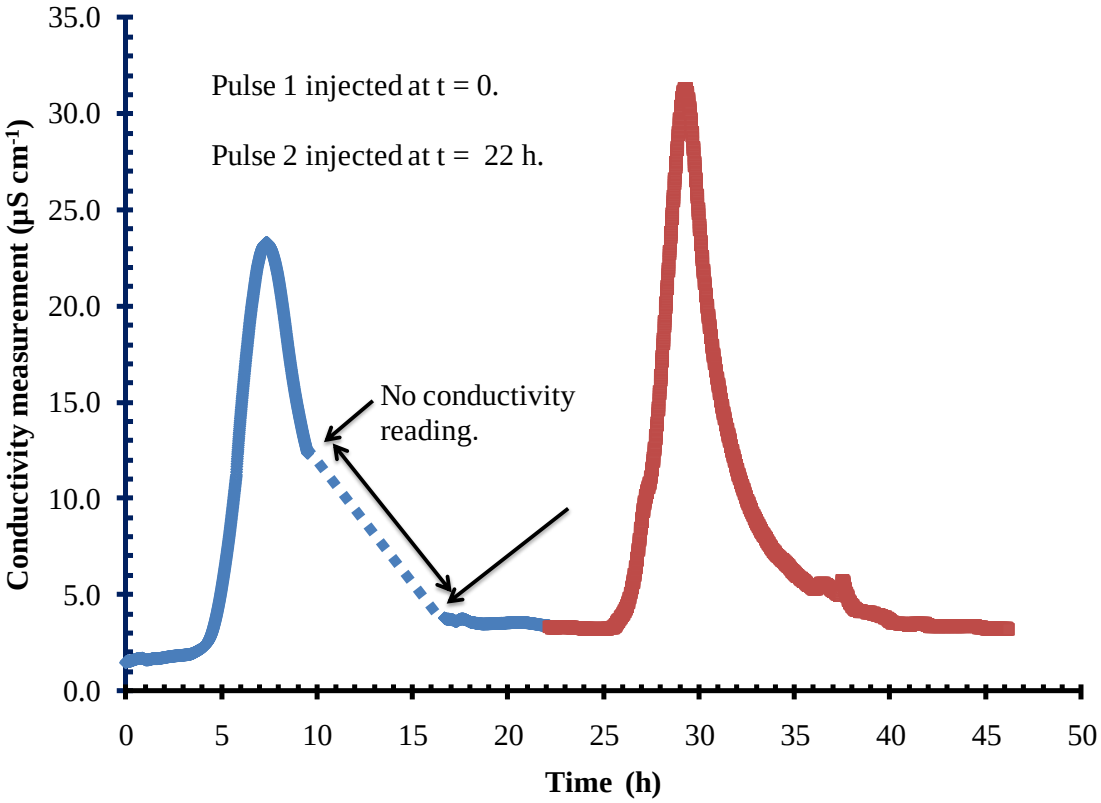

Figure 5.11: Conductivity curve with two-step pulse injection at a flow of 0.1 ml min^{-1}.

5.2.5 Experiments using a dye as a tracer

The stainless tube was replaced with a glass tube, and a dye (potassium permanganate) was injected. The glass tube had the same diameter (i.d. = 6.22 mm) as the steel tube. The experiment set-up is shown in Figure 5.12. A known quantity of dye (1 ml) was injected *via* the injection port, and the time taken for the dye to travel between two marked points was monitored. The retention time was estimated from the time it took the coloured liquid to pass between the two points. The results are shown in Table 5.4. From these, the retention time of the dye is very close to the theoretically calculated valves (assuming plug flow).

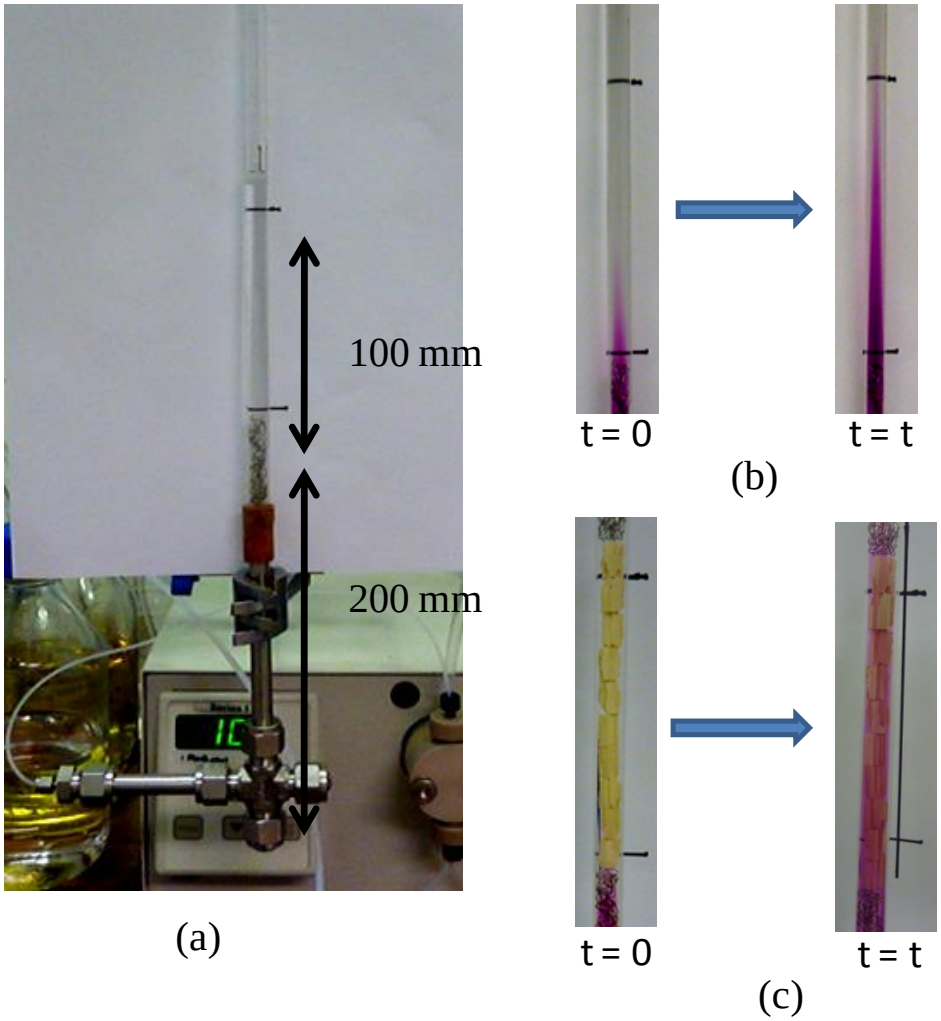

Figure 5.12: Apparatus and visual observations from dye (potassium permanganate) injection: (b) Experiment with an empty glass tube, and (c) Experiments with 10 monolith pieces in the tube.

Table 5.4: Estimated and experimentally measured times for each flowrate.

Flowrate (ml min^{-1})	2.90	1.00	0.10
Theoretical residence time = V/Q (min)	7	20	200
Experimental residence time (min)	8.5 ± 1.5	18.5 ± 1.5	200 ± 10

5.2.6 Interim conclusions from RTD

The tracer method was found not suitable for the RTD study at the flows used in this thesis, for example, at the flowrate of 0.1 ml min, > 80 % of tracer was not seen at the exit. Despite facing many issues with the RTD technique, the method used was able to show some useful qualitative outcomes, which are summarised as follows:

i) At high flows, the C curve shows that the presence of the monolith helps to approach plug flow conditions in the reactor.

ii) The extended trace trail from the C curve most probably signifies the presence of dead volume in the reactor, presumably in the T-connector.

iii) The broadening in concentration response at low flow indicates the presence of back-mixing. Use of salt tracer at such low flows is clearly not appropriate.

iv) Visual dye experiments were useful in confirming that the mean residence time matched expected values from plug-flow calculations.

5.3 Continuous biodiesel production

Figure 5.14 shows the constructed experimental rig which was used for the continuous transesterification reaction. The reactor was packed with pieces of monolith and then connected to the hot oil system. The experiment was started using the following procedure:

i. The temperature of the oil bath was set to 70°C, and hot oil was circulated.
ii. The two HPLC pumps were turned on, and rapeseed oil and methanol were fed into the reactor.
iii. The pressure in the reactor increased and finally this reached a set valve of 20 bar (set with back-pressure regulator).
iv. When a pressure of 20 bar was reached, the temperature of the oil bath was increased to 195°C.

The run-time was started after the pressure and temperature were constant or the system was in pseudo-steady-state. The time for system to achieve steady state was approximately one hour. Then, the reaction was allowed to achieve a constant flowrate for about another 20 to 30 minutes. During the course of an experiment, liquid samples were collected (1 to 2 ml) from time to time (e.g. every 30 minutes). The samples were then analysed using gas chromatography as described in Chapter 3. See page 105 for a discussion on the experimental error.

To shutdown the operation, the pressure of the reactor needs to be decreased to atmospheric. First, the circulating heated oil was shut off and left for 2 or 3 hours for the reactor to cool down. Then, the two HPLC reactant feed pumps were turned off. After the pressure has completely dropped, the back-pressure regulator was turned fully open and the remaining reactants was drained.

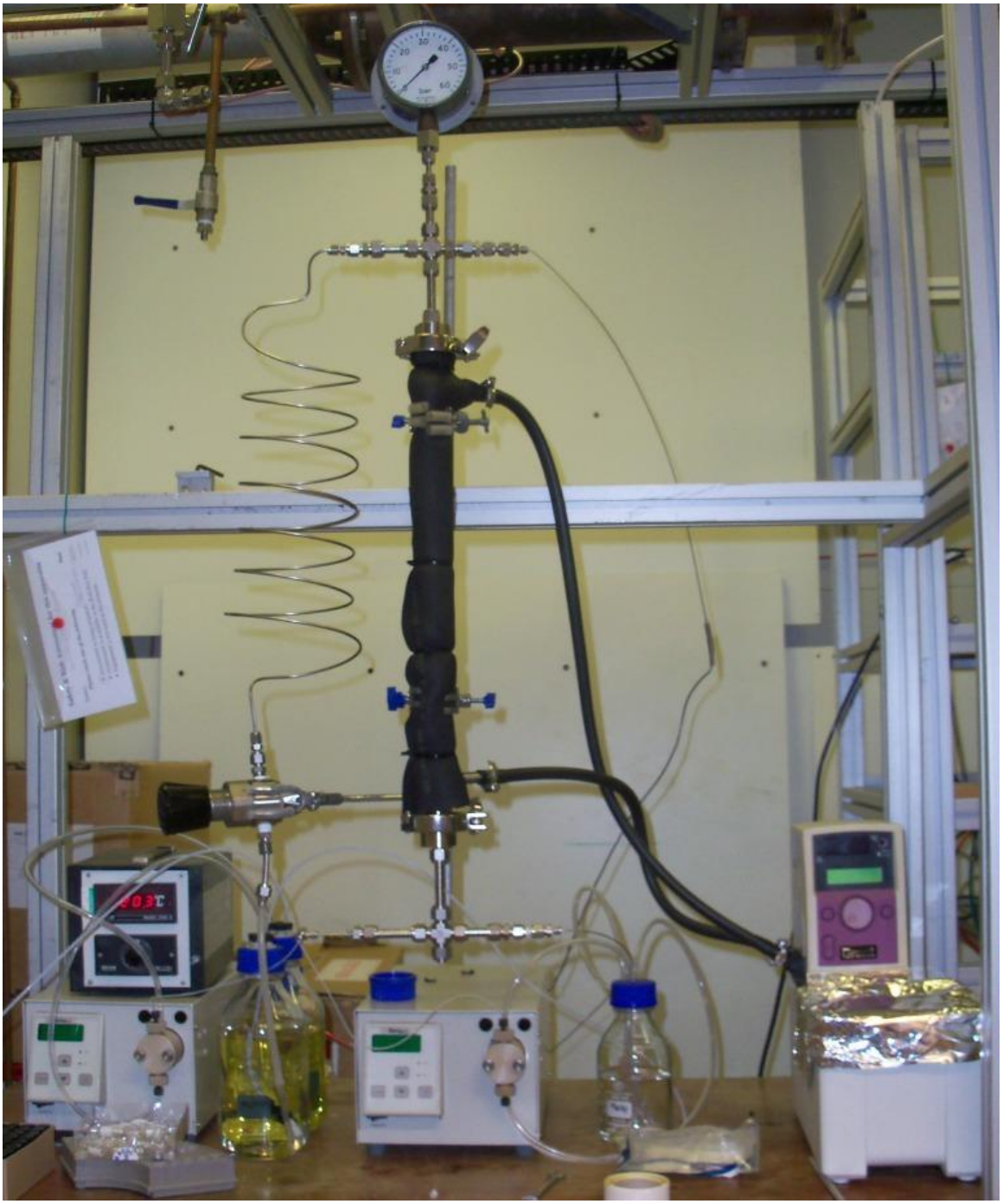

Figure 5.14: The experimental set-up for the continuous reaction experiments.

5.3.1 Performance of the continuous flow monolith reactor

All of these experiments were performed at a constant pressure of 20 bar and a temperature of 195°C. This experiment was to select the most suitable condition (i.e. monolith bed length and inlet flowrates) in order to achieve a high conversion. Reactor performance was assessed by calculating the conversion of triglycerides to methyl esters using the technique described in Chapter 3. Table 5.3 summarises the results of these experiments.

(a) Using 20 monoliths in a 200 mm bed:

The tubular reactor was packed with 20 pieces of monolith. The total coated mass of zinc proline was 38.5 ± 0.5 mg, and coating method A was used. The experiment was run at a high flow of 2.9 ml min^{-1}, with a molar ratio of MeOH to oil = 12:1. As a conversion of 6.29 wt % was obtained in the first run, experiments were performed at lower flows (i.e. 1.0 and 0.11 ml min^{-1}). The maximum conversion obtained was 28 wt% at the lowest flows of 0.11 ml min^{-1} with a FAME yield of 15 wt%.

(b) Using 20 monoliths in a 200 mm bed (with diglyceride in feed):

In order to explore if the miscibility between methanol and oil was limiting the conversion, it was decided to add 0.5 wt% of pure diglyceride with the feed oil. It is mentioned in Babcock *et al.* (1998), that the intermediates diglycerides and monoglycerides contain one and two hydroxyl groups respectively, and therefore have a greater preference for the methanol phase than does the oil. However, the result in Table 5.5 (b) show that the conversion decreased instead. This may have occurred because of catalyst deactivation which is discussed in more detail in subsequent sections. An interesting point to be highlighted, is that although the addition of 0.5 wt% of diglyceride into the oil did not increase the FAME yield, the yield of monoglyceride was 0.5 wt%, indicating that all of the diglyceride that had been added to the feed was converted to monoglyceride.

(c) Using 40 monoliths in a 400 mm bed:

In order to increase the conversion, the monolith bed was extended to 400 mm. The mass of catalyst in this longer bed was approximately 82.3 ± 0.7 mg, approximately twice that of the first run. From the result in Table 5.3 (c), as expected the conversion increased as the flow is decreased, and in general is also higher than obtained in the shorter length of bed. Also, it is encouraging to observe that the yield of FAME has also increased.

At this point it is interesting to compare, the estimated value of conversion obtained. Selecting valves from Table 5.5 (a) and (c), and comparing them with Figure 5.1, then:

At $\nu_0 = 1.0$ ml min^{-1}

For W = 38.5 mg , then X = 0.10 (in experiment, Table 5.3 (a))

and X = 0.04 (in Figure 5.1)

For W = 82.3 mg, then X = 0.13 (in experiment, Table 5.3 (c))

and X = 0.08 (in Figure 5.1)

Next, catalyst stability is considered in more detail.

Note:

Yield : This term is used in this thesis to represent the wt% of product (or intermediate) measured in a sample of solution taken from the reactor.

Table 5.5: Result from the continuous flow reaction experiments (T = 195°C, P = 20 bar, coated using Method A).

(a) 20 pieces of monolith (L = 200 mm)

Experimental conditions		Transesterification result					
Catalyst loading (mg)	**Total Flowrate (ml/min)**	**TG content (wt%)**	**DG content (wt%)**	**MG content (wt%)**	**FAME content (wt%)**	**GL content (wt%)**	**Conversion of reaction (%)**
38.5 ± 0.5	2.9	93.72	5.51	n.d	0.78	n.d.	6.28
	1.0	90.17	8.22	n.d	1.60	n.d.	9.83
	0.1	71.92	12.58	0.19	15.32	n.d.	28.08

n.d. is not detected.

(b) 20 pieces of monolith (L = 200 mm) and with the addition of 0.5 wt% of diglyceride into the feed.

Experimental conditions		Transesterification result					
Catalyst loading (mg)	**Total Flowrate (ml/min)**	**TG content (wt%)**	**DG content (wt%)**	**MG content (wt%)**	**FAME content (wt%)**	**GL content (wt%)**	**Conversion of reaction (%)**
38.5 ± 0.5	0.1	85.66	8.73	0.54	5.08	n.d.	14.34

(c) 40 pieces of monolith (L = 400 mm)

Experimental conditions		Transesterification result					
Catalyst loading (mg)	**Total Flowrate (ml/min)**	**TG content (wt%)**	**DG content (wt%)**	**MG content (wt%)**	**FAME content (wt%)**	**GL content (wt%)**	**Conversion of reaction (%)**
82.3 ± 0.7	2.9	93.99	4.54	n.d	1.47	n.d.	6.01
	1.0	86.61	7.49	0.12	5.78	n.d.	13.39
	0.1	19.53	8.67	8.70	57.16	5.94	80.47

5.3.2 Catalyst stability

Catalyst stability was studied in more detail, using a flowrate of 0.11 ml min^{-1}. The length of the monolith bed used in this study was 400 mm. For this purpose, 3 different sets of monolith were freshly prepared:

(a) Using Method A (62.2 ± 0.5 mg of catalyst).
(b) Using Method B (104.9 ± 0.5 mg of catalyst).
(c) Using uncoated monolith which had been dried in a flow of nitrogen.

The catalyst loading for monoliths prepared by Method A was slightly lower (24.4%) than that used in the previous run. As the geometry of the monolith pieces is cylindrical with a small diameter (o.d. = 5 mm), made it very difficult to be consistent with the level of coating. In Method B, the catalyst loading was higher by 68.7 % than of the catalyst loading in Method A. This was because of the coating technique. Also, the catalyst loading amount was simply quantified by the weight difference of monolith before and after coating. Although this is a common way used by others, to be more accurate, a more sophisticated method need to be explored. This was not covered in this thesis.

The results of these experiments are shown in Figure 5.14, and the following observations can be made:

i) The initial conversion for monoliths coated using method A (54.1 wt%) is lower than in the previous experiment (80.5 wt%), most probably because of the lower catalyst loading (62.2 mg instead of 82.3 mg).
ii) The performance of monoliths coated by Methods A and B is similar. Although the catalyst loading in Method B is higher, this did not improve the level of activity. This had already been discussed earlier in the batch experiments in Chapter 4.
iii) The bare monolith showed catalytic activity, but deactivated after 60 minutes of running time.
iv) There are fluctuations in the conversion, most probably caused by back-mixing and liquid hold-up effects as these low flowrates.

v) In general, for all of the samples tested there is a loss in activity with time, even in the case of the bare (uncoated) monolith.

vi) In Figures 5.15 and 5.16, the composition of the intermediates is followed. Despite the drop in the production of FAME, it is interesting to observe that the level of DG remains relatively constant. There is also consistency in the results for the two methods of coating.

The observed trends show a reduction of conversion in a relatively short period of time (30 to 60 min). This also shows the value of performing extended experiment in a flow reactor of this type. The loss in the performance of the catalyst could be occurring for a number of reasons, for example:

(i) The catalyst may be leaching,

(ii) The catalyst may be fouled,

(iii) The catalyst may be poisoned.

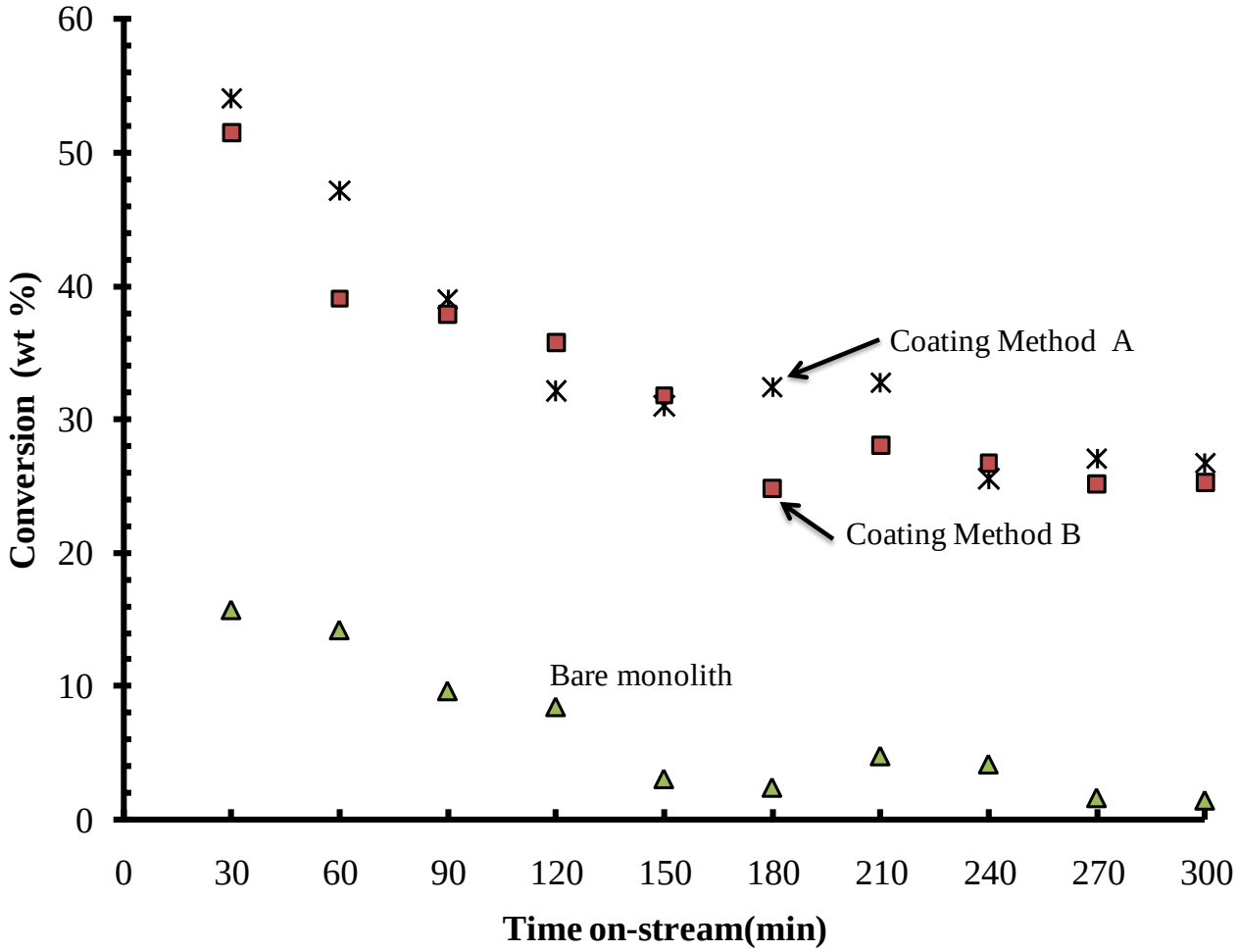

Figure 5.14: Conversion of TG over an extended run: $L_{monolith}$ = 400 mm; ν_0 = 0.11 ml min^{-1}; molar ratio methanol to oil = 12:1; catalyst loading = 62.2 mg (Method A) and 104 mg (Method B)).

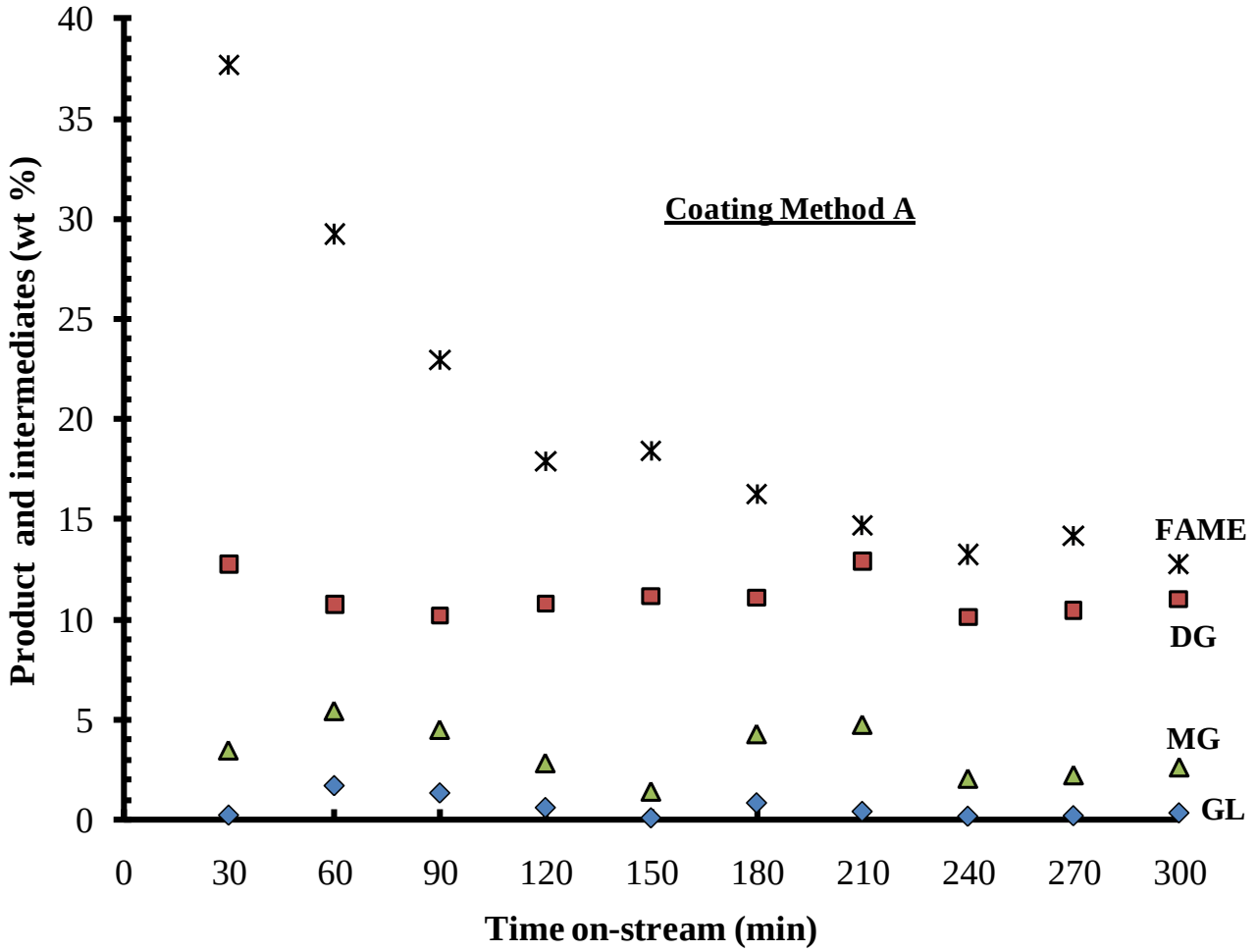

Figure 5.15: Production of FAME and intermediates over an extended run (coating Method A).

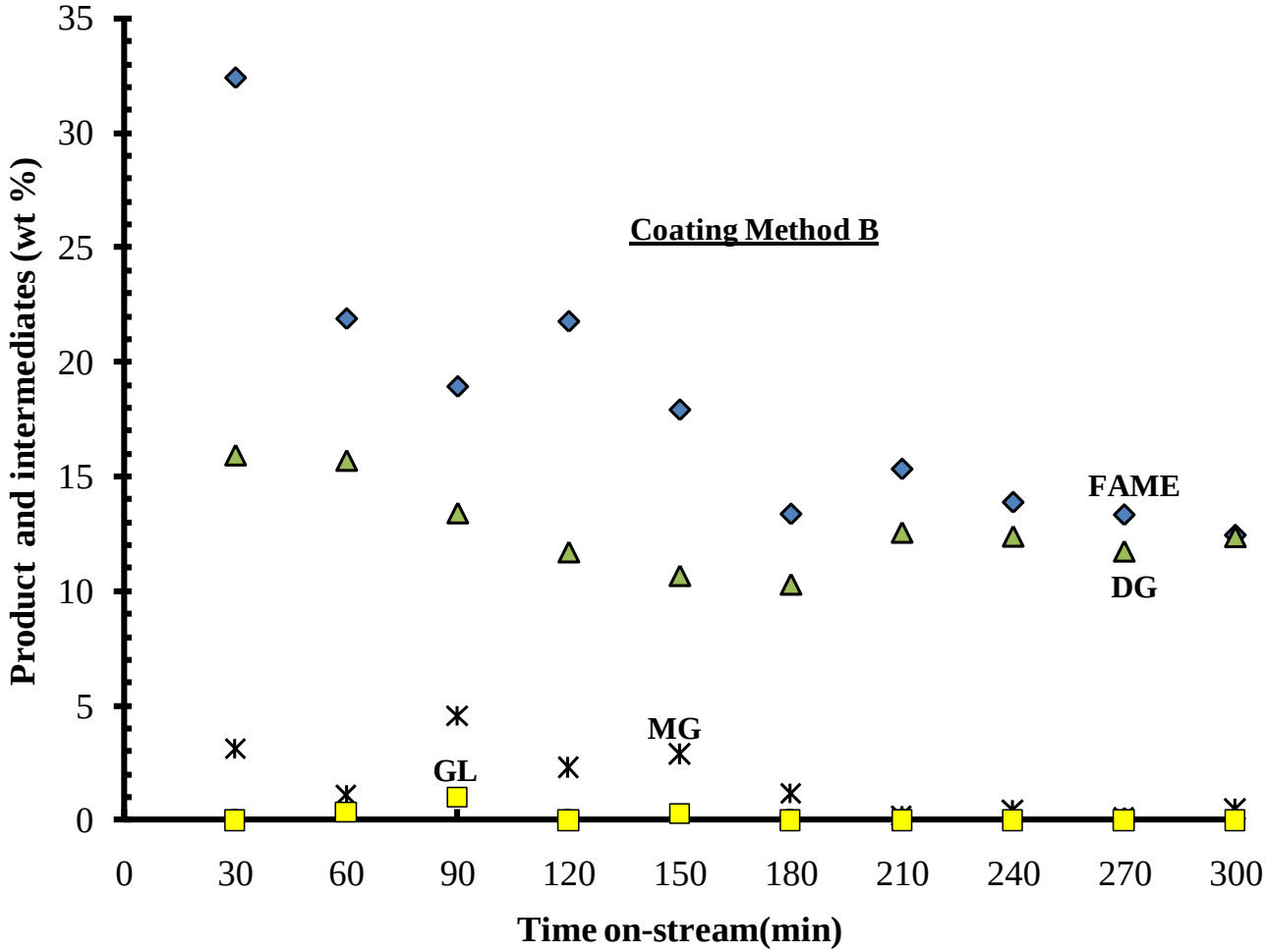

Figure 5.16: Production of FAME and intermediates over an extended run (coating Method B).

i) Catalyst leaching

To investigate the extent to which zinc proline leaches from the monolith, the product stream was analysed by an Atomic Absorption Spectrometer (AAS). Calibration and samples solutions were prepared by dissolving the sample in an organic solvent (4-metyl isobutyl ketone (MIBK)). A Perkin-Elmer® Model AAnalyst 100 atomic absorption spectrometer (with nitrous oxide-acetylene flame, with wavelength = 213.9 nm and slit = 0.7) was used.

Figure 5.18 shows the amount of zinc detected in samples taken for analysis. The total amount of zinc detected in a sample taken after 30 min was nearly 200 ppm, and this links with the sudden drop in reactivity. The samples in this analysis have two distinct layers, which are separated by their density. The upper layer consists mainly of FAME and glycerides as an apolar phase, while the bottom layer containing mainly glycerol and unreacted MeOH as a polar phase. As can be seen in Figure 5.17, most of the Zn is in the mixture of FAME and glycerides. The rate of leaching was approximately the same for both cases. As, the catalyst loading in Method B is approximately twice the amount in Method A, this indicates that catalyst loss is not proportional to catalyst loading. Also, when samples are taken and analyzed after 90 minutes of operation, the quantity of zinc detected is a lot less.

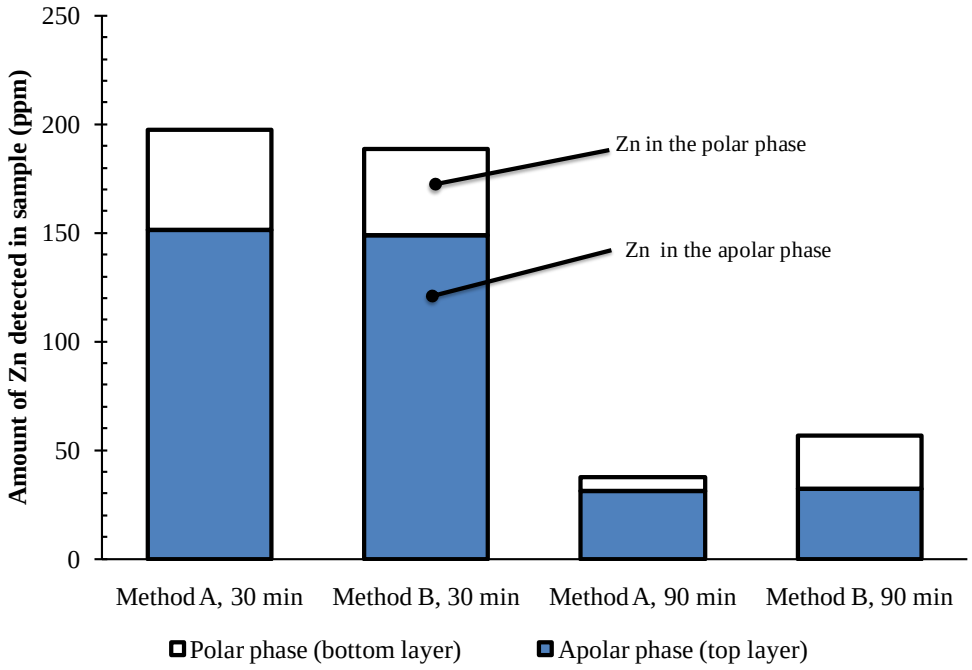

Figure 5.17: Comparison of zinc leached from Methods A and B.

The leaching of zinc compounds during a transesterification reaction has been studied by Pugnet *et al.* (2010). The leached amount reported in Pugnet *et al.* (2010) was as follows: for $ZnAl_2O_4$ catalyst, the zinc amount reaches 4 ppm in the ester phase and 2 ppm in the polar phase (glycerine). When ZnO was used as a catalyst, the zinc amounts reach 259 and 9 ppm in the polar and apolar phases, respectively.

The following are interesting discussion points raised in Pugnet *et al.* (2010)

(a) The leached species were expected to form zinc glycerolate, zinc carboxylate (soaps) or zinc methoxylate.

(b) The higher the FAME content produced, then the higher was the leached zinc content.

(c) There were two ways proposed in which the leached active species could influence the FAME yield, either (i) they stay in solution and cause homogeneous catalysis, or, (ii) they adsorb on the walls of the stainless steel reactor, or on the surface of a solid when present in the medium.

It is roughly estimated that the majority of zinc from the monolith leached into in both biodiesel and glycerol phases. The leached species could have been zinc oleate or zinc glycerolate. The shortcoming of zinc in biodiesel is that zinc can accelerate the oxidation process of biodiesel, creating problems as fuel insolubles or gels and salts (National Biodiesel Board, 2011).

ii) Surface may be fouled

It was decided to examine the surface of the coated used monoliths with SEM imaging. However, this proved to be difficult, as the monolith surface was impregnated with a range of oils/products.

The possibility of active site blockage was reported in Yan *et al.* (2008), when a CaO/MgO catalyst was used in their transesterification reaction experiments. Yan *et al.* (2008) confirmed the phenomenon, by showing that the catalyst could be regenerated by washing with ethanol and reutilised the catalyst. So, the spent monoliths from the experiment in this thesis (Methods A and B) were placed in a heated solution of ethanol at a temperature of 60°C for 3 to 4 hours, then rinsed with methanol three times, and blow dried with cool air and left for 24 hours. Figures 5.18 and 5.19 show the SEM

images of washed monoliths. In both of these images, the clear distinct structure of the zinc proline cannot be easily observed. It is difficult to conclude if this confirms the loss of zinc proline by leaching, or whether the surface remains fouled by reactants/products. Unfortunately, there was a lack of time to explore this further.

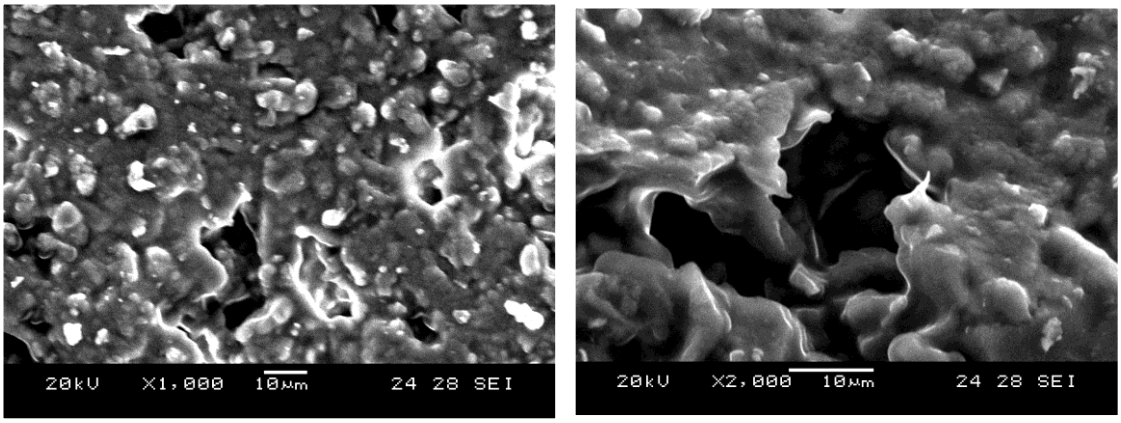

Figure 5.18: SEM images of used monolith coated with zinc proline (Method A).

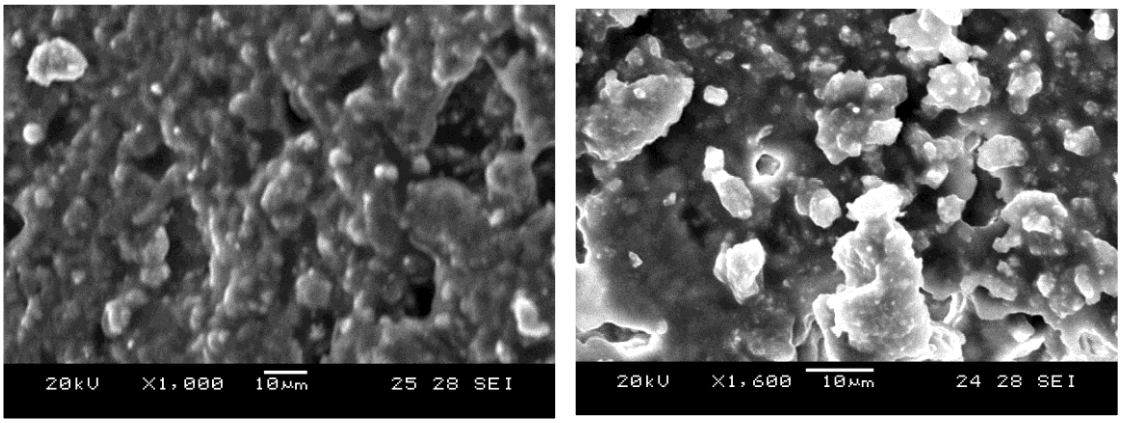

Figure 5.19: SEM images of used monolith coated with zinc proline (Method B).

5.3.3 Effect of methanol:oil ratio

If physical pore blockage was caused by more viscous products, then potentially run-time could be extended by using less viscous feed. Hence, further experiments were done at a higher methanol:oil ratio (36:1), which was three times higher than the ratio used in the previous experiment. The flowrate used for this run was 1.0 ml min^{-1} which was 10× higher than in the previous experiment.

The results from this experiment are shown in Figure 5.20 and the profiles of product and intermediates are shown in Figure 5.21. The results show that after 30 min of run-time complete conversion was achieved and the yield of FAME was 70.1 wt%. However, a sudden drop in reactivity was observed in this experiment, indicating the same trend of loss in catalytic activity as seen in earlier sets of experiments. Figure 5.21 shows the samples collected during this experiment. From the pictures, it is clear the samples have changed colour during the course of the experiment. Samples with a darker brown colour contained more FAME. The reason for the colour difference is uncertain, but it is assumed that the higher FAME content leads to the presence of more organic particulates being dissolved in the mixture, and this gives the darker colour.

From this experiment, it was found that an increase in molar ratio does increase the conversion and FAME yield. A conversion of 100 wt% of oil was achieved, higher than a 13.4 wt% conversion at the same flowrate with a lower MeOH:oil ratio. As found in Encinar *et al.* (2007), an excess of alcohol seems to favour conversion of di- to monoglycerides. In work done by Tonetto and Marchetti (2010), high yields were also obtained using a MeOH to oil ratio of 32:1 (with K/Al_2O_3 catalyst, in a batch reactor).

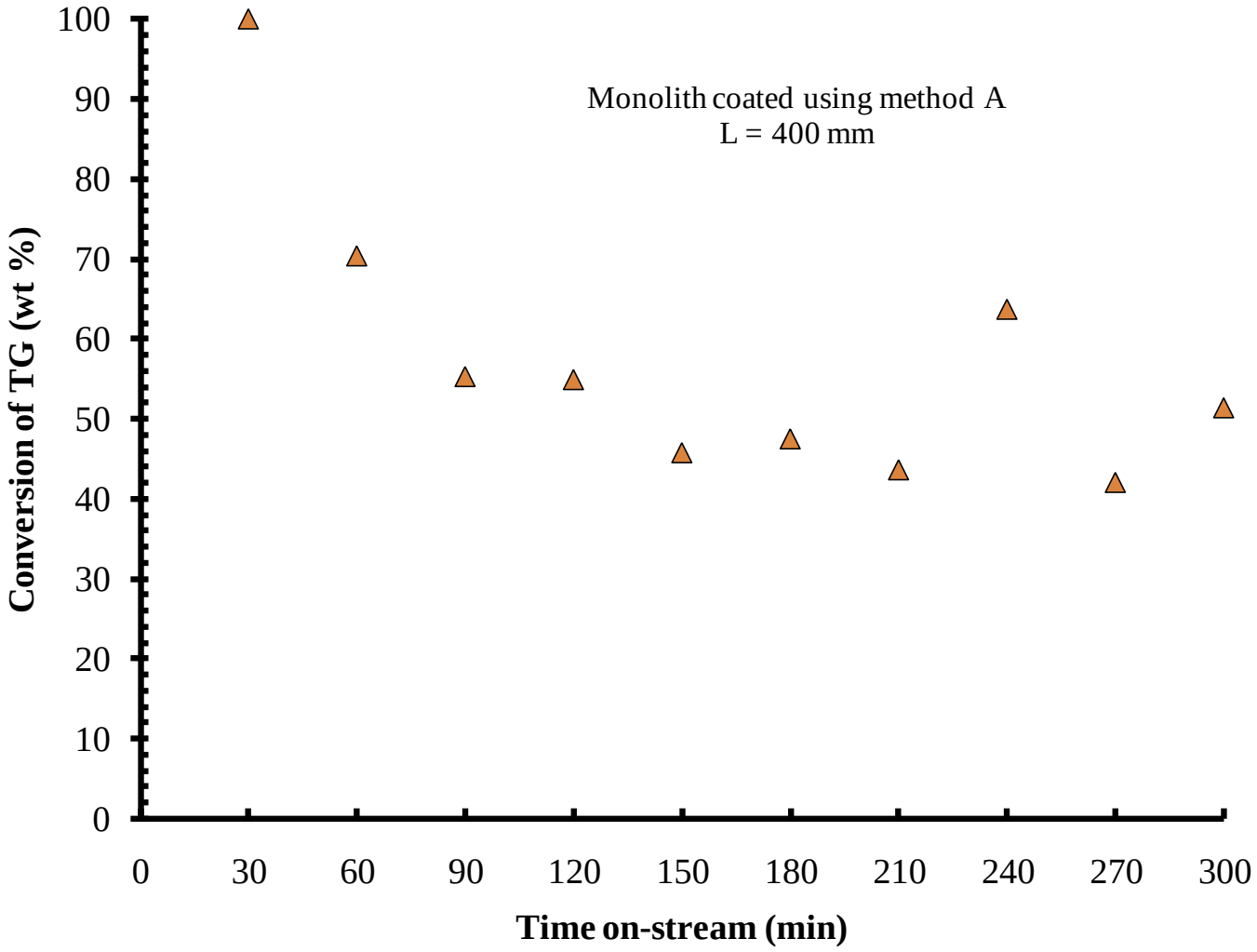

Figure 5.20: Conversion of TG over an extended run using a MeOH : oil ratio 36:1, and ν_0 = of 1.0 ml min^{-1}.

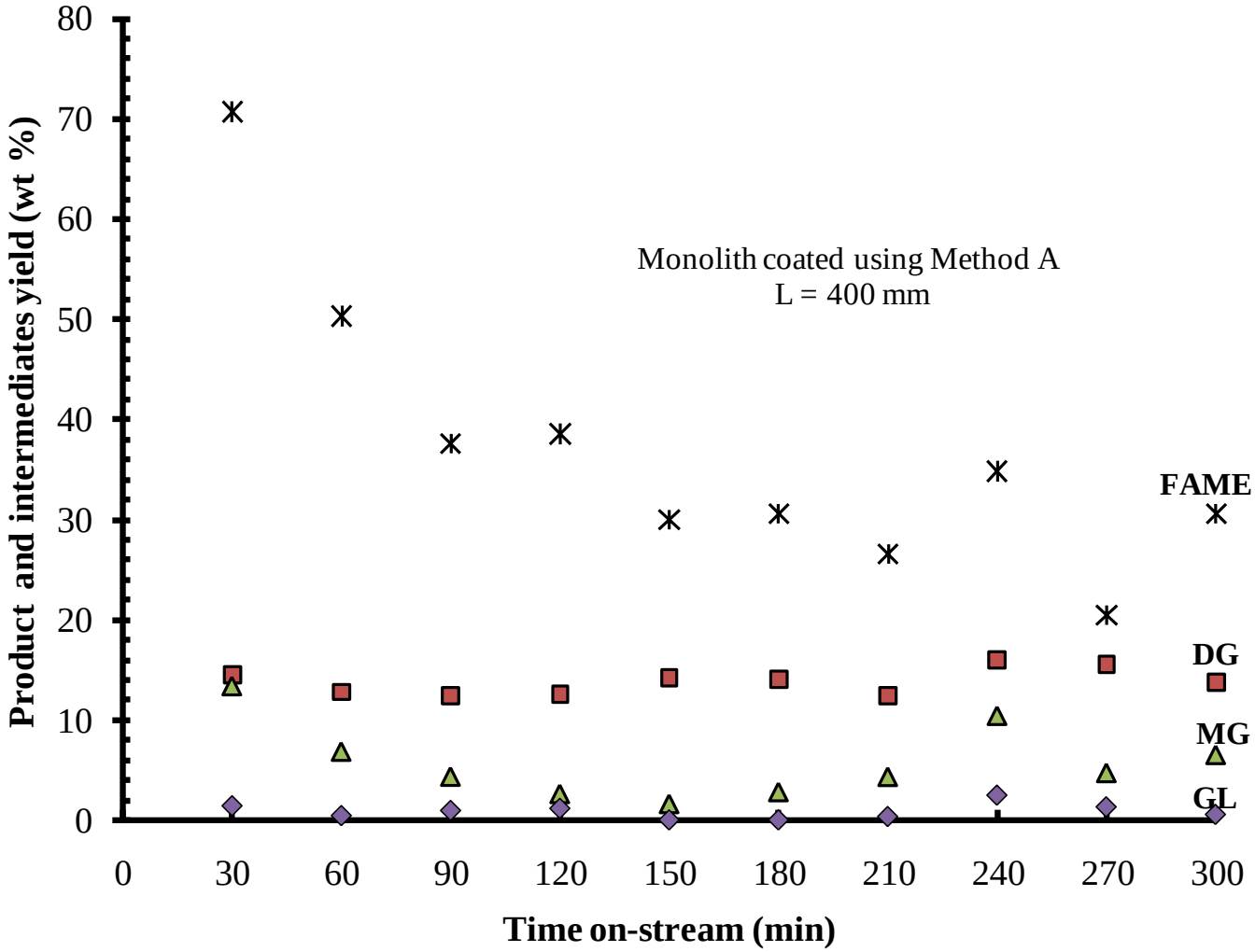

Figure 5.21: Production of FAME and intermediates over an extended run using a MeOH:oil ratio of 36:1 and ν_0= 0.1 ml min^{-1}.

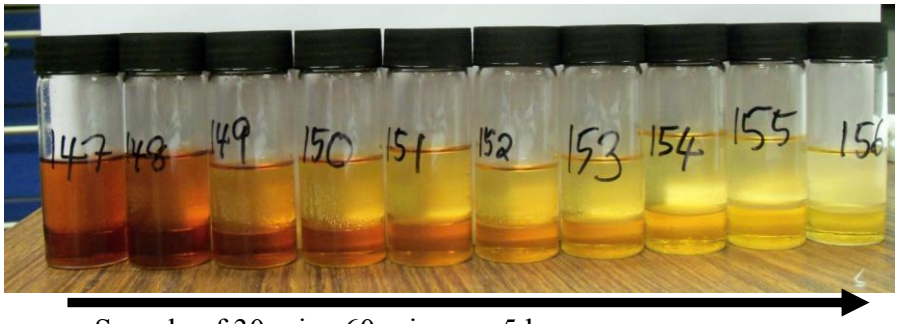

Sample of 30 mins,60 mins,…..5 hours

Figure 5.22: Samples collected every 30 minutes from the continuous experiment.

The main hurdle in this work is that in extended runs it is clear that the reactivity was not sustained. From the analysis of the zinc content in the samples from this experiment, at least 40 ppm zinc was detected in the first 30 minute of run time. This is shown in Figure 5.23. Also, it was noted that zinc compound(s) in this experiment are more bound in the apolar phase (bottom layer in this experiment) containing FAME and glycerides.

The recognition of leaching problems in the use of heterogeneous catalysts for the transesterification reaction is not uncommon. For example:

(a) In D'Cruz *et al*. (2007): approximately 1000 ppm Ba leached from an alkali metal (Li, Na, K) promoted BaO catalyst.

(b) In Noiroj *et al*. (2009): 51 % of K from a 25 wt% KOH/Al_2O_3 catalyst leached from the surface.

As zinc leaching was observed throughout the experiment, then homogenous-heterogeneous catalytic effects cannot be ruled out (Tonnetto and Marchetti, 2010 and Pugnet *et al.*, 2010). Also, as mentioned by Bournay *et al.* (2005), some solid metal oxides such as those of tin, magnesium, and zinc are known catalysts but they actually act according to a homogeneous mechanism and result in metal soaps or metal glycerates. However, to confirm this, more detailed analysis would need to be done.

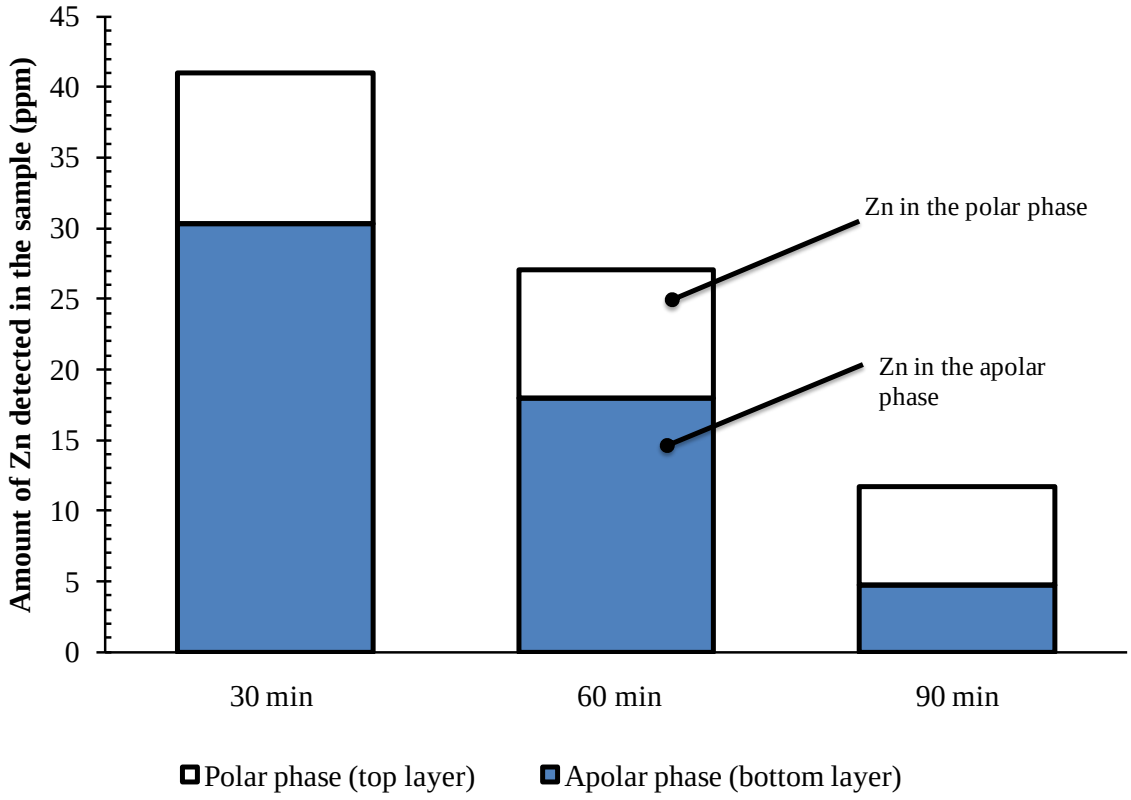

Figure 5.23: Zinc detected in 3 samples (after 30, 60 and 90 min of run time), using a MeOH: oil ratio of 36:1 and ν_0 = 1.0 ml min^{-1}.

5.4 Further testing with alternative catalyst (strontium oxide)

Working jointly in another short project (with Griffen, 2010), a strontium oxide (SrO) catalyst was coated onto the monoliths. It has to be emphasized, this is only a preliminary test to explore the possibility of using different catalysts in the reactor system and apparatus developed in this thesis. The objective of this experiment was to evidence the viability of the reactor system. There is no attempt to study this particular catalyst in detail.

The SrO catalyst was chosen as it has been proposed as a potential catalyst for the transesterification reaction. For example:

Liu *et al.* (2007): they achieved 95% conversion in 30 min of reaction time at temperatures below 70°C with a an oil/catalyst ratio of 3% and a MeOH:oil ratio of 6:1. The SrO catalyst was reported to have a long catalyst lifetime and could maintain sustained activity even after being repeatedly used for 10 cycles.

Yoo *et al.* (2010): they studied the transesterification of rapeseed oil using SrO (at 200°C and 40 bar) and the yield of FAME was 96% in 10 min of reaction time. The amount of catalyst used in their study was 1.0 wt % and the molar ratio of MeOH:oil was 40:1.

Patil and Deng (2009): they achieved a yield of approximately 80% of FAME, using 0.5 wt% of SrO with MeOH:oil molar ratio of 12:1, at 60°C with a 2 h reaction time. The feedstock used was camelina sativa oil.

Some key properties of SrO found in the literature are summarised in Table 5.4. SEM images of SrO in powder form are shown in Figure 5.24.

Table 5.6: Properties of SrO.

Appearance	White powder form
BET surface area [a, b]	0.0637 $m^2 g^{-1}$ to 8.0 $m^2 g^{-1}$
Pore volume[a]	0.00020 $cm^3 g^{-1}$
Pore width[a]	12.64 nm
Basic strength (H_)	15.0 <H_<18.4
Toxicity	Radiogenic (Radioactivity with ^{90}Sr (Half life = 28.9 years)

Taken from [a]Patil and Deng, (2009) and [b]Yoo *et al.* (2010).

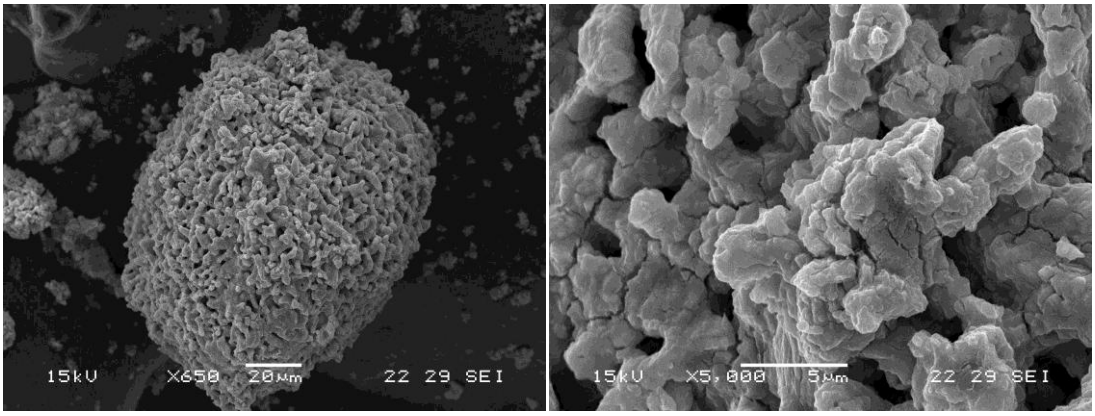

(a) (b)

Figure 5.24: Example SEM of the powdered SrO catalyst: (a) example of a particle, (b) magnified view of surface.

5.4.1 Method of SrO coating onto the monolith

As reported in Griffen (2010), there are two ways of preparing SrO in the literature, one is based on the calcination of $Sr(CO_3)$ at 1200 °C (Liu *et al.*, 2007), and the other were tested the calcination of $Sr(NO_3)_2$ at 600 °C (Yoosuk *et al*., 2010, Yang and Xie, 2007, Yang *et al.*, 2010). According to Griffen (2010), the SrO catalyst on the monolith support gave 64 % conversion to FAME after 4 h of reaction time in a batch system (as used in this thesis). The catalyst loading was 1.8 g (7.1 wt % of the monolith).

Various coating method tested, and the following method was finally selected.

(a) First a slurry was prepared:
   - 8g $Sr(NO_3)_2$ (Sigma-Aldrich, ≥99%) was mixed with 20 ml H_2O and 20 ml of Ludox (colloidal silica, 40 wt % in water, Sigma-Aldrich) with vigorous shaking.

(b) Then dried monoliths were dipped into the slurry, blown dry with pressurised air and then dried with hot air.

(c) The dipping process was repeated two times before calcining at 1200 °C for 5 h.

The coated monoliths were then examined using SEM analysis. The morphology of SrO on the monolith structure is shown in Figure 5.25.

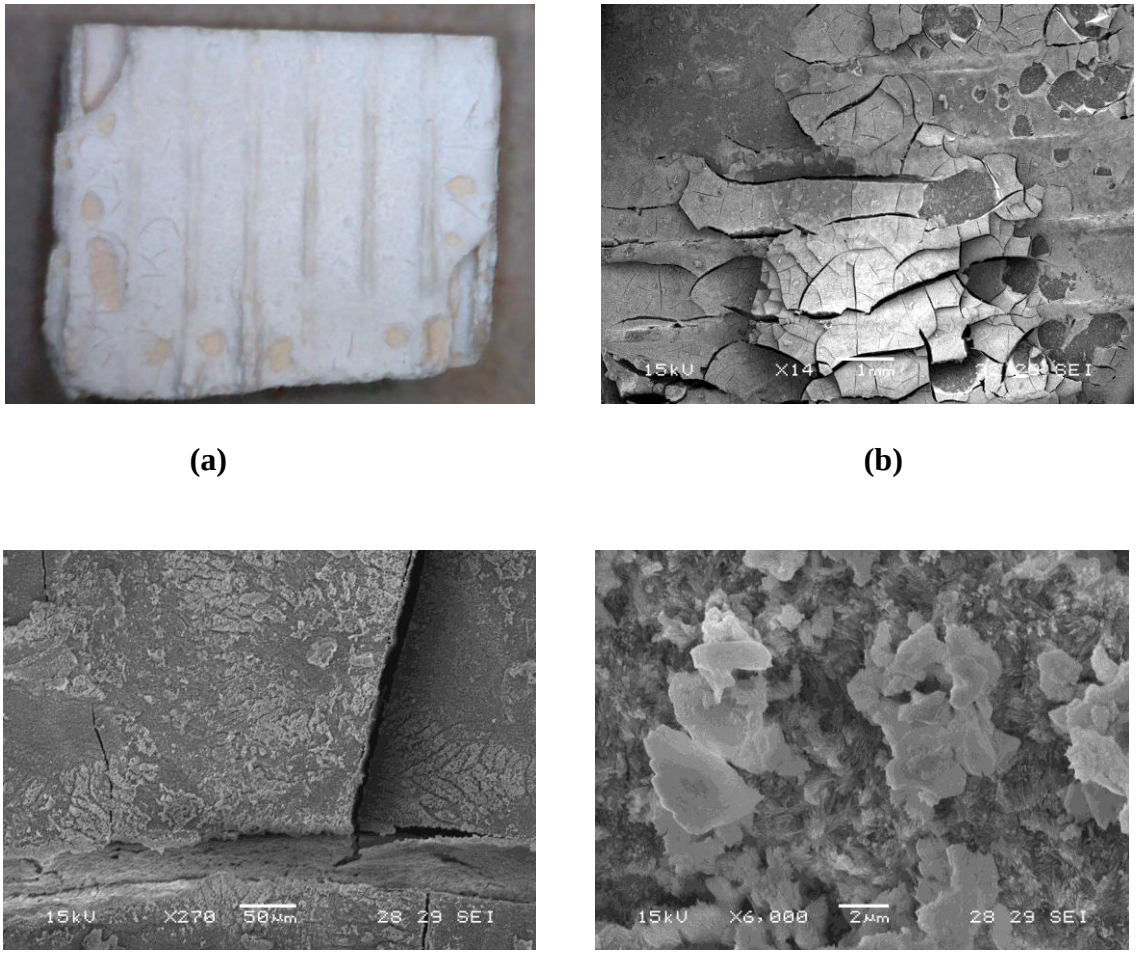

(a) **(b)**

(c) **(d)**

Figure 5.25: A surface view of the SrO catalyst coated onto a cordierite monolith using the slurry method:

(a) microscopic image showing the layer of coating,

(b) SEM view of the surface of the coating,

(c) SEM magnified view of the surface,

(d) SEM magnified view of the surface showing the SrO crystal structure (similar to structure in Figure 5.24 (b)).

5.4.2 Continuous flow experiments using SrO

The continuous experiments were done at the following conditions:

ν_0 = 0.1, 1.0 and 2.9 ml min^{-1},

T = 195°C,

P = 20 bar,

MeOH:oil = 12:1,

Number of monolith pieces = 40,

Total monolith length = 400 mm,

SrO catalyst loading = 0.28 g (method of coating: slurry Method B).

The result obtained are presented in Figure 5.27.

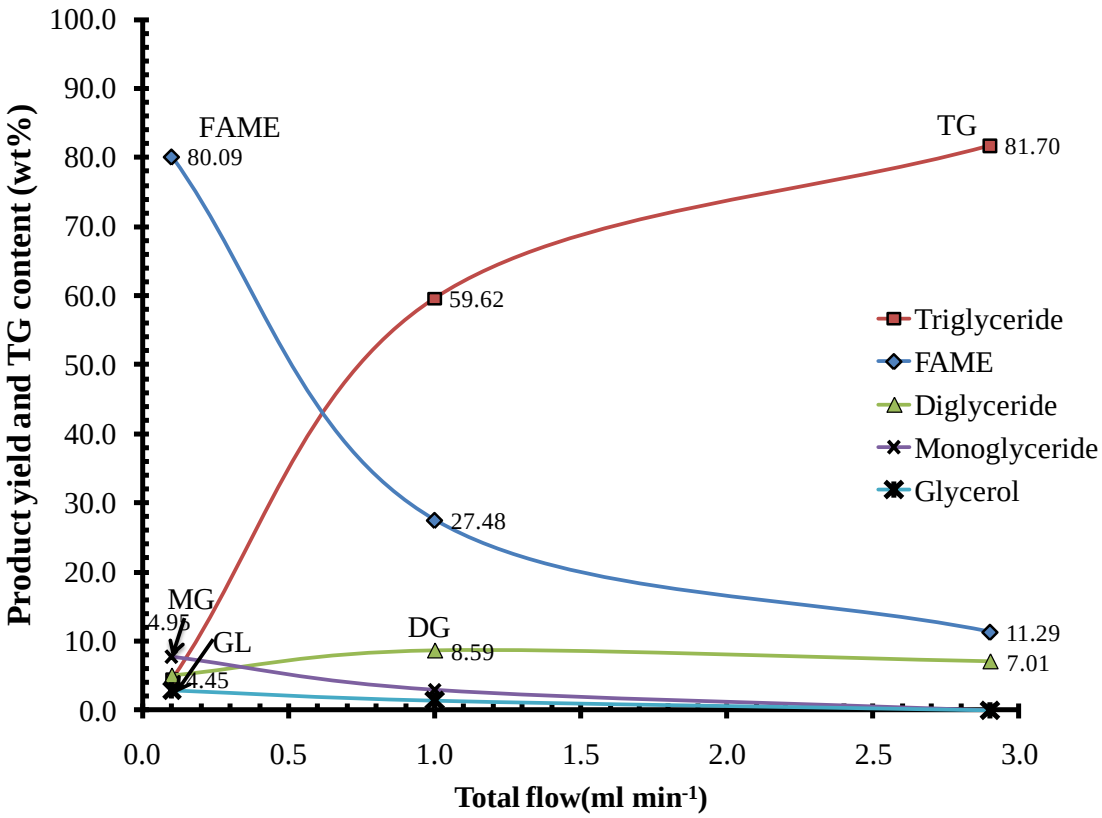

Figure 5.26: Influence of flow on the conversion of TG to FAME using an SrO coated monolith.

As can be seen from Figure 5.26, at the lowest flowrate (0.11 ml min^{-1}), 80 wt % of FAME was produced. The yield then dropped to 12 wt % when the flowrate was increased to 2.9 ml min^{-1}. The experiment was then shut-down and re-started on the next day to see if the catalyst was still active, however, the conversion was negligible, so, no further testing was done.

The used monolith from this experiment was washed to remove any oil substance by placing the monoliths in ethanol at a temperature of 60°C for 3 to 4 hours. It was then rinsed with methanol three times, blow dried with cool air and left for 24 hours. However, it seemed that the monoliths surface were still wet. Then, further drying was done by heating the monoliths under a N_2 flow at 150°C. After the monoliths went through this process, the washed and dried monoliths looked slightly burned. SEM imaging revealed the structure of the used monolith (see Figure 5.27). From the picture, it can be seen, that layers are bound to the cordierite surface, presumably these are layers of binder, and the SrO crystal structure is difficult to distinguish in the SEM image.

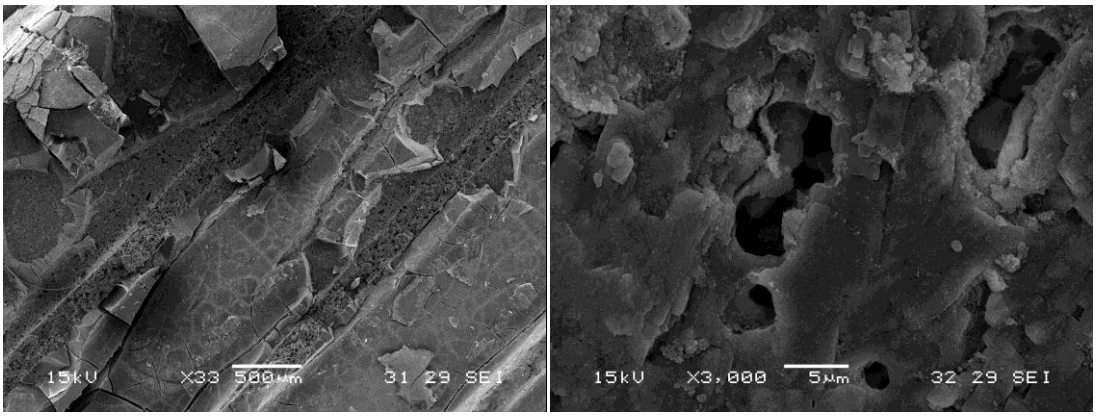

(a) (b)

Figure 5.27: Example SEM of the washed monolith coated with SrO catalyst: (a) view of surface, (b) magnified view of surface.

It is likely that catalyst leaching may have also occurred in this experiment and the catalyst surface may have been damaged during the washing and drying processes. The SrO catalyst was reported to have a strong tendency to react with CO_2 and water in air to form $SrCO_3$ and $Sr(OH)_2$, and can lose its catalytic ability despite having a high activity (Yan *et al.*, 2008). In addition, as reported by Yoo *et al.* (2010), SrO can be leached and dissolved in the product stream. Yoo *et al.* (2010) reported that Sr leaching was 5915.7 mg kg^{-1} of biodiesel and 6811.8 mg kg^{-1} of glycerol.

So despite an initial level of optimism about the possible favourable performance of this catalyst (based on the literature data), tests in this reacting system have revealed that the coated SrO system lost its activity. This was disappointing, but at least it was a good test of the reaction system developed in this thesis. Further work is recommended, to explore :

(a) if this is a real problem with this catalyst,

(b) if it arises from the method used to coat the monoliths, or

(c) if it is a result of the way in which the reactor was re-started after the shutdown.

5.5 Conclusions on work in Chapter 5

i) A continuous flow reaction system was designed and tested, that was shown to be suitable for laboratory scale bench-top experiments. The reactor i.d. = 6.2 mm, and experiments could be performed with multiple sections (500 mm each) of heated length. The monolith pieces were easy to install and remove from the reaction tube.

ii) The reactor was operated at liquid flows that ranged from 0.1 to 2.9 ml/min, and experiments were performed with 200 and 400 mm packed monolith bed lengths. Experiments at the very low flow, although useful (as high conversion can be demonstrated), do not represent realistic conditions in a tubular reactor, as at these flows a lot of back-mixing would have occurred inside the reactor (theoretic mean residence time = 200 min @ 0.1 ml min^{-1}, compared with 7 min @ 2.9 ml min^{-1}).

iii) The method of maintaining the desired back pressure in the reactor worked, and the heating system and method of controlling the temperature of the reactor also worked well. Experiments were performed with a back-pressure of 20 bar(g), and at a temperature of 195 °C.

iv) In a tubular reactor, an approach to plug flow is often considered desirable, in order to minimize undesirable side reactions, and to minimize the length of the reactor. So, to explore this aspect, RTD experiments were performed, using a solution of KCl to act as a tracer. However, these were difficult experiments to perform. Nevertheless, some useful qualitative data was obtained, indicating that the presence of the monolith helped to reduce the amount of dispersion in the reaction tube. This was very clear in the 2.9 ml min^{-1}experiments where, with monoliths, it was clear that plug flow conditions were being approached. Then as the number of monoliths was increased in the tube, this also increased the approach to plug flow conditions.

v) Visual experiments with a dye tracer, were useful in confirming that the mean residence time matched expected values from plug-flow calculations, even at the low flow condition (0.1 ml min^{-1}).

vi) At the base of the reactor, space was provided to enable a pulsating device to be installed in the future. This aspect was not studied in this thesis.

5.5.1 Zinc proline catalyst

i) Monolith pieces (i.d. = 5 mm, L = 10 mm) were coated with zinc proline catalyst, and these were then tested in the reactor. It was shown, that in a 30 min period on-stream, then it was possible to achieve high conversions. For example, at a flow = 0.1 ml min^{-1}, using a MeOH:oil ratio = 12:1, then conversion of TG was 80.5 wt% and a 57 wt% yield of FAME was obtained. However, over time, the catalyst also lost its activity (e.g. achieving 27 wt% after 5 h on-stream), but interestingly the yield of DG appeared to remain relatively constant.

ii) The monoliths were coated using two different methods. The slurry based coating Method B produced a higher loading, than Method A. However, the level of activity remained similar.

iii) Catalyst leaching experiments were performed, and it was shown that significant quantities of Zn can be detected after 30 min in the reactor effluent (e.g. 200 ppm). This factor is likely to be contributing to the loss in activity. The majority of Zn (about 75%) was in the apolar phase (FAME & glycerides), and the rest was in the polar phase (glycerol & unreacted methanol).

iv) In a comparison of catalyst leaching from monoliths coated by Methods A & B, the level of Zn loss was approximately the same, indicating that catalyst loss is not proportional to catalyst loading (Method B had a higher catalyst loading).

v) Interpreting SEM images of the catalyst surface after it had been in use (on-steam), was very difficult as the surface was contaminated with oil/by-products. However,

even after washing the catalyst in hot ethanol, it was still very difficult to distinguish signs of the zinc proline crystal structure. This could mean that these had either been washed away, or the surface was still contaminated.

vi) In comparative studies with an uncoated monolith, it was shown that the cordierite was also catalytically active. This was an interesting observation, and matched earlier experiments in Chapter 4 on the batch reactor. In addition, in this continuous flow reactor, it was very clear that the cordierite also lost its catalytic activity with time.

vii) Experiments (at flow = 1.0 ml min^{-1}) using a higher MeOH:oil ratio = 36:1, revealed that in the initial 30 min period a very high conversion (100%) of TG and a 70.1 wt% yield of FAME was obtained. However, over time, the catalyst also lost its activity (i.e. 51.42% conversion after 5 h on-stream). *Further work is necessary to explore the loss in catalyst activity, and how catalyst life may be extended.*

5.5.2 SrO catalyst

i) A scoping study was performed to test this catalyst, a) in the form of a coating on a cordierite monolith support, and b) in the reaction system and apparatus developed in this thesis. This was done using a MeOH:oil ratio = 12:1, and in the initial 30 min period, a reasonable level of conversion was achieved, e.g. at a flow = 1.0 ml min^{-1}, 40% conversion of TG, with 27 wt% yield of FAME.

ii) Unfortunately after the reactor was shut-down overnight, and then re-started to explore catalyst activity as a function of run-time, there was no activity. *Further work is necessary to explore:*

a) if this is a real problem with this catalysts,

b) if this arises because of the method used to coat the monoliths, and

c) *if this arose because of the method used to re-start the reactor after shut-down.*

iii) Finally in general it was pleasing to see that the reaction system developed, worked well for these types of experiments, and that catalysts can be coated onto specially cut monolith pieces and tested in this continuous flow experiment. This was a big achievement, and the analytical techniques used/developed enabled the reaction and its intermediates to be followed.

REFERENCES

Babcock, D.G.B., Konar, S.K., Mao, V. and Sidi, H., 1996. Fast one-phase oil-rich processes for the preparation of vegetable oil methyl esters. *Biomass & Bioenergy*, 11(1), pp. 43-50.

Bournay, L., Casanave, D. Delfort, B., Hillion , G. and Chodorge, J.A., 2005. New heterogeneous process for biodiesel production: A way to improve the quality and the value of the crude glycerin produced by biodiesel plants. *Catalysis Today*, 106, pp. 190–192.

Dasari, M. A., Goff, M. J. and Suppes, G. J., 2003. Noncatalytic alcoholysis kinetics of soybean oil. *Journal of American Oil Chemists' Society*, 80 (2), pp. 189-192.

D'Cruz, A., Kulkarni, M.G., Meher, L. C and Dalai, A.K., 2007. Synthesis of biodiesel from canola oil using heterogenous base catalyst. *Journal of American Oil Chemists' Society*, 84, pp. 937-943.

Fogler, H. S. 2006. *Elements of Chemical Reaction Engineering*. 4th Edition. United States: Pearson Education International.

Geankoplis, C., 2003. *Transport Processes and Separation Process Principles (includes Unit Operation*. 4th Ed. Prentice Hall Press, USA.

Griffen, J., 2010. Strontium Oxide: A New Biodiesel Catalyst for Use in a Continuous Flow Monolith Reactor. *DTC Project II Report*. Department of Chemistry, University of Bath.

Liu, X., He, H., Wang, Y. and Zhu, S., 2007. Transesterification of soybean oil to biodiesel using SrO as a solid base catalyst. *Catalysis Communications,* 8**,** pp. 1107-1111.

National Biodiesel Board, 2011. *Fuel Fact Sheets* [online]. Available from: http://www.biodiesel.org/pdf_files/fuelfactsheets/Materials_Compatibility.pdf [Accessed 01/04/ 2011].

Ni, X. Continuous Oscillatory Baffled Reactor Technology. *Manufacturing, Innovations in Pharmaceutical Technology* [online]. Available from http://www.nitechsolutions.co.uk/Uploads/ InnovationinPharmaTech.pdf [accessed on 23/01/2010).

Noiroj, K., Intarapong, P., Luengnaruemitchai, A and Jai-In, S., 2009. A comparative study of KOH/Al_2O_3 and KOH/NaY catalysts for biodiesel production *via* transesterification from palm oil. *Renewable Energy,* 34 (4), pp. 1145-1150.

Patil, P.D. and Deng, S., 2009. Transesterification of *Camelina Sativa* Oil using heterogenous metal oxide catalysts. *Energy & Fuels,* 23 (9), pp. 4619-4626.

Pugnet, V., Maury, S., Coupard, V., Dandeu, A., Quoineaud, A., Bonneau, J and Tichit, D., 2010. Stability, activity and selectivity study of a zinc aluminate heterogeneous catalyst for the transesterification of vegetable oil in batch reactor. *Applied Catalysis A: General*, 374, pp.71–78.

Reis, N., Vicente, A.A. and Teixeira, J.A., 2010. Liquid backmixing in oscillarry flow through a periodically constricted meso-tube. *Chemical Engineering and Processing,* 49, pp.793-803.

Tonetto, G.M and Marchetti, J.M., 2010. Transesterification of soybean oil over Me/Al_2O_3 (Me = Na, Ba, Ca, and K) catalysts and monolith K/Al_2O_3-Cordierite. *Topic in Catalysis*, 53, pp.755–762.

Yan, S., Lu, H. and Liang, B., 2008. Supported CaO catalysts used in the transesterification of rapeseed oil for the purpose of biodiesel production. *Energy & Fuels*, 22 (1), pp. 646-651.

Yang, R., Su, M., Li, M., Zhang, J., Hao, X. and Zhang, H., 2010. One-pot process combining transesterification and selective hydrogenation for biodiesel production from starting material of high degree of unsaturation. *Bioresource Technology*, 101, pp.5903-5909.

Yang, Z. and Xie, W., 2007. Soybean oil transesterification over zinc oxide modified with alkali earth metals. *Fuel Processing Technology*, 88, pp. 631-638.

Yoo, S. J., Lee, H. S., Veriansyah, B., Kim, J., Kim, J.D. & Lee, Y.W., 2010. Synthesis of biodiesel from rapeseed oil using supercritical methanol with metal oxide catalysts. *Bioresource Technology*, 101, pp**.** 8686-8689.

Yoosuk, B., Krasae, P., Puttasawat, B., Udomsap, P., Viriya-empikul, N. and Faungnawaki, K., 2010. Magnesia modified with strontium as a solid base catalyst for transesterification of palm olein. *Chemical Engineering Journal*, 162 (1), pp. 58-66.

CHAPTER 6

CONCLUSIONS AND RECOMMENDATIONS

Conclusions

The achievements of this work in regard to aims outlined in Chapter 1 (see 1.3) are as follows

6.1 Use of zinc proline as a catalyst on the cordierite support

- Building on earlier work (in a PhD thesis) on a powdered form of zinc proline, two different monolith coating methods were developed, which demonstrated that the zinc-proline could be attached in a catalytically active form to a cordierite support. This also resulted in some interesting structures on the support. Using the slurry method, it was easier to achieve a higher loading of catalyst, although the catalytic activity (based on monolith volume, and also geometric surface area) remained similar to the method prepared from a colloidal solution. [**Aim (i) to immobilize the catalyst (zinc proline) onto a monolithic support, and demonstrate applicability of the system**]
- In batch experiments, when repeat experiments were performed using used coated monoliths, it was found that the catalyst lost its activity.
- In continuous flow experiments, when coated samples of monolith were packed in a tube, the catalyst was shown to be active, and it was possible to achieve high levels of conversion. [**Aim (i) to immobilize the catalyst (zinc proline) onto a monolithic support, and demonstrate applicability of the system**]. However, over extended run-times (30 to 300 min), the catalyst lost its activity. The

literature concerning other catalyst systems for the transesterification reaction shows that a, loss in catalyst activity has also been encountered by others.

- Measurements also showed that during the course of an experiment, Zn (from the coated zinc proline) was leaching, and this clearly contributed to catalyst deactivation. Leaching of catalyst components in transesterification reactions has also been reported by others in the literature.
- After the catalyst had been used for extended run-times in the reactor, using SEM imaging it was difficult to distinguish the zinc proline crystals on the surface of the cordierite. These may have been washed away, and/or masked by constituents in the reaction.
- Blank uncoated samples of cordierite monolith were also found to be catalytically active, and these also lost their activity in experiments over extended run-times. This was interesting, and evidence was found in the literature that the presence of MgO (present in cordierite) could have contributed to the catalytic activity observed.

6.2 Analytical technique for monitoring the reaction

The analytical technique using the GC was worked well, and intermediates could be detected and the progress of the reaction followed. For example, it was interesting to see that when the zinc proline catalyst lost its activity, although the production of FAME decreased, the production of DG appeared to remain relatively constant.The accuracy and repeatability of the GC analysis was good with error of < 1.0%. [**Aim (ii) to develop the analytical technique on gas chromatography for monitoring the reaction**].

6.3 Continuous flow reactor design

The continuous flow reaction system developed in this thesis was shown to work well, and that it could be used to evaluate the performance of catalytically coated sections of monolith. Reaction temperature (T = 195 ºC) could be maintained, and the back-pressure (20 bar) could also be maintained readily. Small monolith pieces could be formed by cutting a 10 mm slice from a monolith cordierite block, and then using a core-cutter to cut a 5 mm o.d. monolith (10 mm long), which after coating, could be inserted easily into the reaction tube and then removed. [Aim (iii) to study

the viability of turning a batch reaction into a continuous process with the use of immobilised catalyst (zinc proline) on the monolith structure as a fixed bed catalyst, and (iv) to design and construct the continuous flow reactor for the system]

6.4 Residence time distribution study

Some RTD studies were performed, and these provided useful qualitative information, which illustrated that the presence of monoliths in the tube helps to approach plug flow conditions. Unfortunately, experiments using KCl salt solution as a tracer were difficult to perform, especially at low flows when dispersion/backmixing was very high, and the [mass of tracer out] < [the mass of tracer in]. Problems with salt solution tracer studies have also been encountered by others in the literature. Visual experiments with a dye tracer confirmed that the mean residence time approximated expected values from plug-flow calculations, even at low flow. [***Aim (v) to quantify the distribution of residence time under pulsatile flow conditions through Residence Time Distribution (RTD) study, this could not be achieved due to lack of funding, the pulsating device was not included in the experimental rig.***]

6.5 Continuous flow reactor performance

- The reactor packed with zinc proline coated monolith was operated at different liquid flowrate, bed lengths and MeOH/oil ratio. From the experiment, a high conversion can be achieved but at the very low flow. The result has been useful, but such low flow do not represent realistic conditions in a tubular reactor. And also, because of over the time, the catalyst losts its activity, the catalyst deactivation was investigated. To demonstrate the use of this system, a few scoping studies were also performed using SrO as a catalyst, which was coated onto the cordierite monolith. [**Aim (vi) to perform reaction experiments over a wide range of conditions in the continuous flow reactor].**

Recommendations for future work

6.6 Zinc proline as catalyst:

- Further work is necessary to explore the loss in catalyst activity, and how catalyst life may be extended.
- Other monolith coating techniques (e.g. ion-exchange) and also other materials as potential monolith supports (e.g. carbon) should be explored.

6.7 SrO as a catalyst:

- Although the catalyst was active, after the reactor was shut-down overnight and then re-started, it had lost its activity. Further work is necessary to explore: (a) if this is a real problem with this catalyst, (b) if this arises because of the method of coating, (c) if this arose because of the method used to re-start the reactor after shut-down.

6.8 Other catalysts:

- Other catalysts that have been reported to be active should be tested in this reacting system.

6.9 Surface characterisation of coated monolith:

- Other methods such as EDX Energy-dispersive X-ray spectroscopy (EDS or EDX), X-ray photoelectron spectroscopy (XPS), Fourier Transform Infrared Spectroscopy (FTIR) and X-Ray Diffraction (XRD) would have been useful to accurately measure the coated monolith surface.

6.10 Continuous flow reactor:

- Experiments should be performed, to explore any advantages to be gained from the use of a device to create pulsating flow, which could help to mix the MeOH and oil mixture at the inlet to the reactor, and also to enhance mass transfer rates within the catalytic sections.
- Once a reliable catalyst has been identified, kinetic studies could be performed in the flow reactor, the intermediates followed, and basic design equations could be developed for this system. Further experiments could be performed with monoliths with different cell sizes, and the system optimised.

6.11 Reproducibility and accuracy

- To improve the reproducibility and accuracy of the experimental result, it would have been useful to repeat the experiment and perform an error analysis.

APPENDIX A

Table A1: USA standard for biodiesel according to ASTM D6751 standard (National Biodiesel Board, 2008).

Property	Test method	Limits	Unit
Calcium & Magnesium, combined	EN14538	5 maximum	ppm (μg/g)
Flash point (closed cup)	D 93	93 min	° C
Alcohol Control (One of the following must be met)			
1. Methanol Content	EN14110	0.2 maximum	mass %
2. Flash Point	D 93	130 maximum	° C
Water and sediment	D 2709	0.050 max	% volume
Kinematic viscosity,40°C	D 445	1.9 to 6.0	mm^2/ s
Sulfated ash	D 874	0.020 maximum	% mass
Sulfur S 15 Grade S 500 Grade	 D 5453 D 5453	 0.0015 maximum 0.05 maximum	 % mass (ppm) % mass (ppm)
Copper strip corrosion	D 130	No. 3 maximum	
Cetane number	D 613	47 minimum	
Cloud point	D 2500	Report	° C
Carbon residue (100% sample)	D 4530*	0.050 max	% mass
Acid number	D 664	0.80 max	mg KOH/g
Free glycerin	D 6584	0.020 max	% mass
Total glycerin	D 6584	0.240 max	% mass
Phosphorus content	D 4951	0.001 max	% mass
Distillation, T90 AET (atmospheric equivalent temperature)	D1160	360 max	° C
Oxidation Stability	EN 14112	3 minimum	ppm
Cold Soak Filtration For use in temperature below -12° C	Annex to D6751 Annex to D6751	360 maximum 200 maximum	sec sec

* The Carbon residue shall be run on the 100% sample.

Table A2 : European standard for biodiesel (BP Coryton Technical Centre, Essex, 2008).

Test	Method	Limits	Unit
Density at 15 °C	ISO 12185	883.2	kg/m^3
Kinematic Viscosity at 40 °C	EN ISO 3104	4.564	mm2/s
Flash Point	EN ISO 3679	182.0	°C
Sulphur Content	EN ISO 20846	1.8	mg/kg
Microcarbon Residue 10% (ASTM D1160)	EN ISO 10370	0.17	% (m/m)
Cetane Number	EN ISO 5165	49.5	
Water	EN ISO 12937	210	mg/kg
Total Contamination	EN 12662	6	mg/kg
Copper Corrosion 3 hrs at 50 °C	EN ISO 2160	1	
Oxidation Stability, 110 °C	EN 14112	10.8	hours
Acid Number	EN 14104	0.18	mgKOH/g
Iodine Value	EN 14111	112	g/100gFAME
Linolenic Acid Methyl Ester	EN 14103	9.41	% m/m
Polyunsaturated Methyl Ester	EN 14103	<1	% m/m
Ester Content	EN 14103	97.7	% m/m
Methanol Content	EN 14110	0.01	% (m/m)
Monoglyceride Content	EN 14105	0.57	% m/m
Diglyceride Content	EN 14105	0.15	% m/m
Triglyceride Content	EN 14105	0.03	% m/m
Free Glycerol	EN 14105	<0.01	% m/m
Total Glycerol	EN 14105	0.17	% m/m
Sodium	EN 14108	<0.1	mg/kg
Potassium	EN 14109	<0.1	mg/kg
Calcium	EN 14538	<0.1	mg/kg
Magnesium	EN 14538	<0.1	mg/kg
Phosphorus	EN 14107	0.2	mg/kg
Cold Filter Plugging Point	EN 116	-20	°C

Table A3: German standard for biodiesel according to DIN V 51606 standard (Achten *et al.*, 2008).

Property	Limits	Unit
Density	0.87 to 0.90	g/cm^3
Flash point (closed cup)	110.0 minimum	° C
Cetane value	49 minimum	% volume
Viscosity at 30°C	3.5 to 5.0	cSt
Iodin number	115 maximum	mg Iodine/ g
Acid number	0.50 maximum	mg KOH/g
Monoglycerides %	0.80 maximum	% mass
Diiglycerides %	0.4 maximum	% mass
Triglycerides %	0.4 maximum	% mass
Carbon residue (100% sample)	0.030 max	% mass
Sulfur	0.01 maximum 0.05 maximum[a]	% mass
Sulfated ash	0.03 maximum	% mass
Methanol	0.3 maximum	% mass
Acid number	0.80 max	mg KOH/g
Phosphorus content	0.001 max	% mass
Water %	0.030 max	% mass
Free glycerin	0.020 max	% mass
Total glycerin	0.250 max	% mass

[a]The limits are for Grade S15 and Grade S500 biodiesel, respectively. S15 and S500 refer to maximum sulfur specifications (ppm).

Reference

National Biodiesel Board, 2008. *Fuel Fact Sheets* [online]. Available from: http://www.biodiesel.org/resources/ fuelfactsheets /default.shtm [Accessed 12 January 2009].

BP Coryton Technical Centre, Essex. Kolaczkowski,S.T (S.T.Kolaczkowski@bath.ac.uk). 23 January 2008. *Interim Laboratory Test Report*. Email to Asli,U.A. (U.A.Asli@bath.ac.uk)

Achten, W.M.J., Verchot, L., Franken, Y.J., Mathijs, E., Singh, V.P., Aerts, R. and Muys, B., 2008. Review: Jatropha bio-diesel production and use. *Biomass and Bioenergy*, 32, 1063-1084.

APPENDIX B

Paper presented at the 3rd International Conference on Structured Catalysts and Reactors, ICOSCAR-3 (Italy, 27 to 30 September 2009).

This was then published as a paper in Catalysis Today.

APPENDIX C

Example calculation to determine the volume of oil and methanol to achieve a molar ratio of 1:6.

Volume of oil used = 200 ml

$$\text{Moles used} = \frac{\text{Volume of oil} \times \text{Density of oil}}{\text{Molecular weight of oil}}$$

where density of oil = 920 g litre^{-1} and molar mass of oil = 860 g mol^{-1} taken from (Swern,1979).

$$\text{Moles of oil} = \frac{0.2\ l \times 920\ g\ l^{-1}}{860\ g\ mol^{-1}} = 0.214\ mol$$

$$\text{Volume of methanol} = \frac{6 \times \text{Mol of oil} \times \text{Molar mass of methanol}}{\text{Density of methanol}}$$

where density of methanol = 789 *g litre^{-1}* and molar mass of MeOH = 32 g mol^{-1}.

$$\text{Volume of MeOH} = \frac{6 \times 0.214\ mol \times 32\ g\ mol^{-1}}{789\ g\ litre^{-1}} = 0.05\ litre$$

.

Reference

Swern, D., 1979. *Baileys Industrial Oil and Fat Products Volume 1*, 4th ed. Wiley & Sons, New York. pp. 424-435.

APPENDIX D

GG calibration using as standards:

- Glycerol
- Monoglyceride
- Triglyceride
- Diglyceride
- Biodiesel

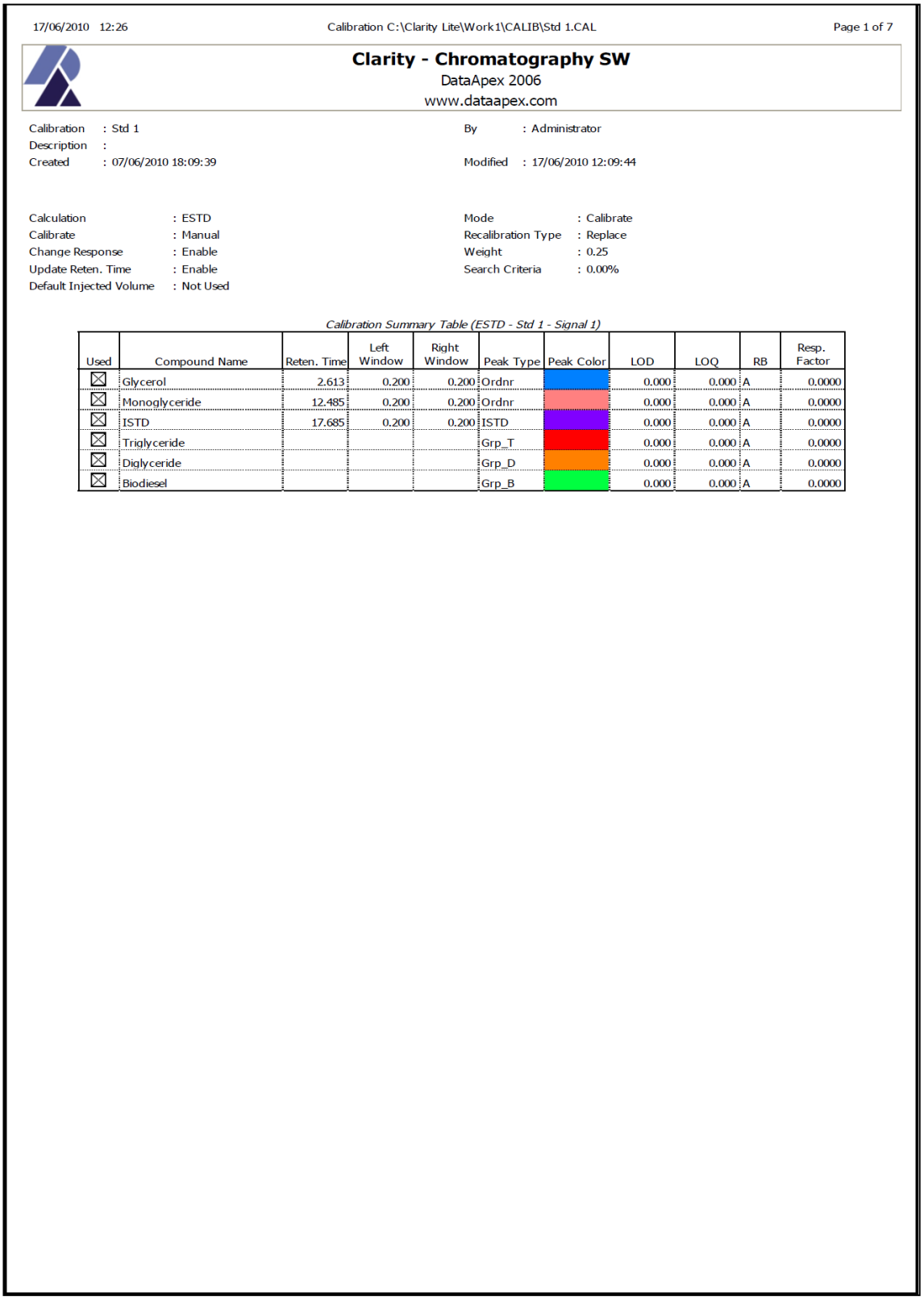

17/06/2010 12:26 Calibration C:\Clarity Lite\Work1\CALIB\Std 1.CAL Page 1 of 7

Clarity - Chromatography SW
DataApex 2006
www.dataapex.com

Calibration : Std 1
Description :
Created : 07/06/2010 18:09:39
By : Administrator
Modified : 17/06/2010 12:09:44

Calculation : ESTD
Calibrate : Manual
Change Response : Enable
Update Reten. Time : Enable
Default Injected Volume : Not Used
Mode : Calibrate
Recalibration Type : Replace
Weight : 0.25
Search Criteria : 0.00%

Calibration Summary Table (ESTD - Std 1 - Signal 1)

Used	Compound Name	Reten. Time	Left Window	Right Window	Peak Type	Peak Color	LOD	LOQ	RB	Resp. Factor
☒	Glycerol	2.613	0.200	0.200	Ordnr		0.000	0.000	A	0.0000
☒	Monoglyceride	12.485	0.200	0.200	Ordnr		0.000	0.000	A	0.0000
☒	ISTD	17.685	0.200	0.200	ISTD		0.000	0.000	A	0.0000
☒	Triglyceride				Grp_T		0.000	0.000	A	0.0000
☒	Diglyceride				Grp_D		0.000	0.000	A	0.0000
☒	Biodiesel				Grp_B		0.000	0.000	A	0.0000

Figure D1: Report page.

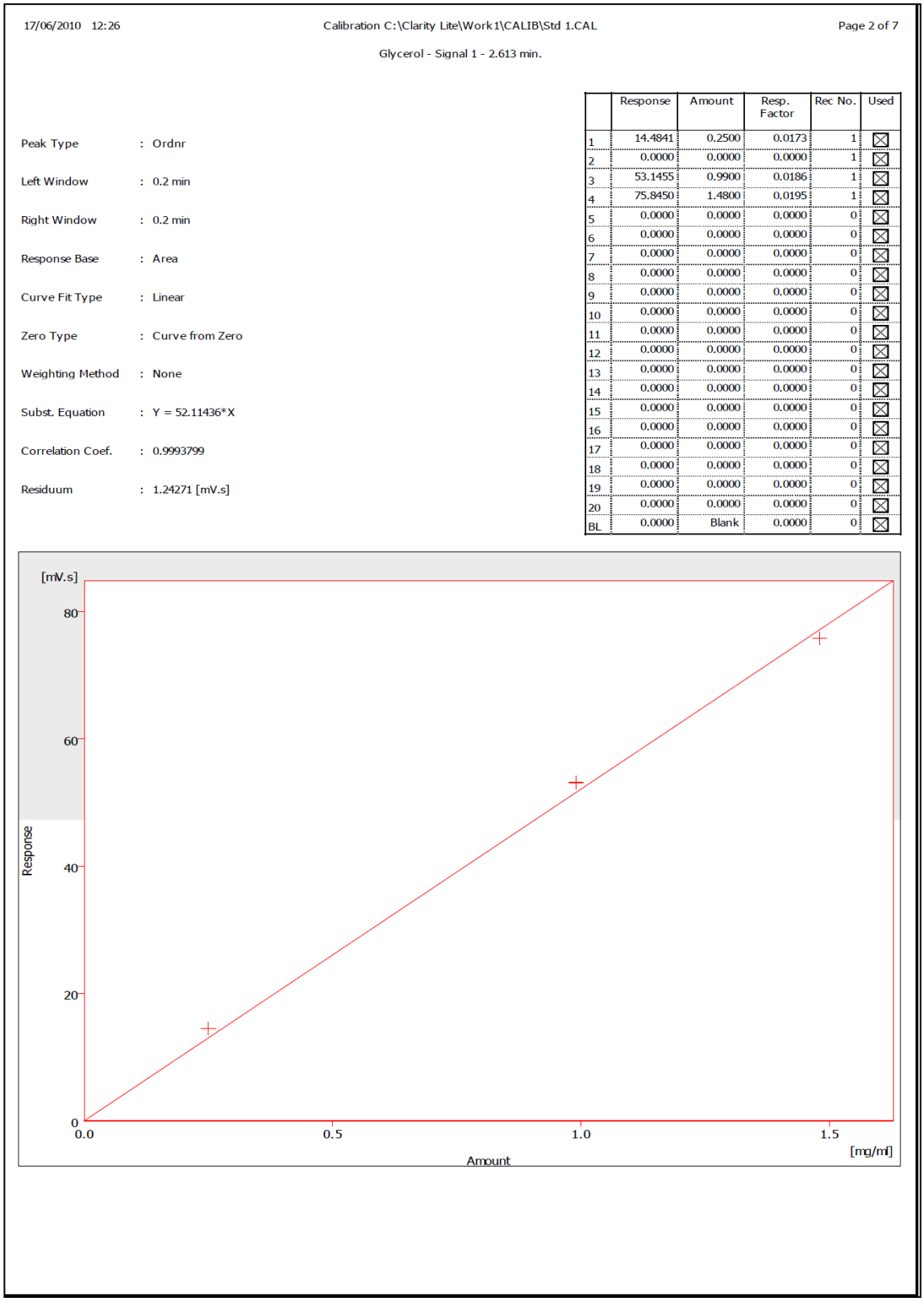

	Response	Amount	Resp. Factor	Rec No.	Used
1	14.4841	0.2500	0.0173	1	☒
2	0.0000	0.0000	0.0000	1	☒
3	53.1455	0.9900	0.0186	1	☒
4	75.8450	1.4800	0.0195	1	☒
5	0.0000	0.0000	0.0000	0	☒
6	0.0000	0.0000	0.0000	0	☒
7	0.0000	0.0000	0.0000	0	☒
8	0.0000	0.0000	0.0000	0	☒
9	0.0000	0.0000	0.0000	0	☒
10	0.0000	0.0000	0.0000	0	☒
11	0.0000	0.0000	0.0000	0	☒
12	0.0000	0.0000	0.0000	0	☒
13	0.0000	0.0000	0.0000	0	☒
14	0.0000	0.0000	0.0000	0	☒
15	0.0000	0.0000	0.0000	0	☒
16	0.0000	0.0000	0.0000	0	☒
17	0.0000	0.0000	0.0000	0	☒
18	0.0000	0.0000	0.0000	0	☒
19	0.0000	0.0000	0.0000	0	☒
20	0.0000	0.0000	0.0000	0	☒
BL	0.0000	Blank	0.0000	0	☒

Figure D2: GC calibration of Glycerol.

17/06/2010 12:26 Calibration C:\Clarity Lite\Work1\CALIB\Std 1.CAL Page 3 of 7

Monoglyceride - Signal 1 - 12.485 min.

Peak Type	: Ordnr
Left Window	: 0.2 min
Right Window	: 0.2 min
Response Base	: Area
Curve Fit Type	: Linear
Zero Type	: Curve from Zero
Weighting Method	: None
Subst. Equation	: Y = 23.29338*X
Correlation Coef.	: 0.9937689
Residuum	: 0.55879 [mV.s]

	Response	Amount	Resp. Factor	Rec No.	Used
1	1.5575	0.0700	0.0449	1	☒
2	4.5465	0.1700	0.0374	1	☒
3	6.6499	0.3300	0.0496	1	☒
4	15.9761	0.6700	0.0419	1	☒
5	0.0000	0.0000	0.0000	0	☒
6	0.0000	0.0000	0.0000	0	☒
7	0.0000	0.0000	0.0000	0	☒
8	0.0000	0.0000	0.0000	0	☒
9	0.0000	0.0000	0.0000	0	☒
10	0.0000	0.0000	0.0000	0	☒
11	0.0000	0.0000	0.0000	0	☒
12	0.0000	0.0000	0.0000	0	☒
13	0.0000	0.0000	0.0000	0	☒
14	0.0000	0.0000	0.0000	0	☒
15	0.0000	0.0000	0.0000	0	☒
16	0.0000	0.0000	0.0000	0	☒
17	0.0000	0.0000	0.0000	0	☒
18	0.0000	0.0000	0.0000	0	☒
19	0.0000	0.0000	0.0000	0	☒
20	0.0000	0.0000	0.0000	0	☒
BL	0.0000	Blank	0.0000	0	☒

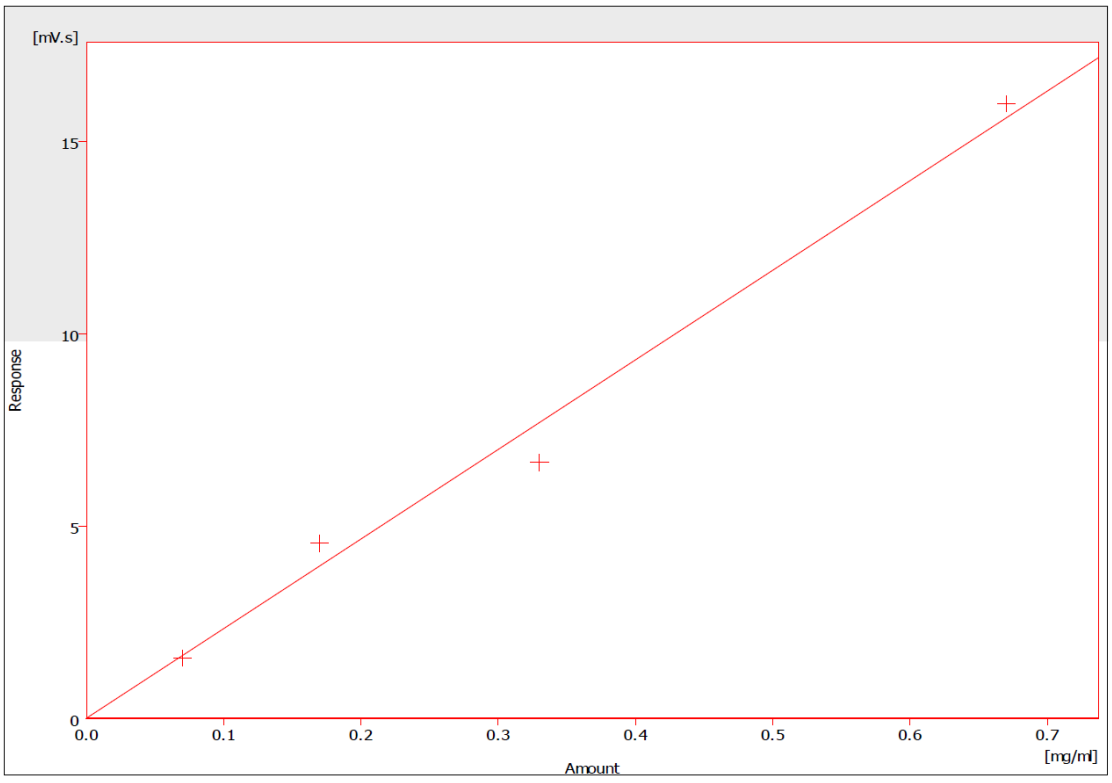

Figure D3: GC calibration of Monoglyceride.

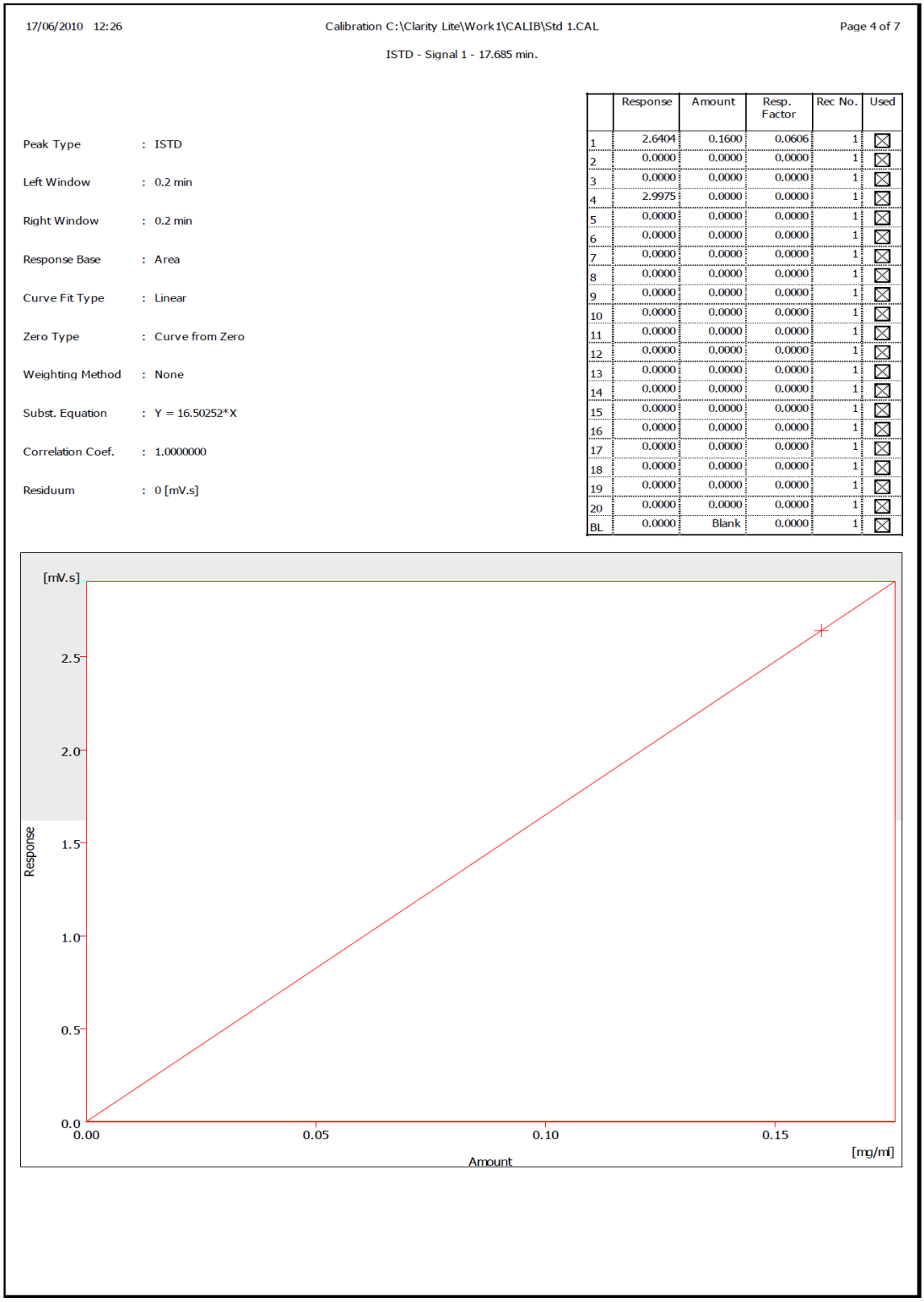

Figure D4: Calibration of Internal Standard (ISTD).
Note : The amount of ISTD was generated from an internal calibration method (*i.e.* using one standard amount calibration). However, the amount of ISTD was not used in the calculation for other components. It is only useful to check the consistency of sample injection.

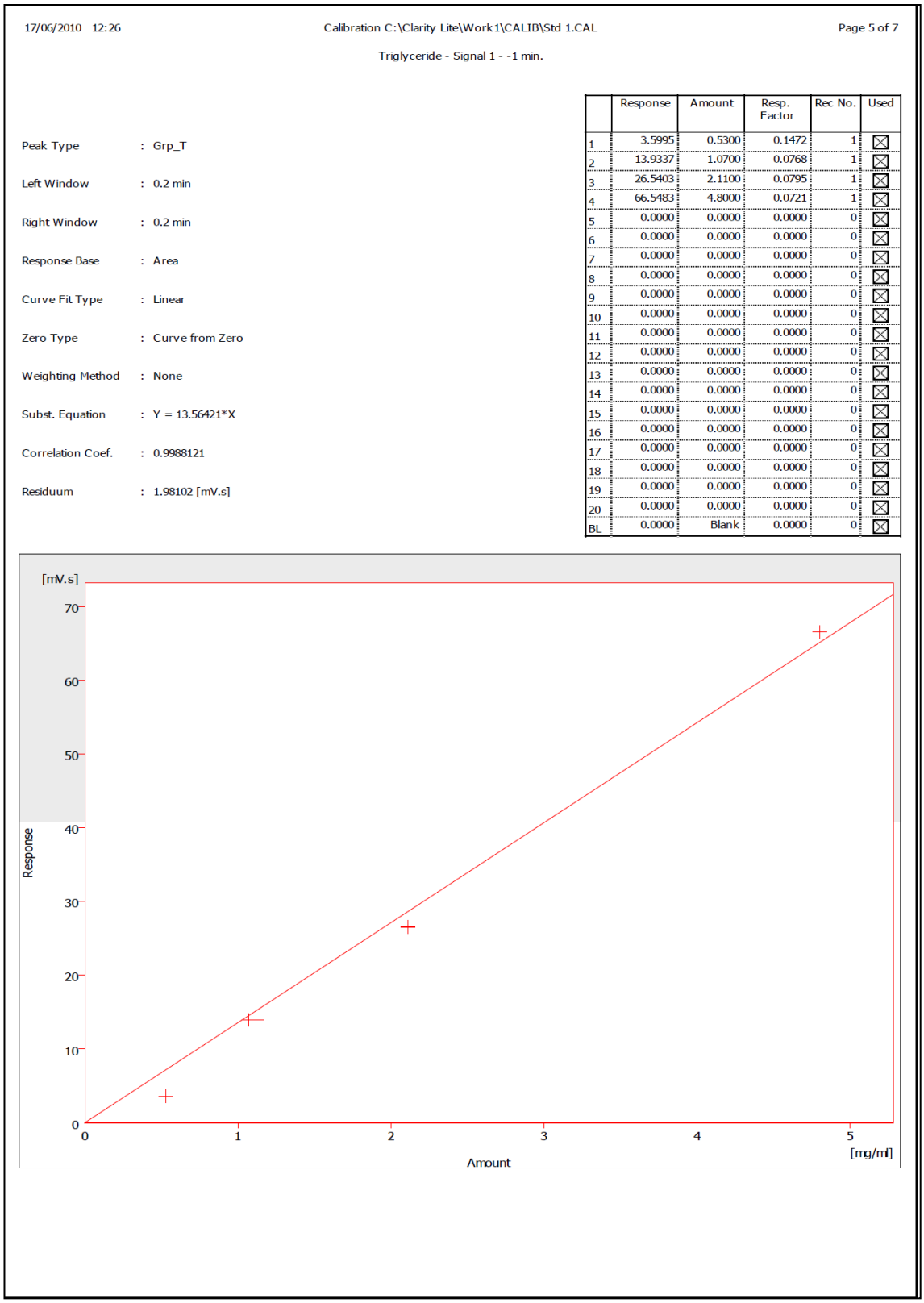

Figure D5: GC calibration of Triglyceride.

17/06/2010 12:26 Calibration C:\Clarity Lite\Work1\CALIB\Std 1.CAL Page 6 of 7

Diglyceride - Signal 1 - -1 min.

Peak Type	: Grp_D
Left Window	: 0.2 min
Right Window	: 0.2 min
Response Base	: Area
Curve Fit Type	: Linear
Zero Type	: Curve from Zero
Weighting Method	: None
Subst. Equation	: Y = 19.90573*X
Correlation Coef.	: 0.9966729
Residuum	: 0.56396 [mV.s]

	Response	Amount	Resp. Factor	Rec No.	Used
1	0.9055	0.0500	0.0552	1	☒
2	2.7300	0.1300	0.0476	1	☒
3	4.5113	0.2100	0.0465	1	☒
4	11.6924	0.5300	0.0453	1	☒
5	19.4226	1.0100	0.0520	1	☒
6	0.0000	0.0000	0.0000	0	☒
7	0.0000	0.0000	0.0000	0	☒
8	0.0000	0.0000	0.0000	0	☒
9	0.0000	0.0000	0.0000	0	☒
10	0.0000	0.0000	0.0000	0	☒
11	0.0000	0.0000	0.0000	0	☒
12	0.0000	0.0000	0.0000	0	☒
13	0.0000	0.0000	0.0000	0	☒
14	0.0000	0.0000	0.0000	0	☒
15	0.0000	0.0000	0.0000	0	☒
16	0.0000	0.0000	0.0000	0	☒
17	0.0000	0.0000	0.0000	0	☒
18	0.0000	0.0000	0.0000	0	☒
19	0.0000	0.0000	0.0000	0	☒
20	0.0000	0.0000	0.0000	0	☒
BL	0.0000	Blank	0.0000	0	☒

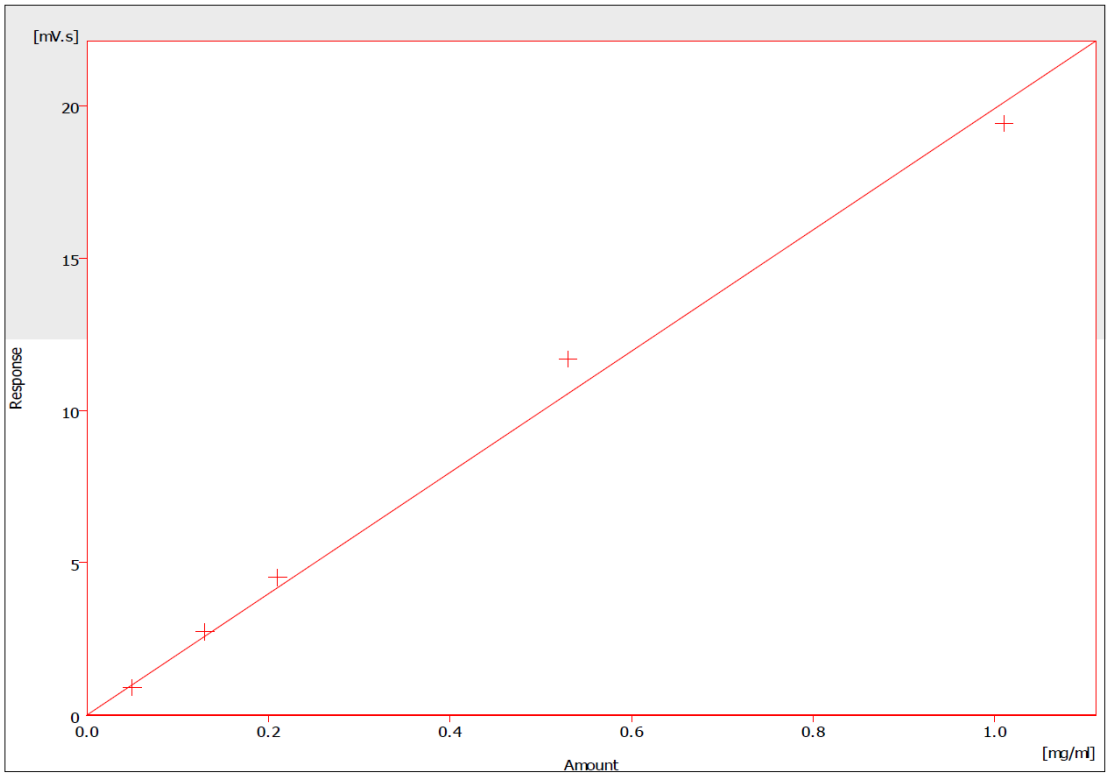

Figure D6: GC calibration of Triglceride.

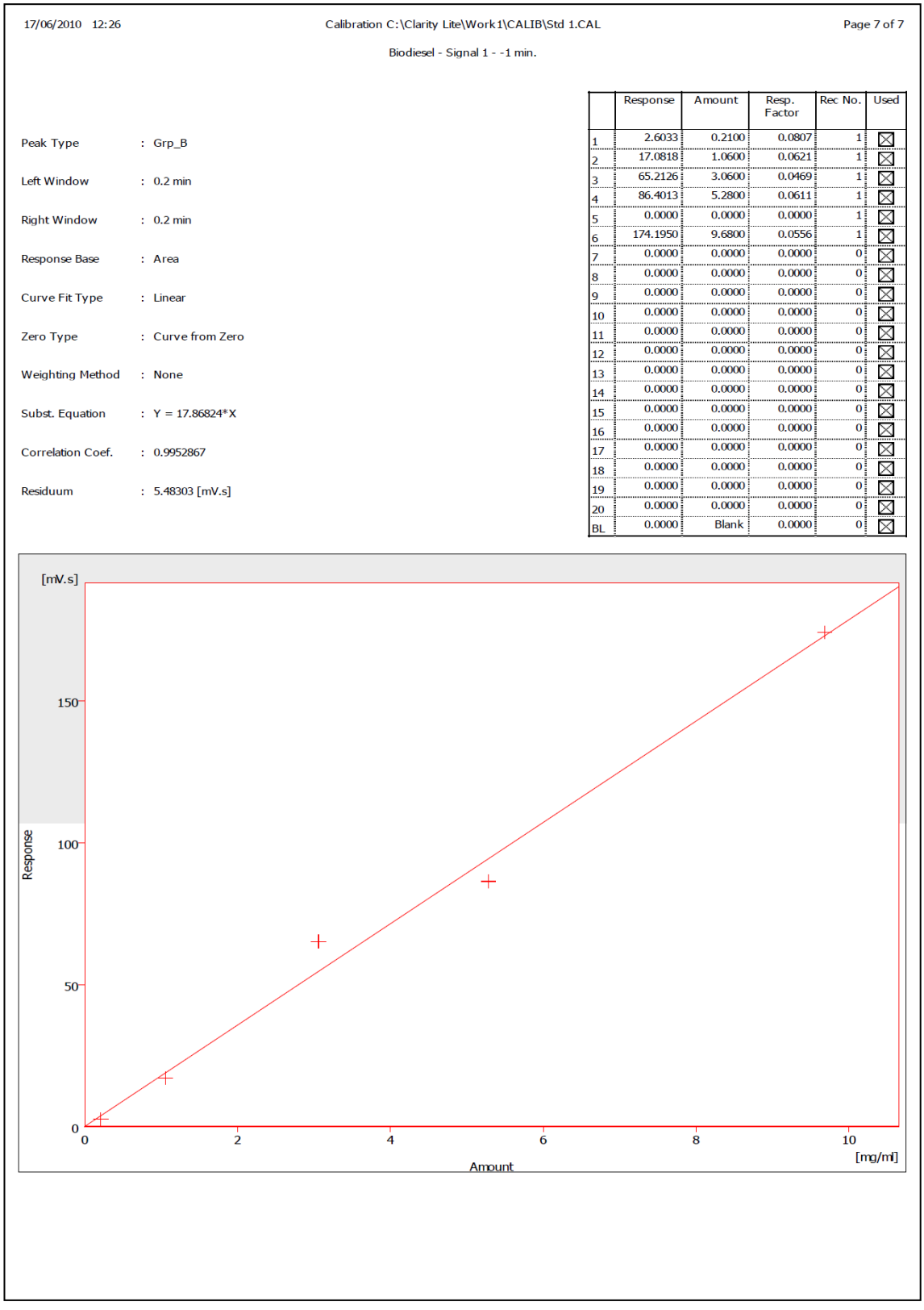

	Response	Amount	Resp. Factor	Rec No.	Used
1	2.6033	0.2100	0.0807	1	☒
2	17.0818	1.0600	0.0621	1	☒
3	65.2126	3.0600	0.0469	1	☒
4	86.4013	5.2800	0.0611	1	☒
5	0.0000	0.0000	0.0000	1	☒
6	174.1950	9.6800	0.0556	1	☒
7	0.0000	0.0000	0.0000	0	☒
8	0.0000	0.0000	0.0000	0	☒
9	0.0000	0.0000	0.0000	0	☒
10	0.0000	0.0000	0.0000	0	☒
11	0.0000	0.0000	0.0000	0	☒
12	0.0000	0.0000	0.0000	0	☒
13	0.0000	0.0000	0.0000	0	☒
14	0.0000	0.0000	0.0000	0	☒
15	0.0000	0.0000	0.0000	0	☒
16	0.0000	0.0000	0.0000	0	☒
17	0.0000	0.0000	0.0000	0	☒
18	0.0000	0.0000	0.0000	0	☒
19	0.0000	0.0000	0.0000	0	☒
20	0.0000	0.0000	0.0000	0	☒
BL	0.0000	Blank	0.0000	0	☒

Figure D7: GC calibration for FAME or biodiesel.

APPENDIX E

Example plots for Case 1 ($\alpha = 0, \beta = 0$)

Estimation of reaction order and rate constant per unit surface area of catalyst.

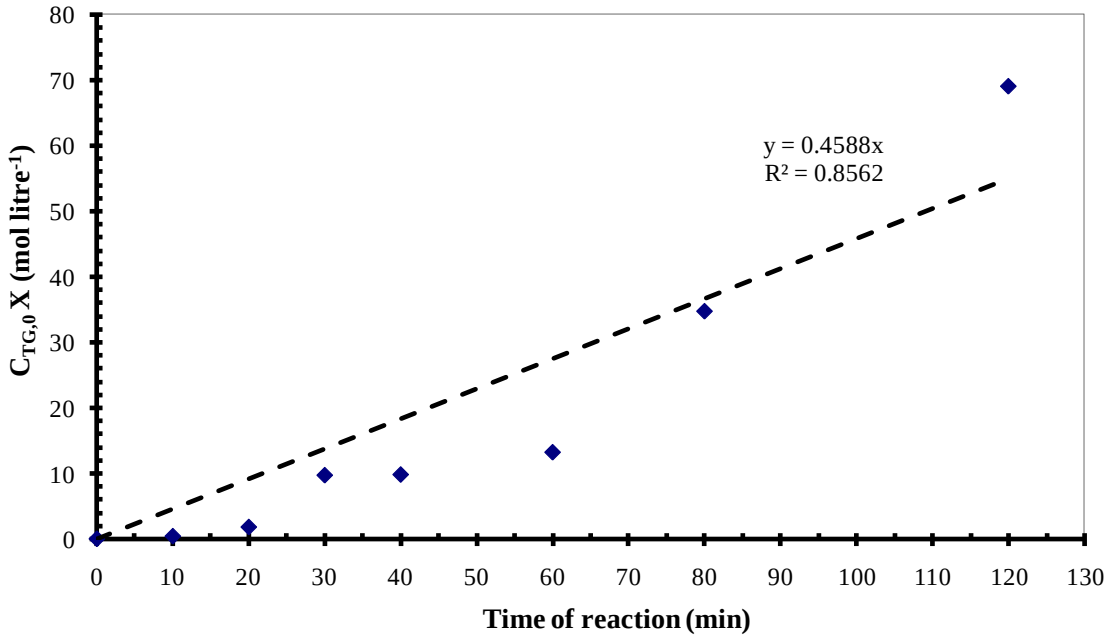

Figure E1(a): Plot for Case 1 for zinc proline powder.

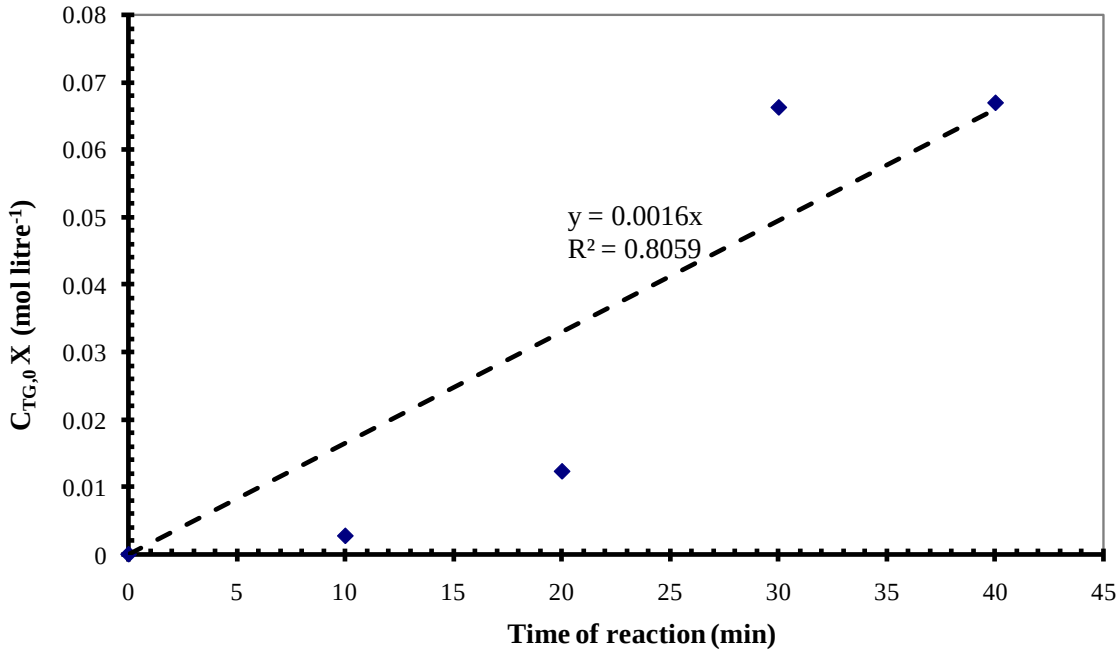

Figure E1(b): The slope for initial rate constant.

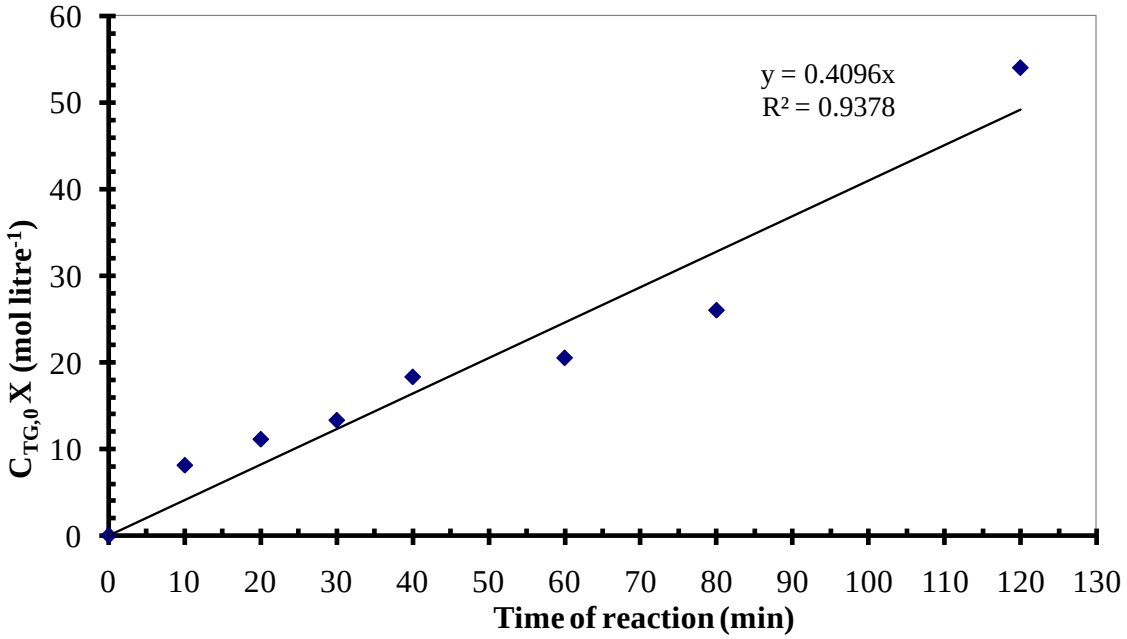

Figure E2(a): Plot for Case 1 using colloidal coating method A.

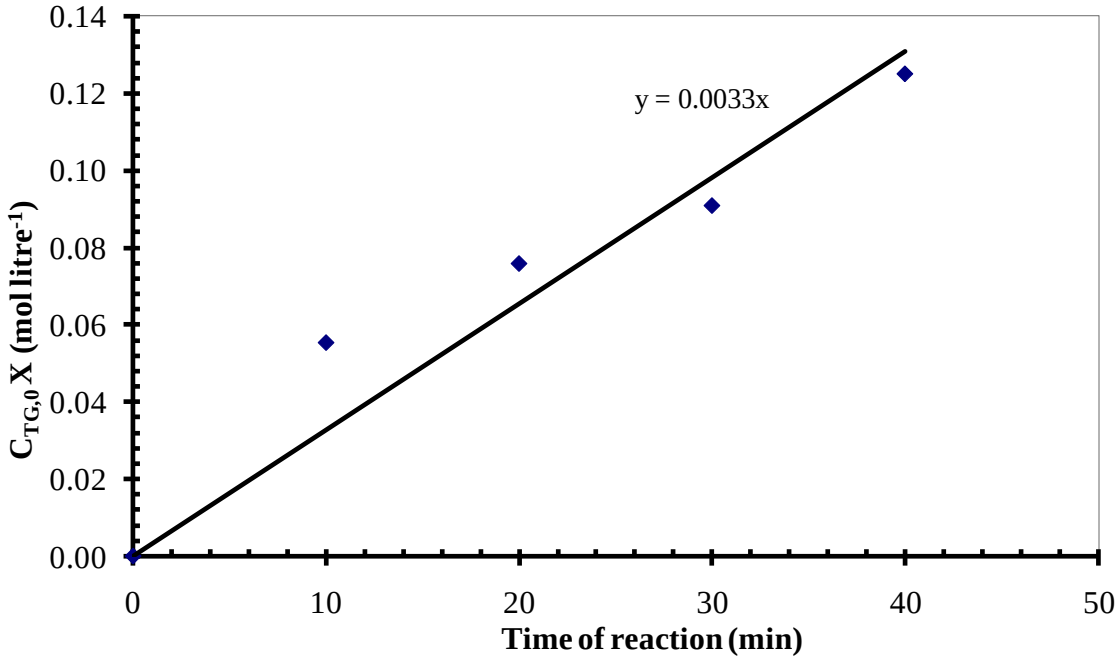

Figure E2(b): Plot to determine initial rate constant**.**

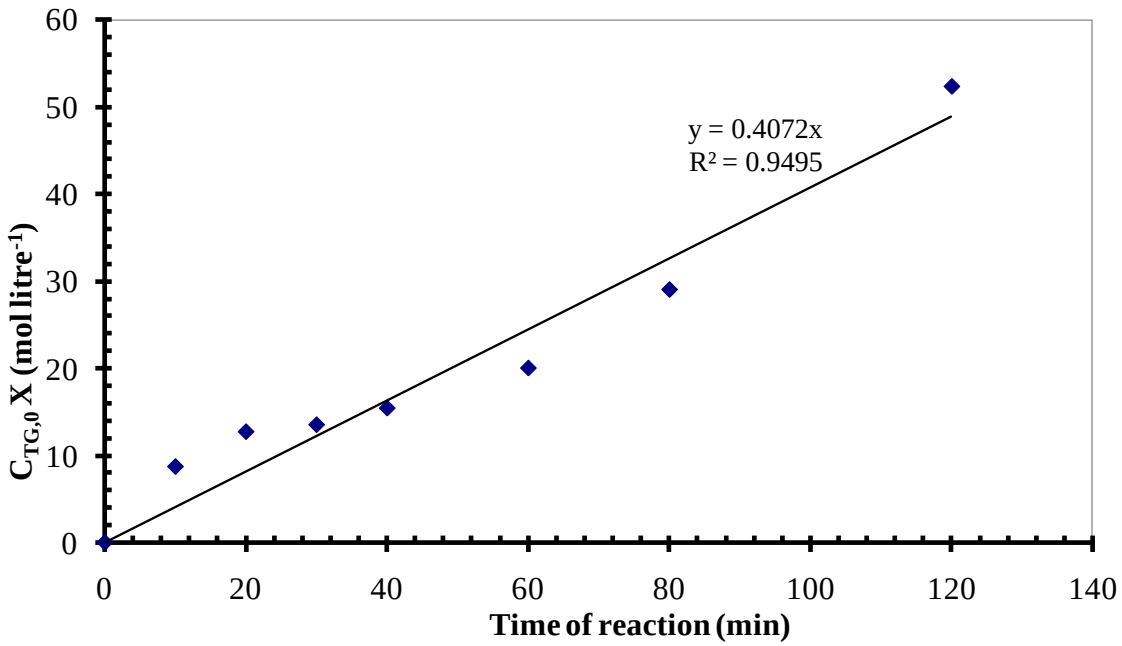

Figure E3(a): Plot for Case 1 using colloidal slurry coating method B.

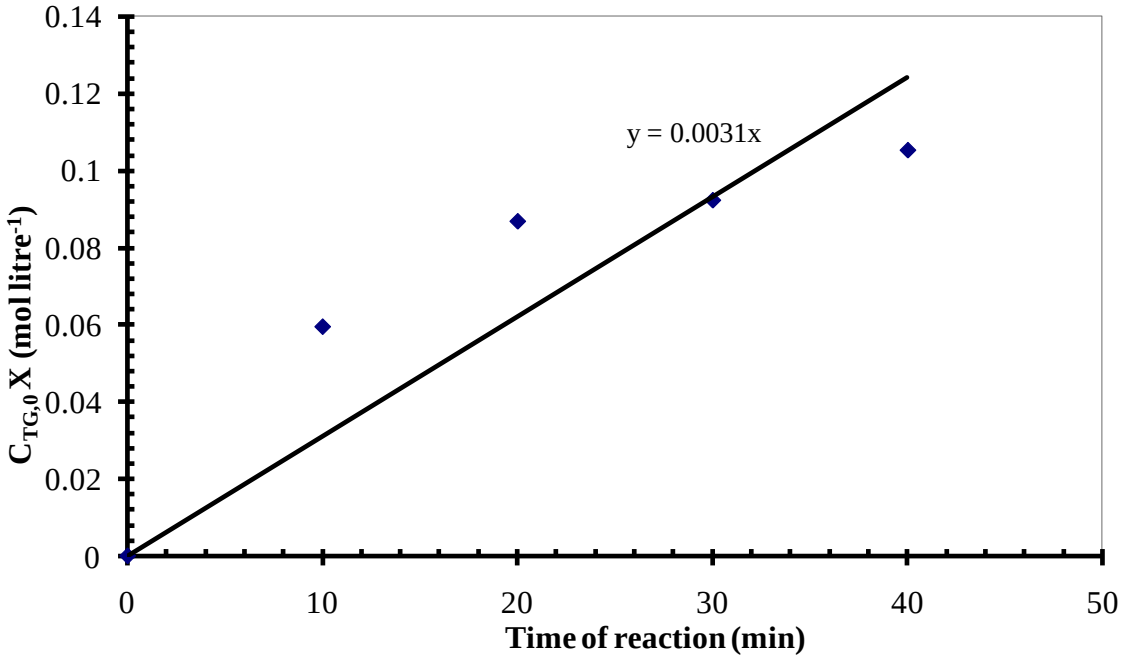

Figure E3(b): Plot to determine initial rate constant

APPENDIX F

Example calculations of geometric surface area.

F1: Calculation of total surface area of zinc proline powder.

To determine the density of zinc proline powder, an amount of zinc proline was placed in the cylinder vial. The mass of the zinc proline was weighed and the level height where zinc proline powder occupied in the cylinder was measured.

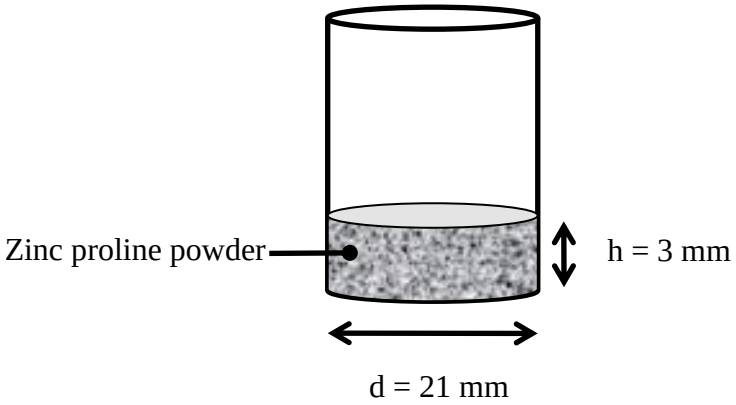

The volume of zinc proline powder is the volume of cylinder where the zinc proline occupied.

$$Volume\ of\ cylinder = \frac{\pi\ d^2\ h}{4}$$

It is assume that the porosity of the catalyst powder, ε = 0.35.

Volume of catalyst = V × (1– ε)

$$= \frac{\pi \times (21\times10^{-3}m)^2 \times (3\times10^{-3}m)}{4} \times (1 - 0.35)$$

= 6.7548 × 10^{-6} m^3 = 6.76 cm^3.

$$Density, \rho = \frac{mass}{volume} = \frac{0.5607\ g}{6.7548 \times 10^{-7} m^3}$$

$$= 8.3 \times 10^5 \text{ g m}^{-3}$$

According to Loweell and Shields (1983), specific surface area for powder, S is

$$S = \frac{3}{\rho\, r}$$

The diameter of particle, $r_{partricle} \approx 1$ μm. Thus,

$$S_{powder} = \frac{3}{8.3 \times 10^5 g\ m^{-3}(1 \times 10^{-6} m)}$$

$$= 3.6144 \text{ m}^2 \text{ g}^{-1}$$

The amount of zinc proline catalyst used in the batch system is 0.3 g. Thus, the geometric surface area of zinc proline powder, A_{powder} in the batch system is

$A_{powder} = 3.6144 \text{ m}^2 \text{ g}^{-1} \times 0.3 \text{ g}$

$= \underline{1.084 \text{ m}^2}$

F2: Calculation of total surface area of monolith

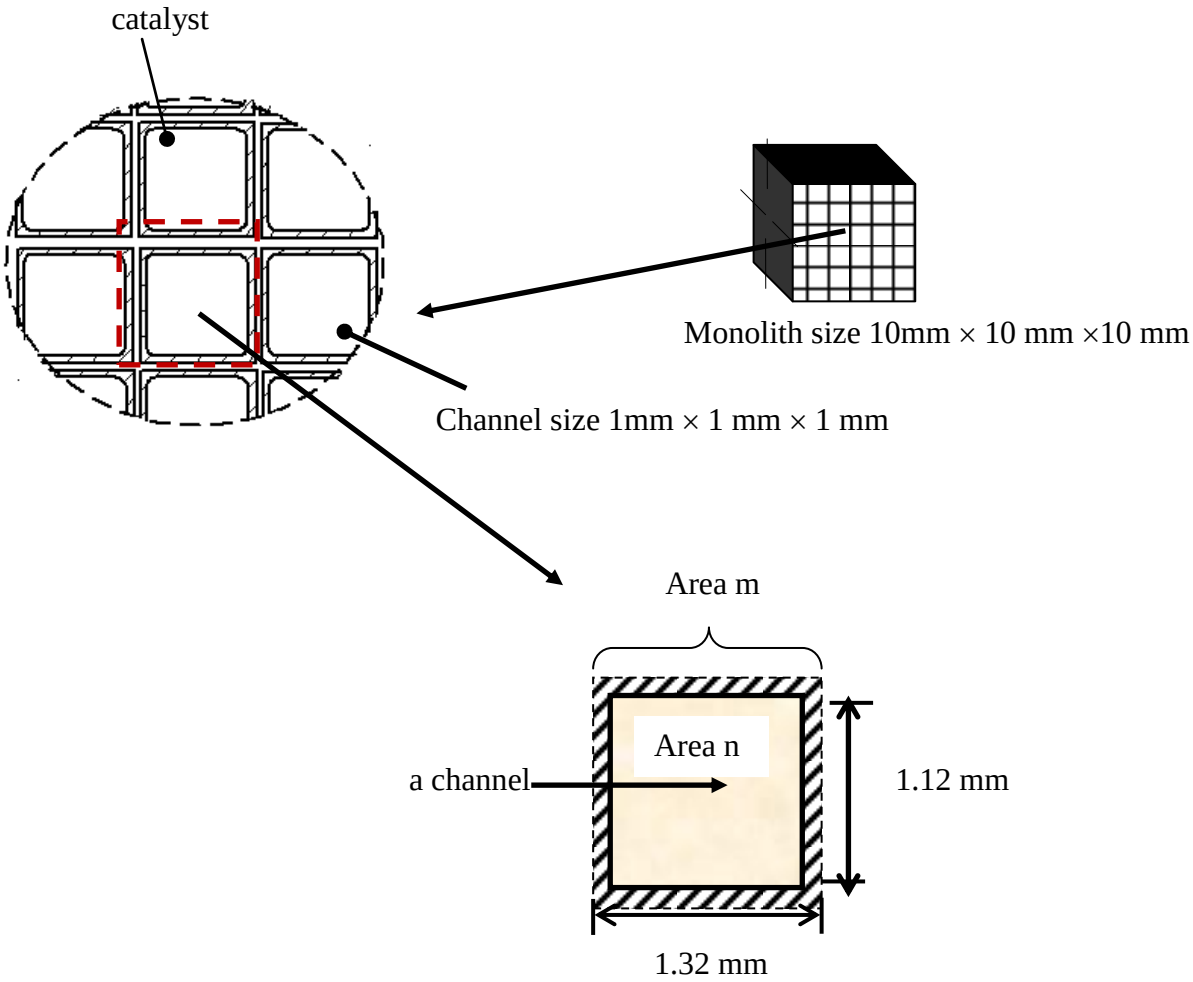

Total area = $A_1 + A_2 + A_3$

Where

A_1 = Area around monolith

A_2 = Area inside the channels

A_3 = Area of top and bottom

Number of monolith pieces = 10 pieces

Number of channel in one piece = 64 channels

For one piece of monolith :-

A_1 = (4 ×10 mm) × 10 mm

= 400 mm^2

A_2 = (4 ×1.12 mm) × 10 mm × 64 channels

= 2867.2 mm^2

A_3 = (m–n) × no of channels × 2 sides

= [(1.32 mm × 1.32 mm)–(1.12 mm × 1.12 mm)] × 64 channels × 2

= 62.464 mm^2

$\Sigma A_1 + A_2 + A_3 = (4 \times 10^{-4}\,m^2) + (2.8672 \times 10^{-3}\,m^2) + (6.2464 \times 10^{-5}\,m^2)$

$= 3.3297 \times 10^{-3} m^2$

Σ A for 10 pieces monoliths = $3.3297 \times 10^{-3}\,m^2 \times 10$ pieces

$= \underline{0.033\ m^2}$

F3: Comparison of global reaction rate

$$r'_{powder} = \frac{0.459\ mol\ l^{-1}\ min^{-1}}{1.084\ m^2} = 0.423\ mol\ l^{-1}\ min^{-1}\ m^{-2}$$

$$r'_{monolith} = \frac{0.410\ mol\ l^{-1}\ min^{-1}}{0.033\ m^2} = 12.424\ mol\ l^{-1}\ min^{-1}\ m^{-2}$$

$$\text{Ratio} = \frac{r'_{monolith}}{r'_{powder}} = \frac{12.42}{0.42} = 30$$

Reference

Lowell, S. and Shields, J. E., 2003. *Powder Surface Area and Porosity*, 3rd Ed. Chapman & Hall. USA.

APPENDIX G

G1: Example calculations to determine weight of catalyst in a reactor.

From Eq. 5.4: $$W = \left(\upsilon_0 C_{TG,0}\right) \frac{X}{k'}$$

where: W is the weight of catalyst (g),

υ_0 is inlet flow (litre min^{-1}),

$C_{TG,0}$ is the concentration of TG (mol $litre^{-1}$) .

X is the fractional conversion of TG, and

k' is the reaction rate (mol min^{-1} $g_{catalyst}^{-1}$).

Using data from Table 4.4 (in Chapter 4), for zinc proline (using Method A), then:

k = 0.0033 mol $litre^{-1}$ min^{-1}

The concentration of catalyst in bulk liquid mixture (20 ml of methanol and 37 ml of oil)

$= \frac{0.3\ g}{0.057\ litre}$ = 5.2631 g $litre^{-1}$.

Then, the value of k' is

$$k' = \frac{0.0033\ mol\ litre^{-1} min^{-1}}{5.2671\ g\ litre^{-1}} = 0.627 \times 10^{-3} \text{ mol g}^{-1} \text{ min}^{-1}.$$

For an X = 0.3, with $C_{TG,0}$ = 0.684 mol $litre^{-1}$, and with υ_0 = 1.0 ml min^{-1}:

$$W_R = (1.0 \times 10^{-3} \text{ litre min}^{-1}) \times 0.684 \text{ mol litre}^{-1} \times \frac{0.3}{0.627 \times 10^{-3} \text{ mol g}^{-1} \text{ min}^{-1}}$$

= 0.327 g.

G2: Calculation to determine volume in a reactor

Catalyst loading per unit volume of monolith $= \frac{W_1}{V_1}$ which was determined to be:

$$= \frac{0.030\ \text{g}}{(1\,\text{cm} \times 1\,\text{cm} \times 1\,\text{cm})} = 0.03\text{g cm}^{-1}$$

From Eq. 5.5, if W = 0.327 g (as calculated in D1), then:

$$V_R = \frac{W_R}{\left(\frac{W_1}{V_1}\right)} = \frac{0.327\ g}{0.03\ g\ cm^{-3}} = 10.9\ cm^3$$

APPENDIX H

Table H1: Properties of oil and methanol at 470K.

Properties	**Rapeseed oil**	**Methanol** (Perry and Green, 1997)
Density, ρ	920 kg m^{-3} (Swern, 1999)	20.061 kg m^{-3}
Viscosity, μ	0.668 Poise = 0.0668 kg m^{-1} s^{-1} (Nwafor and Rice, 1996)	0.0144 kg m^{-1} s^{-1}
Thermal Conductivity, k	0.15 W m^{-1} °K^{-1} (Peterson *et al*.,1995)	0.17 W m^{-1} K^{-1}
C_p	1622.72 J mol^{-1} K^{-1} (Peterson *et al*.,1995)	80.212 J mol^{-1} K^{-1}

Table H2: Estimated properties of a mixture of oil and methanol at 470K

Properties of mixture	**Calculation**
Viscosity, μ	$\mu_{mix} = (x_{oil}\,\mu_{oil}) + (x_{MeOH}\,\mu_{MeOH})$ $= (0.68 \times 0.0668) + (0.32 \times 0.0144)$ = 0.05 kg m^{-1} s^{-1}
Density, ρ	$\rho_{mix} = (x_{oil}\,\rho_{oil}) + (x_{MeOH}\,\rho_{MeOH})$ $= (0.68 \times 920) + (0.32 \times 20.061)$ = 632.02 kg m^{-3}
Thermal Conductivity, k	$k_{mix} = (x_{oil}\,k_{oil}) + (x_{MeOH}\,k_{MeOH})$ $= (0.68 \times 0.15) + (0.32 \times 0.17)$ = 0.156 W m^{-1} K^{-1}
C_p	$C_{p,mix} = (x_{oil}\,C_{p,oil}) + (x_{MeOH}\,C_{p,MeOH})$ $= (0.68 \times 1622.72) + (0.32 \times 80.212)$ = 1129.12 J mol^{-1} K^{-1}

Table H3: Properties of heat transfer fluid (Julabo, 2009)

Properties	Value
Density, ρ	970 kg m^{-3}
Viscosity, μ	50 kg m^{-1} s^{-1}
Thermal Conductivity, k	0.1 W m^{-1} °C^{-1}
C_p	1.37 × 106 J mol^{-1} K^{-1} or °C

Reference

Julabo Product Datasheet [online]. Available from http://www.julabo.de/Download/Safety_Sheets/Julabo_Thermal_H20S_en.pdf. [Accessed on 05/12/2008].

Nwafor, O.M.I. and Rice, G., 1996. Performance of Rapeseed Oil Blends in a Diesel Engine. *Applied Energy*, 54 (4), pp.345-354.

Peterson, C.L. and Auld, Dick., 1991. Technical Overview of Vegetable Oil As A Transportation Fuel. FACT-Vol.,12, *Solid Fuel Conversion for the Transportation Sector*. *ASME 1991*[online]. Available from http://www.biodiesel.org/resource.org/resource/reportdatabase/reports/gen/19910101_GEN.pdf. [Accessed on 05/12/2008].

Perry, R.H. and Green, D.W. ed., 1997. Perry's Chemical Eningeers's Hanbook. 7th Ed. McGraw-Hill, USA.

Swern, D., 1979. *Baileys Industrial Oil and Fat Products Volume 1*, 4th ed. Wiley & Sons, New York. pp. 424-435.

APPENDIX I

I1: Calibration plot for RTD experiments

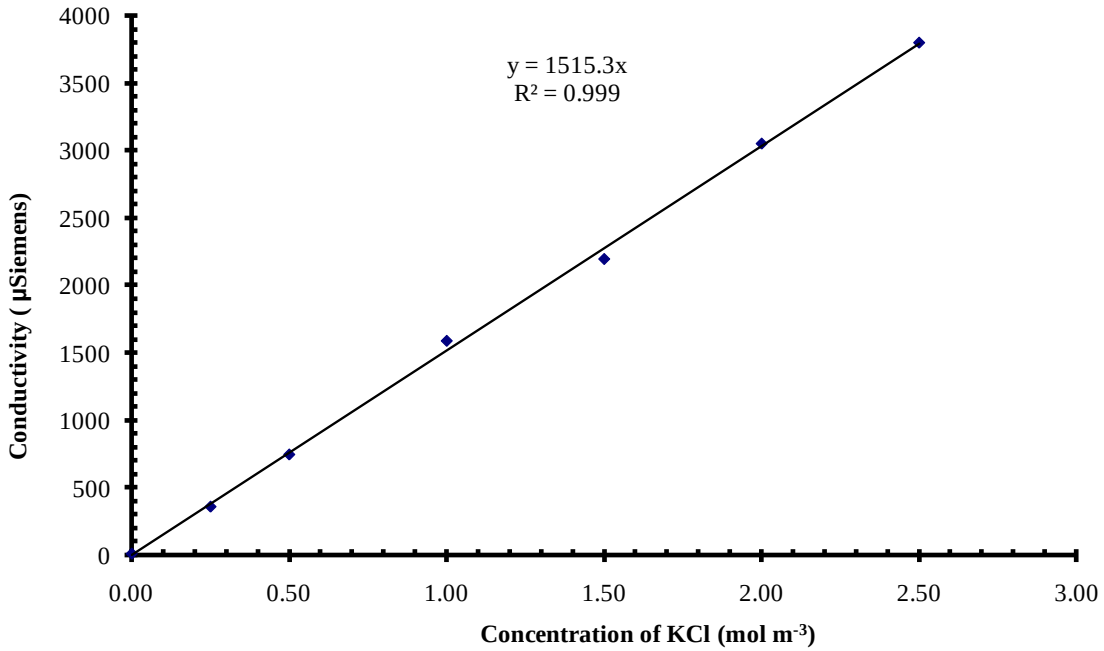

Figure I1: Calibration curve for data interpretation of conductivity meter to tracer concentration

Note: the salt used was KCl solution.

I2: Data for Figure 5.7.

i) Without monolith, inlet flowrate = 2.9 ml min^{-1}.

time (min)	Conductivity reading (µSiemens)	KCl concentration (mol m^{-3})
0	20.58	0.014
2	23.38	0.015
4	28.29	0.019
6	121.20	0.080
8	681.00	0.449
10	758.00	0.500
12	765.50	0.505
14	685.10	0.452
16	516.60	0.341
18	433.30	0.286
20	316.20	0.209
22	221.90	0.146
24	160.00	0.106
26	122.20	0.081
28	104.70	0.069
30	88.21	0.058
32	84.53	0.056
34	79.23	0.052
36	75.07	0.050
38	72.02	0.048
40	69.74	0.046
42	68.05	0.045
44	66.81	0.044
46	65.44	0.043
48	64.13	0.042
50	62.54	0.041
52	60.59	0.040
54	58.54	0.039
56	56.41	0.037
58	54.23	0.036
60	51.74	0.034
70	40.96	0.027
80	33.89	0.022

ii) Without monolith, inlet flowrate = 1.0 ml min^{-1}

time (min)	**Conductivity reading (µSiemens)**	**KCl concentration (mol m^{-3})**
0	18.78	0.012
2	19.82	0.013
4	19.41	0.013
6	19.74	0.013
8	19.15	0.013
10	19.25	0.013
12	25.41	0.017
14	50.89	0.034
16	99.99	0.066
18	130.20	0.086
20	210.50	0.139
22	284.10	0.187
24	361.10	0.238
26	387.98	0.256
28	498.00	0.329
30	508.00	0.335
32	529.12	0.349
34	559.70	0.369
36	575.90	0.380
38	612.50	0.404
40	621.60	0.410
42	611.80	0.404
44	583.80	0.385
46	568.22	0.375
48	547.60	0.361
50	541.12	0.357
52	499.77	0.330
54	485.40	0.320
56	439.30	0.290
58	410.80	0.271
60	380.90	0.251
62	371.30	0.245
64	361.63	0.239
66	335.74	0.222
68	311.87	0.206
70	292.40	0.193
72	262.32	0.173
74	248.53	0.164
76	228.65	0.151
78	196.34	0.130

contd.

time (min)	Conductivity reading (µSiemens)	KCl concentration (mol m^{-3})
80	179.30	0.118
82	164.56	0.109
84	150.34	0.099
86	143.14	0.094
88	124.72	0.082
90	104.00	0.069
92	99.78	0.066
94	94.44	0.062
96	89.56	0.059
98	88.43	0.058
100	87.00	0.057
120	50.00	0.033

iii) Without monolith, inlet flowrate = 0.1 ml/min

time (min)	Conductivity reading (µSiemens)	KCl concentration (mol m^{-3})
0	24.58	0.016
10	25.95	0.017
20	27.71	0.018
30	27.32	0.018
40	28.04	0.019
50	28.87	0.019
60	29.19	0.019
70	29.59	0.020
80	29.40	0.019
90	28.93	0.019
100	28.59	0.019
110	28.77	0.019
120	30.17	0.020
130	31.17	0.021
140	31.75	0.021
150	33.12	0.022
160	36.75	0.024
170	42.12	0.028
180	57.14	0.038

contd.

time (min)	Conductivity reading (µSiemens)	Salt concentration (mol m^{-3})
190	61.43	0.041
200	82.68	0.055
210	135.60	0.089
220	200.50	0.132
230	298.00	0.197
240	377.20	0.249
250	460.80	0.304
260	555.70	0.367
270	649.40	0.429
280	749.00	0.494
290	852.80	0.563
300	924.40	0.610
310	996.70	0.658
320	1098.00	0.725
330	1153.00	0.761
340	1190.00	0.785
350	1220.00	0.805
360	1233.00	0.814
370	1235.00	0.815
380	1226.00	0.809
390	1199.00	0.791
400	1180.00	0.779
410	1146.00	0.756
420	1120.00	0.739
430	982.80	0.649
440	899.26	0.593
450	860.90	0.568
460	848.40	0.560
480	603.20	0.398
500	469.10	0.310
540	294.50	0.194
600	170.20	0.112
660	160.40	0.106

I3: RTD Data for Figure 5.8

i) L = 200 mm, inlet flowrate = 2.9 ml min^{-1}.

Time (min)	**Conductivity reading (µSiemens)**	**KCl concentration (mol m^{-3})**
0	23.29	0.015
2	19.01	0.013
4	21.22	0.014
6	433.80	0.286
8	1143.00	0.754
10	931.50	0.615
12	723.00	0.477
14	460.00	0.304
16	337.00	0.222
18	224.70	0.148
20	159.00	0.105
22	122.60	0.081
24	101.70	0.067
26	89.58	0.059
28	80.26	0.053
30	72.01	0.048
32	64.71	0.043
34	60.30	0.040
36	56.93	0.038
38	50.14	0.033
40	47.63	0.031
42	44.73	0.030
44	40.00	0.026
46	36.25	0.024
48	33.13	0.022
50	30.14	0.020
52	30.03	0.020
54	29.99	0.020
56	28.80	0.019
58	28.90	0.019
60	28.90	0.019

ii) L = 200 mm, inlet flowrate = 1.0 ml min^{-1}.

Time (min)	**Conductivity reading (µSiemens)**	**KCl concentration (mol m^{-3})**
0	23.97	0.016
2	24.85	0.016
4	25.38	0.017
6	26.10	0.017
8	26.44	0.017
10	26.82	0.018
12	27.21	0.018
14	29.66	0.020
16	47.90	0.032
18	137.40	0.091
20	372.00	0.245
22	600.00	0.396
24	758.00	0.500
26	821.80	0.542
28	852.60	0.563
30	849.70	0.561
32	828.40	0.547
34	798.30	0.527
36	753.00	0.497
38	730.50	0.482
40	700.00	0.462
42	675.80	0.446
44	649.30	0.428
46	627.80	0.414
48	594.80	0.393
50	545.80	0.360
52	498.90	0.329
54	470.60	0.311
56	431.00	0.284
58	353.98	0.234
60	306.20	0.202
62	275.90	0.182
64	241.11	0.159
66	223.30	0.147
68	201.00	0.133
70	183.30	0.121

Contd.

Time (min)	**Conductivity reading (µSiemens)**	**KCl concentration (mol m^{-3})**
72	165.00	0.109
74	159.70	0.105
76	150.10	0.099
78	147.50	0.097
80	131.80	0.087
82	123.10	0.081
84	118.45	0.078
86	114.70	0.076
88	110.00	0.073
90	109.70	0.072
92	105.20	0.069
94	97.53	0.064
96	95.93	0.063
98	93.18	0.061
100	94.55	0.062
102	92.11	0.061
104	91.00	0.060
106	89.78	0.059
108	88.55	0.058
110	82.80	0.055
112	78.90	0.052
114	76.32	0.050
116	72.16	0.048
118	68.00	0.045
120	66.12	0.044
122	63.84	0.042
124	61.56	0.041
126	59.28	0.039
128	57.01	0.038
130	54.73	0.036
132	52.45	0.035
134	51.78	0.034
136	51.00	0.034
138	50.90	0.034
140	50.55	0.033

Contd.

Time (min)	Conductivity reading (µSiemens)	KCl concentration (mol m^{-3})
142	50.17	0.033
144	49.00	0.032
146	47.89	0.032
148	45.61	0.030
150	45.21	0.030
152	44.10	0.029
154	43.93	0.029
156	43.75	0.029
158	43.58	0.029
160	42.94	0.028
162	42.74	0.028
164	41.56	0.027
166	40.37	0.027
168	49.98	0.033
170	39.57	0.026
172	42.51	0.028
174	42.11	0.028
176	41.71	0.028
178	41.31	0.027
180	36.76	0.024

iii) L = 200 mm, inlet flowrate = 0.1 ml min^{-1}.

Time (min)	Conductivity reading (µSiemens)	KCl concentration (mol m^{-3})
0	21.9	0.014
10	21.81	0.014
20	27.70	0.018
30	30.54	0.020
40	33.73	0.022
50	38.69	0.026
60	40.77	0.027
70	43.37	0.029
80	49.33	0.033
90	52.01	0.034
100	53.35	0.035
110	54.37	0.036

Contd.

Time (min)	**Conductivity reading (µSiemens)**	**KCl concentration (mol m^{-3})**
120	54.26	0.036
130	53.36	0.035
140	51.78	0.034
150	49.89	0.033
160	49.60	0.033
170	54.33	0.036
180	255.00	0.168
190	341.00	0.225
200	416.90	0.275
210	589.10	0.389
220	737.50	0.487
230	863.30	0.570
240	963.00	0.636
250	999.90	0.660
260	1120.00	0.739
270	1209.00	0.798
280	1263.00	0.833
290	1278.00	0.843
300	1322.00	0.872
310	1322.00	0.872
320	1322.00	0.872
330	1320.00	0.871
340	1304.00	0.861
350	1273.00	0.840
360	1231.00	0.812
370	1174.00	0.775
380	1121.00	0.740
390	1068.00	0.705
400	999.00	0.659
410	962.00	0.635
420	923.80	0.610
430	855.00	0.564
440	823.50	0.543
450	726.90	0.480
460	711.30	0.469
480	687.60	0.454
540	417.60	0.276
600	317.60	0.210

I4: Data for Figure 5.9.

i) L = 400 mm, inlet flowrate = 2.9 ml min^{-1}.

Time (min)	**Conductivity reading (μSiemens)**	**KCl concentration (mol m^{-3})**
0	17	0.011
2	18.90	0.012
4	18.75	0.012
6	297.7	0.196
8	1679.00	1.108
10	1278.00	0.843
12	752.00	0.496
14	431.00	0.284
16	262.30	0.173
18	187.50	0.124
20	164.40	0.108
22	144.80	0.096
24	128.30	0.085
26	111.70	0.074
28	97.48	0.064
30	84.92	0.056
32	76.88	0.051
34	68.70	0.045
36	61.40	0.041
38	55.91	0.037
40	51.03	0.034
42	46.55	0.031
44	42.85	0.028
46	39.80	0.026
48	36.86	0.024
50	34.75	0.023
52	31.27	0.021
54	28.47	0.019
56	25.91	0.017
58	23.45	0.015
60	22.79	0.015

ii) L = 400 mm, inlet flowrate = 1.0 ml min^{-1}.

Time (min)	**Conductivity reading (µSiemens)**	**KCl concentration (mol m^{-3})**
0	23.41	0.015
2	22.50	0.015
4	22.13	0.015
6	21.77	0.014
8	21.66	0.014
10	21.73	0.014
12	21.66	0.014
14	51.44	0.034
16	169.50	0.112
18	344.20	0.227
20	785.00	0.518
22	1199.00	0.791
24	1382.00	0.912
26	1365.00	0.901
28	1242.00	0.820
30	1135.00	0.749
32	1030.00	0.680
34	930.10	0.614
36	848.00	0.560
38	770.00	0.508
40	713.40	0.471
42	632.90	0.418
44	589.70	0.389
46	550.00	0.363
48	490.60	0.324
50	463.80	0.306
52	391.00	0.258
54	332.00	0.219
56	303.00	0.200
58	255.00	0.168
60	217.10	0.143
62	192.00	0.127
64	174.30	0.115
66	162.70	0.107
68	149.10	0.098
70	142.90	0.094

Contd.

time (min)	**Conductivity reading (µSiemens)**	**KCl concentration (mol m^{-3})**
76	124.70	0.082
78	120.70	0.080
80	111.90	0.074
82	110.00	0.073
84	118.45	0.078
86	114.70	0.076
88	109.70	0.072
90	103.10	0.068
100	77.50	0.051
110	65.00	0.043
120	53.31	0.035
130	48.02	0.032
140	43.55	0.029
150	38.76	0.026
160	34.87	0.023
170	30.98	0.020
180	29.27	0.019

APPENDIX J: GC results for continuous experiments

Data for Figure 5.15 and 5.16 (Monolith A).

Run time (min)	Mass concentration (mg ml^{-1})						wt % composition					Conversion (%)
	TG	DG	MG	FAME	GL	Total	TG	DG	MG	FAME	GL	
30	1.817	0.505	0.138	1.492	0.008	3.960	45.88	12.75	3.48	37.68	0.20	54.12
60	1.993	0.406	0.206	1.103	0.063	3.771	52.85	10.77	5.46	29.25	1.67	47.15
90	1.728	0.289	0.128	0.650	0.037	2.832	61.02	10.20	4.52	22.95	1.31	38.98
120	1.409	0.224	0.059	0.372	0.012	2.076	67.87	10.79	2.84	17.92	0.58	32.13
150	3.212	0.520	0.066	0.857	0.003	4.658	68.96	11.16	1.42	18.40	0.06	31.04
180	1.413	0.232	0.090	0.340	0.017	2.092	67.54	11.09	4.30	16.25	0.81	32.46
210	0.873	0.168	0.062	0.191	0.005	1.299	67.21	12.93	4.77	14.70	0.38	32.79
240	3.570	0.485	0.099	0.635	0.007	4.796	74.44	10.11	2.06	13.24	0.15	25.56
270	2.532	0.363	0.078	0.492	0.006	3.471	72.95	10.46	2.24	14.18	0.17	27.05
300	1.864	0.280	0.067	0.325	0.008	2.544	73.27	11.01	2.63	12.78	0.31	26.73

Data for Figure 5.15 and 5.17 (Monolith B).

Run time (min)	Mass concentration (mg ml^{-1})						wt % composition					Conversion (%)
	TG	DG	MG	FAME	GL	Total	TG	DG	MG	FAME	GL	
30	1.608	0.529	0.104	1.075	0.000	3.316	48.49	15.95	3.14	32.42	0.00	51.51
60	1.264	0.326	0.023	0.454	0.007	2.074	60.95	15.72	1.11	21.89	0.34	39.05
90	2.836	0.613	0.208	0.864	0.045	4.566	62.11	13.43	4.56	18.92	0.99	37.89
120	6.288	1.148	0.226	2.132	0.000	9.794	64.20	11.72	2.31	21.77	0.00	35.80
150	4.818	0.755	0.205	1.265	0.021	7.064	68.20	10.69	2.90	17.91	0.30	31.80
180	9.887	1.356	0.153	1.756	0.000	13.152	75.17	10.31	1.16	13.35	0.00	24.83
210	5.752	1.006	0.015	1.225	0.000	7.998	71.92	12.58	0.19	15.32	0.00	28.08
240	4.732	0.801	0.028	0.895	0.000	6.456	73.30	12.41	0.43	13.86	0.00	26.70
270	6.229	0.979	0.010	1.109	0.000	8.327	74.80	11.76	0.12	13.32	0.00	25.20
300	3.800	0.630	0.024	0.632	0.000	5.086	74.71	12.39	0.47	12.43	0.00	25.29

Data for Figure 5.15 (Bare monolith).

Run time (min)	Mass concentration (mg ml^{-1})						wt % composition					Conversion (%)
	TG	DG	MG	FAME	GL	Total	TG	DG	MG	FAME	GL	
30	3.264	0.409	0.000	0.199	0.000	3.872	84.30	10.56	0.00	5.14	0.00	15.70
60	3.422	0.389	0.000	0.177	0.000	3.988	85.81	9.75	0.00	4.44	0.00	14.19
90	4.560	0.377	0.000	0.109	0.000	5.046	90.37	7.47	0.00	2.16	0.00	9.63
120	2.787	0.188	0.000	0.069	0.000	3.044	91.56	6.18	0.00	2.27	0.00	8.44
150	7.690	0.219	0.000	0.023	0.000	7.932	96.95	2.76	0.00	0.29	0.00	3.05
180	5.430	0.118	0.000	0.016	0.000	5.564	97.59	2.12	0.00	0.29	0.00	2.41
210	17.961	0.720	0.000	0.178	0.000	18.859	95.24	3.82	0.00	0.94	0.00	4.76
240	4.202	0.127	0.000	0.055	0.000	4.384	95.85	2.90	0.00	1.25	0.00	4.15
270	9.297	0.077	0.000	0.077	0.000	9.451	98.37	0.81	0.00	0.81	0.00	1.63
300	6.135	0.045	0.000	0.045	0.000	6.225	98.55	0.72	0.00	0.72	0.00	1.45

Data for Figure 5.21 and 5.22.

Running time	Mass concentration (mg/ml)						Weight % composition					**Conversion (%)**
	TG	**DG**	**MG**	**FAME**	**GL**	**Total**	**TG**	**DG**	**MG**	**FAME**	**GL**	
30	0.000	0.103	0.095	0.502	0.010	0.71	0.00	14.51	13.38	70.70	1.41	100.00
60	0.481	0.208	0.111	0.818	0.007	1.625	29.60	12.80	6.83	50.34	0.43	70.40
90	0.856	0.239	0.083	0.720	0.018	1.916	44.68	12.47	4.33	37.58	0.94	55.32
120	0.588	0.165	0.034	0.503	0.015	1.305	45.06	12.64	2.61	38.54	1.15	54.94
150	1.151	0.302	0.034	0.637	0.000	2.124	54.19	14.22	1.60	29.99	0.00	45.81
180	0.789	0.212	0.042	0.461	0.000	1.504	52.46	14.10	2.79	30.65	0.00	47.54
210	1.162	0.257	0.089	0.548	0.007	2.063	56.33	12.46	4.31	26.56	0.34	43.67
240	0.383	0.169	0.110	0.368	0.026	1.056	36.27	16.00	10.42	34.85	2.46	63.73
270	0.579	0.156	0.047	0.205	0.013	1.000	57.90	15.60	4.70	20.50	1.30	42.10
300	0.530	0.150	0.071	0.334	0.006	1.091	48.58	13.75	6.51	30.61	0.55	51.42